FORMULATION, DEVELOPMENT AND ASSESSMENT OF EFAVIRENZ-LOADED LIPID NANOCARRIERS

By
Pedzisai Anotida Makoni

A Thesis Submitted to Rhodes University in Fulfillment of the Requirements for the Degree of

MASTER OF SCIENCE (PHARMACY)

February 2014

Faculty of Pharmacy
RHODES UNIVERSITY
Grahamstown
South Africa

ABSTRACT

The feasibility of incorporating efavirenz (EFV) into innovative solid lipid nanoparticles (SLN) and nanostructured lipid carriers (NLC) using the hot high-pressure homogenization (HHPH) technique was investigated in an attempt to address the shortcomings in therapy associated with the use of conventional dosage forms. The shortcomings include the unpalatable taste of API in solution, instability in the presence of light when in solution and psychiatric side effects of the API. In particular, sustained release approaches may reduce or limit the incidence of adverse psychiatric effects of EFV and alleviate Acquired Immune Deficiency Syndrome (AIDS)-related complications such as AIDS Dementia Complex (ADC) in patients, ultimately improving their quality of life. Prior to initiating pre-formulation, formulation development and optimization studies of EFV-loaded SLN and/or NLC, Response Surface Methodology (RSM) in conjunction with central composite design (CCD), was used to develop and validate suitable methods for the quantitative determination of EFV in pharmaceutical formulations and for monitoring EFV release from SLN and/or NLC *in vitro*. Simple, accurate, precise, sensitive and stability-indicating reversed phase-high performance liquid chromatography (RP-HPLC) methods with UV and electrochemical (EC) detection were developed, validated and optimized for *in vitro* analysis of EFV in formulations. On the basis of risk-to-benefit ratio the RP-HPLC method with UV detection was selected as the most suitable for the quantitative determination of EFV in pharmaceutical formulations, and was applied to *in vitro* release studies of EFV from SLN and/or NLC.

Pre-formulation studies were undertaken to investigate the thermal stability of EFV so as to facilitate the selection of lipid excipients for the manufacture of nanocarriers, and to establish their compatibility with EFV. It was found that EFV was thermostable up to a temperature of approximately 200°C, indicating that HHPH could be used for the manufacture of EFV-loaded SLN and/or NLC. Lipid screening revealed that EFV is highly soluble in solid and liquid lipids, with glyceryl monostearate and Transcutol® HP showing the best solubilizing potential for EFV. Glyceryl monostearate exists in a stable β-modification prior to exposure to heat, but exists in the α-polymorphic modification following exposure to heat. It was established that the addition of Transcutol® HP to glyceryl monostearate revealed the co-existence of the α- and β'-polymorphic

modifications, thereby revealing the existence of the modifications in NLC produced from the optimum lipid combination. Furthermore, an investigation of binary mixtures of EFV/glyceryl monostearate and glyceryl monostearate/Transcutol® HP, in addition to eutectic mixtures of EFV, glyceryl monostearate and Transcutol® HP, revealed no interaction between EFV and the lipids selected for the production of the nanocarriers.

Due to the significantly higher solubility of EFV in Transcutol® HP than in to glyceryl monostearate, NLC are most likely to have a higher LC and EE than SLN. In addition, the existence of both the α- and β'-polymorphic modifications in the binary mixture of the lipid implies that EFV expulsion on prolonged storage is unlikely to occur from NLC when compared to SLN. Consequently formulation development and optimization studies of SLN and NLC were performed to investigate the potential to deliver EFV from a novel technology with an appropriate LC and EE for EFV.

Tween®80 was selected for use in these formulations as the use of this surfactant facilitates the targeting of nanocarriers to the CNS. RSM in conjunction with a Box-Behnken Design (BBD) was used to establish the effects of process variables, such as number of homogenization cycles and pressure, in addition to formulation variables such as amount of EFV and Tween®80 on the particle size (PS), polydispersity index (PDI), zeta potential (ZP), visual assessment (VA) and release rate (RR) of EFV after 24 hours. In addition the LC and EE, degree of crystallinity and lipid modification, shape and surface morphology of the optimized batches were investigated to ensure that EFV-loaded SLN and NLC of desirable quality were produced.

On the day of manufacture the mean PS and PDI of EFV-loaded SLN was 59.00 ± 23.16 nm and 0.382 ± 0.054 respectively. The mean PS and PDI of EFV-loaded NLC was 34.73 ± 0.7709 nm and 0.394 ± 0.027 respectively. The formulations were in the nanometer range and exhibited a narrow particle size distribution, as indicated by the PDI values. The ZP values for optimized SLN and NLC generated on the day of manufacture using HPLC grade water as the dispersion

medium were -32.5 ± 4.99 mV and -22.4 ± 3.72 mV respectively. In addition the optimized batches of SLN and NLC revealed a decrease in crystallinity in comparison to bulk lipid material. DSC, WAXS and FT-IR revealed that EFV was molecularly dispersed in the nanocarriers. In addition EFV-loaded SLN existed in a single α-polymorphic form, whereas EFV-loaded NLC exhibited the co-existence of α- and β'-polymorphic forms. Generally SLN and NLC were spherically shaped when viewed under transmission electron microscopy (TEM) and scanning electron microscopy (SEM). On the day of manufacture the EE and LC of EFV-loaded SLN was found to be 96.77 ± 0.453 % and 9.68 ± 1.772 % respectively. The EE and LC of EFV-loaded NLC was 99.93 ± 0.413 and 9.995 ± 0.672 respectively. The release profiles for the optimized formulations of SLN and NLC exhibited an initial burst release over the first 0-3 hours of testing, after which the release was sustained for up to 24 hours. The cumulative % EFV released over 24 hours was higher from SLN (91.5±3.423 %) than that observed for NLC (73.6±4.34 %).

Stability studies performed for 8 weeks on the optimized batches of the SLN and the NLC were also conducted so as to ensure product quality. The formulations were assessed in terms of parameters considered benchmarks of stability, and included ZP, PS, PDI, LC and EE. Generally these parameters remained unchanged following storage for 8 weeks at 25°C/60% RH but showed considerable changes following storage for 8 weeks at 40°C/75% RH. These studies reveal that SLN and NLC when stored at 25°C/60% RH have the potential to be used as colloidal delivery systems for EFV that have the potential to protect EFV from photodegradation and sustain release into brain tissue. The latter will ultimately reduce or limit the incidence of adverse psychiatric effects and potentially alleviate AIDS-related complications such as ADC in patients with HIV/AIDS, ultimately improving their quality of life.

ACKNOWLEDGEMENTS

I would like to express my sincere gratitude to the following people and organizations:

My supervisor, Doctor K. WaKasongo for his expert guidance, encouragement, continuous support and patience during the research and the writing of this thesis.

My co-supervisor, Professor R.B. Walker for his availability, guidance and assistance during the research and the writing of this thesis.

The Dean and Head, Professor R.B. Walker and the staff of the Faculty of Pharmacy for the use of facilities in the Faculty at Rhodes University.

Mr T. Samkange for his technical support and Mr L. Purdon for his assistance and continuous help throughout the duration of this project.

Dr Sandile Khamanga for the tremendous assistance especially with the use of the Electrochemical Detector and guidance during my studies.

Dr Grooff Driekus in conjunction with the Nelson Mandela Metropolitan University for allowing me to use the Differential Scanning Calorimetry.

My colleagues and friends in the Department of Pharmacy for their academic assistance, objectiveness, honesty, and pleasant company for the duration of my project: Ms. Ayesha Fauzee, Ms. Ashmita Ramanah, Ms. Samantha Mukozhiwa, Mr. Tawanda Dube, Mr. Chiluba Mwila, Mr. Tendai Chanakira, Ms. Chiedza Zindove, Mr. F Mhaka, Mr. Byron Mubaiwa, Mr. Francis Moyo, Mr. Maynard Chiwakata, Mr. Denzil Mubare, Ms. Chikomborero Chakaingesu, Mr. Jameel Fakee, Ms. Faith Kuzeeko, Ms. Amanda Siruma, Ms. Sonal Patel, Mr. Mohammed Adam, Ms. Tafadzwa Mutsvairo, Ms. Nosiphiwe Ngqwala, Mr. Archibald Svogie and Ms. Olivia Motsi. Special thanks to Ms. Samantha Mukozhiwa for listening to all my research anguishes and continuous support during this project.

My parents, Mr. E.J. and Mrs. S. Makoni for giving me a life that I have come to love and treasure, for their prayers, encouragement, love, support and financial assistance. I am forever indebted to my parents for the values, teachings and beliefs that they instilled in me as well as for the sacrifices and decisions that they made to support my education.

My immediate and extended family members for their encouragement, love, support and understanding throughout my years as a student. Special thanks to my uncle and aunt Mr. H.T. and Mrs. V. Matangaidze for their encouragement, love, support and financial assistance not only throughout the duration of my university academic career, but also during part of my life. My late grandmother, Mrs M. Matangaidze for having played a major role in my upbringing. My sisters, Miriro, Tendai, Nyaradzo and my brother Mauru for their encouragement and support, during my academic career.

Adcock Ingram® Limited (Johannesburg, Gauteng, South Africa) for their kind donation of efavirenz. Gattefossé SAS (Saint-Priest Cedex, France) for their kind donation of lipidic excipients. Special thanks to the Gattefossé representative in South Africa, Ms. Nathalie Jelonek for responding to my emails requesting for samples and sending me the requested samples in a timely manner.

The Almighty God for giving me protection, strength and determination to succeed throughout my life and for allowing me to carry out and complete this work in a timely manner.

STUDY OBJECTIVES

Human Immunodeficiency Virus (HIV) is the causative agent of Acquired Immune Deficiency Syndrome (AIDS), and affects the immune system. However the virus also invades the central nervous system (CNS), causing AIDS Dementia Complex (ADC) leading to neurological disorders that may include psychosis and behavioral changes which further affects the quality of life of patients. Efavirenz (EFV) is a WHO-listed drug used in highly active antiretroviral therapy (HAART) against HIV-1 infections in adults, adolescents and children older than 3 years. EFV is effective and requires once-a-day dosing. EFV reaches therapeutic levels in the CNS and may potentially be used to manage HIV in the CNS. However EFV levels in the CNS are generally high due to "dose-dumping" that is associated with the use of conventional dosage forms and can lead to severe psychiatric effects which further exacerbate ADC. In addition solutions of EFV are susceptible to photodegradation and an aqueous solution of EFV for the oral management of HIV in adult and/or paediatric patients is not readily available as EFV causes a strong burning sensation in liquid formulations. Innovative lipid carriers such as solid lipid nanoparticles (SLN) and nanostructured lipid carriers (NLC) have the potential to mask unpalatable tastes, protect API from photodegradation, sustain release of API into brain tissue and may reduce or limit the incidence of adverse psychiatric effects. This may potentially alleviate AIDS-related complications such as ADC in patients with HIV/AIDS, ultimately improving their quality of life.

The objectives of this research were:

1. To obtain data from the literature and experimentation relating to the physicochemical properties of EFV that would aid in the development of innovative formulations.
2. To develop, optimize and validate RP-HPLC methods for the quantitative analysis of EFV using RSM and select the simplest, sensitive, precise, accurate and linear method for use during formulation development and optimization studies of EFV-loaded SLN and/or NLC.
3. To establish the thermal stability of EFV and select and characterize lipidic excipients for the manufacture of EFV-loaded SLN and NLC.
4. To design, develop and optimize EFV-loaded SLN and NLC using a minimum number of experimental runs using RSM and to evaluate the critical quality attributes (CQA) of the formulations.
5. To study the release kinetics of EFV during the formulation, development and optimization process.
6. To investigate and identify an optimum and stable nanoparticulate delivery system for EFV with the appropriate loading capacity (LC) and encapsulating efficiency (EE), and that sustains EFV release over 24 hours.

TABLE OF CONTENTS

LIST OF FIGURES

LIST OF TABLES

LIST OF ACRONYMS

% RSD	Percentage relative standard deviation
^{1}H-NMR	Proton magnetic resonance
ACN	Acetonitrile
ADC	AIDS Dementia Complex
AIDS	Acquired Immunodeficiency Syndrome
ANOVA	Analysis of variance
API	Active pharmaceutical ingredient
Apo E	Apolipoprotein E
ARV	Antiretroviral
BBB	Blood brain barrier
BBD	Box Behnken Design
BCS	Biopharmaceutical Classification System
CCD	Central Composite Design
CE	Capillary electrophoresis
CNS	Central nervous system
CQA	Critical quality attributes
CYP 2B6	Cytochrome 2B6
CYP 2C19	Cytochrome 2C19
CYP 2C9	Cytochrome 2C9
CYP 3A4	Cytochrome 3A4
CYP P450	Cytochrome P450
DLS	Dynamic light scattering
DNA	Deoxyribonucleic acid
DPPC	Dipalmitoyl-phosphatidylcholine

DSC	Differential scanning calorimetry
ECD	Electrochemical detection
EE	Encapsulation efficiency
EFV	Efavirenz
ERMBT	Erythromycin breath test
FDA	Food and Drug Administration
FT-IR	Fourier transform infrared spectroscopy
GC	Gas chromatography
GC-MS	GC-mass spectroscopy
GIT	Gastrointestinal tract
GM	Glyceryl monostearate
GRAS	Generally regarded as safe
HAART	Highly active antiretroviral therapy
HCL	Hydrochloric acid
HBV	Hepatitis B virus
HCV	Hepatitis C virus
HDV	Hydrodynamic voltammogram
HHPH	Hot high-pressure homogenization
HIV	Human Immunodeficiency Virus
HLB	Hydrophilic lipophilic balance
HMG-CoA	Hydroxymethylglutaryl coenzyme A
HPH	Hot pressure homogenization
HPLC	High-pressure liquid chromatography
ICH	International Conference of Harmonisation
IMI	Imipramine
IR	Infrared
IS	Internal standard
K_a	Acid dissociation constant
KBr	Potassium bromide
KOH	Potassium hydroxide
LC	Loading capacity

LC	Liquid chromatography
LC-MS	LC-mass spectrometry
LD	Laser diffractometry
LDA	Laser Doppler anemometry
LDL	Low density lipoprotein
LOD	Limit of detection
LOQ	Limit of quantitation
Log P	Partition coefficient
LRT	Loratidine
MALDI-TOF/TOF	Matrix-assisted laser desorption ionization source and tandem-of-flight
MP	Melting point
NaOH	Sodium hydroxide
NLC	Nanostructured lipid carriers
NNRTI	Non-nucleoside reverse transcriptase inhibitor
NRTI	Nucleoside reverse transcriptase inhibitor
NVP	Nevirapine
PCS	Photon correlation spectroscopy
PDI	Polydispersity index
PEG	Polyethylene glycol
PHR	Peak height ratio
PI	Protease Inhibitor
PS	Particle size
QSRR	Quantitative structure (reversed-phase)-retention relationships
RH	Relative humidity
RI	Recrystallization index
RNA	Ribonucleic acid
RP-HPLC	Reversed phase-HPLC
RR	Release rate
RSM	Response surface methodology
R_t	Retention time

RT	Reverse transcriptase
SAR	Structure activity relationships
SD	Standard deviation
SEM	Scanning electron microscopy
SLN	Solid lipid nanoparticles
SLS	Sodium lauryl sulphate
TB	Tuberculosis
TEM	Transmission electron microscopy
TGA	Thermogravimetric analysis
THP	Transcutol® HP
Tris	Tris (hydroxymethyl) aminomethan
USA	United States of America
USP	United States Pharmacopeia
UV	Ultraviolet
UV-Vis	UV-visible
Vd	Volume of distribution
WAXS	Wide-angle X-ray scattering
WHO	World Health Organization
WP	Width of the peak
ZP	Zeta potential

CHAPTER 1

EFAVIRENZ

1.1 INTRODUCTION

The Human immunodeficiency virus (HIV) is the causative agent of acquired immune deficiency syndrome (AIDS) [1]. By the year 2003 the World Health Organization (WHO) declared AIDS a global pandemic and the disease continues to cause numerous deaths worldwide. In 2011 WHO reported that 34 million people are living with HIV worldwide, of whom 3.3 million are children under 15 years of age. During the same year a reported 1.7 million deaths worldwide were caused by the virus [2]. HIV primarily affects the immune system [3] and can also invade the central nervous system (CNS) causing AIDS dementia complex (ADC) [3].

ADC is caused by the migration, replication and ultimate accumulation of HIV in the CNS. The HIV invades the CNS and significantly resides in the microglial cells of the brain [4]. The characteristic attribute of ADC is the progressive degeneration of specific cognitive and psychomotor functions of the patient [5,6]. Initially ADC is characterized by deterioration in memory, concentration and attention of the patient, followed by the late onset of paraparesis, spasticity, mutism and psychosis [7]. Late stages of ADC are characterized by mental slowness, reduced rate of speech and alterations in speaking volume [8,9]. ADC impairs the quality of life of patients living with HIV/AIDS and it has been estimated that these patients have a one in four chance of developing ADC [10].

To date there is no known cure for AIDS and effective therapy involves the administration of highly active antiretroviral therapy (HAART). HAART requires the use of three or more drugs such as tenofovir, lamivudine or emtricitabine and efavirenz or nevirapine, used in combination so as to suppress the rapid progression of the HIV [1,11].

Efavirenz (EFV) is a non-nucleoside reverse transcriptase inhibitor (NNRTI) listed by WHO as a component of HAART for treating HIV-1 infections in adults, adolescents and children. EFV was first approved by the United States Food and Drug Administration (FDA) in September 1998 [1,12,13]. Although EFV was approved in 1998, to date no dosing regimens for children under 3 years of age or weighing less than13 kg have been established [13,14]. EFV has thus been included in the Medécins Sans Frontières list as one of the ARV agents that is not available in an appropriate paediatric formulation [13,15]. Due to the absence of such data, treatment options for HIV/ tuberculosis (TB) co-infected children under 3 years of age or weighing less than 13 kg becomes difficult due to interactions between nevirapine and TB therapy [13,14].

EFV is available commercially as a 30 mg/ml solution, in addition to 50 mg, 100 mg, 200 mg and 600 mg capsules and tablets [13]. The primary dosage forms available in South Africa are capsules and tablets [14].

Commercially available products containing EFV in South Africa include Stocrin®, Aspen Efavirenz®, Cipla Efavirenz®, Adco-Efavirenz®, Auro-Efavirenz® and Sonke® Efavirenz [14].

1.2 PHYSICO-CHEMICAL PROPERTIES

1.2.1 Description

EFV is (S)-6-chloro-4-(cyclopropylethynyl)-1,4-dihydro-4-(trifluoromethyl)-2H-3,1-benzoxazin-2-one [16,17]. It is a white to slightly pink crystalline powder, has an empirical formula of $C_{14}H_9ClF_3NO_2$ and a molecular weight of 315.7. The structural formula is shown in Figure 1.1 [16,17].

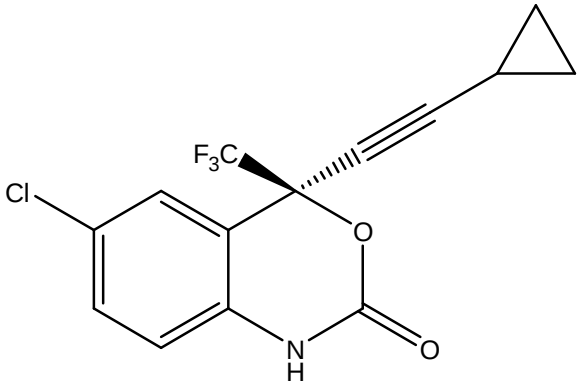

Figure 1.1: *Chemical structure of EFV*

1.2.2 Solubility

EFV is a highly lipophilic compound, practically insoluble in water and soluble in methanol [15,17]. EFV has an intrinsic aqueous solubility of 9.2 µg/mL at a pH of 8.7 at 25°C. Alcohols have been shown to increase the solubility of EFV to 725 mg/mL, 663 mg/mL and 598 mg/mL in methanol, ethanol and isopropanol, respectively [18]. The solubility of EFV is pH dependent and increases in solutions of pH > 9.0, which is consistent with the loss of a proton on the carbamate amine functional group [19].

1.2.3 Biopharmaceutical Classification System (BCS)

EFV has low aqueous solubility and high intestinal permeability and is classified as a Class II compound in the Biopharmaceutical Classification System (BCS) of drugs [20].

1.2.4 pKa and Partition Coefficient (Log P)

EFV is weakly acidic, with a pKa of 10.1 ± 0.1 [21,22] and is therefore mostly unionized at physiological pH. Log P values determine the relative distribution of a specific active pharmaceutical ingredient (API) into *n*-octanol-saturated water (lipid bilayer-like) or *n*-octanol (lipid-like) [22]. EFV has been shown to be highly lipophilic and has a Log P of 2.07 ± 0.12,

established using the *n*-octanol-water shake-flask method [22], and 5.4 using an unknown method [18].

1.2.5 Ultraviolet (UV) Absorption Spectrum

The wavelength of maximum absorption (λ_{max}) of EFV is 247 nm [16,23]. Some studies have reported a λ_{max} of 248 nm [24]. The absorption spectrum of EFV was determined using a solution of phosphate buffer (pH = 5) and acetonitrile (50:50) over a wavelength range of 200-300 nm at a scan speed of 600 nm/min. The spectrum was generated using a double beam Model GBC 916 UV-VIS spectrophotometer (GBC Scientific Equipment Pty Ltd, Melbourne, Australia). The UV absorption spectrum of EFV shown in Figure 1.2 reveals a λ_{max} of EFV of 246.24 nm, and this wavelength was used for the quantitation of EFV in these studies.

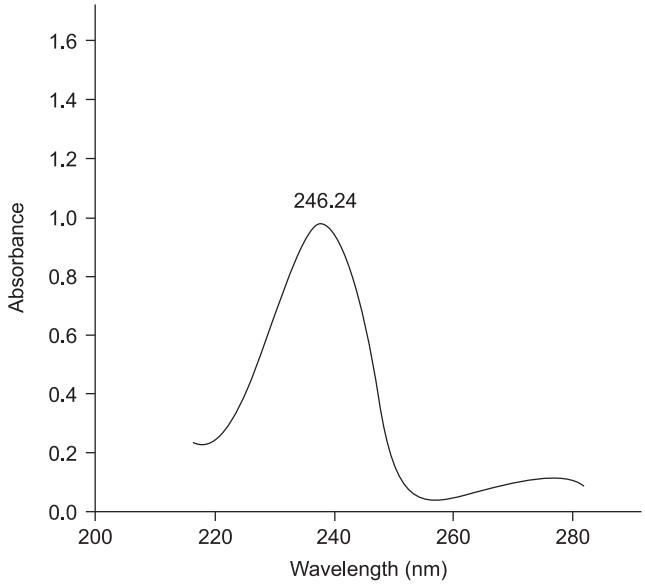

Figure 1.2: *Absorption spectrum of EFV*

1.2.6 Melting Point Range

The melting point of EFV is reported to fall between 138 and 142°C [23]. To determine the purity of anhydrous EFV powder, a melting point determination was performed using a Stuart® SMP 30 melting point instrument (Bibby Scientific Limited, Stone, Staffordshire, STI50SA,

United Kingdom). The melting range was found to be 138.6-141.0°C, which falls into the range 138-142°C reported in the literature.

1.2.7 Hygroscopicity

EFV remains unchanged at a relative humidity as high as 90% [18] and is therefore not considered to be hygroscopic.

1.2.8 Stereochemistry and Polymorphism

It has been reported that EFV exists in as many as 19 solid forms, *viz.* Forms I-V, H1, α, β, γ, γ1, γ2, ω, δ, N, O and P, in addition to 3 amorphous forms [25]. Form I of EFV is used for the manufacture of pharmaceutical products [25]. EFV also exhibits isomerism. The S (Figure 1.1) isomer is used in EFV formulations as the R isomer has no effect on reverse transcriptase enzyme inhibition activity [22,26].

1.2.9 Optical Rotation

The specific optical rotation of a 3 mg/mL solution of EFV in methanol is -89 and -100° at 20°C [23].

1.2.10 Infrared Spectrum (IR)

The IR spectrum of solids can be established by preparing a sample as a compressed disc composed of Potassium Bromide (KBr) by mixing the compound with Nujol® mull, or by dissolving the solid compound in a solvent such as carbon tetrachloride [27,28]. The KBr method was used to generate an IR spectrum for EFV using a Perkin-Elmer® Precisely FT-IR spectrometer Spectrum 100 (Perkin-Elmer® Pty Ltd, Beaconsfield, England). The scan was performed in the range of 4000-650 cm^{-1}. The IR absorption spectrum of EFV is shown in Figure

1.3 and the band assignments are listed in Table 1.1. The principal bands were observed at wave numbers of 3311 (stretching of the –NH bond), 2250 (C-C triple bond stretching), 1749 (carbonyl stretching), 1602 (C=C stretching), 1350-1120 (CF_3 stretching), 1096-1089 (C-Cl stretching) and 900-650 cm^{-1} (aromatic ring detection) and are similar to those reported in literature [23,24,29].

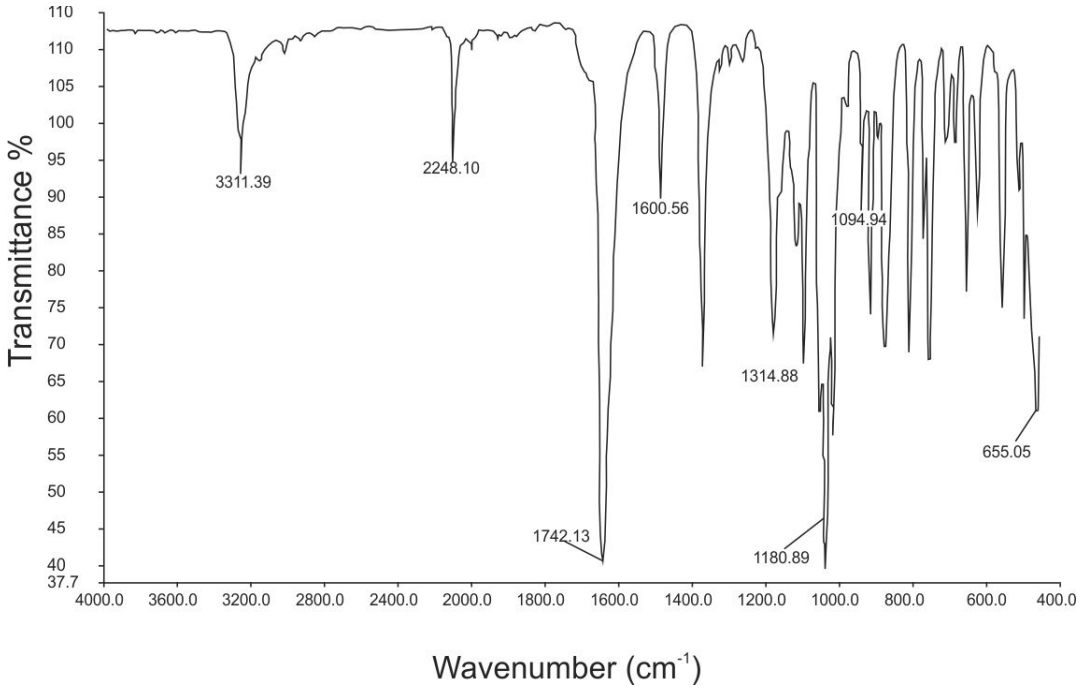

Figure 1.3: *IR absorption spectrum of anhydrous EFV*

Table 1.1: *IR frequency bands of EFV*

Frequency (cm^{-1})	**Vibrational Assignments**
3311	-NH stretching of benzoxazi-2-one ring
2250	C-C triple bond stretching
1749	C=O stretching
1602	C=C stretching
1350-1120	CF_3 stretching
1096-1089	C-Cl stretching
900-650	Aromatic ring

1.3 STABILITY

Stability studies are useful for detecting whether storage or other conditions may result in changes to an API or product, and may provide useful information about potential degradation pathways and/or products that could form during manufacture and/or storage [30,31]. Furthermore such studies provide a useful indication of what may be appropriate storage conditions for EFV.

1.3.1 pH

The stability of EFV is pH dependent, and EFV degradation follows first-order kinetic reactions [19]. EFV solutions were found to exhibit maximum stability in solutions of pH between 4 and 5 [18] and EFV solutions within this pH range have been shown to be stable for up to 72 hours [32-34]. The degradation of EFV at 80°C after 4 hours in 0.1 M NaOH has been reported by Kumar *et al* [32]. Other studies reported the degradation of EFV at 80°C after 6 hours in 0.1 M NaOH, and the degradation products were isolated [33,34]. The proposed alkali-catalyzed degradation pathway of EFV is shown in Figure 1.4. Base-catalyzed hydrolysis may proceed through two interchangeable mechanisms, *viz*. via direct attack on the carbonyl forming carbamic acid intermediate (1), or via an elimination-addition reaction forming the isocyanate intermediate (2), with the latter being consistent with conventional carbamate hydrolysis [35,36]. Base-catalyzed hydrolysis would predominate via elimination-addition forming the isocyanate intermediate based on the inductive effect of CF_3 stabilization on the leaving group [19]. EFV does not undergo significant degradation following exposure to 0.1 M HCI and neutral solutions [32].

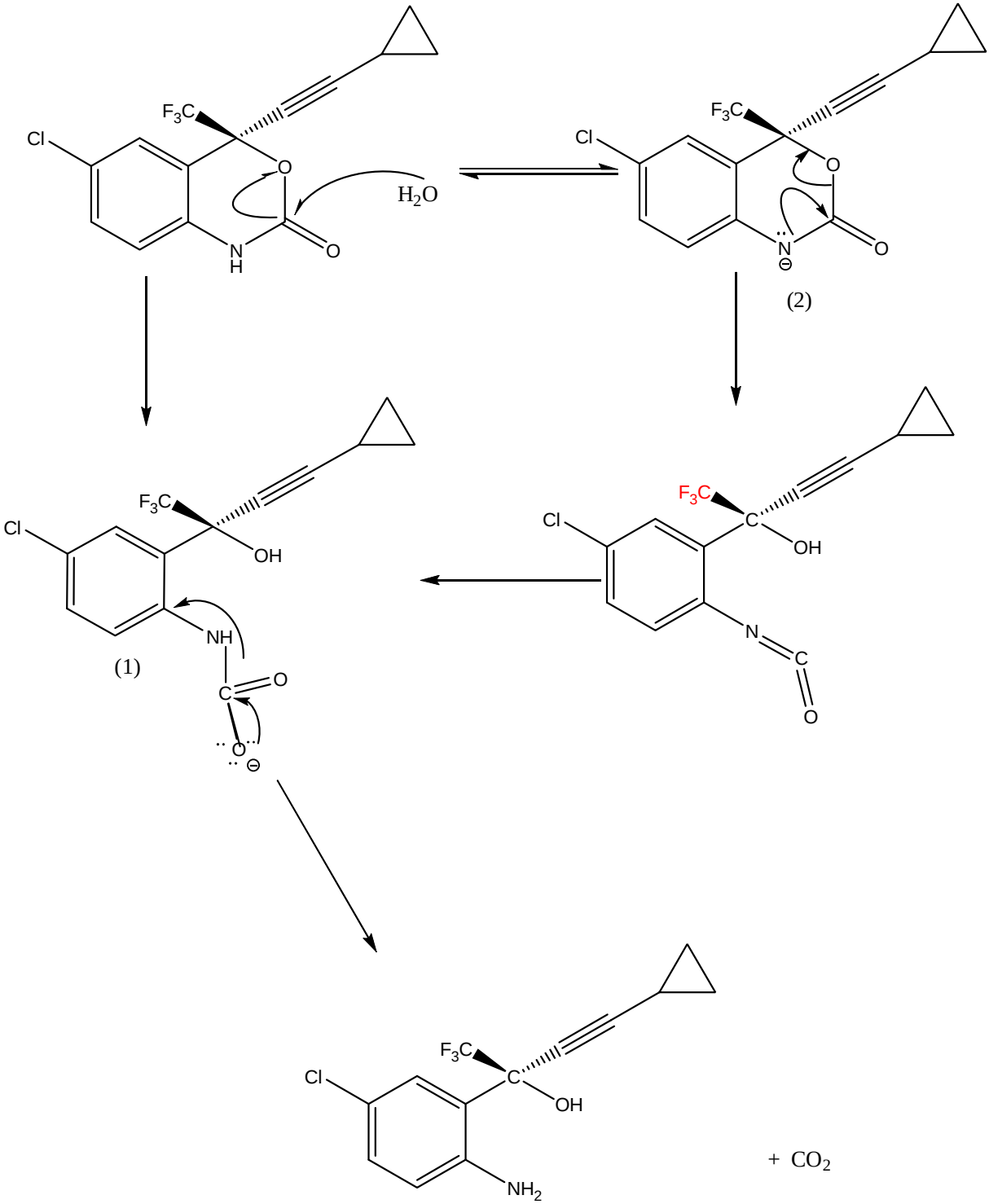

Figure 1.4: *Proposed base hydrolysis pathway of EFV (adapted from [19])*

As the pH of solution increases towards an alkaline pH of 7-9, EFV undergoes base-catalyzed hydrolysis at the carbamate functional group, as proposed in the degradation pathway shown in Figure 1.4. At pH values ≥ 10 EFV ionizes at the carbamate functional group, resulting in stabilization of the negative charge present on the ionized species. This in turn inhibits base-catalyzed hydrolysis of EFV under highly alkaline conditions [19] as shown in Figure 1.5. The mobile phase used to prepare EFV solutions, and used for all HPLC analyses, was buffered to a pH between 4-5 using a phosphate buffer.

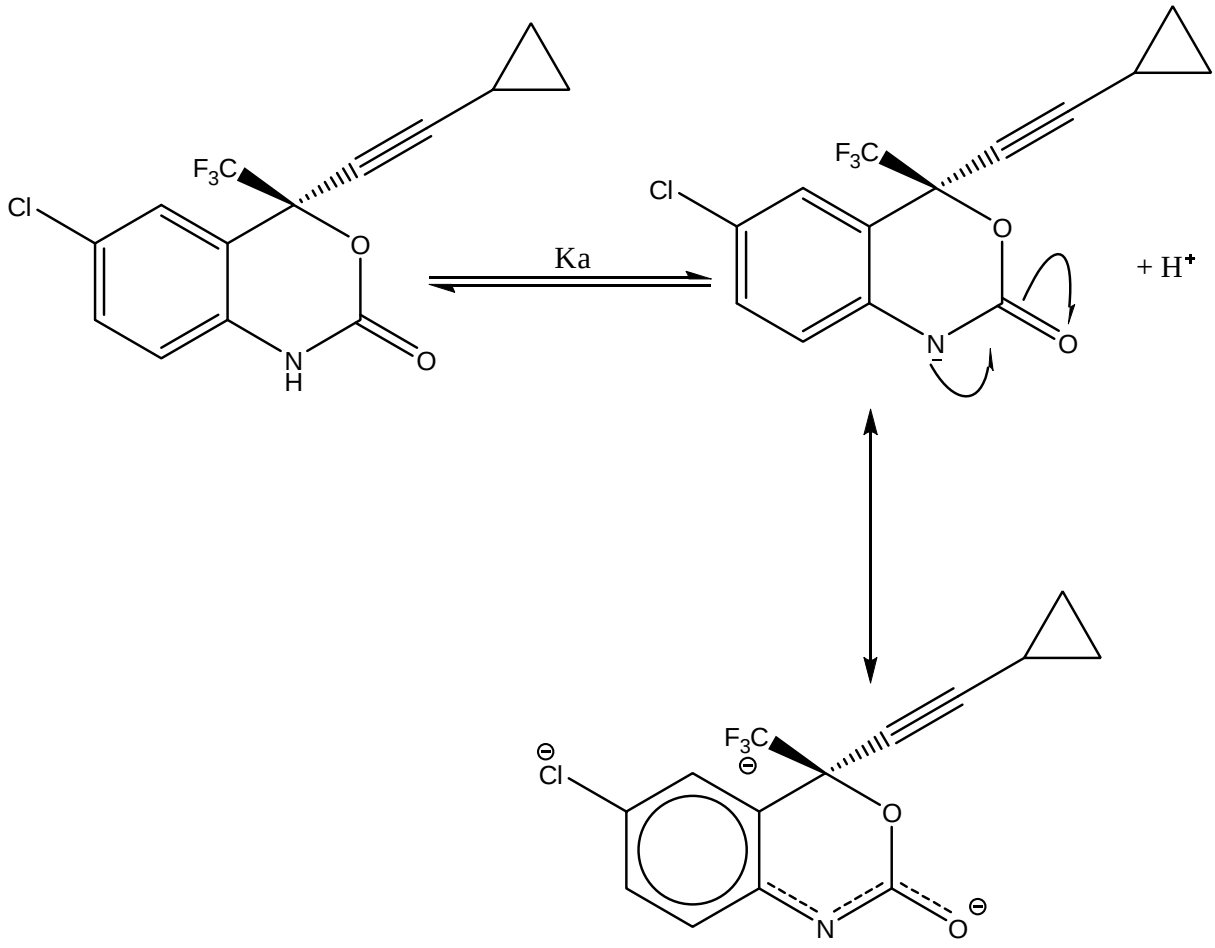

Figure 1.5: *Ionization of the carbamate proton and stabilization of negative charge on the ionized species (adapted from [19])*

1.3.2 Oxidation

EFV has been found to undergo oxidative degradation following exposure to 3% v/v H_2O_2 solution at 80°C for 6 hours [33,34].

1.3.3 Photodegradation

EFV undergoes photolytic degradation following exposure of EFV in solution to ultraviolet (UV) light at a wavelength of 254 nm [34]. EFV solutions were therefore protected from light using aluminum foil and amber colored vials at all times during these studies.

1.3.4 Exposure to dry heat

Anhydrous EFV powder was found to be stable following exposure to dry heat in an oven maintained at 97°C for 8 hours.

1.3.5 Temperature

EFV is susceptible to thermal degradation in mobile phase following exposure at 80°C for 8 hours under reflux conditions. All degradation studies performed on EFV in solution were performed at 70°C so as to minimize the potential for thermal instability.

1.4 SYNTHETIC PATHWAY

The manufacture of EFV follows a series of chemical reactions as outlined by the synthetic pathway shown in Figure 1.6 [37-39].

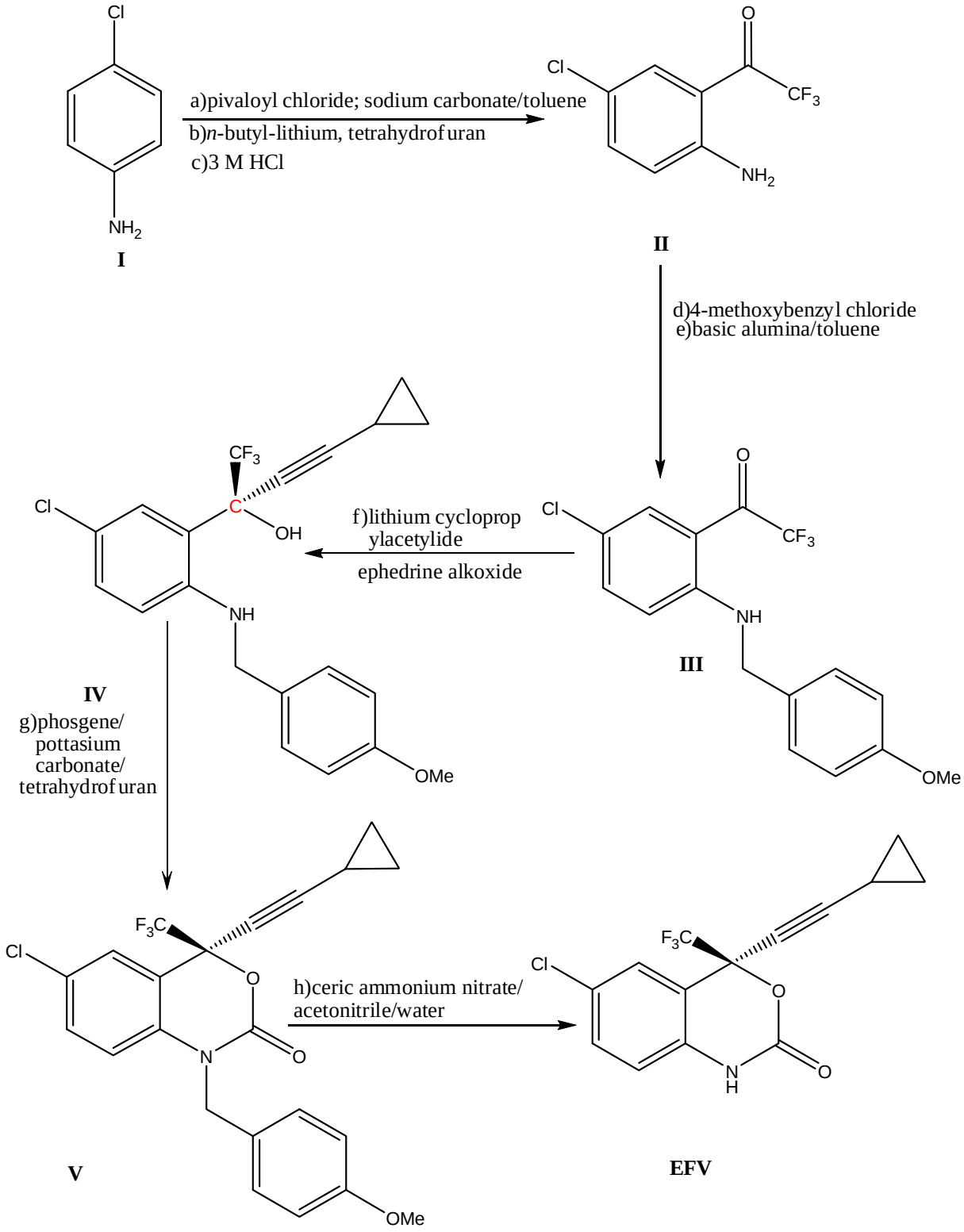

Figure 1.6: *Synthesis of EFV*

4-chloroanaline (**I**) is acylated with pivaloyl chloride using sodium carbonate in toluene. This produces an anilide that is acylated by means of ethyl trifluoroacetate using *n*-butyl-lithium in tetrahydrofuran (THF), which is then hydrolyzed with 3 M HCl to yield 2-amino-5 chloro-2, 2, 2-trifluoroacetophenone (**II**). The aniline nitrogen of (**II**) is benzylated with 4-methoxybenzyl chloride using basic alumina in toluene as the reaction catalyst to form trifluoromethyl ketone (**III)**. Lithium cyclopropylacetylide is added to (**III)** in the presence of ephedrine alkoxide to form an alcohol (**IV),** which has a significant active asymmetric bond (C, Figure 1.6). Compound (**IV)** is reacted with phosgene in the presence of potassium carbonate and THF to yield a benzoxazinone (**V**). The p-methoxybenzyl group is removed by reacting (**V)** with ceric ammonium nitrate in acetonitrile and water to yield (**EFV),** which is then purified by recrystallization from hexane and toluene [38,39].

1.5 STRUCTURE ACTIVITY RELATIONSHIPS (SAR)

The emergence of resistant forms of HIV is one of the major challenges encountered in ARV therapy. Some of the resistant viral strains are the consequence of a single mutation K 103 N and the double mutation K 103 N/ L 100 I. A novel series of 4, 4-disubstituted quinolinones were discovered in a continuing attempt to develop second generation NNRTI with improved viral resistance profiles [40]. The parent quinolinone shown in Figure 1.7 exhibits good antiviral activity but poor enzyme inhibitory activity and therefore has poor activity against single mutation strains. The most potent 4, 4-disubstituted quinolinone discovered (R = *O*-4-pyridylmethyl) has been shown to have an improved resistance profile compared to EFV against single mutation strains. However the disubstituted quinolinone did not show significant potency against the K 103 N/ L 100 I double mutation strain [40].

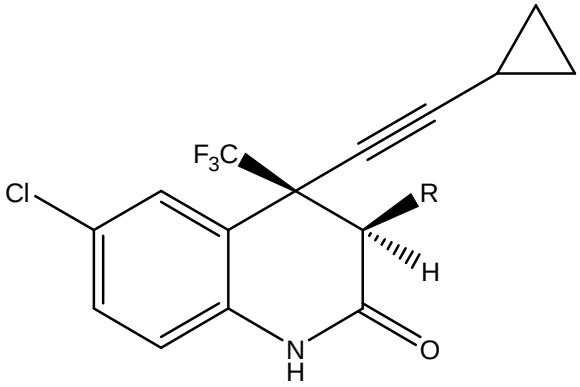

Figure 1.7: *Structure of parent quinolinone derivative*

1.6 CLINICAL PHARMACOLOGY

1.6.1 Mechanism of Action

EFV is a non-competitive potent NNRTI of the wild type HIV-1 reverse transcriptase (RT) with a small component of competitive inhibition. RT is a heterodimer with 66 kDa (p66) and 51 kDa (p51) subunits [37,41,42]. A p66/p51-EFV crystal complex structure showed that EFV attaches adjacent to the hydrophobic p66 subunit pocket of RT enzyme, producing a conformational change in the enzyme, thus inhibiting its function [12,42-44]. This conformational change prevents the enzyme from converting RNA to DNA during DNA polymerization. In contrast to nucleoside reverse transcriptase inhibitors (NRTI), EFV is active in the administered form and does not require phosphorylation to prevent cell infection by HIV [12,42]. Apart from EFV being a selective potent enhancer of HIV-1 RT p66/p51, hetero-dimerization studies have shown that EFV was found to promote RT p66/p66 and p51/p51 homo-dimer interactions significantly and enhanced proteolytic cleavage of the model HIV-1 Pol polyprotein precursor that is expressed in bacteria. The data suggest that potent mediators of RT dimerization such as EFV might interfere with the late stages of viral replication [45]. HIV-2 RT and other retrovirus strains and human cellular DNA polymerase γ, β and γ are not inhibited by EFV [42].

1.6.2 Clinical Indications

EFV is used in combination with other antiretroviral drugs for the treatment of HIV-1 infected adults, adolescents and children weighing more than 13 kg and/or older than 3 years [14,42]. In a clinical study, the superiority of the combination of EFV/zidovudine/lamivudine to that of indinavir/zidovudine/lamivudine in suppressing plasma HIV-1 RNA to undetectable levels was shown [46]. Since nevirapine (NNRTI)-based HAART has been reported to be more hepatotoxic than EFV-based HAART, EFV in combination with two NRTI is the recommended option to initiate therapy and is the most widely used NNRTI [14,43,47]. EFV is also indicated for post-HIV exposure prophylaxis [14].

1.6.3 Dosage and Administration

1.6.3.1 Adult Patients

In adult patients on a regimen containing EFV, 600 mg is administered orally once daily at night so as to minimize the impact of CNS side-effects. EFV should not be used for single-agent therapy [14,48].

1.6.3.2 Paediatric Patients

EFV dosage in children on combination therapy is based on body weight calculations. The following once-at-night daily dosing for children weighing > 13 kg and/or > 3 years of age has been established as follows for patients of 13 kg - 15 kg: 200 mg; 15 kg - 20 kg: 250 mg; 20 kg - 25 kg: 300 mg; 25 kg - 32.5 kg: 350 mg; 32.5 kg - 40 kg: 400 mg, and for a 40 kg or heavier patient: 600 mg [14].

1.6.3.3 Dosage Adjustment

If EFV is taken concomitantly with voriconazole the maintenance dose of voriconazole must be increased to 400 mg 12 hourly and the EFV dose must be reduced by 50% to 300 mg once daily

in order to achieve appropriate systemic exposure similar to standard mono-therapy doses (§ 1.6.6.1). The initial dosage of EFV should be restored once treatment with voriconazole has ceased [49-51]. Co-administration of EFV and rifampicin in patients weighing > 50 kg may require an increase in the dose of EFV to 800 mg daily (§ 1.6.6.1) so as to achieve systemic exposure similar to a 600 mg EFV dose in these patients [49,52].

1.6.3.4 Overdose

Overdose with EFV has been observed in patients accidentally taking 600 mg twice daily, resulting in an increased prevalence of CNS symptoms [49,53,54]. Treatment of overdose should include general supportive measures such as monitoring vital signs and administration of activated charcoal so as to adsorb EFV from the GIT. EFV is highly protein bound and it is highly unlikely that dialysis would remove significant amounts of EFV from the blood [49].

1.6.4 Contraindications

EFV should be avoided in patients with known clinically significant hypersensitivity to EFV, e.g Stevens-Johnson syndrome or toxic skin eruptions or any of the excipients used in the formulations [14,49]. EFV is also contradicted in patients with severe hepatic disease and is not recommended in patients with moderate liver function due to the lack of sufficient data to determine whether dose adjustments are required. EFV should be used with caution in such patients and liver tests should be performed on a regular basis in patients with mild liver disease [14,17,42].

1.6.5 Precautions or Use in Special Patient Populations

1.6.5.1 Geriatric Patients

The pharmacokinetic aspects of EFV have not been studied in patients over the age of 65. Geriatric patients are more likely to present with hepatic conditions and EFV should therefore be

used with caution in elderly patients and regular monitoring of liver function is appropriate if EFV is the drug of choice in such patients [42,55].

1.6.5.2 Paediatric Patients

The safety of EFV in children under the age of 3 has not yet been established. The most common side effect in children is development of a rash. EFV should therefore not be given to children < 3 years of age or weighing < 13kg. In a study conducted in children, 46% of children treated with EFV developed a rash. Antihistamine prophylaxis has been suggested as prophylactic therapy when initiating EFV therapy on children [14,42,49]. However it should be noted that co-administration of the antihistamines terfenadine and astemizole with EFV is contraindicated (§ 1.6.6.3) and should therefore be avoided.

1.6.5.3 Breastfeeding Mothers

Excretion of EFV in human breast milk has not yet been investigated and is therefore unknown. Concentrations much higher than those in maternal plasma have been excreted in studies conducted in rat models, thereby indicating a possible risk to infants. HIV-positive lactating mothers should be advised not to breastfeed during EFV therapy so as to prevent any harm to the infant or transmission of HIV [49].

1.6.5.4 Pregnancy

Administration of EFV during the first trimester in pregnant patients leads to neural tube defects and should be avoided in these patients if alternative therapies are available. Pregnancy should therefore be discounted before commencing treatment with EFV. In women of child bearing age adequate contraception measures should be prescribed and used during EFV therapy and continued for 12 weeks following discontinuation of therapy as EFV has a long half-life [14,42,49,56].

1.6.5.5 Renal Impairment

Less than 1% EFV is excreted unchanged in urine and therefore there should be minimal impact on the pharmacokinetics in patients presenting with renal insufficiency [49].

1.6.5.6 Hepatic Impairment

EFV use is contraindicated in patients with severe hepatic impairment and not recommended in patients with moderate hepatic impairment (§ 1.5.3). EFV undergoes extensive cytochrome P450 (CYP P450)-mediated metabolism leading to elevated liver enzyme values during the first 6 weeks of treatment. Caution should be taken when administering EFV to patients with hepatic impairment and dose-related measurement of EFV levels and liver enzymes as well as monitoring of dose-related side effects are advised in this group of patients [49,57].

Patients with HIV co-infected with the hepatitis B (HBV) or hepatitis C (HCV) virus have an increased progression rate of cirrhosis and liver cancer by four-to five-fold compared to patients with hepatitis only. Clinical evidence has shown that antiretroviral therapy significantly reduces the rate of progression to cirrhosis and death in co-infected patients, suggesting that early initiation of treatment in these patients is beneficial. NNRTI have been shown to have a significant role in managing HBV or HCV co-infected patients with constant and vigilant monitoring of liver function. The data were insufficient to indicate whether EFV or NVP is the preferred treatment of choice in these patients [58-61].

1.6.6 Drug Interactions

1.6.6.1 EFV: A CYP 3A4 substrate

EFV is mainly metabolized in the liver by the CYP P450 isoenzymes CYP 3A4 and CYP 2B6 to form hydoxylated metabolites (§ 1.7.3) [62]. The concomitant use of EFV with substances that inhibit or induce CYP 3A4 or CYP 2B6 may lead to either increased or decreased plasma concentrations of EFV. The drugs, herbs and/or traditional medicines listed in Table 1.2 are known to interact with EFV.

Table 1.2: *Drug interactions resulting from EFV as a CYP 3A4 substrate*

Drug, herb and/or traditional medicine	Interaction effects during co-administration	Recommendations	Reference
Rifampicin	Induces CYP 3A4 and CYP 2B6 decreasing EFV plasma concentrations	Dose adjustments for patients weighing > 50 kg. Daily dose of 800 mg of EFV is suggested to provide similar exposure to 600 mg of EFV taken without rifampicin	[52,63]
St John's Wort (*Hypericum perforatum*)	EFV plasma levels are reduced due to enzyme induction or induction of drug-transporting proteins by the St John's Wort. The inducing effect of St John's Wort may last up to 2 weeks after stopping treatment		[49]
Voriconazole	Co-administration with EFV shows competitive inhibition of an oxidative metabolism process	The maintenance dose of the voriconazole must be increased to 400 mg twice daily and the dose of EFV reduced to 300 mg daily	[49,64]
Carbamazepine	Induces both CYP 3A4 and CYP 2B6 leading to decreased EFV levels. A two-way pharmacokinetic interaction is actually observed with concomitant administration of carbamazepine and EFV as the plasma levels of carbamazepine are also reduced due to self-induction and induction of CYP 3A4 by EFV		[49,65]

1.6.6.2 Induction of CYP 3A4

EFV is a potent inducer of CYP 3A4 *in vivo* and may induce CYP 2C9 in addition to CYP 2C19, leading to a clinically significant decrease in plasma concentrations of CYP 3A4-metabolized API that are co-administered with EFV [66,67]. A study on dose-dependent CYP 3A4 enzyme induction of EFV using the erythromycin breath test (ERMBT) showed that EFV significantly increased the mean ERMBT result in a dose-and time-dependent manner. Induction dissipation occurred 21 days after the last 400 mg dose of EFV due to its long half-life [68]. The metabolism of the compounds listed in Table 1.3 is altered differently by the inductive effects on CYP 3A4 by EFV.

Table 1.3: *Drug interactions of EFV resulting from induction of CYP 3A4*

Drug(s)	Interaction Effects during co-administration	Recommendations	Reference
Protease inhibitors (PI)	Plasma concentrations of PI such as amprenavir/fosamprenavir, atazanavir, darunavir, indinavir, lopinavir, and saquinavir are decreased	There is an increased risk of adverse effects from the concomitant use of EFV and ritonavir and liver enzyme levels should be monitored in patients on this therapy	[17,69]
Antimycobacterials e.g rifabutin	The plasma concentrations of antimycobacterials are reduced	An increase in rifabutin dose from 300 mg to 600 mg was found necessary to compensate for the reduced rifabutin plasma concentration	[70]
Hydroxymethylglutaryl coenzyme A (HMG-CoA) reductase inhibitors such as simvastastin, atorvastatin and pravastatin	EFV reduces the plasma concentrations of simvastastin, artorvastatin and pravastatin by 58%, 48% and 40%, respectively	EFV is associated with hyperlipidemia when co-administered with other ARV and therefore a reduction in inhibition of HMG-CoA reductase activity should be monitored and considered in patients on combination therapy	[71]
Antifungals such as ketoconazole and voriconazole	Co-administration of EFV and voriconazole leads to a significant decrease in the plasma concentration of voriconazole and a concurrent increase in EFV levels (§ 1.6.5.1). EFV was shown to significantly increase the metabolism of ketoconazole, leading to a reduction in the plasma concentration as well as the half-life of this antifungal agent. This could be attributed to the induction of CYP 3A4 by EFV since ketoconazole is metabolized by the CYP 3A4 isoenzyme system		[50,72]

Methadone	Is metabolized by CYP 3A4 and when co-administered with EFV leads to decreased methadone plasma concentrations	In patients on this regimen, signs of opiate withdrawal are seen to re-emerge and therefore the dose of methadone should be adjusted and increased by 22% so as to alleviate withdrawal symptoms	[73]
Carbamazepine (§ 1.6.6.1)			

1.6.6.3 Inhibition of CYP3A4

EFV is an inhibitor of some CYP 450 iso-enzymes including CYP 3A4. EFV must not be co-administered with terfenadine, astemizole, cisapride, midazolam, triazolam, pimozide, bepridil or the ergot alkaloids ergotamine and ergonovine [58,74]. These molecules compete with EFV for CYP 3A4, resulting in inhibition of metabolism and creating the potential for life-threatening adverse effects such as cardiac arrhythmias, prolonged sedation or respiratory depression [49,58].

1.6.7 Adverse Effects

The most common adverse effects of EFV are dermatological and neurological, and more than 50% of patients commencing EFV therapy experience neuropsychiatric adverse effects [49]. Mild to moderate rash that is typically maculopapular in nature usually appears within the first 14 days following the commencement of treatment and may resolve after one month if treatment is discontinued. Severe skin rashes such as those observed with Stevens-Johnson syndrome have been reported in less than 1% of patients treated with EFV [17,48]. The central nervous system (CNS) effects of EFV include dizziness, depression, insomnia, anxiety, headache, impaired concentration, abnormal dreams and agitation [17,48,75]. Severe CNS effects include suicidal ideation, severe depression, abnormal dreams, convulsions, depersonalization and hallucination. Some patients treated with EFV have committed suicide, but these patients generally have a history of mental illness. The effects evolve on initiation of therapy and resolve after 2-4 weeks of therapy. It is recommended that EFV be administered on an empty stomach so as to reduce plasma concentrations, thereby reducing the frequency of incidence of severe CNS effects [17,48,49,76]. Other adverse effects of EFV include diarrhea, nausea and an increase in serum cholesterol and triglyceride levels. A comparative study of the metabolic reactions of EFV and NVP revealed that switching a patient from EFV to NVP was associated with a significant reduction in low-density lipoprotein cholesterol levels, a risk factor in coronary heart disease after 52 weeks of therapy [17,48,77].

1.6.8 Efficacy

The efficacy of the therapeutic response to NRTI/NNRTI treatment regimens in HIV-1-infected African patients co-infected with either *Mycobacterium tuberculosis* or human herpes virus-8 was highly effective in eliminating the rapidly replicating (phase I) virus [78]. Superior virological, immunological and clinical outcomes were observed for EFV compared to NVP in large observational studies [79,80]. The efficacy of EFV has also been evaluated in a study comparing the use of three or four ARV in an HIV regimen [81]. There was no significant difference in this study, thereby supporting the current HIV guidelines recommending therapy with two NRTI and EFV when initiating treatment for HIV-1 infection [81,82].

1.6.9 Resistance

Despite high levels of treatment success mutations have been shown to develop in CYP 3A4 due to EFV although high levels of resistance to EFV are uncommon. The K 103 N substitution is an HIV-1 RT mutation frequently observed in patients not responding to HIV combination therapy. EFV is characterized by an improved resistance profile to most HIV-1 single mutations, including K 103 N [58,83]. However EFV has a long half-life as well as a low genetic barrier to resistance and stopping EFV treatment during combination therapy may lead to functional EFV monotherapy ultimately leading to the development of drug resistant HIV-1. The plasma half-life of EFV is prolonged in patients of the CYP 2B6 516 TT genotype, thereby increasing susceptibility to mutations conferring drug resistance [26,58,84]. Poor adherence to therapy also leads to fluctuation of plasma concentration of EFV that can ultimately result in resistance to EFV mutations [85].

1.7 CLINICAL PHARMACOKINETICS

1.7.1 Absorption

EFV is highly lipophilic and has poor aqueous solubility, thus EFV exhibits relatively low oral absorption and bioavailability (40–45%) and high inter-subject variability [86]. Peak EFV plasma concentrations are observed 5 hours after administration of a single dose in healthy

volunteers. Steady state plasma concentrations of EFV are usually achieved in 6-7 days. The bioavailability of EFV is increased by 17-22% if administered with food, and more specifically by 50% if taken with a high fat meal relative to fasted conditions. The pharmacokinetics of EFV are linear, with plasma concentrations increasing with increasing dose [14,58,87,88].

1.7.2 Distribution

EFV is lipophilic and is highly protein bound to albumin (~99.5-99.75%). It has a high affinity for human adipose tissue due to its lipophilic nature [87,89]. EFV has been found in cerebrospinal fluid in concentrations approximately three times higher than that of the non-protein bound fraction in plasma [86]. The concentrations of EFV in brain tissue have been reported to reach therapeutic concentrations from cerebral spine fluid (CSF)-EFV concentration studies [58,90]. The apparent volume of distribution (Vd) of EFV in a cohort study involving 235 HIV-infected patients was found to be approximately 252 L, implying that EFV is widely distributed in the body [86,88].

1.7.3 Metabolism

The metabolism of EFV is primarily catalyzed by the CYP 450 enzyme system to form hydoxylated metabolites which ultimately undergo glucuronidation, making them ineffective against HIV-1 [88,91,92]. EFV metabolites in humans are mainly excreted in urine with plasma mostly showing levels of unchanged EFV. The proposed metabolic pathway of EFV in humans showing eight metabolites (**M1**-**M8**) is shown in Figure 1.8 [93]. Patients homozygous for the G 516 T genotype of the CYP 2B6 isoenzyme tend to have increased plasma exposure of EFV leading to higher rates of CNS side effects. Gender and race are significant when considering EFV metabolism, with the G 516 T genotype being more significant in African Americans than in European Americans and EFV exposure was reported to be higher in women than in men [94,95].

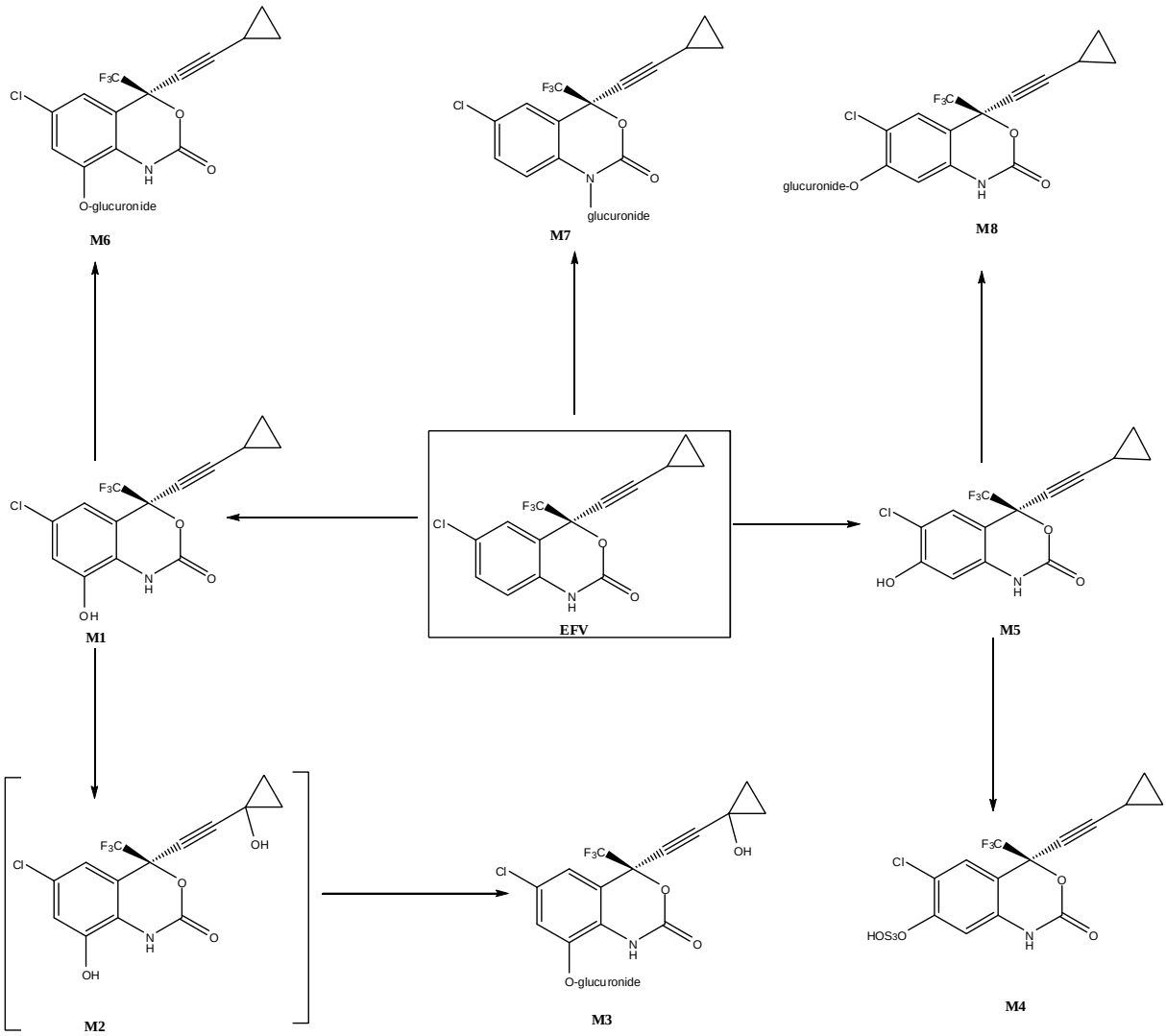

Figure 1.8: *Metabolic pathway of EFV in humans (adapted from [93])*

1.7.4 Elimination

The terminal elimination half-life of EFV is at least 52 hours following a single dose, and is 40-55 hours following multiple dosing as EFV induces its own metabolism. The half-life of EFV is reduced when EFV is taken in combination with didanosine and emtricitabine, however this combination has been shown to be well tolerated on long-term therapy [96,97]. The long half-life of EFV makes it suitable for once-daily dosing. EFV is excreted in the urine as metabolic products (§ 1.7.3) (14-34%) and as unchanged drug in the feces (16-41%) [48,58,68,93].

1.8 CONCLUSIONS

EFV is a NNRTI that has been an important addition for the treatment of HIV for 14 years and has significantly contributed to the emergence and evolution of HAART due to its efficacy and essentially once-a-day low dose requirement [58,98]. As EFV has a long half-life it can be administered as the once-daily dose, which may improve patient adherence to therapy.

Solutions of EFV are susceptible to photodegradation, thus requiring special packaging when formulating liquid dosage forms. An aqueous solution of EFV for the oral management of HIV in adult and/or paediatric patients is not readily available as EFV causes a strong burning sensation when dissolved in water [32,33,98].

EFV has a relatively high partition coefficient of 5.4 and is widely distributed in fat cells due to its lipophilic nature. The concentration of EFV in brain tissue has been reported to reach therapeutic concentrations from cerebral spine fluid (CSF)-EFV concentration studies [58,90]. However severe psychiatric effects such as severe depression and suicidal ideation have been reported in patients treated with EFV, leading to discontinuation of this potent, durable and relatively simple addition to HAART [99].

Clearly there is a need for a potential drug carrier for EFV that can mask the unpalatable taste, protect the API from photodegradation in solution, sustain release into brain tissue so as to reduce or limit the incidences of adverse psychiatric effects, and potentially alleviate AIDS-related complications such as ADC in patients with HIV/AIDS, ultimately improving their quality of life. Overcoming these challenges by formulating EFV into solid lipid nanoparticles and/or nanostructured lipid carriers was undertaken in an attempt to address these clinical needs. The data are reported in this thesis.

CHAPTER 2

SOLID LIPID NANOPARTICLES AND NANOSTRUCTURED LIPID CARRIERS

2.1 INTRODUCTION

2.1.1 Colloidal drug delivery systems

Over the last decade, the use of nanometric devices in medicine has emerged as an enlivening area of research that can be used to solve a number of challenges linked to inadequate therapeutic outcomes from so-called 'old drugs'. The discontent stems from inadequate biodistribution following administration, leading to inadequate therapeutic responses and side effects that affect healthy organs [100]. In an attempt to eliminate these problems, numerous approaches have been used to protect the API, by slowing degradation, optimization of targeting, reducing potential side effects and accumulation in healthy organs whilst also controlling release. The biodistribution of API molecules encapsulated in a nano-carrier that can act as vector can be used therapeutically by modification of the nanovector so as to alter therapeutic efficacy [100,101].

Pharmaceutically-relevant colloidal systems consisting of small molecules, with their sizes typically ranging between 10 nm and 1 µm, are being used to achieve different therapeutic outcomes. The carriers include technologies such as liposomes [102-106], nanoemulsions [107-111], nanocapsules [112-118], polymeric nanoparticles [119-123], solid lipid nanoparticles [124-130] and nanostructured lipid carriers [131-135]. The small size of these systems ensures an entirely different biodistribution from that of other relatively small molecules or carrier systems [136]. Schematic representations of the different families of colloidal systems used for drug delivery are shown in Figure 2.1.

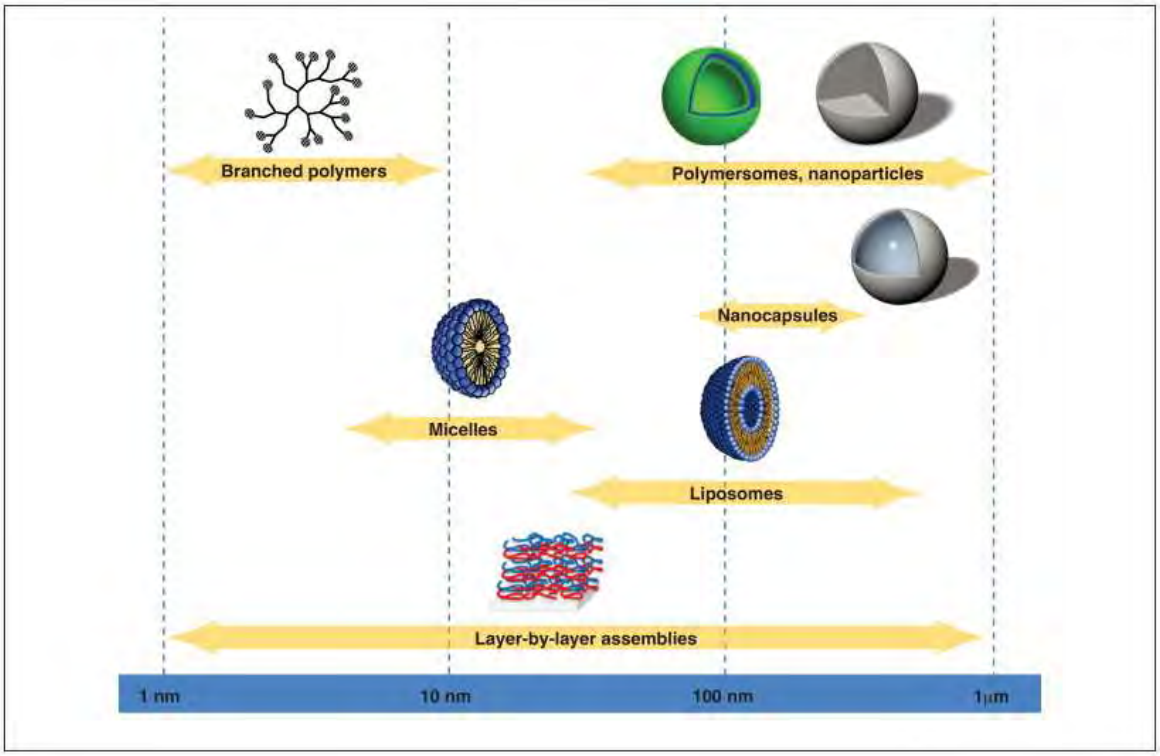

Figure 2.1: *Colloidal systems used for drug delivery (adapted from [100])*

The successful design of nanocarriers intended for particular applications requires careful consideration of various factors, including size and morphology that may have the potential to affect functionality. The mode of administration and intended therapeutic outcome may require the carrier system to have the ability to cross different biological barriers with different characteristics that must also be taken into account [137,138]. Furthermore, the materials used to manufacture carrier systems must be biocompatible and preferably biodegradable or easily eliminated following delivery of the API to the target organ [100]. Consequently, nanovectors have generally been manufactured using lipid-based compounds such as dipalmitoyl-phosphatidylcholine (DPPC) and polymeric materials such as natural polymers, e.g. proteins and biocompatible synthetic polymers such as poly (ε-caprolactone), poly (ethylene oxide) and poly (alkyl cyanoacrylate) [100]. The particle size of the carrier is a major factor determining the biological fate and the internalization process of the API-loaded particles [100]. The choice of upper limit of the size of nanoparticles is usually based on the intended target for the API carrier. For example, particles with a size < 400 nm are considered suitable when the intended therapeutic purpose is accumulation in cellular structures that are tumorous [100,139]. Particles

with sizes ranging between 10 and 100 nm have been shown to evade mechanical filtration through the spleen and liver, and therefore usually accumulate at intended targets within the human body [100,139].

The surface charge and chemistry of the particles have been shown to be vital in designing nanovectors. Positively charged polymeric nanoparticles may interact with negatively charged components of the cell membrane in an electrostatic manner, the consequence of which is internalization of the particles by the cell through a clathrin-mediated endocytosis mechanism [140]. In addition, caveolae-mediated endocytotic pathways could be essential when targeting monocytes or macrophages after successful internalization of negatively charged polymeric nanoparticles and liposomes has taken place [141-143]. Neutral poly (ethylene glycol) or (PEG)-ylated particles are able to avoid uptake by the macrophage system and play a major role in facilitating opening of tight junctions of the blood brain barrier (BBB), which permits adequate delivery of API to the brain [144,145].

Currently used nanovectors can be categorized into three main generations, as shown in Figure 2.2.

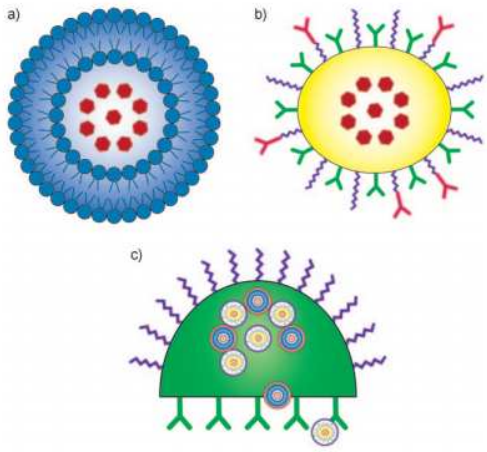

Figure 2.2: *Schematic representation of first generation (a), second generation (b) and third generation (c) nanovectors (adapted from [152])*

The first generation of nanovectors such as liposomes were produced using self-assembling lipids or polymers to achieve aggregated systems [100]. Liposomes have been used to encapsulate hydrophobic and hydrophilic molecules [100,146]. However, the major drawbacks to the use of liposomes are their limited stability when stored over an extended period of time, poor batch-to-batch reproducibility and low drug loading capacity [100]. In addition, these systems are prone to acid-catalyzed or enzymatic degradation in the gastrointestinal tract (GIT) and are difficult to sterilize [100]. Consequently, there has been limited success in attempting to develop liposomal-based pharmaceutical products for oral drug administration [100,147]. However, the incorporation of API such as tamoxifen into lipid bilayers has been shown to impart stability to the liposomes due to the cholesterol-like structure of tamoxifen [148,149]. Freeze drying has also been shown to retain the chemical integrity of lipids and the key physicochemical properties, *viz.* particle size, zeta potential and dynamic viscosity of liposomes [150]. In addition, liposomes of varying antigen loading have been prepared by design [151].

The second generation of nanovectors has specific functionalities which assist in molecular recognition for target tissue and/or the activation of release of API incorporated into systems at the target site, such as antibody-functionalized liposomes and nanoparticles [152,153]. The nanovectors in this generation include responsive systems such as pH-sensitive polymers and enzyme-activated polymers [152]. However, it should be acknowledged that molecular recognition between a vector and target organ plays only a minor role compared to that played by biological membrane barriers that the vector must overcome to achieve efficient delivery of API to the target site and elicit a therapeutic effect [152]. Third generation nanovectors were therefore developed with the primary aim of circumventing the biological barriers to drug delivery.

This family of nanovectors includes nanoparticles that are manufactured using polymers, e.g. nanospheres [126], and those prepared using solid lipids, e.g. solid lipid nanoparticles (SLN) [126] or a combination of solid and liquid lipids, *viz.* nanostructured lipid carriers (NLC) [126,152]. These systems have the ability to perform more complex functions, such as controlled

delivery of API across different biological membrane barriers and consequently to intended target organs [152].

A number of different API have been incorporated into SLN and NLC for oral [154,155], parenteral [156,157], and cosmetic or dermatological use [158,159]. Muller *et al.*, [158] and Garud *et al.,* [160] have reported a broad list of API molecules that have been incorporated into SLN and NLC using different manufacturing approaches [127,160]. EFV has been incorporated into SLN using the solvent emulsification and evaporation technique [98]. However, use of the toxic organic solvent chloroform [161] makes these SLN unsuitable for human use. Therefore a major objective of this research was to develop and characterize EFV-loaded SLN and NLC using hot high-pressure homogenization with the primary aim of controlling the rate of EFV release to the CNS in order to minimize psychiatric side effects associated with the use of this molecule.

2.2 DESCRIPTIONS OF SLN AND NLC

2.2.1 SLN

SLN were developed and introduced at the beginning of the 1990s as a substitute colloidal carrier system for controlled drug delivery [162]. SLN are usually manufactured using lipids that are solid at room and body temperatures, and are stabilized using one or more surfactant(s) [163]. The lipids used can be highly purified triglycerides, mixtures of complex glyceride or waxes [163]. The small nature of these particles (10 nm-1 µm), and the fact that they consist of biodegradable materials makes these carriers superior to previous colloidal systems [164,165]. Due to the lipid based nature of SLN, their popularity has developed rapidly due to biocompatibility and biodegradability, formulation flexibility and the ability to use well-characterized generally regarded as safe (GRAS) excipients. In addition, the possibility of controlled drug release and targeting, increased stability, increased loading capacity, avoidance of organic solvent use and limited issues with scale-up production and sterilization has also

facilitated their use [126,166]. SLN have been manipulated to combine the advantages of using other colloidal systems whilst avoiding associated disadvantages of those technologies.

2.2.1.1 Morphology of SLN

The morphology of SLN is dependent on the method used for incorporation of API into the nanoparticles [158,166]. The incorporation of an API into SLN is reliant on a number of factors, including the solubility of the API in the lipid, miscibility of the API and lipid melt, physicochemical properties of solid lipid matrix and the API, and the method of manufacture [127]. Consequently, three different models of drug incorporation into SLN have been described [158,166] and are schematically summarized in Figure 2.3.

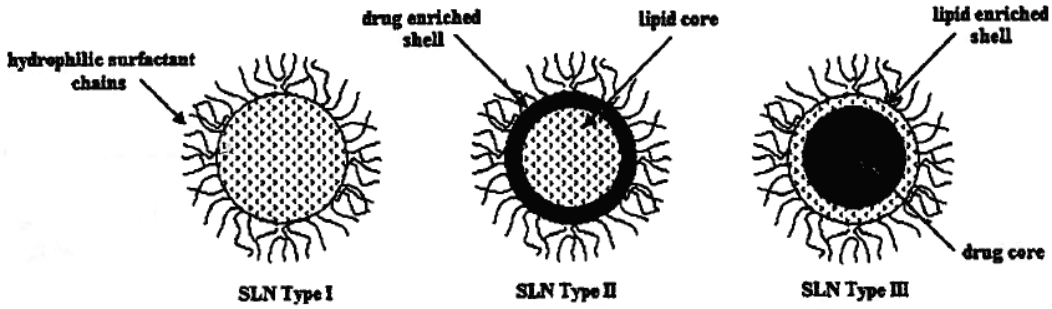

Figure 2.3: *Structure of SLN (adapted from [166])*

SLN type I, or the homogenous matrix type, consists of API that has been molecularly dispersed within the lipid core or amorphous clusters of API that become homogenously dispersed in the lipid core [166]. This model can exhibit controlled drug release properties [166]. The manufacture of a homogenous matrix SLN can be achieved using either hot (HPH) or cold (HPH) high-pressure homogenization [127,158,166].

Type II SLN or the drug-enriched shell model is produced when the lipid is allowed to recrystallize prior to the addition of API during the cooling stages of the manufacturing process, leading to phase separation [127,166,167]. This occurs when the API concentration in the lipid

melt is low, and the production process used is hot HPH (HHPH). Briefly, following high-pressure homogenization, the nano-emulsion is allowed to cool and the lipid begins to precipitate, leading to a gradual increase in the concentration of API in the remaining molten lipid as the solidified lipid fraction increases [166]. Ultimately this leads to the formation of an API-free or reduced lipid core as the API achieves saturation solubility in the remaining molten melt, which then forms an outer core containing both the API and the lipid [127,166]. Since the drug is mainly located at the surface of the lipid carrier, the model cannot be used to control the release of API incorporated into the lipid, although burst release can be achieved due to the occlusive nature of the lipid core [166].

In contrast to the drug-enriched shell model, SLN type III, or the drug-enriched core model, occurs when the API precipitates prior to lipid recrystallization, leading to the formation of a lipid shell containing less drug [127,166-168]. This state occurs when the concentration of API in the formulation is close to or at saturation solubility in the molten lipid [127,166]. As the nano-emulsion is cooled, the solubility of the API decreases and it precipitates when saturation solubility is exceeded. The precipitated API is therefore enclosed in a lipid shell and as a result the model can be used to prolong the release of incorporated API [166].

2.2.2 NLC

The major drawbacks of SLN such as API leakage during storage, insufficient drug loading and the high water content of SLN dispersions led to the development of NLC [158,162,168,169]. API expulsion in SLN has been attributed to polymorphic transitions of solid lipids [170]. Polymorphism is the ability of a compound to crystallize into more than one discrete crystalline type, and these exhibit diverse interior lattice structures [166,171]. Lipid molecules exhibit polymorphism and can therefore transition into consecutive crystalline forms without any alterations in their internal structure [171]. Pure lipids exist as low energy and highly ordered crystalline compounds which present as the β-polymorphic form [172]. When the lipids are melted during production of SLN, they may recrystallize into high energy and less ordered α-

and/or *β*' polymorphic forms [163]. Due to the amorphous nature of these transitional compounds, they allow for incorporation of API which is retained in the lipid matrix. During prolonged storage, the lipid matrix of SLN undergo reversal of polymorphic modifications leading to a reduction in the amorphous regions of the matrix owing to α- and/or *β*' transition to the stable *β* form [127,158,166,170], ultimately leading to API expulsion from the SLN.

NLC have similar physicochemical properties to SLN, however, they have been developed by nano-structuring of the architecture of the lipid matrix in order to increase API loading in addition to preventing drug leakage during storage, thereby resulting in greater flexibility for targeting specific API release profiles [162,166]. The structural matrix of NLC is derived from a mixture of solid and liquid lipids that are mixed in specific combinations, resulting in a less ordered lipid matrix with numerous imperfections that can accommodate a greater amount of API. NLC particles therefore solidify on cooling but do not recrystallize and remain in the amorphous state [158,166,168,170]. API expulsion on prolonged storage is less likely to occur from NLC as compared to SLN due to the differences in architecture of the lipid matrices, as shown in Figure 2.4.

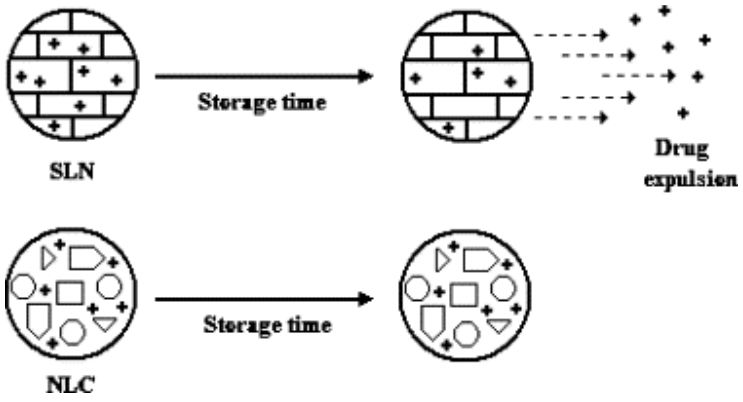

Figure 2.4: *Formation of the perfect lipid crystal in SLN and a crystal lattice with many imperfections in NLC (adapted from [168])*

2.2.2.1 Morphology of NLC

Similar to SLN, three main morphological types of NLC have been described and are shown in Figure 2.5.

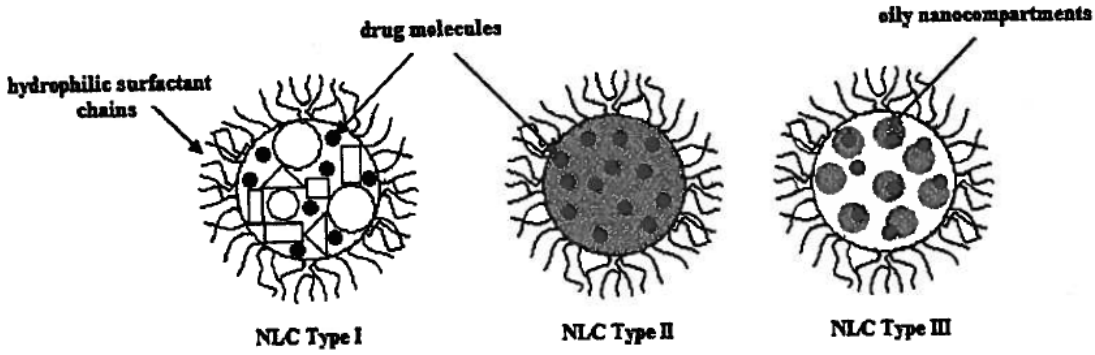

Figure 2.5: *Structure of different types of NLC (adapted from [166])*

Type I NLC, or the imperfect type of NLC, consists of a lipid matrix with numerous imperfections that are able to accommodate API molecules. This model is obtained by mixing solid lipids with sufficient liquid lipid(s) to avoid the formation of a highly ordered structure on cooling. The voids created in the structure that accommodate the API molecules are formed as a result of different chain length fatty acids and mixtures of mono-, di-, and tri-acylglycerols [158,166,173].

Type II NLC, or the amorphous type, are obtained by mixing lipids such as hydroxyoctacosanyl hydroxystearate, isopropyl myristate, or dibutyl adipate that fail to recrystallize following homogenization and cooling of nano-emulsions. These lipids are therefore able to form amorphous NLC that prevent recrystallization of the lipid matrix following cooling, thereby allowing the retention of API within the lipid structure whilst minimizing API expulsion on storage [158,166].

Type III NLC are multiple model systems comparable to multiple emulsions such as w/o/w emulsions. These systems are comprised of minute nano-compartments within the solid-lipid matrix that are formed as a result of phase separation [158,166]. These systems are obtained by mixing solid and liquid lipids such as, for example, medium-chain or long-chain triacyl glycerols

and oleic acid in a ratio such that the amount of liquid lipid is greater than that of the solid lipid [158,162,166,174]. At high temperatures, the molten solid lipid and the liquid lipid are miscible. However, on cooling (40°C) of the nano-emulsion, the solubility of the liquid lipid in the solid lipid is exceeded, i.e. a miscibility gap is achieved and phase separation occurs. This leads to precipitation of the liquid lipid and the formation of tiny droplets in the molten solid lipid. Subsequent solidification of the solid lipid leads to concentration of oily nano-compartments [158,166]. This model has been shown to permit an increased loading capacity for API that have a higher solubility in liquid lipids than in solid lipids [175].

2.3 FORMULATION OF SLN AND NLC

SLN are usually used as aqueous dispersions and are produced using a solid lipid, an API and surfactant(s), which impart stability to the system [126]. NLC differ from SLN only from an excipients point of view, in that binary mixtures of solid and liquid lipids are used during the formulation process [176]. The preparation of SLN or NLC formulations involves melting of a solid lipid or a binary mixture of solid and liquid lipid, followed by redispersion of molten lipids as submicron-size droplets in an aqueous medium containing surfactant(s) [176]. Different mechanical and thermal approaches exist for the production of aqueous dispersions of SLN and NLC [126,163,177]. Acute and or chronic toxicity during *in vivo* use has been associated with carriers of traditional colloidal systems, including polymeric-based systems [170]. Thus, a prerequisite for manufacture is that only pharmaceutical grade excipients with GRAS status are used for the production of SLN and NLC [163,170,177]. Mehnert and Mäder [126], in addition to Souto and Müller [178], have reported broad lists of lipids and surfactants that have been used for the manufacture of SLN and NLC.

2.4 PRODUCTION APPROACHES FOR THE MANUFACTURE OF SLN AND NLC

Different production methods have been used for the production of SLN and NLC [166]. The choice of a suitable production method depends on factors such as particle size requirements, thermal and chemical stability of the API, reproducibility of the release profiles, physicochemical stability of the colloidal system, and residual toxicity that may be imparted to the final product [166]. In certain instances, the possibility of scaling up may also be considered essential as this is usually a pre-requisite for the introduction of a drug product to the market [163].

The different methods that have been developed and used in production of SLN and NLC include high-pressure homogenization (HPH) [179-182], microemulsion [183-185], high shear homogenization and ultrasound [179,186,187], solvent emulsification [188-190], and phase inversion [191,192], among several others or modifications of these techniques [166]. In comparison to all other production techniques, HPH has been broadly applied in a variety of research fields, and is also a well-established technology used for the production of pharmaceutical formulations on a large scale [193,194]. HPH can therefore be also adapted for scale-up production of SLN and NLC [178]. HPH is a powerful and reliable production tool that avoids the use of toxic organic solvents during the manufacturing process, and has been used since the 1950s to produce nanoemulsions such as Intalipid® and Lipofundin® for use in parenteral nutrition [195]. The HPH production technique was selected for use in the production of SLN and NLC in these studies.

2.4.1 High-Pressure Homogenization (HPH)

The HPH technique can be performed either at elevated temperatures, i.e. hot HPH, or below room temperature, i.e. cold HPH technique [163]. The basic principle of high-pressure homogenizers is to force a liquid dispersion through a narrow gap using an elevated pressure of

between 100 and 2000 bar [126]. The liquid accelerates with high velocities of over 1000 km/hr over a very short distance, resulting in breakdown of the particles to submicron sizes by high shear stress and cavitation forces [126,163]. Before entering a narrow gap, the liquid dispersion is contained in a cylinder with a relatively large diameter in comparison to the width of the gap it will subsequently pass through [196]. The overall concept is explained by the Bernoulli equation [197] (Equation 2.1).

$$K = P_1 + \frac{1}{2}\rho V_1^2 \qquad \textbf{\textit{Equation 2.1}}$$

Where

K = constant
P_1 = static pressure
ρ = density
v = velocity
$\frac{1}{2}\rho V_1^2$ = dynamic pressure

According to the Bernoulli law, a reduction in diameter leads to a remarkable increase in dynamic pressure, with a simultaneous drop in static pressure when a liquid dispersion is in the narrow or homogenization gap. The static pressure in the gap drops below the dispersion vapor pressure, leading to boiling of the dispersion and the formation of gas bubbles which ultimately implode after leaving the gap as minute particles in a dispersion, as schematically shown in Figure 2.6 [196].

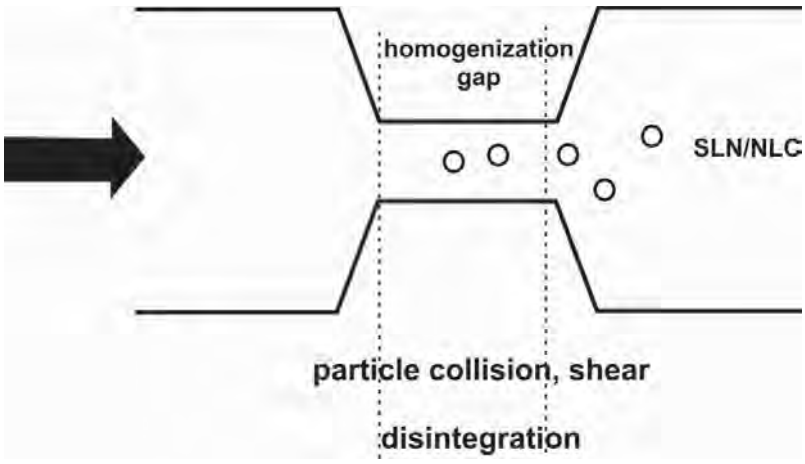

Figure 2.6: *Change of the diameter of the streaming dispersion in a piston-gap homogenizer from a cylinder containing bulk dispersion to a narrow homogenization gap (adapted from [196])*

The particle size distribution of SLN or NLC by HPH is dependent on power density and power distribution in the dispersion volume [166]. Application of a uniform power density allows for uniform power distribution, thus ensuring that all particles experience the same dispersing forces, resulting in uniform particle size distribution [166]. A high power density therefore leads to a narrow particle size distribution due to more effective particle disruption leading to an increase in the physical stability of the dispersion [166]. The power density is the amount of energy generated by the high-pressure homogenizer per unit volume over a specific period [178]. High-pressure homogenizers reach extremely high power densities, of up to 10^{12}-10^{13} W/m^3 [178].

Lipid concentrations in the range of 5-10% w/w are typically homogenized with ease using high-pressure homogenizers [126]. Lippacher *et al*., [198-201] have achieved homogenization of high lipid concentrations of up to 50% w/w to form lipid nanodispersions using HPH. In contrast to hot HPH, cold HPH is a suitable technique used for encapsulation of thermolabile or hydrophilic drugs, which tend to partition from a molten lipid into an aqueous phase, resulting in high API loss, with resulting low encapsulation efficiency [163,195]. EFV is highly hydrophobic (§ 1.2.4) and thermostable (§ 5.3.1.1) to temperatures as high as 90°C that may be used in hot HPH [126]. Consequently, hot HPH was considered a suitable method for use in the production of SLN and NLC in these studies.

2.4.1.1 Hot High-Pressure Homogenization

The hot HPH can be regarded as the homogenization of a solid lipid aqueous dispersion at a temperature above the melting point of the solid lipid or of a binary mixture of solid and liquid lipids [126]. The schematic procedure for the production of SLN and/or NLC is shown in Figure 2.7.

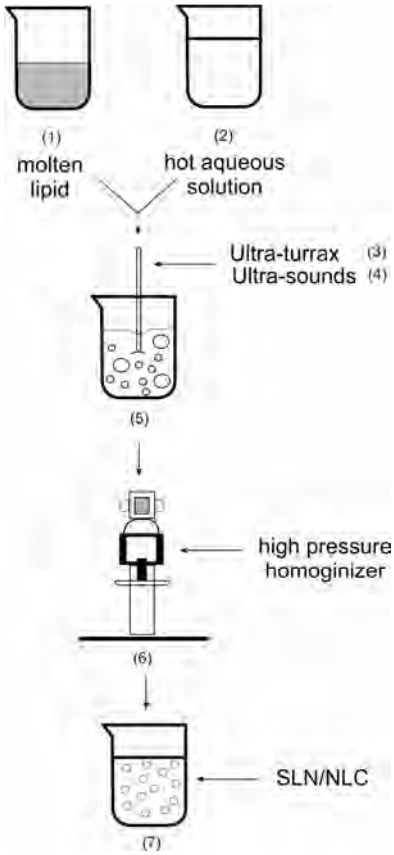

Figure 2.7: *Schematic representation of the production of SLN and/or NLC (adapted from [178])*

The solid lipid or binary mixture of solid and liquid lipids is melted at approximately 5-10°C above the melting point, and the API is dissolved or dispersed in the molten lipid [163]. The drug-containing molten lipid (1) is then dispersed in a hot aqueous surfactant solution (2) that should be maintained at the same temperature as the molten lipid phase. The dispersion of the lipid phase into the aqueous phase is achieved using high-speed stirring (3) [202] or ultrasound (4) [190,203]. The resultant hot pre-emulsion (5) is then homogenized by passing through a high -pressure homogenizer at a pressure ranging between 200 and 500 bar, using 3-5 homogenization cycles (6). The nano-emulsion obtained is cooled to room temperature, leading to recrystallization of the solid lipid and subsequent formation of SLN or NLC *in situ* (7) [178].

The use of very high homogenization pressures (> 1500 bar) and homogenization cycles (> 5 cycles) has been shown to result in increased particle size due to particle coalescence, which

results from high kinetic energy imparted to the particles [126]. In addition, the use of relatively high temperatures may lead to the degradation of an API or an API carrier [178]. Previous studies on the influence of homogenizer type, applied pressure, number of homogenization cycles and temperature on size and size distribution have been published [204,205], and these are important parameters that must be taken into account during the development and optimization of SLN or NLC formulations.

2.5 CHARACTERIZATION OF SLN AND NLC

Adequate characterization of SLN or NLC dispersions is essential to ensure that a quality product is produced. The characterization of these systems poses a serious challenge due to their colloidal size and complex nature, which includes dynamic phenomena such as hysteresis or super cooling [126,127]. Direct measurements of various critical quality attributes (CQA) of aqueous SLN or NLC in their undiluted form are not feasible using the majority of analytical tools currently available. Consequently there exists the possibility of introducing artefacts arising from sample preparation, such as, for example, induction of crystallization processes, lipid transition modifications and removal of surfactant from the surface of the particles [126]. Several parameters that have a direct impact on the stability and release kinetics of nanoparticles must also be considered. These include particle size and zeta potential, extent of crystallinity, lipid modifications, and co-existence of other colloidal structures (micelles, super cooled melts, drug nanoparticles) and dynamic phenomena [126,127].

2.5.1 Particle size and polydispersity index

Particle size (PS) has generally been used as a CQA for the characterization of colloidal systems when the composition, manufacturing technique, or process parameters are modified in an attempt to optimize formulations and/or manufacturing conditions [205-208]. Well formulated nanoparticles should have a narrow PS distribution [176,209]. Recent studies have shown that

factors affecting crystallization processes may have an influence on the mean particle diameter of SLN and NLC [210]. These factors include API composition [211], lipid composition [198,212], formulation and process factors [205,206], dispersion medium [213], lyophilization [207,208], and storage conditions [214]. PS measurements are therefore a useful indicator of the stability of aqueous dispersions of SLN or NLC, as any increase in the size of particles often occurs prior to visible macroscopic changes [176,210].

Bunjes *et al*., [215] concluded that the concentrations of surfactant and lipid significantly affect the particle size of lipid nanoparticles. They observed smaller particle sizes when higher surfactant and lipid ratios were used. Lippacher *et al*., [199] also found surfactant concentration to be inversely proportional to particle size on long-term storage. It has also been suggested that low processing temperatures lead to the formation of nanoparticles of large particle size [176]. In addition, the use of the cold HPH rather than the hot HPH technique produces larger particles, with the latter technique producing particles that are generally < 500 nm in size with a narrow PS distribution [176]. High homogenization pressures lead to an increase in the homogenization efficiency [216], for example, the mean PS and polydispersity index (PDI) have been reported to decrease when homogenization pressure is increased to 1500 bar using between 3-7 homogenization cycles [216]. Consequently, a combination of homogenization pressure and the number of homogenization cycles may be manipulated to obtain particles of the desired PS and PDI [216].

The process of lyophilization may be required to achieve long-term stability of nanoparticles [213]. This process increases the kinetic energy of particles, resulting in increased collisions, and therefore particle growth, with wider size distribution due to the presence of nanoparticle aggregates [213]. A suitable cryoprotectant can be introduced to protect the nanoparticles during the lyophilization process, thereby preventing particle growth [207,208,217].

API composition ultimately affects the amount of entrapped API in nanoparticles. Dingler *et al.*, [125] concluded that high drug entrapment leads to increased particle size, while API

concentrations of up to 1% do not result in a change in size when evaluated using both the photon correlation spectroscopy (PCS) and laser diffractometry (LD) measurements [176].

Movement of particles in the submicron size range is believed to occur in a random manner [126], the consequence of which is that various techniques used to determine the sizes of SLN and NLC are often based on random movements. Photon correlation spectroscopy (PCS) or dynamic light scattering (DLS) is the most frequently used technique in measuring the sizes of nanoparticles [126]. PCS operates on the principle of measuring scattered light intensity fluctuations resulting from particle movement, which in turn yields the mean diameter of the bulk population of the particles [210]. In addition, the PDI provides information pertaining to the width of the distribution of these particles. Monodisperse systems generally give a PDI value of 0, which increases to 0.500 for systems with a relatively broad particle size distribution [210,218]. The major drawback of using PCS is that the technique cannot accurately measure the size of particles that are larger than 3 µm in diameter [210]. However, since it is vital to keep the size of particles in a nanodispersion system within a submicron range, it is recommended that PCS be used in combination with other analytical tools, such as for example laser diffraction (LD), to facilitate the detection of relatively large particles [210]. LD determines the size of the particles by detecting the light diffracted from the surfaces of particles [210].

2.5.2 Imaging Analysis

Although PCS and LD are complementary analytical tools that can be used to determine PS and PDI of SLN and NLC, these techniques cannot provide information on the shape and surface morphology of nanoparticles. These parameters can be determined only by using microscopic tools such as transmission electron microscopy (TEM) and scanning electron microscopy (SEM) [126,219]. SEM operates by forming a focused beam of electrons that is scanned over the sample while the desired signal is unravelled to form a 3-dimensional image of the particle under investigation [220]. The preparation of samples for visualization with SEM under high vacuum requires pre-treatment of the SLN and/or NLC dispersions. The lipid dispersion is first

lyophilized for approximately 24 hours. The dried sample is then sputter coated with a conductive metal such as gold, for 15 minutes prior to imaging. The drying process of the lipid dispersion causes shrinkage, leading to a decreased mean particle diameter when using SEM, [220,221] and could therefore have an effect on the shape and surface morphology of the particles.

In contrast, TEM displays 2-dimensional images and usually has a higher resolution. Staining, freeze-fracturing and cryo-electron microscopy are techniques used in sample preparation for TEM analysis [222,223]. The choice of the most suitable technique is dependent on the type of data to be generated. For the purposes of size, shape and surface morphology of SLN and/or NLC, a staining sample preparation technique is adequate. The lipid dispersion is placed onto a carbon-coated copper grid and left to dry for 24 hours at room temperature (22°C) prior to staining with phosphotungstic acid for 30 seconds at room temperature, following which the sample is visualized using TEM [222,223].

2.5.3 Particle charge, zeta potential and electrophoretic mobility

It has been postulated that almost all particles in contact with a liquid will develop a surface charge [210]. The potential at the shear plane, which is an imaginary surface separating a thin layer of liquid bound to a solid surface in motion, is known as the zeta potential [210]. The electrophoretic mobility of a particle is defined as one of the electrokinetic phenomena of charged colloidal particles [224]. The prediction of stability of colloidal dispersions following storage is dependent on measurement of the zeta potential of the system [225]. The zeta potential therefore describes ion adsorption and electrostatic interactions between charged particles [176,225]. The Laser Doppler Anemometry (LDA) technique can be used to determine the electrophoretic mobility of particles in an aqueous dispersion, which in turn can be used to obtain the zeta potential according to Smoluchowski’s formula, as shown in Equation 2.2 below [210,224].

$$\gamma = \frac{\varepsilon_r \varepsilon_o}{\eta} \zeta \qquad \textit{Equation 2.2}$$

Where

γ = electrophoretic mobility
ε_r = relative permittivity
ε_o = permittivity of a vacuum
η = viscosity of surrounding fluid
ζ = zeta potential

Highly charged particles have high zeta potential values, and these particles tend to repel each other [176]. Particle aggregation is thus not an issue in these situations. Low values of the zeta potential have been associated with a reduction in the physical stability of colloidal dispersions [176]. However, this does not apply to colloidal systems containing steric stabilizers, as the presence of these stabilizers leads to a decrease in the zeta potential due to a shift in the shear plane of the particle [127]. For excellent physical stability, a minimum zeta potential of greater than ±60 mV is mandatory, and values greater than ±30 mV may impart good physical stability [210,226]. The zeta potential decreases with an increase in the energy of the system i.e. light and temperature due to increased particle kinetic energy, thus leading to particle aggregation and gelation [176].

2.5.4 Crystallization, polymorphism and compatibility

The assessment of CQA such as particle size is essential in characterizing SLN/NLC, however, they are not sufficient to fully characterize the quality of these colloidal systems. The characterization of degree of crystallization and polymorphic transitions of lipids should be taken into consideration as this is vital in determining the quality of SLN and NLC products and these aforementioned parameters play a major role with respect to API entrapment and release rates [126,127,176]. Differential Scanning Calorimetry (DSC), wide-angle X-ray diffraction scattering (WAXS) and high-resolution proton nuclear magnetic resonance (^{1}H NMR) may be used to characterize the state and thermodynamic behavior of solid lipids [126,176,227,228]. In addition,

Fourier Transform Infrared Spectroscopy (FT-IR) has been widely used to investigate drug-lipid interactions of bulk material as well as SLN and/or NLC [98].

DSC is usually used to elucidate the crystallization and melting behavior of lipid nanoparticles, and operates on the principle that modifications of different lipids will result in different melting points with different enthalpies [126]. The heating and cooling processes lead to a breakdown and/or fusion of the lattice and provide information about internal polymorphism, crystal ordering, presence of eutectic mixtures and/or glass transition processes [176]. Thermal events can thus be used to provide information on the purity, melting and crystallization behavior of the solid and liquid constituents of particles [126,176,227,228]. Two types of DSC systems have been reported, *viz*. power compensation and heat-flux or heat leak systems [229].

The power compensation system independently controls and monitors the temperature of reference and sample cells. Both cells are supplied with constant energy, resulting in a steady rate of increase in temperature. A thermally induced transition will therefore result in a temperature lag of the sample cell in comparison to the reference. The excess heat capacity is then calculated using the additional heat required to maintain the same temperature between the two cells [229,230]. With the heat-flux or heat leak system, a low resistance heating flow-path thermoelectric disk is used to connect both cells. The temperature-measuring device records differences in voltage and this is proportional to the temperature difference which is ultimately used to calculate heat capacity [229,230]. The melting enthalpy values obtained using DSC can be used to assess the degree of crystallinity in lipid nanoparticles using the recrystallization index (RI). The RI for SLN and NLC can be calculated using Equation 2.3 [231].

$$RI(\%) = \frac{\Delta H_{SLN\ or\ NLC\ dispersion}}{\Delta H_{bulk\ lipid} x Lipid\ conc} X\ 100 \qquad \textbf{\textit{Equation 2.3}}$$

Where

RI = Recrystallization Index
ΔH = Molar melting enthalpy

WAXS is used as a tool to distinguish different lipid polymorphs. WAXS assesses the length of the long and short spaces of a lipid lattice, and these differences in spacing are thus used to characterize the different polymorphic forms [126,176,232]. The major difference between WAXS and DSC is that WAXS is able to discriminate between crystalline and amorphous materials and assess the influence of the lipid constituents on the long spacings of lipid nanocrystals, whereas DSC can be manipulated to distinguish between amorphous solids and liquids [176]. The polymorphism behavior of the material as recognized by DSC can be confirmed by WAXS. WAXS can therefore be used in combination with DSC to elucidate the crystallinity and polymorphic nature of SLN and NLC [175,233].

^{1}H NMR spectroscopy is generally used to characterize liquid lipids inside solid lipid nanoparticles. The principle behind ^{1}H NMR is based on different proton relaxation times in liquid, semi-solid and/or solid states. Sharp signals with high amplitudes for protons are observed in the liquid state, whereas lipids in the semi-solid or solid state produce weak and broad signals [126,176].

The qualitative aspect of FT-IR works on the principle of different vibrational energies possessed by specific chemical bonds in a molecule. It can thus be used for fingerprint identification of a molecule, and is also able to reveal potential interactions at a molecular level as specific functional groups will show molecular vibrations at specific frequencies [234].

2.5.5 Drug loading capacity and encapsulation efficiency

An essential characterization parameter in determining the appropriateness of a novel drug carrier system is its loading capacity (LC) in addition to the long term stability of the system in ensuring the API remains entrapped [127,235]. The optimization of SLN and/or NLC-incorporated API is therefore considered in terms of the LC and the encapsulation efficiency (EE) [166]. The lipid core of the system should be able to shield incorporated API from degradation, and therefore the importance of ensuring high EE in addition to long term maintenance of the API in the lipid matrix is critical [163]. The LC and EE of SLN and/or NLC

are essential parameters in the production process as these can affect API release kinetics, particle size distribution, zeta potential and lipid modification [126]. The LC is defined as the ratio of the weight of incorporated API to the total weight of the lipid composition, and can be calculated using Equation 2.4 [127,166]. The EE is presented as the ratio between the weight of the incorporated drug and the total weight of the drug and similarly to the LC can be calculated using Equation 2.5 [166,168].

$$LC = \frac{W_a - W_s}{W_a - W_s + W_L} \; x \; 100 \qquad \textbf{\textit{Equation 2.4}}$$

$$EE = \frac{W_a - W_s}{W_a} \; x \; 100 \qquad \textbf{\textit{Equation 2.5}}$$

Where

W_a = weight of drug added to formulation
W_s = weight of drug analyzed in supernatant (after centrifugation)
W_L = weight of lipid added to the formulation

2.5.6 *In vitro* release studies

In-vitro dissolution studies have become vital for the characterization of dosage form performance in formulation and development studies [236]. It has been shown that the nature of API release profile from SLN and/or NLC is influenced by modification in the lipid matrix [163]. Three release mechanisms are possible from these colloidal systems, and include (i) release through diffusion from the surface of the particles, (ii) release through diffusion from the matrix, and (iii) release through erosion at the surface of the particle. In most instances, API release can be explained by more than one release mechanism. The API release mechanism is mostly dependent on the structure of the lipid system produced. For example, diffusion from the surface is observed with a burst release effect of API on contact with dissolution medium of an API-enriched shell model of SLN. However, diffusion-controlled release is observed from matrix models and API-enriched cores lead to the release of the API in a controlled manner (§ 2.2.1.1, Figure 2.3) [163].

Different dissolution apparatus and techniques have been used to study the *in-vitro* release of API from SLN and/or NLC. The most frequently used methods include the Franz diffusion cell [168,175,212,237,238] and the dialysis bag approach [98,239-241]. Bhardwaj *et al*., [242] categorized the *in vitro* release testing of colloidal systems into three groups, *viz*. (i) membrane dialysis that involves the use of dialysis sac, reverse dialysis sac, micro-dialysis or Franz-diffusion cells, (ii) the sample and separate methods that include the use of a vial/tube/bottle with centrifugation or filtration following sampling, and (iii) the use of flow-through cell methods or USP IV apparatus [242].

There is dearth in data published in which the suitability and therefore the use of dissolution apparatus for testing API release for SLN and/or NLC is confirmed [236]. Heng *et al*., [236] compared the applicability of four commonly used dissolution approaches, *viz*. paddle, rotating basket, dialysis and the flow-through cell for use as dissolution test methods for API release from nanoparticles. The experimental data obtained revealed that the flow-through cell was the most robust dissolution approach to study *in vitro* API release from nano-particulate systems [236]. Consequently, the flow-through apparatus was used to investigate the release of EFV from SLN or NLC during formulation development and optimization studies.

2.6 CONCLUSIONS

Over the years, colloidal drug delivery systems such as liposomes, nano-emulsions, nano-capsules and polymeric nanoparticles have been developed in order to eliminate the challenges or disadvantages associated with delivery of ‘old drugs’. However, these colloidal systems have advantages and disadvantages associated with their use. SLN and NLC are innovative solid lipid carriers developed as drug delivery systems that eliminate some of the disadvantages associated with colloidal drug delivery systems. SLN and NLC consist of a matrix of biocompatible lipid(s) that are solid at room and body temperatures and have a mean particle size ranging between 10 and 1 µm.

In comparison to other colloidal drug delivery systems such as liposomes and emulsions, SLN and NLC may protect an API, thereby slowing potential photodegradation and/or oxidation, optimize targeting, reduce potential side effects, reduce API accumulation in healthy organs and control API release *in vivo*. These delivery systems may also eliminate the problem of inadequate biodistribution [100,101]. SLN and NLC have been used as drug delivery systems through a number of routes of administration including topical [169], oral [240], parenteral [133], dermal [158], pulmonary [243], rectal [244] and ocular [245] routes.

The morphology of SLN and NLC is dependent on the method of API incorporation into the lipid matrix. Factors such as solubility of the API in the lipid(s), miscibility of the API with the molten lipid, physicochemical properties of the lipid matrix and API, polymorphic nature of the lipid material as well as the production method may affect incorporation of API into the lipid matrix. Three API incorporation models have been postulated for SLN and include a homogenous matrix, API-enriched shell and the API-enriched core models. NLC have similar physicochemical properties to SLN, however in contrast, they have an increased API loading capacity and prevent API leakage on prolonged storage. Similar to SLN, three main morphological types of NLC have been described, including the imperfect type, amorphous type and multiple model system. Several production methods have been used to produce SLN and NLC. Amongst these, HPH can be used for the scale-up manufacture and commercial production of SLN and/or NLC.

Different parameters are monitored when characterizing SLN and/or NLC. PS and PDI can be measured using photon correlation spectroscopy (PCS), or dynamic light scattering (DLS). PCS is usually used in combination with laser diffraction (LD) as a complementary tool. However, PCS and DLS fail to characterize SLN and/or NLC according to shape and surface morphology, therefore transmission electron microscopy (TEM) and scanning electron microscopy (SEM) are used to assess the shape and surface morphology of colloidal systems. The crystallization and polymorphic transitions of SLN and NLC can be investigated using DSC, WAXS and ^{1}H NMR, while FT-IR can be used to investigate API-lipid interactions of bulk material, SLN and /or NLC, and laser doppler anemometry (LDA) can be used to determine electrophoretic mobility

and ultimately the zeta potential of SLN and/or NLC. A validated RP-HPLC can be used to determine the LC, EE as well as the release rate of API during *in vitro* studies of SLN and NLC.

The encapsulation of EFV into SLN and/or NLC was achieved using hot high-pressure homogenization. The aforementioned techniques were used to characterize colloidal systems in terms of PS, PDI, ZP, shape, surface morphology, crystalline structure and polymorphic transitions, LC, EE and release rate of EFV-loaded SLN and/or NLC.

CHAPTER 3

DEVELOPMENT AND VALIDATION OF A RP-HPLC METHOD WITH UV DETECTION FOR THE ANALYSIS OF EFAVIRENZ

3.1 INTRODUCTION

The quantitative determination of EFV in pharmaceutical formulations and/or in biological fluids has been achieved using reversed-phase high performance liquid chromatography (RP-HPLC) [246-252], liquid chromatography with mass spectrometry (LC−MS) [253,254], gas chromatography with mass spectroscopy (GC-MS) [255], capillary electrophoresis (CE) [256], matrix-assisted laser desorption ionization source and tandem-of-flight (MALDI-TOF/TOF) [257] and spectrophotometric methods [258,259]. However RP-HPLC is considered the method of choice for the *in vitro* analysis of API, mainly due to the stable and reproducible nature of HPLC columns [260]. In addition the significantly large ratio of aqueous components used in the mobile phase, in addition to the ease of reproducing the analytical method in a variety of laboratory settings, makes RP-HPLC an ideal analytical method [248,260]. HPLC is the recommended compendial method for the analysis of EFV in pharmaceutical dosage forms [16]. However the method does not provide adequate sensitivity for the quantitative determination of EFV release from colloidal drug delivery systems such as SLN and NLC *in vitro*. Consequently the objective of these studies was to develop a simple, precise, accurate, selective and sensitive RP-HPLC method with ultraviolet (UV) detection for the quantitative analysis of EFV in SLN and NLC and *in vitro* release studies.

3.2 PRINCIPLES OF HPLC

Modern HPLC has been developed from older liquid chromatography (LC) theory combined with gas chromatography (GC) instrumentation [261]. The term LC refers to any procedure in which a liquid phase moves along a stationary phase [261]. This includes liquid-liquid, liquid-solid, ion-exchange, paper, thin layer in addition to size-exclusion chromatography [261,262]. In classical or modern LC such as HPLC, a mixture of compounds is separated on a column by use of a liquid or mobile phase due to the differences in affinity of a compound for the mobile and stationary phases, the latter of which could be solid, liquid, ion exchange or a porous polymer [263,264]. HPLC is more advanced than traditional LC in terms of speed and separation power, and is less dependent on the skill or technique of the analyst, resulting in greater accuracy, precision and improved reproducibility of an analytical method [263-265].

The concept and theory of HPLC has been applied to various fields of analysis and has found major application for the analysis of pharmaceutical dosage forms [266-268], in biochemical and biomedical research [269-272], cosmetic products [273-276], the food industry [277-279] and clinical applications [280-283]. In addition HPLC is used in the biotechnological, energy and environmental fields [284]. Chromatographic modes of separation are distinguished by differences in column packing materials, mobile phase composition and the nature of functional groups in an analyte. The specificity and selectivity of an analytical method is achieved by interaction of the functional groups of the analyte molecule(s) with the column packing material and/or mobile phase [284].

RP-HPLC is mostly used in the pharmaceutical environment and it is estimated that 80-90% of chromatographic separations use RP-HPLC [284]. In reversed-phase chromatography the use of a polar mobile phase and a non-polar stationary phase facilitates the separation. Most pharmaceutical compounds are water soluble, are generally polar in nature and are therefore ionizable, resulting in rapid elution of the compound from non-polar stationary phases [261,284,285].

Silica-based columns are normally used as non-polar stationary phases in RP-HPLC [284]. The phases comprise of C_3, C_4, C_8, C_{18} alkyl chains bonded to silica to produce non-polar backbones for use with mobile phases. The latter are buffered solutions containing an organic modifier such as methanol or acetonitrile to reduce the polarity of the mobile phase, therefore reducing the retention time of the solute [286]. The solutes pass through the column, are separated and are viewed as an electrical signal from a detector that is subsequently captured for analysis. [284]. Due to different affinities and interaction of solutes and the stationary and mobile phases, differential rates of migration are observed, leading to separation of the compounds [261,284,286].

The process of separation in RP-HPLC is a function of the differences in the equilibrium distribution (*K*) of solute molecules between the stationary and mobile phases, and can be calculated using Equation 3.1 [287].

$$K=\frac{C_s}{C_m} \qquad \textbf{\textit{Equation 3.1}}$$

Where

C_s = the concentration of the solute is the stationary phase
C_m = the concentration of the solute in the mobile phase

The solute molecules migrate only when they are distributed in a mobile phase, causing more polar compounds to elute faster than hydrophobic compounds, as the latter are attracted to the stationary phase [285]. Ultimately, differential migration in RP-HPLC will be influenced by experimental factors affecting the distribution of an analyte molecule into a particular phase *viz.* mobile and stationary phase compositions [265,285,288-290].

Interactions between a solute and the mobile phase have been shown to be significant in controlling the retention time of the solute molecule [290]. Karger *et al.*, [290] studied solvophobic interaction impact on the retention time of solutes, using a topological index called molecular connectivity to represent the surface area of the hydrophobic solute. It was suggested that molecular connectivity is proportional to the surface area of the cavity formed by the solute

[290]. When solvophobic interactions occur, non-polar compounds in aqueous media tend to cluster, form a non-polar cavity and interact with the stationary phase, resulting in longer retention times if they have a high molecular connectivity [290,291].

Stationary phases used in RP-HPLC differ in the nature of silica particles used, silane and the process used to bond the two components [291]. Mean-field statistical mechanics theory has been used to describe the retention time of molecules [287]. In this model, the retention factor (k') is used to explain the outcome of experimental procedures. The retention factor (k') can be calculated using Equation 3.2 [287].

$$k' = \Phi K \qquad \textbf{\textit{Equation 3.2}}$$

Where

Φ = the phase ratio of relative volumes of stationary to mobile phases
K = the equilibrium constant or the ratio of molar concentrations of solute in the stationary and mobile phases

Retention of a compound on a stationary phase may occur through adsorption of the solute to the end of stationary phase chains and/or via partitioning of the solute into the chain phase [292]. Mean-field statistical mechanics theory strongly suggests that the primary mechanism of retention of a solute in a stationary phase is partitioning of the solute between two phases [293]. It has been suggested that an increase in the surface density of stationary phase chains leads to an increase in partitioning, with a minimal effect on the adsorption process leading to shorter retention times [293]. Alkane stationary phases have therefore been shown to exhibit shorter retention times than grafted stationary phases [294]. Linear solvation energy relationships have revealed that partitioning in RP-HPLC at a molecular level is a function of three microscopic processes. These are the creation of a solute cavity in the stationary phase, the transfer of solute molecule from the mobile phase to the pre-formed cavity in the stationary phase, and sealing of the cavity created in the mobile phase [295].

Although partitioning has been considered the key mechanism of molecular retention, Reido *et al.,* [296] proposed an experimental interpretation explaining the theory of adsorption and its involvement in RP-HPLC molecular retention. A more realistic and generally well-accepted

proposal describes three different approaches that can be used to elucidate the mechanism of molecular separation or retention. These include the partitioning of an analyte between the stationary and mobile phases [292,297], the adsorption of the analyte onto the surface of the non-polar adsorbent [296,298], and the mobile phase organic modifier being preferentially adsorbed onto the surface of the adsorbent prior to partitioning of the analyte into the adsorbed layer [299].

The adsorption and partitioning processes are therefore fundamental parameters explaining how molecules are retained on a stationary phase. The retention of most compounds that are analyzed using PR-HPLC occurs as a result of a combination of several independent mechanisms [300]. In addition the molecular retention of different analytes, including acidic ionizable compounds such as EFV, is influenced by mechanisms that involve other factors such as temperature and flow rate [301,302], pressure, pH, ionic strength, mobile phase composition, nature of organic or ionic modifier and the nature of stationary phase packing materials [301-305].

Logarithmic and linear free energy model relationships have been used in an attempt to further clarify the theory of separation in RP-HPLC systems [306-310]. Various statistical relationships have been used to derive explanations for molecular retention mechanisms, and quantitative structure (reversed-phase)-retention relationships (QSRR) have been applied to explain structural factors affecting retention in addition to understanding the mechanism of separation and biological activity of compounds [311,312].

3.3 METHOD DEVELOPMENT

3.3.1 Background

The development of a RP-HPLC method is initiated by considering the nature of the sample to be analyzed i.e. the chemical composition, acidic or basic nature, impurities and any degradation products of the compound [313]. The chemistry of the compound is then matched to the best choice for initial HPLC conditions to be used. In contrast, proceeding directly to initial chromatographic conditions without consideration of the nature of the analyte of interest is

another approach [314-317]. In addition, the intended purpose of the HPLC method must be taken into account [313,318,319].

Traditionally HPLC methods are developed by changing individual chromatographic conditions while keeping others constant in order to achieve a desired response, e.g. sufficient peak resolution in a short analysis time. Method optimization is generally focused on mobile phase composition, i.e. the type and concentration of an organic modifier, mobile phase pH, column type and temperature [320,320,321]. However this approach of determining optimum operating conditions by changing a single parameter at a time while keeping the others constant does not provide information pertaining to potential interactive effects between the variables, the consequence of which is that it fails to depict the complete effect of parameters on the separation [322]. In addition the conventional approach is tedious and requires the performance of a vast number of experiments and is not cost effective [322,323].

Technological advances have now led to the development of analytical methods using experimental design with the aid of software such as Dry Lab® [324,325], Delfi-2® [326,327], Goldworks® [326,328], Mylog® [326], Nexpert Object® [326] and Response Surface Methodology (RSM) [323]. These systems speed up method development in respect to consistency, provision of critical parameters of a separation in addition to indicating potential challenges through identification of the robustness of the method [320,321,329]. Consequently these systems are used to overcome the limitations associated with the development of HPLC methods using a conventional approach.

3.3.2 Response Surface Methodology (RSM)

RSM encompasses a group of mathematical and statistical techniques applicable to the development of an appropriate functional relationship between a number of input variables (x_1, $x_{2,\ldots,}$ x_k) and an associated response (Y) that may take the form of a polynomial model as shown in Equation 3.3.

$$Y = \boldsymbol{f}'(x)\,\beta + \epsilon \qquad \textit{Equation 3.3}$$

Where

$x = (x_1, x_2 \ldots, x_k)$ are the input variables
$\boldsymbol{f}'(x)$ = a vector function of elements consisting of powers and cross- products of powers of $x_1, x_2 \ldots, x_k$ up to a certain degree d (≥ 1)
β = is a vector of unknown constant coefficients known as parameters
ϵ = a random experimental error observed in the response Y assumed to have a zero mean

The relationship described in Equation 3.3 holds provided $\boldsymbol{f}'(x)\,\beta$ represents a mean response (response surface) that has an expected value of Y. The response can be represented as 3-dimensional and/or contour plots so as to aid visualization of the shape of the response surface [330]. Two significant models commonly used in RSM include first degree (d=1) and second degree models (d=2), mathematically given in Equations 3.4 and 3.5 [330].

$$Y = \beta o + \sum_{i=1}^{k} \beta i x i + \varepsilon \qquad \textit{Equation 3.4}$$

Where

Y = response surface
βo and βi = constant coefficients
xi = coded independent factor
ε = experimental error

$$Y = \beta o + \sum_{i=1}^{k} \beta i x i + \sum\sum_{i<j} \beta i j x i x j + \sum_{i=1}^{k} \beta i i x_i^2 + \varepsilon \qquad \textit{Equation 3.5}$$

Where

βo ,βi ,βij = constant coefficients
xi and xj = coded independent factors
ε = experimental error

To apply RSM as an optimization approach, different stages are followed in the application of the design [331]. Initially independent variables likely to have a major effect on the system are

selected on the basis of the study objectives in addition to experience. The experimental design is then selected and the experiments are conducted according to the appropriate experimental matrix. The data are treated through fitting to polynomial functions, and the fitness of the model is subsequently evaluated. The final stages of analysis include verification of the possibility of initiating steps necessary to perform displacement in the direction of an optimal region and then generating the optimum values for each variable investigated.

The procedures adopted in these studies involved generating experimental data that could be explained by linear and polynomial functions, and therefore both models (Equations 3.4 and 3.5) were used. The polynomial model was used to describe the interaction between different experimental variables and was therefore able to determine the critical point according to the quadratic terms in Equation 3.5. To estimate the parameters in Equation 3.5 all variables in the design should be investigated at three factor levels. Common second-order symmetrical designs include three-level or 3^k factorial, Box-Behnken, Central Composite and Doehlert Designs [330-334].

In a factorial experiment the design variables are modified in combination and not individually. A 3^k factorial design is comprised of all combinations at levels of k, the control variable, at least at three levels each. Equally spaced levels can be coded to correspond to -1, 0 and 1. For a large number of variables the number of experiments increases exponentially (3^k) and this approach tends to become impractical. Typically a full factorial approach is used when five or fewer variables are to be investigated and a fractional approach of 3^k design cannot be considered as a mechanism to reduce the cost of running a large number of experiments [330].

The Box-Behnken Design provides for three levels of each factor under investigation and consists of a specific subset of factorial combinations from the 3^k factorial design. The three levels are coded -1, 0 and 1, and the number of experiments (N) required for a Box-Behnken Design is defined using Equation 3.6.

$$N = 2k\,(k-1) + Co \qquad \textbf{Equation 3.6}$$

Where

k = number of factors
Co = number of central points

The Box-Behnken Design may be rotatable but is generally not rotatable as a number of design arrangements for k were reported by Box and Behnken [330,332,335].

For the Doehlert Design the number of levels is not the same for all variables to be investigated, and the design can be built on itself and extended to other factor intervals. This approach permits the prediction of all main effects, all first order interactions and all quadratic effects without any interchangeable effects. The number of experiments (N) required for a Doehlert Design are defined using Equation 3.7 [336].

$$N = k + k^2 + 3 \qquad \textbf{Equation 3.7}$$

Where

k = number of factors

The Central Composite Design (CCD) is the most popular of second-order designs. CCD is a first-order 2^k design developed by the addition of center and axial points allowing for the adjustment of parameters of a second-order model. CCD is therefore a second-order design consisting of a complete $2k$ factorial design, or fraction thereof, with factor levels coded as 1, -1, an axial component consisting of $2k$ points at a distance α from the design center point and n_o center points [330]. The number of experiments (N) required for a CCD design is defined using Equation 3.8.

$$N=2^k+2k+n_o \qquad \textbf{\textit{Equation 3.8}}$$

Where

k = number of factors
n_o = number of center points

The number of experiments (N) of a CCD with three or more design variables is significantly smaller than that of a 3^k factorial design [330]. The symmetric graphs of CCD for two and three variables are shown in Figures 3.1 and 3.2, in which the CCD factor levels are marked in blue while the axial points are shown in green. The center points shown in red indicate replicate experiments of the CCD that enhance the precision of the model, thereby minimizing model error [334].

+/-α Level +/-1 Level Centre Point

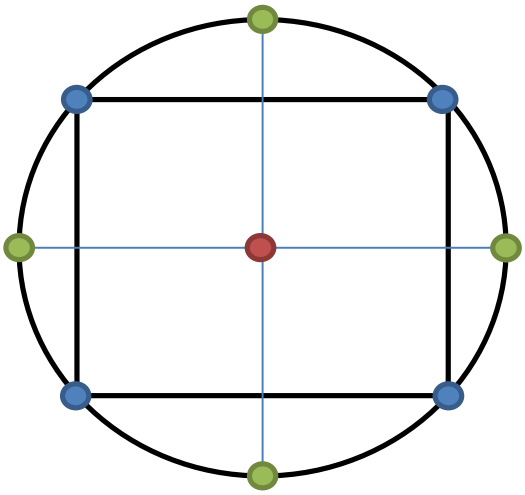

Figure 3.1: *Schematic representation for a CCD with two design variables (adapted from [334])*

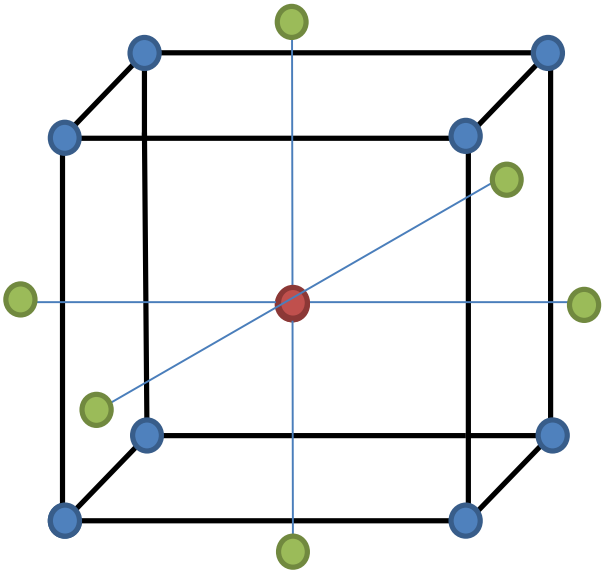

Figure 3.2: *Schematic representation for a CCD with three design variables (adapted from [334])*

If the CCD is rotatable all factors and axial points are the same distance from the center point, as shown in Figures 3.1 and 3.2. The rotatability of the design confers better statistical balance on the model, leading to equal precision for points equidistant from the center point [330,334].

The use of experimental design has been reported for the optimization of a number of HPLC methods, including the analysis of captopril [323], pramipexole [337] and variconazole in pharmaceutical formulations [338]. Furthermore CCD was used for the optimization of naloxene microemulsions for transdermal delivery [339] and in determining the purity of samples obtained from natural products [340]. Consequently a CCD was used to establish optimum operating chromatographic conditions for the analysis of EFV, *in vitro*.

3.3.3. Experimental

Prior to developing a method for the analysis of EFV using RSM, preliminary studies were undertaken on the basis of published data. A summary of methods using RP-HPLC with UV detection that have been published and used for the quantitative determination of EFV in pharmaceutical formulations and biological fluids is listed in Table 3.1.

The analysis of EFV in pharmaceutical dosage forms and biological samples has been achieved using silica-based columns, specifically C_{18} columns, microparticulate phenethyl (Zorbax® SB Phenyl) and cyanopropyl (Zorbax® SB-CN) bonded columns [341,342]. A binary mobile phase consisting of acetonitrile and phosphate buffer [32-34,250,343-347] is commonly used, but ternary mixtures consisting of methanol, ammonium acetate buffer, Tris buffer, formic acid and trifluoroacetic acid in combination with acetonitrile, water or both have also been used [34,247,248,348-351].

EFV is a weakly acidic drug (§ 1.2.4), and its analysis has been successfully performed using mobile phases buffered at pH $\leq$ 7.4 [32-34,247,343,344,346,348,349,351], although analysis

using unbuffered solutions has also been achieved [248,350]. The data contained in the published manuscripts were used to establish the preliminary RP-HPLC conditions for the development of an analytical method for the quantitation of EFV.

Table 3.1: *Summary of HPLC methods of analysis for EFV*

Column	Mobile Phase	Flow Rate	Detector	Retention Time	Reference
Spherisob® C_8,10µm, 250x4.6mm	60:40 % (v/v) acetonitrile :potassium dihydrogen phosphate, 25mM, pH=2.9	1.0mL/min	UV 220-390nm	7.7mins	[343]
C_{18} Inertsil® ODS 3V, 5µm, 250x4.6mm	(A): 0.02M sodium dihydrogen orthophosphate monohydrate (B): methanol :water (85:15)	1.5mL/min	UV 265nm	12.02mins	[344]
C_{18}, 5µm, 150x4.6mm	100mM ammonium acetate: acetonitrile (40:60) v/v	1.2mL/min	UV 246nm	3.0mins	[34]
Zorbax® RX C_{18},4.6x250mm, 5µm	50:50; ACN: 0.86% w/w ammonium dihydrogen phosphate, pH=3	1.5mL/min	UV 252nm	-	[32]
C_{18},250x4mm ,10µm	Acetonitrile: water: 85% H_3PO_4 (70:30:0.1)	1.0mL/min	UV 252nm	-	[345]
Thermo BDS hypersil C_{18}, 250x4.6mm, 5µm	Methanol: acetonitrile: 0.05M phosphate buffer (60:20:20) v/v/v ,pH=4.5	1.0mL/min	UV 254nm	4.25mins	[346]
Novapak® 150x 3.9µm	Monobasic potassium phosphate buffer and dibasic sodium phosphate buffer, pH=6. Buffer solution : acetonitrile 55:45 v/v.	1.0mL/min	UV 247nm	6.5mins	[33]
Hypersil® BDS C_{18}, 250x4.6 mm, 5 µm	Acetonitrile and 0.03 M KH_2PO_4 in water (pH =3.2 with orthophosphoric acid) in the ratio of 60:40 v/v	0.8 ml/min	UV 260 nm	10.55 mins	[347]
Zorbax® SB-CN, 150 mmx4.6 mm	(A): 90% water, with 0.05% trifluoroacetic acid: 10% methanol (B): 90% methanol:10% water, with 0.05% trifluoroacetic acid	1.5 ml/min	UV 250 nm	40 mins	[248]
Phenomenex® Luna C_{18} , 150 mm × 2.0 mm, 5 µm	0.1 M formic acid, acetonitrile and methanol (43:52:5)v/v/v, pH=2.2	0.3 ml/min	UV 247 nm	-	[349]
Zodiac® C_{18}, 250x4.6mm	Methanol: acetonitrile (80:20)	1.0ml/min	UV 280 nm	4.08 mins	[350]
Symmetry® C_{18} 250×4.6, 5µm	(A): Potassium phosphate buffer 50mM pH 5.65 (B): Acetonitrile	1.5 ml/min	UV 260 nm	27.2 mins	[250]
Waters C_{18}, 150mm×3.9mm, 4µm	(A): acetonitrile–10mM ammonium acetate buffer (0.1% acetic acid) (10/90, v/v), (B): acetonitrile–10mM ammonium acetate buffer (0.1% acetic acid) (90/10, v/v)	1mL/min	UV 280nm	8.7mins	[348]
Hypersil® C_{18} BDS 150x4.6 mm	Acetonitrile:20 mM Tris buffer (pH 7.4) (60:40 v/v)	1.2 mL/min	UV 248 nm	-	[247]
Agilent Zorbax® SB Phenyl, 150 mm x 4.6 mm , 5µm	Ammonium acetate (pH 4.75, 20 mM), acetonitrile and methanol (40:45:15, v/v/v)	0.8mL/min	UV 246nm	6.7mins	[351]

3.3.3.1 Chemicals and Reagents

All reagents were at least of analytical reagent grade. EFV was donated by Adcock Ingram® Limited (Johannesburg, Gauteng, South Africa) and the internal standard, loratidine (LRT) was donated by Aspen Pharmacare® (Port Elizabeth, Eastern Cape, South Africa). Stocrin® 600 mg tablets were purchased from a local pharmacy. HPLC-grade water was prepared by reverse osmosis using a Milli-RO® 15 water purification system (Millipore®, Bedford, MA, USA), consisting of a Super-C carbon cartridge, two Ion-X® ion-exchange cartridges and an Organex-Q® cartridge. The water was filtered through a 0.22 µm Millipak® stack filter (Millipore®, Bedford, MA, USA) and used to prepare all buffer solutions. HPLC far UV-grade acetonitrile (ACN) was purchased from Microsep® (Port Elizabeth, Eastern Cape, South Africa). Potassium dihydrogen orthophosphate, *o*-phosphoric acid (85% v/v) and sodium hydroxide pellets were purchased from Merck® Laboratories (Merck®, Wadeville, South Africa).

3.3.3.2 Instrumentation

The HPLC system consisted of a Waters® Alliance Model 2695 separation module equipped with a solvent delivery module, an autosampler, an online degasser and a Model 2996 Photodiode Array Detector (Waters®, Milford, MA, USA) set at a λ_{max} of 246.24 nm (§ 1.2.5). Data acquisition, processing and reporting were achieved using Waters® Empower 2 software (Waters®, Milford, MA, USA). The separation between the internal standard and EFV was achieved under isocratic conditions using a Nova-Pak® C_{18}, 4 µm (150 mm x 3.9 mm i.d) (Waters® Corporation, Milford, MA, USA) cartridge column with a mobile phase consisting of 31.5 mM phosphate buffer (pH 4.5) and acetonitrile in a 50:50 v/v ratio. The flow rate of the mobile phase and the injection volume were 1.0 mL/min and 20 µL respectively. The analytical column was maintained at 30°C using a temperature controller (Waters®, Milford, MA, USA).

3.3.3.3 Preparation of stock solutions and calibration standards

Standard stock solutions of EFV (100 µg/mL) and LRT (150 µg/mL) were prepared by accurately weighing approximately 10 mg and 15 mg of each API using a Model AE 163 Mettler® analytical balance (Mettler® Inc., Zurich, Switzerland), transferring into 100 ml A-grade volumetric flasks and diluting with a small volume of mobile phase. The stock solutions were sonicated using a Model B12 Branson® ultrasonic bath (Branson® Inc., Shelton, Conn, USA) until a clear solution was observed, after which the solutions were made to volume with mobile phase. Calibration standards of EFV over the concentration range 0.1-50 µg/mL were prepared by serial dilution of the standard stock solution on the day of analysis using mobile phase as the diluent. A concentration of 150 µg/mL LRT was added to all calibration standards and test samples prior to analysis. The stock solutions were protected from light using aluminum foil, stored in a refrigerator at 4°C and used within three days of preparation.

3.3.3.4 Preparation of buffer and mobile phase

Phosphate buffer solutions (31.5 mM) were prepared by accurately weighing 4.2868 g of potassium dihydrogen orthophosphate into a 1 L A-grade volumetric flask and making to volume with HPLC grade water. The pH of the buffers was monitored at 25°C using a Model GLP 21 Grison pH-meter (Crison Instruments, Barcelona, Spain) and was adjusted to 4.5 using *o*-phosphoric acid. The mobile phase was prepared by mixing specific volumes of the buffer and HPLC-grade acetonitrile using A-grade measuring cylinders and transferring into a 1 L Schott® Duran bottle (Schott Duran GmbH, Wertheim, Germany), mixing and degassing under vacuum with the aid of a Model A-2S Eyela Aspirator degasser (Rikakikai Co., Ltd, Tokyo, Japan) and filtering through a 0.45 µm HVLP Durapore® membrane filter (Millipore® Corporation, Bedford, MA, USA) prior to use.

3.3.3.5 Column Selection

The column packing for most RP-HPLC separations is produced using silica microspheres that are completely porous, with sizes ranging between 3 and 5 µm, and a single pore size distribution. API molecules are generally separated on columns with packing materials in the size range 80-100 Å [265,352].

Silica is the most popular packing material in HPLC columns as it has a combination of highly desirable characteristics [265,352], such as a silica surface that can be easily manipulated using covalent reactions and made into a variety of shapes and sizes with the desired pore size to produce columns suitable for different types of analytical procedures [316]. Further, silica is compatible with water and most organic solvents [352], and does not swell when the solvent is changed, the consequence of which is that variations in the dimensions of the column packing are minimal [316,352].

Silica is also a physically strong material and is superior to other packing materials for use as a RP-HPLC column backbone [316,352], permitting the formation of efficiently packed silica beads that are stable under high operating pressures and last for long periods of time [316,352].The strong particles also produce columns that operate with low back pressure [316,352], which assists in extending the lifespan of a column. Silica forms narrow pore size distributions without any “ink-bottle-like” pore structures, leading to reduced band broadening and faster separations for analysis. Extremely pure particles can be produced with almost a neutral pH surface [316,352].

Silica does however have a number of undesirable properties as a column support material. The most significant of these is the instability of silica and chemically modified silica at extreme pH [353]. Therefore the typical operating range of pH for silica-based columns is 2 to 8. The bonded organo-silane material undergoes decomposition and dissolution at low and high pH [353,354], increasing the ratio of free to bound silanol groups that results in shorter retention times for neutral and hydrophobic solutes [353-355]. Furthermore, the increase in the number of exposed silanols results in a reduction in peak asymmetry and peak width of organic cations [353-356].

Similarly the dissolution of silica is associated with column clogging, the consequence of which is a reduction in the longevity of the column [356].

The retention times and selectivity of ionizable compounds change significantly when pH modification or changes occur during analysis [357]. For instance the retention time of an unionized fraction is relatively longer than that of its ionized counterpart [357]. EFV is a weakly acidic molecule, and a medium with low pH was therefore selected for use in the mobile phase during the initial stages of the development process to ensure EFV was unionized and stability was maintained during analysis.

3.3.3.6 Column suitability testing

The performance of an analytical column is central to the efficiency of a separation of compounds of interest. Prior to method development and validation the suitability of the column [263,358] should be evaluated to ensure that the performance is adequate for the intended purpose.

3.3.3.6.1 Theoretical plate number

The column efficiency (*N*) is the relative ability of a column to provide narrow bands, and therefore improved separations, and is usually assessed by determination of the number of theoretical plates of the column, calculated using Equations 3.9 or 3.10 [264].

$$N=16\left(\frac{t_r}{w_b}\right)^2 \qquad \textit{Equation 3.9}$$

$$N=5.54\left(\frac{t_r}{w_{1/2}}\right)^2 \qquad \textit{Equation 3.10}$$

Where

N = number of theoretical plates of a column
t_r = the retention time of the probe molecule
w_b = the width of the peak at the baseline
$w_{½}$ = the width of the peak at one half the maximum height

The suitability of the column was evaluated using a test solution mixture of uracil, naphthalene, acetophenone, benzene and toluene in ACN. Separation was achieved using a mobile phase of ACN/H_2O (65/35) and was performed at ambient temperature (22°C) with an injection volume of 20 µL. The flow rate and detection wavelength were 1.0 mL/min and 254 nm respectively. A column may be considered suitable for routine HPLC analysis if a theoretical plate number is > 2000 [359]. The average theoretical plate number of the column was 7256 ± 0.176. Consequently on the basis of the value for *N* the column was considered suitable for use in the development and validation of a RP-HPLC method for the analysis EFV.

3.3.3.6.2 Resolution factor

The resolution (R_s) indicates the extent and quality of a separation between peaks of interest in a sample matrix. The resolution is a function of the column and operating conditions, instrumental effects or variable separation conditions, and can be used to assess the quality of separation between adjacent peaks [316]. The resolution factor (R_s) is calculated using Equation 3.11.

$$R_S = \frac{t_{2-}t_1}{0.5(w_{1+}w_2)}$$ ***Equation 3.11***

Where

R_s = peak resolution
t_2 = Retention time for second eluting peak
t_1 = Retention time for first eluting peak
W_1 = Width of first eluting peak at the base
W_2 = Width of second eluting peak at the base

On one hand, a baseline separation with *Rs* > 1.5 allows for the accurate integration and quantitation of individual peaks, whereas on the other hand values < 1.5 are indicative of poor peak resolution and are unacceptable for quantitative analyses [316,360]. The R_s between EFV and LRT was 1.81 (0.21% RSD), indicating that the peaks were well-resolved and the column was suitable for these studies.

3.3.3.6.3 Asymmetry factor

Peak asymmetry is a measure of peak tailing [316]. While the use of columns and experimental conditions that provide symmetrical peaks may be preferred, most chromatographic peaks are not perfectly symmetrical. Poor peak symmetry can result in inaccurate plate number and resolution measurement, imprecise quantitation, poor resolution and poor reproducibility of retention [316].The peak tailing factor (PTF) or the peak asymmetry factor (A_s) is used to estimate the degree of peak asymmetry, and is found using Equations 3.12 and 3.13 respectively [316,360].

$$PTF = \frac{A+B}{2A}$$ ***Equation 3.12***

$$A_S = \frac{B}{A}$$ ***Equation 3.13***

Where

PTF = peak tailing factor
A_s = peak asymmetry factor
A = Distance between the middle point and the left side of the peak
B = Distance between the middle point and the right side of the peak

The PTF and A_s value are measured at 5% and 10 % of the full peak height as depicted in Figure 3.3.

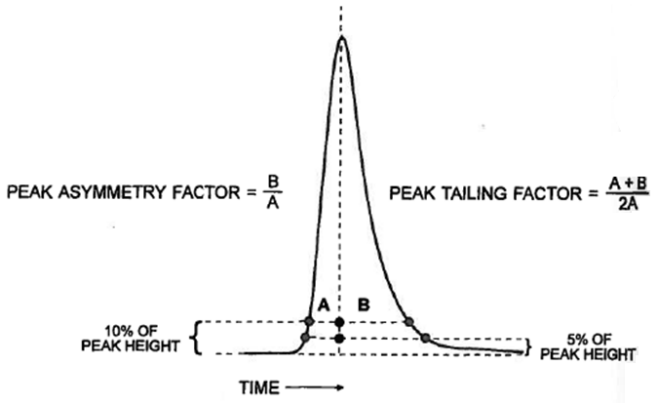

Figure 3.3: *Peak asymmetry and peak tailing factor determination (adapted from [316])*

Efficient columns produce A_s values ranging between 0.95 and 1.1. When the value of A_s is > 1.2 the apparent *N* value calculated using Equations 3.9 and 3.10 (§ 3.4.4.1) will be high, therefore A_s values > 1.2 are generally not appropriate [316]. The A_s values for EFV and LRT at 10% of the peak height were estimated to be between 1.0 and 1.1. The conversion of A_s to PTF resulted in values ranging between 1.0 and 1.1. Ideally the A_s value should be ≤ 2 according to FDA guidelines [316,359]. Therefore these data reveal that peak symmetry was acceptable and the column was deemed suitable for chromatography.

3.3.3.6.4 Capacity factor

The capacity factor or mass distribution (D_m) ratio is a measure of the retention of a solute in a column [361] and can be calculated from a chromatogram using Equation 3.14.

$$D_m = \left(\frac{t_r - t_m}{t_m}\right) \qquad \textit{Equation 3.14}$$

Where

D_m = Capacity factor (mass distribution ratio)
t_R = solute retention time
t_R = retention time of an unretained component

Low values for D_m are indicative of a peak that elutes close to the solvent front and may affect the selectivity of a method [361]. The minimum recommended D_m for a peak of interest is usually 1 [361]. The D_m value for EFV was 1.27 (0.14% RSD) using LRT as an un-retained compound and on this basis the column was appropriate for use.

3.3.3.7 Selection of Internal Standard

The addition of an internal standard (IS) to calibration standards and samples of unknown concentration is used as an approach to improve the performance of an analytical method by compensating for analytical error [316,316]. The internal standard is usually a compound of known purity that has physicochemical characteristics similar to those of the analyte of interest and can be separated without interference [359,362]. The IS permits compensation for changes in sample volume or concentrations that may be a consequence of instrumental variability [316,359,362,363].

The selection of an IS was based on evaluating compounds with a structure similar to EFV. Nevirapine, citalopram, amlodipine, imipramine, nitrazepam and loratidine were evaluated as potential IS candidates using a preliminary mobile phase consisting of 50 mM phosphate buffer

and acetonitrile (55:45) maintained at pH = 5. The data obtained are summarized in Table 3.2, and reveal that LRT was an ideal IS for this separation.

Table 3.2: *Selection of Internal Standard*

Internal Standard	Retention Time(minutes)	Comments
Nevirapine	1.6	Too close to solvent front
Citalopram	2.0	Too close to solvent front
Amlodipine	1.6	Too close to solvent front Presence of unknown second peak
Imipramine	4.8	Ideal to be considered as IS but peak tailing observed
Nitrazepam	2.0	Too close to solvent front
Loratidine	14.4	Ideal to be considered as IS

3.3.3.8 Method of detection

Ultra-violet (UV) has been used as a primary detection technique for the analysis of EFV and other antiretroviral agents [247,250,364]. Most organic compounds absorb light in the UV region (190-400 nm) and only a few in the visible region (400-750 nm) [284]. Furthermore most HPLC-grade solvents are generally transparent in the UV-vis region, which enhances the specificity of the method. However non-polar solutes lacking UV-absorbing chromophores would not be able to absorb light within this range and this is a major drawback to the use of UV-vis detectors. [284,365]. Nevertheless UV-vis detectors have the best combination of sensitivity, linearity, versatility and reliability of all the HPLC detectors developed to date [284,365]. UV-vis detectors are simple to use, are relatively inexpensive and easy to maintain [284,365]. The intensity of light transmitted through the detector cell is proportional to the solute concentration and can be predicted by Beer's law, as illustrated in Equation 3.15 [366].

$$I_T = I_o\, e^{-kLc} \qquad \textit{Equation 3.15}$$

Where

I_T = intensity of the transmitted light
I_o = intensity of light entering the cell
L = optical path length
c = solute concentration
k = constant

The λ_{max} of EFV was 246.24 nm (Figure 1.2, § 1.2.5). This wavelength was used for the quantitation of EFV in subsequent studies.

3.4 METHOD OPTIMIZATION

A computer-generated rotatable CCD design consisting of 20 experiments, 6 center points and 14 axial points was generated using Version 8.0.2 Design Expert® statistical software (Stat-Ease Inc., Minneapolis, MN, USA) and is summarized in Table 3.3. The experimental levels investigated are listed in Table 3.4. The minimum and maximum values for buffer molarity (X_1) were maintained at 30 mM and 50 mM, with the lower and upper axial points at 23 mM and 57 mM. Similarly pH 4 and pH 6 were the minimum and maximum values for buffer pH (X_2), with the lower and upper axial values maintained at pH 3.3 and pH 6.7. The ACN concentration (X_3) was kept at minimum and maximum values of 40% v/v and 50% v/v with respect to buffer concentration, with the lower and upper axial levels of 36.6% v/v and 53.4% v/v. The independent input variables and ranges were selected on the basis of preliminary studies, and the retention time (Y_1) of the last peak eluted, peak symmetry (Y_2) and peak resolution (Y_3) were the dependent output responses monitored. The data generated from the responses monitored were analyzed using Design Expert® version 8.0.2 statistical software (Stat-Ease Inc., Minneapolis, MN, USA). Fisher's test for Analysis of Variance (ANOVA) was used to establish whether significant differences existed between the mean of the factors investigated.

Table 3.3: *Randomized coded experimental runs for method optimization using CCD*

		Factor 1	Factor 2	Factor 3
Std	**Run**	**A:Buffer Molarity mM**	**B:Buffer pH**	**C:ACN con %**
4	1	1	1	-1
13	2	0	0	-1.682
14	3	0	0	1.682
8	4	1	1	1
17	5	0	0	0
11	6	0	-1.682	0
3	7	-1	1	-1
15	8	0	0	0
10	9	1.682	0	0
1	10	-1	-1	-1
6	11	1	-1	1
12	12	0	1.682	0
20	13	0	0	0
9	14	-1.682	0	0
16	15	0	0	0
18	16	0	0	0
5	17	-1	-1	1
7	18	-1	1	1
2	19	1	-1	-1
19	20	0	0	0

Table 3.4: *Actual design values used in CCD experiments*

Variable	**Level**			
	-α	**-1**	**1**	**+α**
X_1**(Buffer mM)**	23.18	30	50	56.82
X_2**(Buffer pH)**	3.32	4	6	6.68
X_3**(Organic solvent %)**	36.59	40	50	53.41

The overall design summary consisted of one linear and two 2FI models. The experiments were randomly performed to eliminate any possible experimental bias. The mathematical models used for the analysis of the four independent factors were developed, and optimization of the significant model variables was undertaken with the primary aim of obtaining the best response. The influence of three factors *viz*. buffer molarity, buffer pH and ACN concentration, in addition to their interactions on three critical quality attributes (CQA) of retention time, peak symmetry and peak resolution, were described using one-factor graphs and two-dimensional contour plots.

3.4.1 Retention time

The retention time (Y_1) is considered the most critical HPLC response to monitor as it is used to determine the run time of an analytical method. It should lie between 5-10 minutes in order for the method to be regarded as rapid [316].The concentration of ACN in the mobile phase was found to be the only significant factor affecting the retention time of EFV in these studies, and the impact of this variable is shown in Figure 3.4. A summary of ANOVA analysis of the linear model on retention time is listed in Table 3.5.

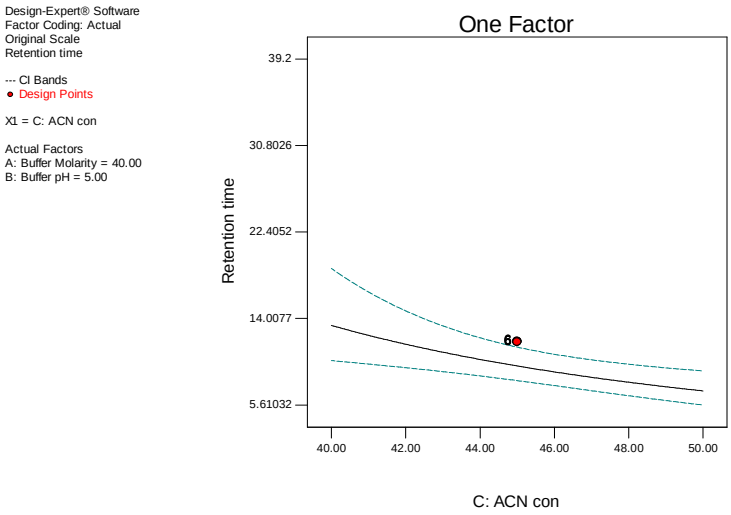

Figure 3.4: *The effect of ACN concentration on retention time*

The data shown in Figure 3.4 reveal that increasing the concentration of ACN from 40-50% v/v led to a decrease in the retention time of EFV, which is due to rapid elution of the analyte due to a change in polarity of the mobile phase. ACN has an intermediate dielectric constant, and an increase in the ACN concentration leads to a decrease in the polarity of the mobile phase [367] that leads to preferential partitioning of EFV into the mobile phase, and hence rapid elution as the drug is hydrophobic. Retention times of ≤ 10 minutes were observed with 45-50% v/v ACN content in the mobile phase. The final equation of Y_1 (retention time) is shown in Equation 3.16.

$$\frac{1}{\sqrt{Y_1}} = +0.33 + 0.052X_3 \qquad \textit{Equation 3.16}$$

The data summarized in Table 3.5 reveal that the Model F-value is 3.20, implying that the model is insignificant, with only a 5.17% probability that the Model F-Value could be a consequence of noise. In this case C (ACN concentration) is a significant model term as it has a p-value of 0.0071 which is < 0.05.

Table 3.5: ANOVA table for response surface linear model for retention time

Source	Sum of Squares	df	Mean Square	F Value	p-value Prob > F	
Model	0.038	3	0.013	3.20	0.0517	Not Significant
A-Buffer Molarity	2.067E-004	1	2.067E-004	0.053	0.8215	
B-Buffer pH	5.764E-005	1	5.764E-005	0.015	0.9051	
C-ACN conc	0.037	1	0.037	9.54	0.0071	Significant
Residual	0.063	16	3.927E-003			
Lack of fit	0.063	11	5.712E-003	19133.98	< 0.0001	Significant
Pure error	1.493E-006	5	2.985E-007			
Cor Total	0.10	19				
Std.Dev.	0.063	R^2	0.3751			
Mean	0.33	Adj R^2	0.2579			
C.V. %	19.21	Pred R^2	-0.1022			
PRESS	0.11	Adeq. Precision	6.285			

A Box-Cox plot is used when data transformation is required to increase the applicability and usefulness of an applied statistical test [368]. Box-Cox plots prior to and following transformation of the data are shown in Figure 3.5 and 3.6, respectively. The blue line reflects the current transformation. Inspection of the data shown in the Box-Cox plot reveals the need for data transformation using the inverse square root, since λ was not located within the confidence interval. Following data transformation, λ was located in the optimum region of the parabola, thereby confirming aqeduate data fit to the model. The red lines demarcate the 95% confidence interval and include -0.5 (blue line), indicating that the data are approximately in the optimum region of the parabola [369-371].

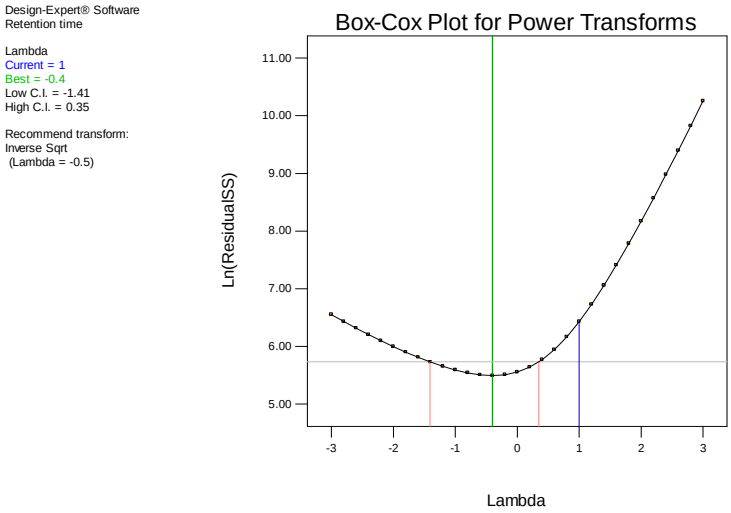

Figure 3.5: *Box–Cox plot for power transformation of retention time data for EFV*

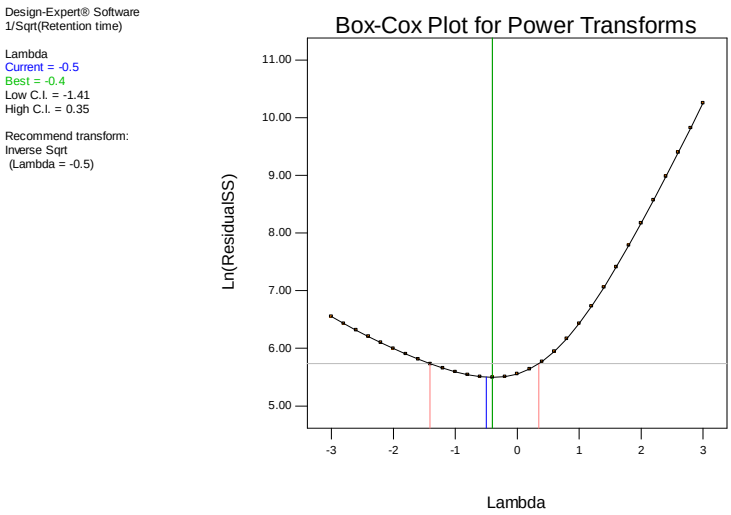

Figure 3.6: *Box–Cox plot for power transformation of 1/square root retention time data for EFV*

Due to a number of insignificant model terms, model reduction of the transformed data was performed using backward elimination to improve the model, as shown in Table 3.6. The backward method is considered the most robust for algorithmic model reduction since all model terms are considered for inclusion in the model [372]. Forward elimination and stepwise selection procedures commence with a minimal core model and therefore some terms are never included [372]. An "Adeq Precision" ratio of 9.408 (Table 3.6) was observed and is > 4, indicating that there is adequate signal for the model to be used in navigating the design space.

Table 3.6: *ANOVA for response surface reduced linear model*

Source	**Sum of Squares**	**df**	**Mean Square**	**F Value**	**p-value Prob > F**	
Model	0.037	1	0.037	10.68	0.0043	Significant
C-ACN conc	0.037	1	0.037	10.68	0.0043	Significant
Residual	0.063	18	3.506E-003			
Lack of fit	0.063	13	4.854E-003	16258.40	< 0.0001	Significant
Pure error	1.493E-006	5	2.985E-007			
Cor Total	0.10	19				
Std.Dev.	0.059	R^2	0.3725			
Mean	0.33	Adj R^2	0.3376			
C.V. %	18.15	Pred R^2	0.1980			
PRESS	0.081	Adeq Precision	9.408			

The normal probability plot of residuals for retention time is shown in Figure 3.7 and reveals that the data points generally fall on a straight line, suggesting that the model is adequate to navigate the design space. The normal distribution of errors shown in Figure 3.7 further confirms the suitability of the model for use in navigating the design space.

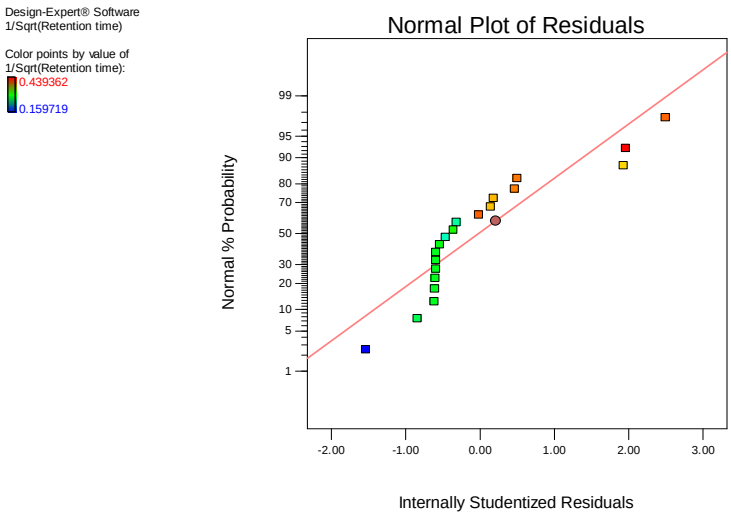

Figure 3.7: *Normal plot of residuals for retention time*

3.4.2 Peak asymmetry

ANOVA analysis reveals that the overall model for peak asymmetry (Y_2) was not significant (p = 0.0869). However ACN concentration had a significant effect (p = 0.0447) on the peak asymmetry of EFV. The combination of ACN concentration and buffer pH was also significant (p = 0.0124). The combined effect of ACN concentration and buffer pH on peak asymmetry is shown in Figure 3.8

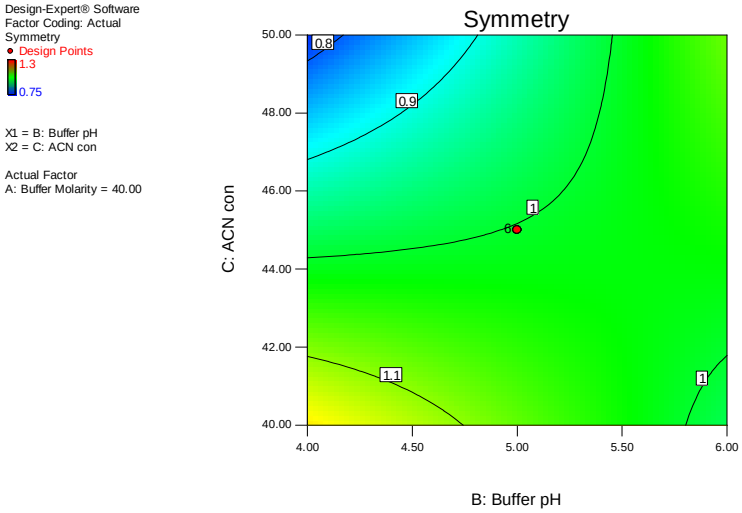

Figure 3.8: *Contour plot for peak asymmetry as a function of buffer pH and ACN concentration*

These data reveal that an optimal peak asymmetry of 1 exists when the concentration of ACN used is approximately 44% v/v in combination with a buffer in the pH range of 4-5, which is the range of maximum stability of EFV [18]. An increase in ACN concentration leads to a decrease in peak asymmetry, probably due to preferential partitioning of EFV into the mobile phase rather than the stationary phase, leading to less peak tailing and sharp peaks. The overall equation of peak asymmetry is given in Equation 3.17.

$$Y_2 = +1.00+7.322E\text{-}003X_1+0.031X_2-0.073X_3-0.012X_1X_2-0.012X_1X_3+0.13X_2X_3 \qquad \textbf{\textit{Equation 3.17}}$$

3.4.3 Peak resolution

The resolution (Y_3) between EFV and LRT was also investigated, and the resulting model was found to be statistically significant (p = 0.0215). The significant factors for this response were the combination of buffer pH and ACN concentration. An "Adeq Precision" of 8.234 was generated for the model, implying that the model is suitable to navigate the design space. The contour plot of the synergistic effect of buffer pH and ACN concentration on the resolution of EFV and LRT is shown in Figure 3.9.

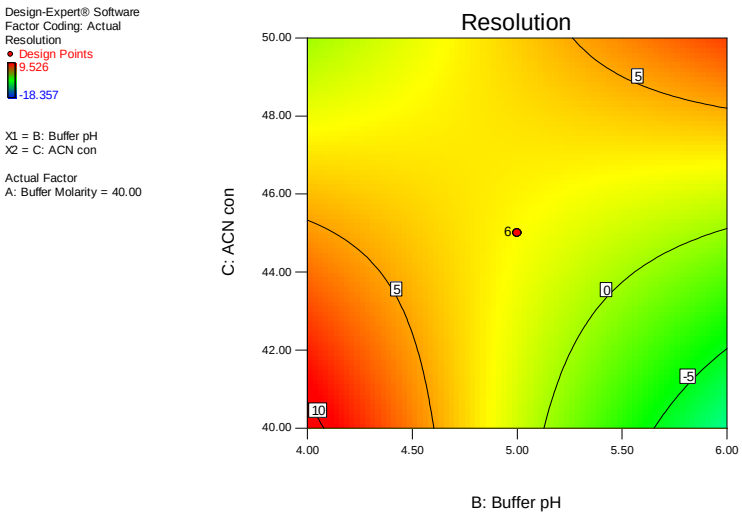

Figure 3.9: *Contour plot for peak resolution as a function of buffer pH and ACN concentration*

The resolution (Y_3) of EFV and LRT was significantly affected by an increase in buffer pH when the ACN concentration was constant, as shown in Figure 3.9. The ionic state of EFV is influenced by mobile phase pH, and a change in pH results in a change in migration due to the polarity of EFV. The resolution of EFV improved with a decrease in pH as the molecule is unionized and stable at low pH, since it has a pKa of 10.1 ± 0.1 [21,22]. The resolution was also improved when lower concentrations of ACN were used. The R_s of the optimized chromatographic conditions was found to be 1.81, with a % RSD of 0.21, and was deemed adequate resolution for the quantitative studies performed. The overall equation for resolution is expressed in Equation 3.18.

$$Y_3 = +2.58-0.83X_1-2.77X_2+1.37X_3-1.58X_1X_2+1.63X_1X_3+6.75X_2X_3 \qquad \textbf{\textit{Equation 3.18}}$$

3.4.4 Optimized Chromatographic conditions

The overall chromatographic analyses of EFV and LRT were identified through optimization of the models using Design Expert® statistical software. The optimized conditions for the overall response *Y* are listed in Table 3.7.

Table 3.7: *Optimized chromatographic conditions for analysis of EFV*

Process variable	**Optimized condition**
X_1 **(buffer molarity)**	31.5 mM
X_2 **(buffer pH)**	4.5
X_3 **(% ACN)**	50 % (v/v)

Sharp, symmetrical and well resolved peaks following the separation of 50 µg/mL EFV and 75 µg/mL LRT solutions were observed when the optimized chromatographic conditions were used. A typical chromatogram of the separation is shown in Figure 3.10. The % RSD for retention time of EFV using the optimized conditions in relation to the predicted retention time was 4.02%, which was less than the set value of 5% for our laboratory. The low value of the calculated percentage prediction error indicates the robustness of the mathematical modeling approach. In addition, the high predictive ability of RSM is demonstrated and suggests the efficiency of RSM as a fitting tool for process optimization [373].

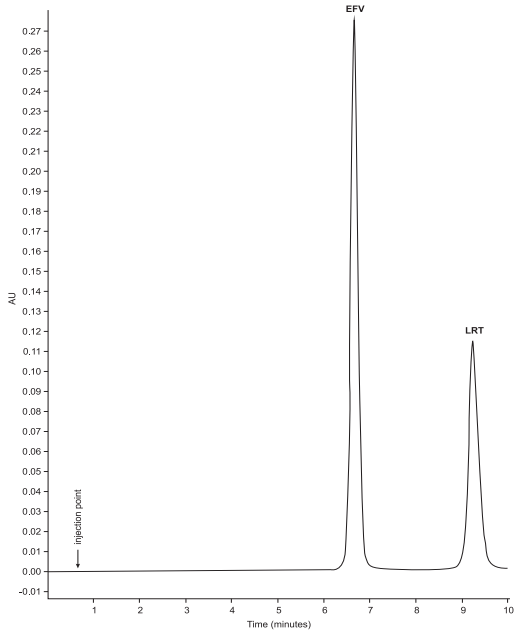

Figure 3.10: *Typical chromatogram of the separation of EFV (50 µg/mL) and LRT (75 µg/mL) obtained using the optimized chromatographic conditions*

3.5. METHOD VALIDATION

3.5.1 Introduction

The validation of an analytical method ensures the performance characteristics of an analytical method and its fitness for its intended purpose [359]. Method validation includes an assessment of the adequacy of the analytical procedure by means of statistical testing, and includes linear regression analysis and the determination of the relative standard deviation to demonstrate the validity of a method [374-376]. The method should be reliable, accurate, precise and robust when used by other analysts when using equivalent instrumentation or analysis on different days throughout the lifecycle of a product [359,374-377].

The International Conference of Harmonisation (ICH) [378], Food and Drug Administration (FDA) [379] and United States Pharmacopoeial Convention (USP) [16] have developed

guidelines for analytical method validation. The ICH Q2 (R1) guideline on validation of analytical procedures [378] recognizes accuracy, precision (repeatability and intermediate precision), specificity, detection limit, quantitation limit, linearity and range as essential parameters for establishing the performance characteristics of a method and that they meet the requirements for the intended analytical application of that method.

The HPLC method developed for the analysis of EFV was validated in accordance with the ICH [378] guidelines, and stress studies were conducted as described in accordance with the FDA [377] guidelines.

3.5.2 Calibration, linearity and range

The linearity of an analytical method is an indication of the ability of the method to produce results directly proportional to the concentration of the analyte in samples over a defined range [380,381]. The interval between the upper and lower concentrations, inclusive of the two extremes, is defined as the range of the analytical method [380,381]. Linearity can be demonstrated by analysis of samples of increasing concentration using the proposed method. The regression coefficient (R^2) is used to evaluate the plot of signal height or peak area as a function of the analyte concentration [316,382]. For assay purposes the ICH [378] recommends that linearity be determined using a series of three to six injections of not less than five standards, with concentrations ranging between 80 and120% of the expected concentration of test samples.

The linearity of the method was established by repeat injections (n=6) of seven calibration standards containing EFV/LRT. Calibration standards (0.1, 0.2, 1.0, 2.5, 5.0, 20.0 and 50.0 µg/mL) spiked with LRT (IS) were prepared as described in § 3.3.3.3 and were injected (n=6) onto the chromatographic system using the conditions described in § 3.3.3.2. The peak height ratios (PHR) of EFV/LRT were calculated and a calibration curve of PHR *versus* concentration

was plotted as shown in Figure 3.11. Least squares regression analysis was performed on the data to establish linearity.

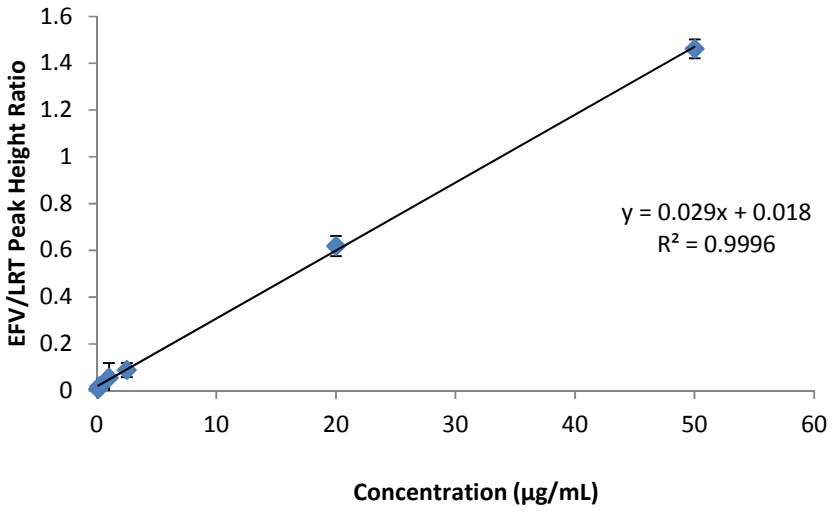

Figure 3.11: *Typical calibration curve for EFV over the concentration range 0.1-50 µg/mL*

The equation for the best-fit linear regression line was y = 0.0292x+0.0174 with a correlation coefficient of 0.9996, indicating that the calibration curve was linear. The correlation coefficient is normally used to assess linearity of a method and a value of ≥ 0.99 is usually considered sufficient to describe linearity of the data across the concentration range [383,384]. Furthermore the regression plot should have a y-intercept of < 2% of the response or close to zero [380,384]. The intercept of 0.0174 satisfies this criterion for linearity.

3.5.3 Precision

The precision of an analytical method is the degree of scatter of a data set. It is assessed using multiple injections of a homogenous solution [380] and is represented as the percent relative standard deviation (% RSD) [381]. Precision may be assessed at three levels *viz.* repeatability (intra-day precision), intermediate precision (inter-day precision) and reproducibility (between

laboratories precision) [376,382]. In these studies, repeatability and intermediate precision were used to assess this parameter, with a RSD tolerance level set at ≤ 5%.

3.5.3.1 Repeatability

The repeatability of an analytical procedure expresses the precision of a method when used under the same operating conditions over a short period of time [376,382]. Repeatability is used to determine the sensitivity of the HPLC instrument under experimental conditions, and in turn eliminates any possibility of variability introduced by the chromatographic conditions [359]. The ICH guideline [378] recommends that repeatability be assessed using a minimum of nine analyses covering the specified range of the method, for example use of three replicate analyses of three concentrations. A minimum of six determinations at 100% of the test target concentration may also be used when assessing repeatability [378]. Repeatability was established by performing six analyses at three different concentrations (low, medium and high) over the calibration range. The repeatability data generated following analysis are summarized in Table 3.8, and reveal that in all cases the % RSD values were < 5%, indicating that the intra-day precision of the method is adequate.

Table 3.8: *Repeatability data for EFV analysis (n=6)*

Concentration (µg/mL)	Calculated concentration Mean ± SD	% RSD
1.50	1.48 ± 0.012	0.81
10.00	10.18 ± 0.027	0.27
50.00	49.89 ± 0.055	0.11

3.5.3.2 Intermediate precision

The intermediate precision experiments are performed to express variations that may occur within laboratories through application of a method on different days using a different analyst with different equipment amongst other potential variations [378,382]. Evaluation of intermediate precision indicates whether the method will produce similar results when similar samples are analyzed. The extent to which the intermediate precision is assessed depends on the

manner in which the analytical method is to be used, and thus on the expected variation [378,382]. The intermediate precision was assessed by analyzing six replicate injections of solutions of three different concentrations on three consecutive days using the same analytical equipment. A summary of the data generated in these studies is listed in Table 3.9. All % RSD values were < 5%, suggesting that the method conforms to the specifications for intermediate precision.

Table 3.9: *Inter-day precision data for EFV analysis (n=6)*

Quality control	**EFV**								
	Day 1			**Day 2**			**Day 3**		
Theoretical concentration (µg/mL)	1.00	20.00	50.00	1.00	20.00	50.00	1.00	20.00	50.00
Calculated concentration (µg/mL)	0.94	21.15	52.04	1.14	20.69	49.08	1.09	19.96	52.03
% RSD	1.12	0.07	0.28	0.76	0.12	0.18	0.83	0.09	0.08

3.5.3.3 Reproducibility

According to the ICH guideline [378] the reproducibility of an analytical method expresses the precision of analysis between laboratories in shared studies. Reproducibility is therefore assessed by means of an inter-laboratory trial [374]. Reproducibility was not assessed in these studies as all analyses were to be performed by a single analyst in the same laboratory for the duration of the project.

3.5.4 Accuracy and bias

The accuracy of an analytical procedure is defined as the closeness of measured experimental values to the true values for a sample or an accepted reference value [359]. It is recommended that accuracy studies for an API and/or a drug product be performed at the 80, 100 and 120% levels of their label claim [359,382,385]. Accuracy is usually established after precision, linearity and the specificity of a method have been established [359].

The measurement of accuracy can be achieved in a number of ways and the experimental data may be compared with results from an established reference method if available [382]. The accuracy can also be determined by analyzing samples of known concentration and comparing the data generated to the true value for the specific samples. A blank sample can be spiked with a known concentration by weight or volume of a material if certified reference material is unavailable [382].

The ICH guideline [378] recommends that accuracy be assessed using a minimum of nine determinations at three concentration levels within the specified calibration range. The accuracy data are reported as % recovery of the added amount of analyte in a sample or as the difference between the mean and the accepted true value of a sample with confidence intervals [378,382]. The analytical method is considered accurate if the % recovery is close to 100% with a % Bias < 2% [381]. However a % Bias of ≤ 5% was set in our laboratory as the test limit since the % Bias is the extent of deviation of a sample result from the sample true value. The extent of deviation of the experimental data from the true value can be expressed as % Bias, which is calculated using Equation 3.20.

$$\% \text{ Bias} = \frac{True\ Value - Measured\ Value}{\text{True Value}} x100 \qquad \textbf{\textit{Equation 3.20}}$$

The accuracy was assessed at three concentrations with each sample injected in replicates (n=6), and the data generated are summarized in Table 3.10. These data show that the method is accurate for the analysis of EFV.

Table 3.10: *Accuracy results for EFV*

Theoretical concentration (µg/mL)	Mean concentration determined (µg/mL)	% RSD	% Bias
0.36	0.35 ± 0.0066	1.89	-2.86
9.00	9.20 ± 0.011	0.12	+2.17
46.50	46.80 ± 0.056	0.12	+0.64

3.5.5 Specificity

The specificity of a chromatographic method is the ability of the method to accurately measure the response of an analyte in the presence of all potential contaminants and sample components [381]. The chromatographic conditions should resolve peak(s) of interest from any possible excipients or contaminants that may be present in a dosage form. The specificity of the method was established by analysis of commercially available EFV tablets. The peaks observed were well resolved from the solvent front and did not interfere with the analysis of EFV. EFV solutions exposed to stress conditions (§ 3.5.7) also revealed well-resolved peaks, thus confirming the specificity of the analytical method.

3.5.6 Limits of quantitation and detection

Von Richter *et al*., [386], Marin *et al*., [387] in addition to Washington *et al*., [388], have extensively addressed the concept of the limits of quantitation (LOQ) and limits of detection (LOD) as an indication of the sensitivity of an analytical method. The LOQ is defined as the lowest concentration of an analyte that can be quantitated with adequate accuracy and precision [387]. Conversely the LOD of an analytical method is the lowest amount of an analyte that can be detected but not quantitated to an exact numeric value [387]. The LOD is detectable above the noise level of a system and is characteristically reported three times above the noise level [382,387,389].

The ICH guideline [378] describes three approaches for establishing the LOQ and LOD of analytical methods [378,382]. The detection and quantitation limits are determined by analyzing samples of known concentration of the analyte of interest and establishing the minimum level at which the analyte can be reliably detected.

The signal-to-noise ratio can be used to determine the detection limits of an analytical method [374,378,390,391]. However this approach can only be applied to analytical methods that exhibit sufficient baseline noise. The signal-to-noise ratio approach is performed by measuring the signals of an analyte at low concentration and comparing the resultant signal to those of a blank sample. A signal-to-noise ratio of between 3 or 2:1 and 10:1 is generally considered acceptable for identifying the limits of detection and quantitation respectively [374,382]. Variability in detector noise indicates that the method is not practical to use as different signals to those obtained during method development may arise when the detector is changed [374].

Another approach for the determination of detection limits depends on the standard deviation of a response that is based on the standard deviation of a blank sample or the slope of the calibration curve [382,389]. The calculation of these limits can be established using Equations 3.21 and 3.22, respectively.

$$\text{LOD} = \frac{3.3\sigma}{S} \qquad \textit{Equation 3.21}$$

$$\text{LOQ} = \frac{10\sigma}{S} \qquad \textit{Equation 3.22}$$

Where

σ = standard deviation of the response
S = slope of the calibration curve

The slope (*S*) is estimated from the calibration curve for an analyte. An estimation of σ can be obtained from the standard deviation of a number of blank sample responses. In addition σ can

be obtained using a specific calibration curve with samples containing an analyte in the LOD and LOQ range. The standard deviation of the y-intercept of regression lines can be used as the standard deviation [378].

The detection limits can also be evaluated from the minimum concentration for which the % RSD is less than a predetermined value. The LOQ can be evaluated as the minimum concentration of an analyte for which the % RSD for the peak area or peak height of the compound of interest (n=6) does not exceed 5% RSD. The LOD is then calculated as 0.3 x LOQ [392,393]. The LOQ and LOD were established using the % RSD approach and the data generated are summarized in Table 3.11. The LOQ was set at 0.10 µg/ml and by convention the LOD was calculated as 0.03 µg/mL.

Table 3.11: *LOQ data for HPLC analysis of EFV*

Conc(µg/mL)	MPHR (EFV/LRT)	SD	% RSD
0.50	0.0264	0.00027	1.02
0.25	0.0175	0.00033	1.86
0.20	0.0152	0.00056	3.68
0.15	0.0117	0.00041	3.50
0.10	0.0076	0.00037	4.87

3.5.7 Forced degradation studies and stability of EFV

A stability-indicating method is a validated quantitative analytical procedure that should detect relevant changes in the properties of API and/or drug product [31]. A stability-indicating method accurately measures API without interference from degradation products, process impurities, excipients or other potential impurities [30]. Forced degradation or stress studies are performed to demonstrate that degradants and impurities of an API or excipients do not interfere with the quantitation of the API [377]. In addition, forced degradation studies may provide information that would be useful in identifying the degradation pathway(s) and/or degradation products of a chemical entity and/or drug products on storage [30].

Stress studies were conducted by exposing EFV to acidic, alkaline, neutral, hydrogen peroxide, light and heat conditions [30,31,377]. These studies were performed in solution except when the drug was exposed to dry heat, in which case the powder form of EFV was used. Stock solutions (100 µg/mL) were prepared as described in § 3.3.3.3 using mobile phase. These solutions were then exposed to the different stress conditions, prior to analysis using the validated analytical method. A tolerance level of between 5 and 20% degradation of API is considered acceptable for the purpose of validating an analytical method intended for assay [30]. Consequently a tolerance of 5% was used in determining if EFV had degraded as a result of exposure to stress conditions. The untreated chromatogram of EFV was used as a reference and is shown in Figure 3.12. Typical chromatograms for EFV following exposure to stress conditions are shown in Figure 3.13.

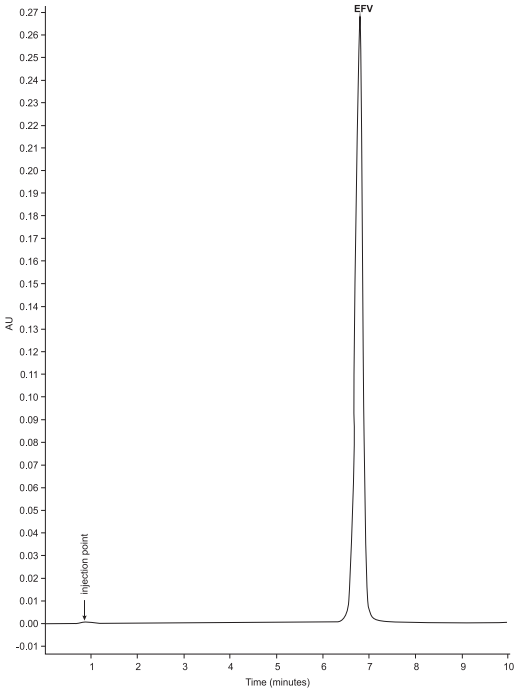

Figure 3.12: *Typical chromatogram of an untreated EFV solution*

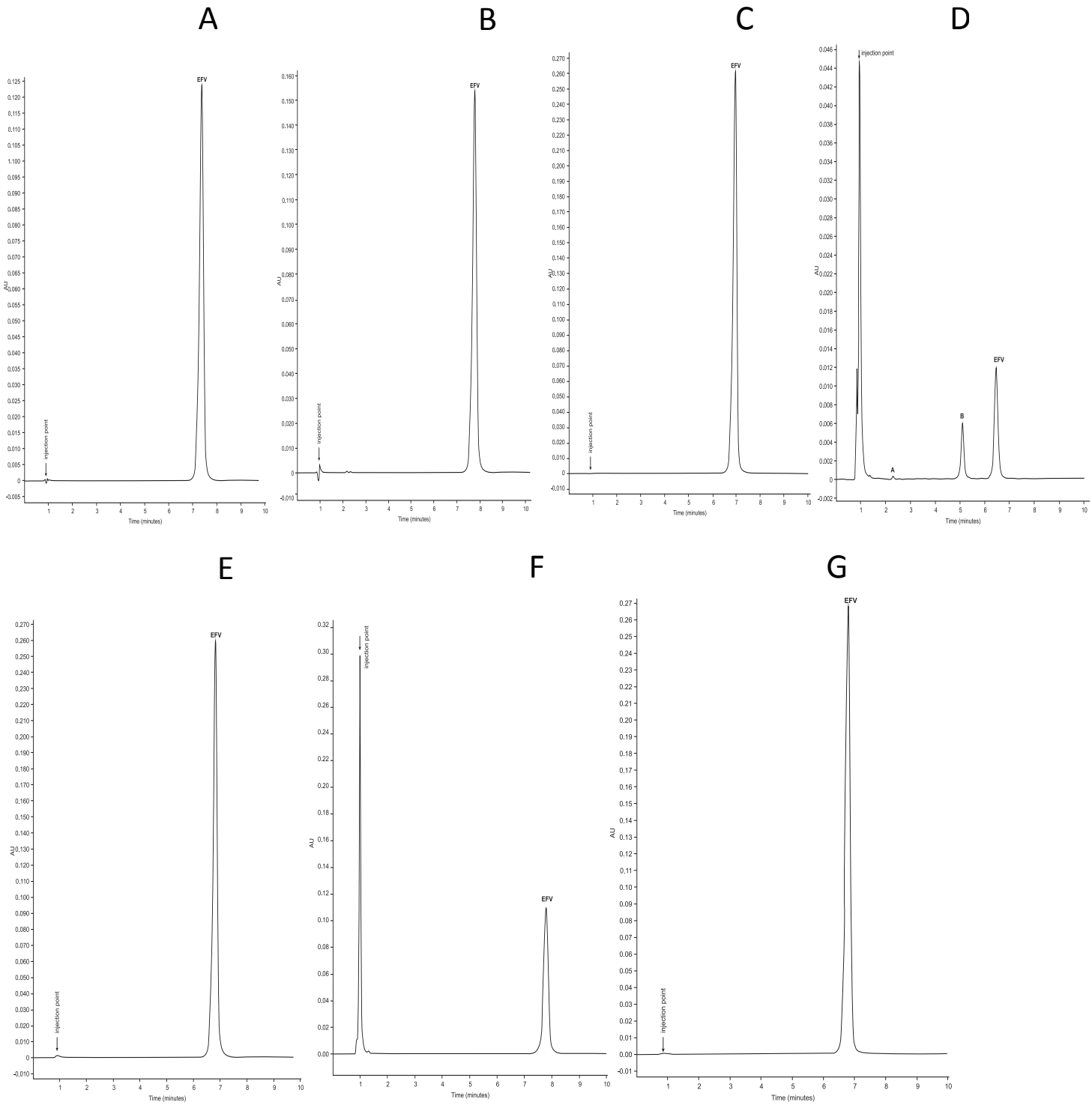

Figure 3.13:*Typical chromatograms for EFV following exposure to 500 W h/m2 (A), 70 °C (B), 0.1M HCL at 70 °C (C), 0.1 M NaOH at 70°C (D) HPLC grade water at 70 °C(E), 3% v/v H2O2 (F) and dry heat at 97 °C (G)*

3.5.7.1 Photostability studies

The ICH recommends exposing an API to light as an essential part of stress studies [394]. The photostability characteristics of a new API are necessary in order to demonstrate that light exposure does not result in unacceptable changes to the compound [394]. Photostability testing may be conducted by exposure of an API to light designed to produce a similar output to D65 or ID65 emission standards [31,394]. The exposure energy should be a minimum of 200 W h/m^2, or at least 1.2 million lux hours for UV photolytic analysis [31,394]. Photolytic degradation was performed by exposing a 100 µg/mL solution of EFV to 500 W h/m^2 for 8 hours in a photostability test chamber (Suntest® CPS+, Atlas, Linsengericht, Germany) prior to analysis. The resultant chromatogram generated following injection of a sample exposed to photolytic conditions for 8 hours is shown in Figure 3.13 (A). The extent of degradation under these conditions was determined and it was observed that 46.64 ± 0.0297% EFV had been recovered.

3.5.7.2 Temperature stress studies

The ICH guidelines [378] recommend that temperature stress testing of an API substance be conducted using temperatures over 10°C increments above that used for accelerated stability studies. For these studies it was deemed necessary to determine the temperature at which EFV becomes thermolabile in solution and whether or not the degradation products could be resolved from the parent drug. Consequently 100 µg/mL of EFV was exposed to heat and maintained at 50, 60, 70 and 80°C for 8 hours using a Colora® Model NB-34980 Ultra-Thermostat water bath (Colora®, Lorch, Germany), and allowed to cool to room temperature (22°C) prior to analysis using the validated method.

The resultant chromatogram generated from exposing the solution to a temperature of 80°C is shown in Figure 3.13 (B). The extent of degradation under these conditions was determined and it was observed that 59.28 ± 0.0681% of EFV had been recovered.

3.5.7.3 Acid degradation studies

Bakshi and Singh [31] recommended that acid and basic hydrolytic studies of new chemical entities be performed by refluxing the API in 0.1 M HCL and NaOH for 8 hours. Therefore 50 ml of a 100 µg/mL of EFV solution was mixed with 50 ml of 0.1 M HCL and the mixture refluxed at 70°C for 8 hours and left to cool to room temperature (22°C) prior to HPLC analysis. The resultant chromatogram generated from acid degradation of EFV is shown in Figure 3.13 (C). The extent of degradation under these conditions was determined and it was observed that 97.71 ± 0.0359% of EFV had been recovered.

3.5.7.4 Alkali degradation studies

Briefly, 50 mL of 100 µg/mL solution of EFV was mixed with 50 mL of 0.1 M NaOH and the mixture was refluxed at 70°C for 8 hours as described in § 3.5.7.3. The solution was allowed to cool to room temperature (22°C) prior to HPLC analysis. The resultant chromatogram generated from alkali degradation of EFV is shown in Figure 3.13 (D). The extent of degradation under these conditions was determined and it was observed that 4.28 ± 0.0134% of EFV had been recovered. Following exposure of EFV to a solution of NaOH, degradation peaks (**A** and **B**) were observed in the chromatogram, as shown in Figure 3.13 (D). This confirms the alkaline instability of EFV through hydrolysis of the carbamate functional group as reported in Chapter 1 (§ 1.3.1).

3.5.7.5 Neutral hydrolysis

Hydrolytic studies in a neutral solution of compounds can be performed by refluxing an aqueous solution of the API for 12 hours [31]. Therefore 50 mL of 100 µg/mL solution of EFV was mixed with 50 mL of HPLC-grade water, and the resultant mixture was refluxed at 70°C for 8 hours. Once again the solution was then allowed to cool down to room temperature (22°C) prior to HPLC analysis. The resultant chromatogram generated from neutral degradation of EFV is shown in Figure 3.13 (E). The extent of degradation under these conditions was determined and it was observed that 98.35 ± 0.0559% of EFV had been recovered.

3.5.7.6 Oxidative studies

Bakshi and Singh [31] suggested the use of hydrogen peroxide in 3-30% v/v concentration for the evaluation of oxidation of compounds. Approximately 50 mL of 100 µg/mL of EFV solution was mixed with 50 mL of 3% v/v hydrogen peroxide. The mixture was refluxed at 70°C for 8 hours prior to cooling to room temperature (22°C) and analysis using HPLC. The resultant chromatogram generated from oxidative stress studies of EFV is shown in Figure 3.13 (F). The extent of degradation under these conditions was determined and it was observed that 44.94 ± 0.0286% of EFV had been recovered. Following exposure to hydrogen peroxide for eight hours EFV was found to degrade and an additional peak was eluted in the solvent front, which may be a degradation product.

3.5.7.7 Dry heat

EFV powder was exposed to 97°C for 8 hours in a drying cabinet (Weiss, Gallenkamp®, Loughborough, UK). A 100 µg/mL stock solution was prepared using EFV powder that had been exposed to heat, following which the true concentration was determined by HPLC. The resultant chromatogram generated from dry heat studies of EFV is shown in Figure 3.13 (G). The extent of degradation under these conditions was determined and it was observed that 98.98 ± 0.0809% of EFV had been recovered.

3.5.7.8 Stability of the analyte

An analyte is said to be chemically stable under specific conditions and time by comparison of the response to that observed for freshly prepared samples [395]. The stability of an analyte in mobile phase ensures that the integrity of the compound is maintained throughout the analytical process [396]. The stability of EFV in solution was established in mobile phase by analyzing a 100 µg/mL solution of the molecule that had been maintained at 4°C for a period of 3 days. A tolerance level of 1% RSD was considered acceptable in order to infer stability. These studies

revealed that the concentration of EFV remained constant with a % RSD value of 0.23%. EFV was therefore considered stable in the mobile phase, and the stock solution could be stored under the stated conditions and used within three days of preparation.

3.6 APPLICATION OF THE ANALYTICAL METHOD

The validated method was applied to the analysis of EFV in commercially available Stocrin ® 600 mg tablets [397], and for the quantitative determination of EFV in samples collected during *in vitro* release testing of EFV in SLN and NLC. Briefly, 20 tablets were crushed in a mortar and pestle and an aliquot of powder equivalent to the weight of one tablet was then quantitatively transferred to a 100 mL A-grade volumetric flask. Approximately 80 mL of the mobile phase was then added to the volumetric flask and the mixture was sonicated using a Branson® B12 sonicator (Branson® Inc., Shelton, Conn, USA) with regular shaking until complete dissolution of the powders had been observed [33]. The solution was allowed to cool to room temperature (22°C) prior to making up to volume with mobile phase. An aliquot of the resultant mixture was centrifuged at 500 rpm for 10 minutes [33] using an IEC Model HN-SII centrifuge (Damon, Needham HTS, MA, USA), filtered through a 0.45 µm Millipore® Millex-HV Hydrophilic PVDF filter membrane (Millipore® Co., Bedford, MA, USA) and analyzed using the validated HPLC method.

The data generated from assay studies (n=3) revealed that the tablets contained on average 100.68 ± 2.015% of the label claim, with a precision of 2.00% RSD. These data fall within the limits of 92-110% as specified in the USP [397]. A typical *in vitro* release profile (n=3) generated during these studies is shown in Figure 3.14. The data obtained from assay and *in vitro* release studies reveal that the HPLC-UV method is suitable for the quantitative determination of EFV in pharmaceutical formulations and the assessment of the *in vitro* release rate of EFV from colloidal drug carriers such as SLN and/or NLC.

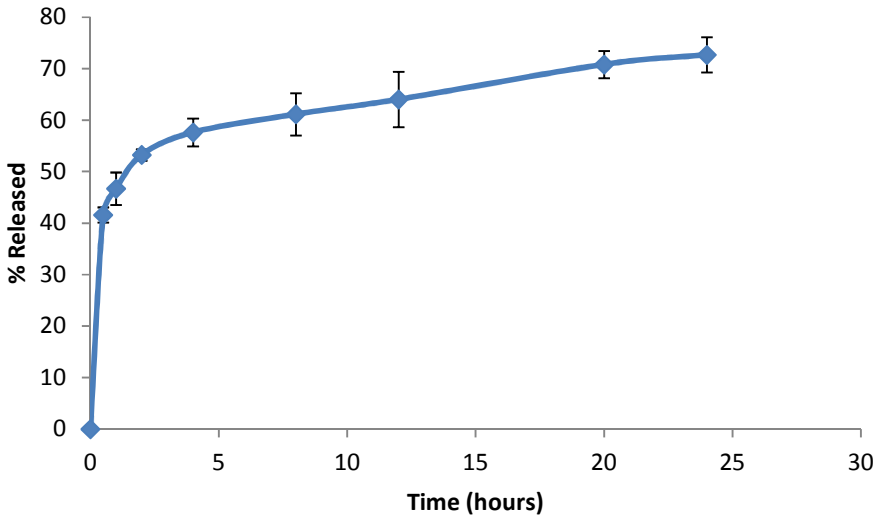

Figure 3.14: *Typical dissolution profile of EFV from EFV-loaded SLN (n=3)*

3.7 CONCLUSIONS

The use of Response Surface Methodology (RSM) is a popular approach for optimization experiments [322], including the development of HPLC methods. A Central Composite Design (CCD) approach was used to develop and optimize a RP-HPLC with UV detection for the analysis of EFV. The optimization studies investigated the effect of three variables *viz.* buffer pH, buffer molarity and ACN concentration on three critical quality attributes of a separation, *viz*. peak asymmetry, peak resolution and retention time.

The results of statistical analysis for the model reveal that it can be used to navigate the design space. Contour plots were used to explain the interactive effects of factors on the responses. Statistical analysis of the models showed that of all factors studied, only ACN concentration had a significant effect on the retention time of EFV. Furthermore the responses observed for the method were closely related to the predicted values generated using the optimized method. The analytical method was developed and optimized using a small number of experimental runs in a short experimental run time. It is clearly evident that RSM is an important and efficient tool that

can be used to identify the optimum chromatographic conditions for the purpose of achieving adequate separation, resolution and retention time in an HPLC analysis.

A stability-indicating RP-HPLC method has been developed that is simple, precise, accurate, selective and rapid. The method can be used for the quantitative determination of EFV in pharmaceutical dosage forms. In addition the method is sensitive and could be used for the assessment of *in vitro* release rate of EFV from colloidal drug delivery systems such as SLN and/or NLC. EFV is photolabile and undergoes extensive photolytic degradation following exposure to ultraviolet (UV) light, confirming published data [34,343], and therefore the use of HPLC with UV detection for the quantitative determination of EFV may be undesirable. It was decided that a RP-HPLC method with electrochemical detection (ECD) be developed and validated for the analysis of EFV. Data generated from these studies are highlighted in Chapter 4.

CHAPTER 4

DEVELOPMENT AND VALIDATION OF A RP-HPLC ECD METHOD FOR THE ANALYSIS OF EFAVIRENZ

4.1 INTRODUCTION

The use of HPLC-UV for quantitative analysis of EFV in dosage forms either alone [33,248,343] or in combination with ARV has been reported in Chapter 3 [250]. However the use of HPLC with UV detection for the quantitaive analysis of EFV may be inappropriate as the molecule is photolabile and has been reported to undergo extensive photolytic degradation following exposure to light at wavelengths of 254 nm [34] and 320-400 nm [343].These conditions may be unsuitable and there is a need to explore the use of an alternate detector for HPLC analysis of EFV. EFV has a nitrogen atom on the benzoxazine ring that is susceptible to electrochemical oxidation [398]. Consequently the use of electrochemical detection (ECD) may be suitable for the analysis of EFV in dosage forms. Dogan-Topal *et al.*, [398] reported the use of an HPLC-ECD method for the determination of EFV in formulations using a pencil graphite electrode. However this method was not stability-indicating and involved the use of an electrochemical biosensor with the primary aim of studying DNA–EFV interactions and therefore may not be suitable for the routine analysis of the EFV in dosage forms.

HPLC-ECD has been successfully used for trace determination of oxidizable and reducible organic compounds. Electrochemical approaches such as pulse polarography, anodic stripping voltammetry and differential pulse voltammetry have been applied to the analysis of API and drug products [365,399]. HPLC-ECD has been used for the detection of tricyclic antidepressant compounds using boron-doped diamond electrodes [400], *p*-nitrophenol and acid phosphatase in urine [401], penicillins [402,403], phenols in environmental waters [404], cyclizine and

norcyclizine in biological fluids [405], and for the bioequivalence study of trimetazidine in human plasma [406] amongst other separations and applications.

ECD is a sensitive and specific technique requiring the compound of interest to have a functional moiety that has the potential to undergo a redox reaction [365]. The detection limit of compounds with oxidizable functional groups has been reported to be as low as 0.1 picomols. However the limit of detection is relatively high for molecules with reducible functional groups due to challenges associated with dissolved oxygen and electrode stability [284,365,407]. Despite the advantages of ECD, i.e. adequate selectivity, low limits of detection and cost, significant drawbacks are associated with the use of ECD, including unreliability due to constant electrode fouling, especially when operated at high potentials [365], resulting in the cell having to be removed and cleaned on a regular basis [365]. Electrode fouling can be limited by use of pulsed electrochemical detection in which gold or platinum electrodes are used [284,365,408-410]. A schematic representation of the principle behind the operation of ECD is shown in Figure 4.1 [411].

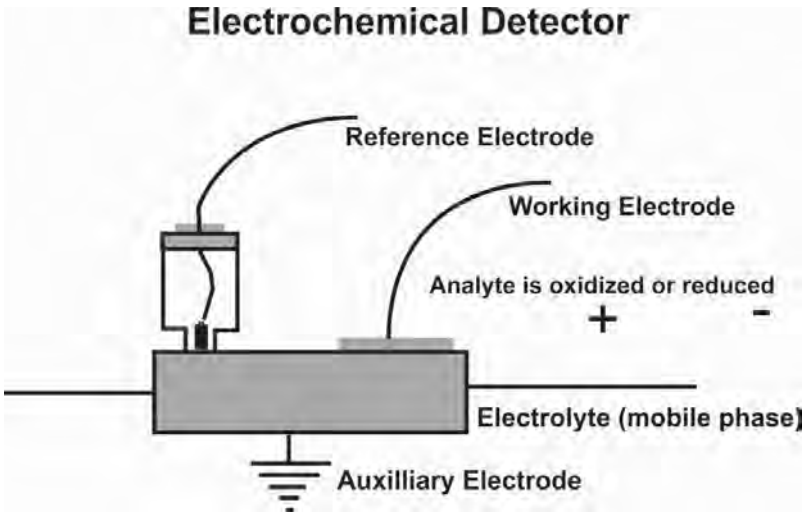

Figure 4.1: *Schematic representation of an electrochemical detector (adapted from [411])*

The potential required for activation of the API and subsequent detection of the compound is applied to the working reference electrode connected to a flow cell, with the auxiliary electrode being used to control the potential [411]. As oxidation or reduction occurs at the working electrode the flow of current changes and is monitored, amplified and recorded as a chromatographic response [284,411]. When using coulometric detection, the reaction goes to completion by use of the high surface area of a working electrode and exhausting all reactants in the flow cell [412]. The number of coulombs of charge transferred is then measured. For amperometric detection, solute molecules located at the surface of an electrode in addition to those in close proximity to that surface, are oxidized or reduced by maintaining a constant working electrode potential [412]. The reaction is diffusion-controlled and is proportional to the concentration of analyte present. In this case the flow of current is measured, amplified and the signal recorded as a function of time [284,412].

The objectives of this study were to develop and validate an HPLC-ECD method for the quantitation of EFV in pharmaceutical dosage forms, and to compare the method to the HPLC-UV method (Chapter 3) in terms of simplicity, precision, accuracy and selectivity prior to selecting the most appropriate approach for the analysis of SLN and/or NLC formulations.

4.2 EXPERIMENTAL

4.2.1 Chemicals and Reagents

All chemicals and reagents, except for imipramine (IMI), were similar to those used in the development of the RP-HPLC with UV detection described in § 3.3.3.1. The internal standard (IS) IMI was donated by Aspen Pharmacare® (Port Elizabeth, Eastern Cape, South Africa).

4.2.2 Preparation of stock solutions and calibration standards

Standard stock solutions of EFV (140 µg/mL) and IMI (5µg/mL) were prepared and stored as described in § 3.3.3.3. The range of concentrations for the calibration standards was 5-70 µg/mL for ECD studies.

4.2.3 Preparation of Buffer and Mobile Phase

Phosphate buffer (30 mM) was prepared by accurately weighing 4.0789 g of potassium dihydrogen orthophosphate into a 1 L A-grade volumetric flask and making up to volume with HPLC grade water. The pH was adjusted as described in § 3.3.3.4, and the mobile phase was prepared as described in § 3.3.3.4.

4.2.4 Instrumentation

The modular HPLC system consisted of a Model 510 Waters® solvent delivery system (Waters® Associates, Milford, MA, USA), a Waters® Wisp 710 B autosampler (Waters® Associates, Milford, MA, USA) and a Model 464 pulsed amperometric electrochemical detector (Waters® Associates, Milford, MA, USA) operated in the DC mode with the potential and current set at +1400 mV and 1 µA respectively. Separation between IMI and EFV was achieved under isocratic conditions using a Nova-Pak® C_{18}, 4 µm (150 mm x 3.9 mm i.d) (Waters® Corporation, Milford, MA, USA) cartridge column and a mobile phase consisting of 30 mM phosphate buffer (pH 4.5): acetonitrile (55:45 v/v). The flow rate of the mobile phase and the injection volume were 1.0 mL/min and 20 µL respectively. The temperature of the analytical column was maintained at 30°C using a Model LC-22 temperature controller (Bioanalytical Systems, West Lafayette, IN, USA). Data acquisition was achieved using a SP Thermo Separation Datajet Integrator (Waters® Associates, Milford, MA, USA) which had been set at an attenuation of 128.

4.3 METHOD DEVELOPMENT

The development and optimization studies of the ECD method were performed in a similar manner to the approach outlined in Chapter 3, § 3.4. EFV has an oxidizable functional group that oxidizes at a potential of +1250 mV [398]. Consequently in these studies an electrochemical (EC) detector was used for the detection of EFV. Preliminary studies were designed to establish the oxidization potential and analytical current for EFV. A hydrodynamic voltammogram (HDV)

for EFV and IMI generated in the DC mode in a potential range between +1000-1800 mV and a scan of the background current ranging between 0.5-5.0 µA are shown in Figure 4.2 (A) and (B) respectively. These data reveal that the maximum oxidizing potential for the analyte of interest (EFV) was reached at +1400 mV, corresponding to oxidation of the secondary amine electroactive site [398] (Figure 1.1), and the limiting current for both EFV and IMI reached plateau at 1.0 µA. However the optimal detector potential is selected only when the chromatographic conditions have been optimized as the electrochemical behavior of an analyte depends on other conditions such as mobile phase composition and pH [413]. Consequently a potential range between +1300 mV and +1500 mV was included as a factor for the CCD to generate the optimum chromatographic conditions for this analysis. The plateau background current of +1.0 µA (Figure 4.2 B) was used in all subsequent method development experiments to achieve the detection and separation of EFV (70 µg/mL) and IMI (5 µg/mL).

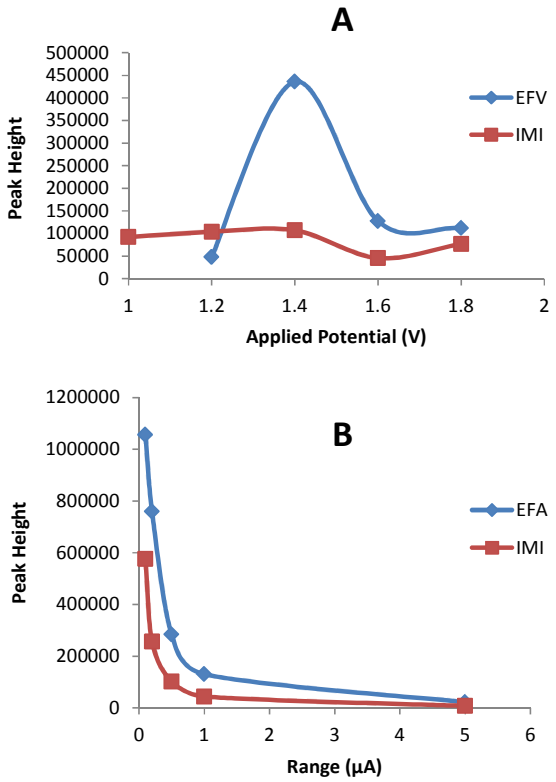

Figure 4.2: *HDV for EFV and IMI generated in DC mode (A) and scan for background current (B)*

4.3.1 Method optimization

A computer-generated rotatable CCD design consisting of 30 experiments, 6 center points and 24 non-center points was generated and is listed in Table 4.1. The experimental levels studied are summarized in Table 4.2. The minimum and maximum values of the buffer molarity (X_1) were 30 mM and 50 mM with the lower and upper axial points of 20 mM and 60 mM. Similarly the values of 4 and 6 were the minimum and maximum values of the buffer pH (X_2), with the lower and upper axial values maintained at pH 3 and pH 7. The ACN concentration (X_3) was kept at minimum and maximum values of 40% and 50% with respect to buffer concentration, with lower and upper axial levels of 35% and 55% respectively. Detector voltage (X_4) was set to a minimum of +1350 mV and maximum of +1450 mV, with the lower and upper axial levels of (X_4) set at +1300 mV and +1500 mV respectively. The independent input variables and ranges were selected on the basis of preliminary studies of the chromatographic system. The retention time (Y_1) of the last peak eluted, peak symmetry (Y_2) and peak resolution (Y_3) were selected as dependent output responses or variables. Data analysis was performed using Design Expert® statistical software as described in § 3.4, and the design summary selected was best represented with four quadratic models.

Table 4.1: *Randomized coded experimental runs for CCD*

		Factor 1	Factor 2	Factor 3	Factor 4
Std	**Run**	**A:Buffer Molarity mM**	**B:Buffer pH**	**C:ACN conc % v/v**	**D:Voltage mV**
6	1	1	-1	1	-1
9	2	-1	-1	-1	1
11	3	-1	1	-1	1
29	4	0	0	0	0
7	5	-1	1	1	-1
25	6	0	0	0	0
16	7	1	1	1	1
19	8	0	-2	0	0
21	9	0	0	-2	0
22	10	0	0	2	0
3	11	-1	1	-1	-1
2	12	1	-1	-1	-1
12	13	1	1	-1	1
30	14	0	0	0	0
24	15	0	0	0	2
14	16	1	-1	1	1
13	17	-1	-1	1	1
20	18	0	2	0	0
4	19	1	1	-1	-1
15	20	-1	1	1	1
1	21	-1	-1	-1	-1
8	22	1	1	1	-1
23	23	0	0	0	-2
27	24	0	0	0	0
26	25	0	0	0	0
18	26	2	0	0	0
28	27	0	0	0	0
5	28	-1	-1	1	-1
17	29	-2	0	0	0
10	30	1	-1	-1	1

Table 4.2: *Actual variable and experimental design values*

Variable	Level			
	-α	**-1**	**1**	**+α**
X_1**(Mobile phase mM)**	20	30	50	60
X_2**(Mobile phase pH)**	3	4	6	7
X_3**(Organic solvent %)**	35	40	50	55
X_4**(Voltage mV)**	1300	1350	1450	1500

4.3.1.1. Effect on retention time

Retention time (Y_1) was considered the most critical response as it affects the analytical run time of a method. ACN concentration was found to be the most statistically significant factor affecting retention time and the influence of ACN concentration on retention time is shown in Figure 4.3.

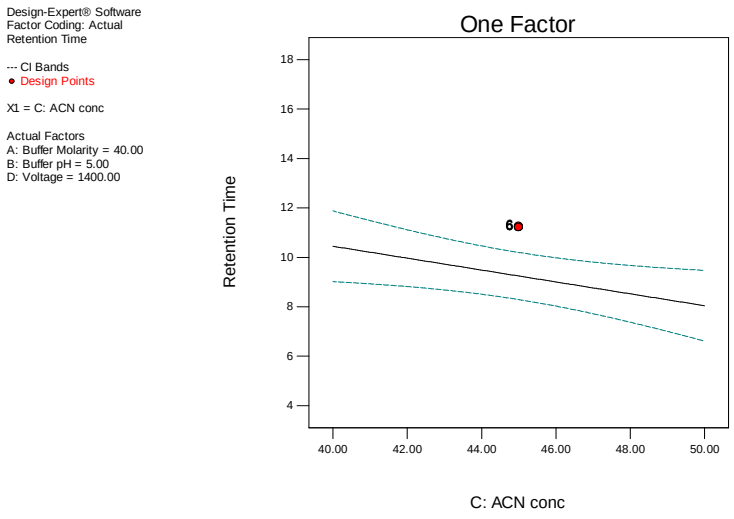

Figure 4.3: *The effect of ACN concentration on retention time*

A decrease in the retention time of EFV was observed when the ACN concentration was increased from 40 to 50% v/v. ANOVA was used to analyze the quadratic model for retention time and Fisher's F-ratio was calculated to identify significant terms in the model, with the error term of p = 0.05. Values of "Prob > F" < 0.0500 indicate model terms that are significant,

however values greater than 0.1000 indicate that the model terms are not significant. The overall contribution of the model factors to retention time was not statistically significant as summarized in Table 4.3, as the “Prob > F” > 0.1. The "Model F-value" of 0.89 implies that the model is not significant relative to noise and that there is a 58.25% chance that a "Model F-value" this large could occur due to noise.

Table 4.3: *ANOVA Data for the response surface quadratic model for retention time*

Source	Sum of Squares	df	Mean Square	F Value	p-value Prob > F	
Model	98.59	14	7.04	0.89	0.5825	Not significant
A-Buffer Molarity	1.23	1	1.23	0.16	0.6983	
B-Buffer pH	7.59	1	7.59	0.96	0.3424	
C-ACN conc	34.75	1	34.75	4.40	0.0533	
D-Voltage	0.066	1	0.066	8.325E-003	0.9283	
AB	0.30	1	0.30	0.038	0.8488	
AC	5.50	1	5.50	0.69	0.4171	
AD	2.28	1	2.28	0.29	0.5989	
BC	12.78	1	12.78	1.61	0.2227	
BD	0.40	1	0.40	0.050	0.8256	
CD	1.66	1	1.66	0.21	0.6528	
A^2	12.87	1	12.87	1.63	0.2212	
B^2	4.87	1	4.87	0.62	0.4446	
C^2	17.77	1	17.77	2.25	0.1543	
D^2	8.76	1	8.76	1.11	0.3090	
Residual	118.46	15	7.90			
Lack of fit	118.46	10	11.85	27764.19	< 0.0001	Significant
Pure Error	2.133E-003	5	4.267E-004			
Cor Total	217.05	29				
Std. Dev.	2.81	R^2	0.4542			
Mean	9.25	Adj R^2	-0.0582			
C.V. %	30.44	Pred R^2	-2.1437			
Press	682.34	Adeq. Precision	3.859			

The "Lack of Fit F-value" of 27764.19 indicates that the Lack of Fit is significant and may be due to insignificant model terms, which is undesirable. Therefore model reduction through a background elimination procedure was used to improve the model fit. In this way insignificant model terms were reduced, resulting in identification of a significant model as summarized in Table 4.4.

Table 4.4: *ANOVA table for the response surface reduced linear model*

Source	Sum of Squares	df	Mean Square	F Value	p-value Prob > F	
Model	34.75	1	34.75	5.34	0.0285	Significant
C-ACN conc	34.75	1	34.75	5.34	0.0285	Significant
Residual	182.30	28	6.51			
Lack of fit	182.30	23	7.93	18576.27	< 0.0001	Significant
Pure error	2.133E-003	5	4.267E-004			
Cor Total	217.05	29				
Std.Dev.	2.55	R^2	0.1601			
Mean	9.25	Adj R^2	0.1301			
C.V. %	27.60	Pred R^2	-0.0048			
PRESS	218.09	Adeq. Precision	7.306			

The Model F-value of 5.34 is indicative of a significant model, as the probability that a "Model F-Value" of such magnitude could occur due to noise is only 2.85%. Following model reduction the lack of fit was still significant, as observed in Table 4.4. However, an "Adeq Precision" of 7.306 indicates a signal that is satisfactory. The "Adeq Precision" measures the signal to noise ratio, and a ratio > 4 is considered desirable. Therefore this model was used to navigate the design space as summarized in Table 4.4. The method was used to predict the retention time of EFV within the limits of the design space. The resultant model equation for Y_1 (retention time) is shown in Equation 4.1.

$$Y_1 = 9.25\text{-}1.20X_3 \qquad \textbf{\textit{Equation 4.1}}$$

The normal probability plot of residuals for retention time is shown in Figure 4.4.

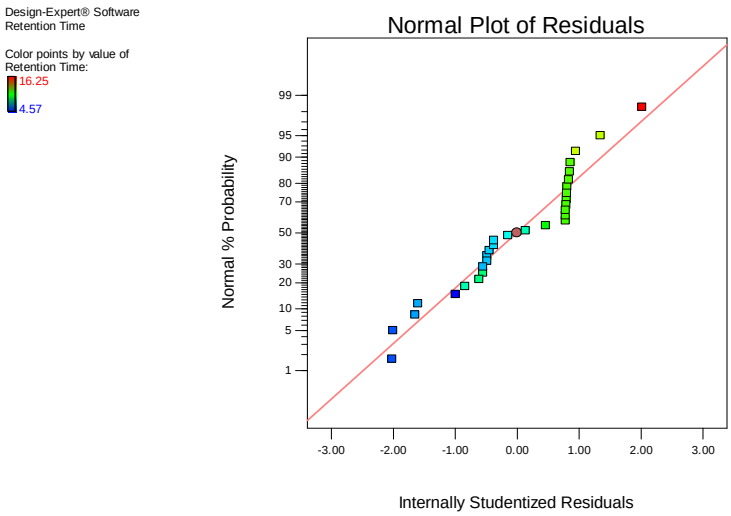

Figure 4.4: *Normal plot of residuals for retention time*

The normal plot of residuals shows that the points generally lie on a straight line, and is indicative of a relatively normal distribution of error and therefore is confirmation of adequate fitting of the data to the model. A Box-Cox plot for power transformations for this model is shown in Figure 4.5, and the observed current value of 1 indicates that a transformation of the model data is not necessary, confirming that the data were normally distributed, and further implies that the data are located at the best possible and optimal region of the parabola [369-371].

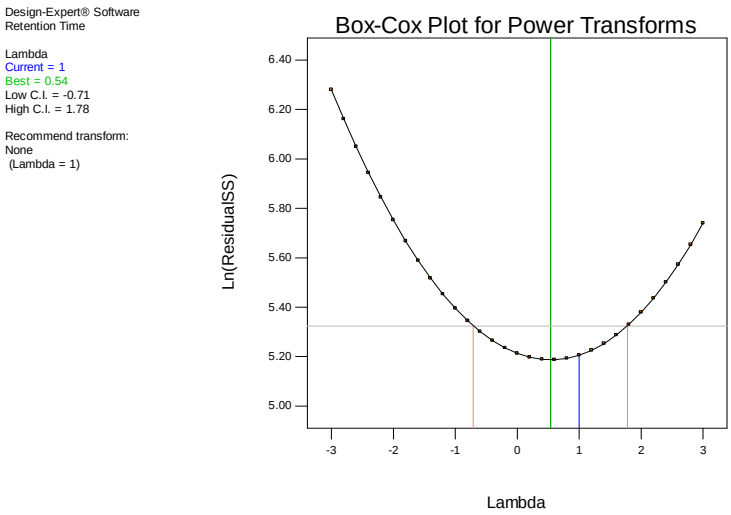

Figure 4.5: *Box –Cox plot for power transformation for retention time of EFV*

4.3.1.2. Effect on peak asymmetry

The peak symmetry response (Y_2) was evaluated using the peak asymmetry factor (As), and was determined using Equation 3.13 (§ 3.3.3.6.3). The analysis of data using ANOVA revealed that the model was insignificant (p = 0.0852) with respect to As. Consequently model reduction was performed using background elimination. Evaluation of the significant model (p = 0.0005) suggests that ACN concentration (p = 0.0256) and detector voltage (p = 0.0256) alone or in combination (p = 0.0032) were major factors affecting peak symmetry for EFV. These factors can therefore be manipulated to improve the EFV peak symmetry during analysis. The synergistic effect of ACN concentration and voltage on the peak symmetry is shown in Figure 4.6.

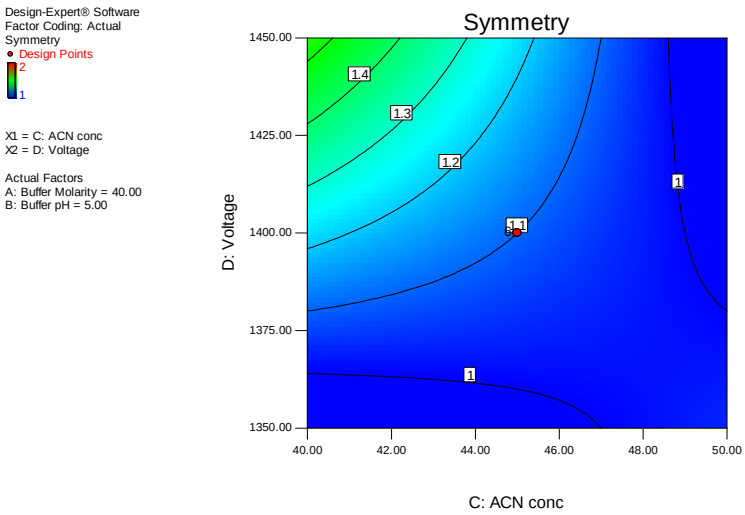

Figure 4.6: *Contour plot for peak symmetry as a function of ACN concentration and voltage*

These data indicate that in order to generate a symmetrical peak for EFV the optimal ACN concentration and voltage should lie between 40-47% v/v and +1375 mV-+1450 mV respectively. An experimental run performed using the optimized chromatographic conditions resulted in an As value of 1.1 (0.18% RSD) and was considered adequate peak symmetry for analysis of EFV. The equation for the peak symmetry response is shown in Equation 4.2.

$$Y_2 = +1.00 - 0.042X_1 + 0.042X_2 - 0.13X_3 + 0.12X_4 + 0.063X_1X_2 + 0.063X_1X_3 - 0.062X_1X_4 - 0.062X_2X_3 + 0.063X_2X_4 - 0.19X_3X_4 + 0.031X_1^2 + 0.031X_2^2 + 0.031X_3^2 + 0.031X_4^2 \quad \textbf{Equation 4.2}$$

4.3.1.3. Effect on peak resolution

The resolution between EFV and the IS was considered an essential HPLC response and was therefore also investigated during the optimization stage of method development. The quadratic model was not significant (p = 0.4265) and an F-value of 1.10 was calculated. The "Model F-value" was 1.10, with a 42.65% probability of this value occurring as a consequence of noise, indicating that the model was not significant. Furthermore the ratio of maximum to minimum resolution was 23.67, and a ratio >10 indicates that transformation of the data is required in order to validate the ANOVA. Consequently an inverse transformation was used to transform the data and a significant (p = 0.0412) two-factor interaction (2FI) model was obtained. The buffer pH

was a significant model term with a *p*-value of 0.0233. Furthermore the interactive effects of buffer pH and ACN concentration, and between ACN concentration and voltage, were significant model terms with *p*-values of 0.0179 and 0.0371 respectively. Two-dimensional contour plots of the influence of these interactive effects on peak resolution for EFV are shown in Figures 4.7 and 4.8.

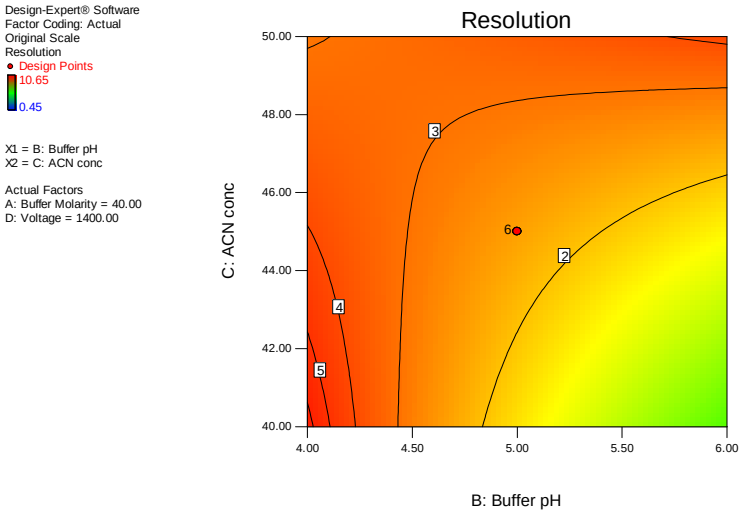

Figure 4.7: *Contour plot for peak resolution as a function of buffer pH and ACN concentration*

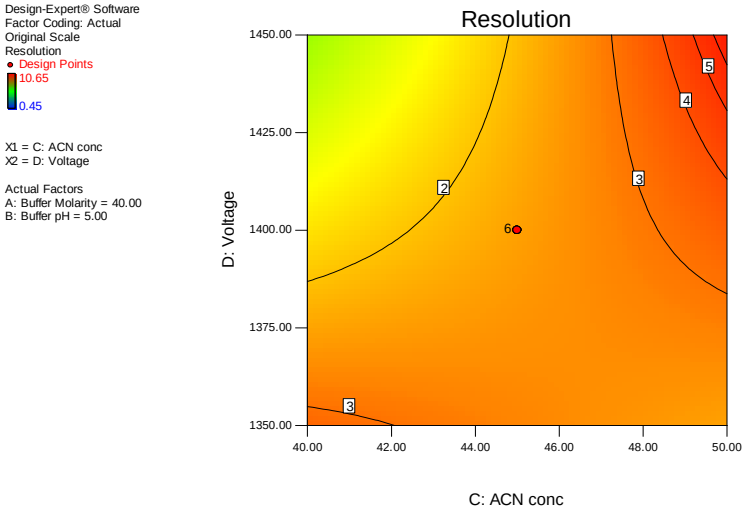

Figure 4.8: *Contour plot of peak resolution as a function of ACN concentration and voltage*

The data depicted in Figure 4.7 reveal that adequate peak resolution could be observed when the pH of the buffer was < pH 5 with any concentration of ACN. Furthermore the data in Figure 4.8 suggest that acceptable peak resolution could be obtained when the ACN content and detector voltage were within the range of 44%-50% v/v and +1380 mV–+1450 mV respectively. An experimental run performed using the optimized chromatographic conditions resulted in a peak resolution value of 3.52 (0.59% RSD), suggesting that adequate resolution between EFV and IMI had been achieved. The equation for the peak resolution response is shown in Equation 4.3.

$$\frac{1}{Y_3} = +0.43+5.086\text{E-}003X_1+0.18X_2-0.14X_3+0.059X_4+0.021X_1X_2-0.11X_1X_3+0.084X_2X_3+0.063X_2X_4-0.20\,X_3X_4 \qquad \textit{Equation 4.3}$$

4.3.1.4. Optimized chromatographic conditions

The overall solutions for chromatographic conditions were generated through optimization of the models using Design Expert® statistical software (Stat-Ease Inc., Minneapolis, MN, USA). The optimized conditions for the overall response *Y* are given in Table 4.5.

Table 4.5: *Optimized chromatographic conditions for HPLC-ECD analysis of EFV*

Process variable	Optimized condition
X_1 **(buffer molarity)**	30 mM
X_2 **(buffer pH)**	4.5
X_3 **(% ACN)**	45% (v/v)
X_4 **(Voltage)**	+1400 mV

The optimized chromatographic conditions were applied to the quantitative analysis of EFV, and a typical chromatogram of the separation of EFV and IMI generated using these conditions is shown in Figure 4.9. It is evident that sharp and well-resolved peaks for EFV and IMI were obtained with retention times (R_t) of 3.70 and 8.89 minutes respectively. The retention times were considered suitable for the routine analysis of EFV as the total run time for sample analysis was < 10 minutes. Furthermore the % RSD for the retention time of EFV in relation to the predicted retention time was 2.54%, and was considered adequate as it was less than the criterion of 5% RSD set in our laboratory.

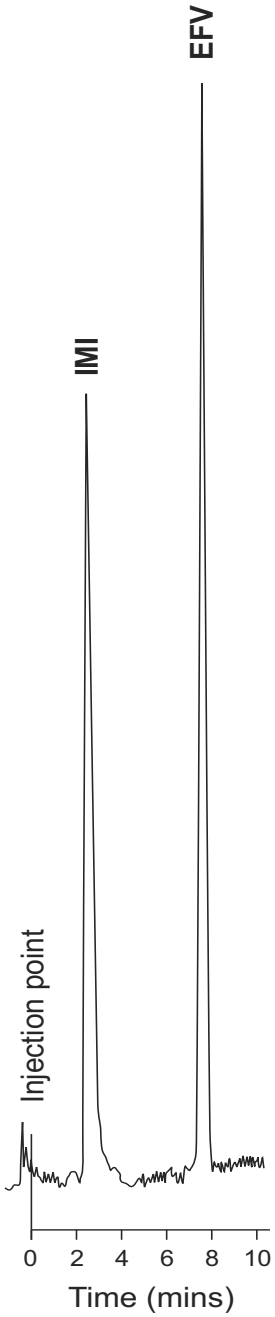

Figure 4.9: *Typical chromatogram showing separation of EFV (70 µg/mL) and IMI (50 µg/mL)*

4.4. METHOD VALIDATION

To compare the versatility of the two HPLC methods using UV and EC detection, the same validation limits and standards as described in Chapter 3, § 3.5 were carried out during validation of the HPLC-ECD method.

4.4.1 Calibration, linearity and range

The linearity of the method was demonstrated as in § 3.5.2 by analyzing (n=6) seven calibration standards of EFV i.e. 5.0, 10.0, 15.0, 30.0, 40.0, 50.0 and 70.0 µg/mL. A plot of the peak ratio (PHR) of EFV to IMI was plotted against the concentration as shown in Figure 4.10. Least squares regression analysis was performed to establish linearity of the data. The R^2 value and equation for the line were 0.9979 and y = 0.0151x+0.0163 respectively.

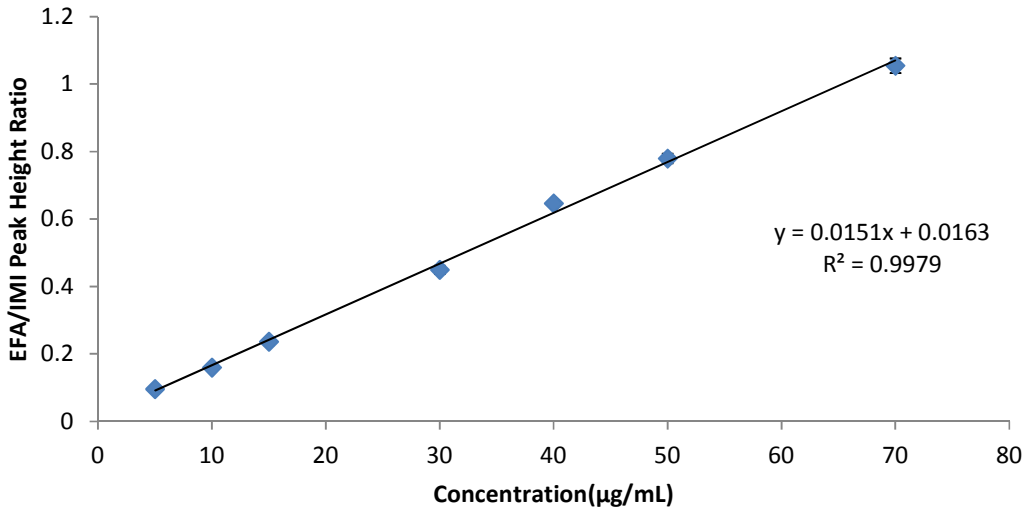

Figure 4.10: *Typical calibration curve for EFV over the concentration range 5-70 µg/mL*

4.4.2. Precision

4.4.2.1 Repeatability or intra-day precision

The repeatability of the method was established using three different concentrations (low, medium and high) across the calibration range and the data are summarized in Table 4.6. These results reveal that the intra-day precision of the method was acceptable in accordance with the criteria set in our laboratory as defined in Chapter 3,§ 3.5.3.1.

Table 4.6: *Intra-day data for EFV analysis (n=6)*

Concentration (µg/mL)	Calculated concentration Mean ± SD	% RSD
10.00	9.86 ± 0.428	4.34
30.00	29.67 ± 0.999	3.37
50.00	48.54 ± 1.937	3.99

4.4.2.2 Intermediate precision

Intermediate precision was determined on three consecutive days using three concentrations (n=6) and the resultant data are listed in Table 4.7. The % RSD < 5% for each concentration tested confirming that the method was precise with respect to intermediate precision as defined in Chapter 3,§ 3.5.3.2.

Table 4.7:*Inter-day precision and accuracy data for EFV analysis*

Quality control	EFV Day 1			Day 2			Day 3		
Theoretical concentration (µg/mL)	10.00	30.00	50.00	10.00	30.00	50.00	10.00	30.00	50.00
Calculated concentration (µg/mL)	10.23	29.87	48.95	9.88	30.12	50.04	9.96	29.97	51.03
% RSD	4.24	2.79	1.86	4.26	1.67	1.31	3.58	2.29	1.35

4.2.3 Accuracy and bias

Accuracy and bias were assessed at three concentrations (n=6) and the resultant data are summarized in Table 4.8. They indicate that the method was accurate in accordance with the criteria set in our laboratory as defined in Chapter 3, § 3.5.4.

Table 4.8: *Accuracy results for blinded EFV samples*

Theoretical concentration (µg/mL)	Mean concentration determined (µg/mL)	% RSD	% Bias
7.50	7.80 ± 0.240	3.08	+3.85
33.50	32.78 ± 0.954	2.91	-2.20
65.50	64.94 ± 1.507	2.32	-0.86

4.2.4 Specificity

The peaks for EFV and IMI were well-resolved from the solvent front and no additional extraneous peaks were observed (Figure 4.9). A similar trend was also evident when EFV powder and solutions that had been exposed to stress conditions prior to analysis (§ 3.5.7) were analyzed, confirming that the method was specific for EFV.

4.2.5 Limits of quantitation (LOQ) and detection (LOD)

The LOQ and LOD were determined as described in Chapter 3 § 3.5.6. Different concentrations of EFV were analyzed (n=6) and LOQ data generated are listed in Table 4.9. A concentration of 5.0 µg/mL resulted in a % RSD value < 5% and this concentration was considered the LOQ for the method. The LOD was calculated as 0.3 x LOQ producing an LOD of 1.5 µg/mL.

Table 4.9: *LOQ data for HPLC analysis of EFV*

Conc(µg/mL)	MPHR (EFV/IMI)	SD	%RSD
1.0	0.0389	0.0044	11.39
1.5	0.0569	0.0046	8.01
2.0	0.0747	0.0132	17.67
2.5	0.1013	0.0136	13.41
5.0	0.1608	0.0069	4.29

4.2.6 Forced degradation studies and stability of EFV

EFV was exposed to different stress conditions including acid, base and neutral hydrolysis, dry heating, light, thermal and oxidation as described in Chapter 3, § 3.57. The data generated in these studies are summarized in Table 4.10 and typical chromatograms for EFV following exposure to stress conditions are shown in Figure 4.11. The acceptable degradation criteria used were similar to those stated in § 3.5.7.

Table 4.10: *Forced degradation results for EFV*

STRESS CONDITION	% RECOVERY	REMARKS
Light	64.78 ± 0.0055	Degradation
Heat (80°C)	94.39 ± 0.0221	Degradation
Acid Hydrolysis	99.58 ± 0.0463	No degradation
Alkali Hydrolysis	0.000 ± 0.0000	Degradation
Neutral Hydrolysis	99.50 ± 0.0357	No Degradation
Oxidative	0.000 ± 0.0000	Degradation
Dry Heat	98.64 ± 0.0604	No degradation

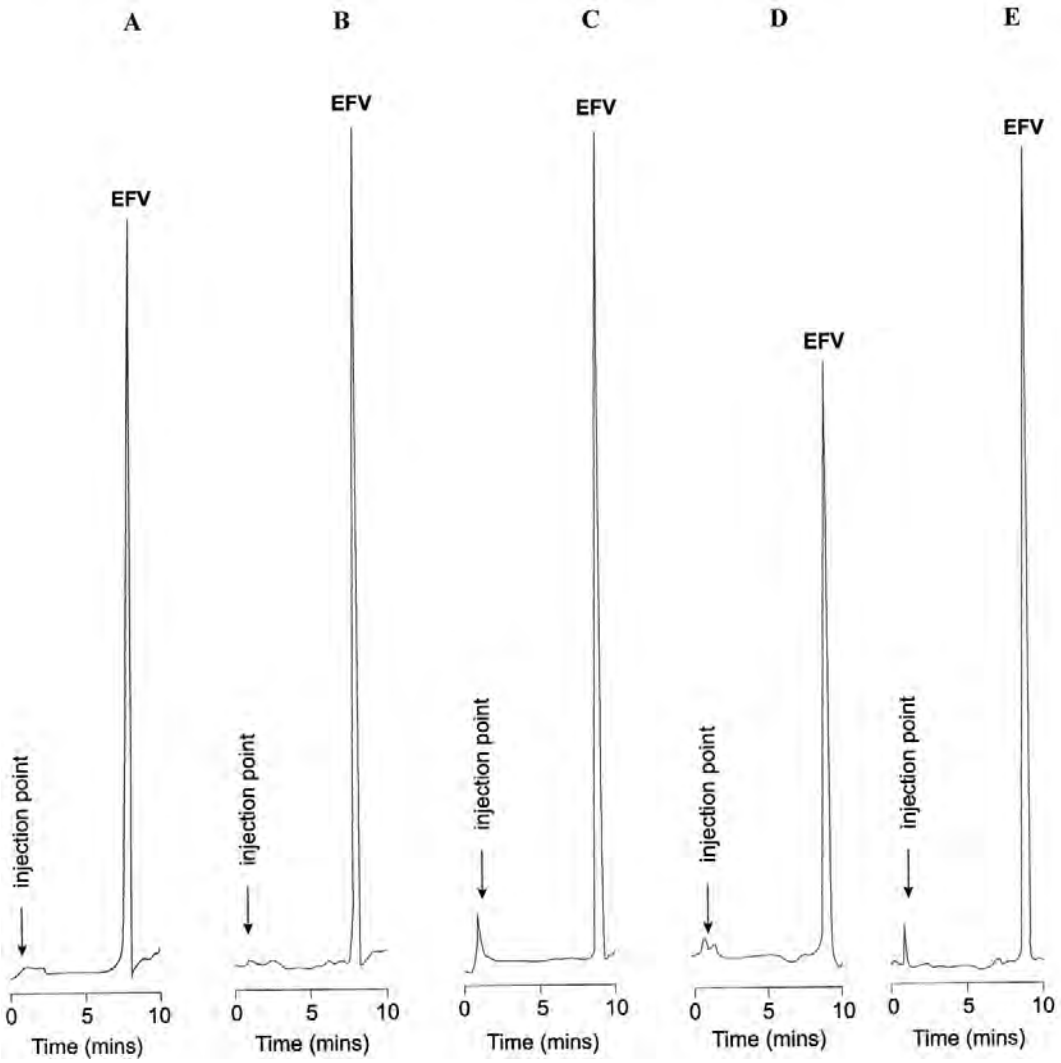

Figure 4.11:*Typical chromatograms showing stability and degradation of EFV following exposure to 70 °C(A), 0.1M HCL at 70 °C(B), HPLC grade water at 70 °C(C), 500 W h/m2 (D) and dry heat at 97 °C (E)*

Solutions of EFV undergo degradation to some extent when exposed to heat at 70°C for 8 hours (A). Base hydrolysis has been reported to be the major degradation pathway of EFV solutions due to the presence of a cyclic carbamate functional group [34].Consequently no peaks and ultimately no chromatograms were observed following exposure of EFV to alkaline conditions, confirming the loss of the oxidizing carbamate moiety of the molecule. Hydrogen peroxide facilitates oxidation of EFV, the consequence of which is the impairment of the ability of the drug to undergo electrochemical oxidation during HPLC-ECD analysis, resulting in no detection

of the analyte of interest. Exposure of EFV to UV light (D) resulted in approximately 35% degradation of EFV, confirming reports of the photolabile nature of EFV [343]. However UV-induced degradation does not result in the loss of the oxidizing potential of EFV, which implies that the molecule may be detectable in the presence of degradation products. EFV is stable when exposed to acidic (B), neutral (C) and dry heat (E) conditions.

The stability of EFV in the mobile phase was assessed over 3 days, resulting in a recovery of 99.963 ± 0.170 µg/mL (0.17% RSD). These data were adequate for the studies, as limits of ≤ 1 % RSD had been achieved for this parameter. Thus EFV was considered stable in the mobile phase for this period and the stock solution could be stored under the stated conditions and used within three days (§ 3.5.7.8).

4.3 APPLICATION OF THE METHOD

Commercially available Stocrin® 600 mg tablets were analyzed as described in § 3.6, Chapter 3, using the HPLC-ECD method that had been developed and validated. Similar to HPLC-UV, no interfering peaks were observed in the chromatograms, eliminating the possibility of any interference from excipients used by the manufacturer in the production of the tablets. A typical chromatogram of the analysis of EFV tablets is shown in Figure 4.12. Data generated from the assay studies revealed that the tablets contained on average 95.4 ± 3.244% of the label claim with a precision of 3.40% RSD. These data fall within the limits of 92-110% as specified in the USP [397].

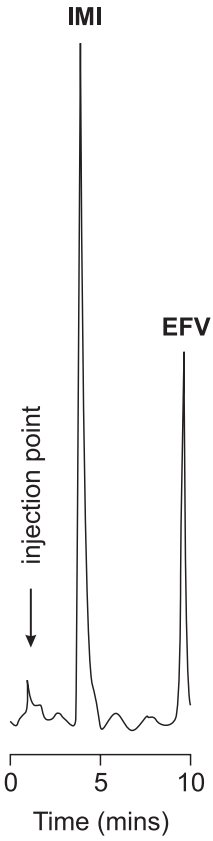

Figure 4.12: *Typical chromatogram for the assay of Stocrin®-600 mg tablets*

4.4 CONCLUSIONS

A stability-indicating RP-HPLC method using ECD has been developed and validated for the analysis of EFV in pharmaceutical dosage forms. The method is specific for EFV in the presence of degradation products. However the method is not as sensitive as the method using RP-HPLC with UV detection. In addition, the ability of EFV to oxidize appears to be relatively poor, as evidenced by the extremely high potential of +1400 mV required to achieve its oxidation. This high potential is attributed to the amine functional group attached to the carbamate portion of the molecule, which is known to have high oxidation potentials [400]. Furthermore EFV contains a highly electronegative substituted chlorine functionality that stabilizes the compound and makes oxidation difficult [400]. These high detector potentials lead to increased background noise and increased detector fouling and a loss of detector sensitivity, requiring the electrode to be

regenerated daily by cleaning and/or polishing [414,415]. This is a tedious process when large numbers of samples are to be analyzed on a daily basis. The relatively low sensitivity also suggests that the method may not be suitable to analyze *in vitro* release of EFV from SLN/NLC, which will contain relatively low doses of the drug. Therefore on the basis of risk-to-benefit ratio the RP-HPLC method with UV detection (Chapter 3) was selected as the most suitable method for the quantitative determination of EFV in pharmaceutical formulations. This method was applied to *in vitro* release studies of EFV from SLN and/or NLC.

CHAPTER 5

PRE-FORMULATION

5.1 INTRODUCTION

Hot high-pressure homogenization is the most effective and reliable technique for the manufacture of nanoparticles, compared to methods using high shear mixing and ultrasound [126,232]. Hot high-pressure homogenization (HHPH) was therefore selected for the production of EFV-loaded SLN and NLC. The technique involves exposing an API/ lipid(s) mixture to temperatures 5-10°C above the melting point of the solid lipid used, and then mixing with a surfactant solution maintained at the same temperature, resulting in the formation of a pre-emulsion [163]. The pre-emulsion is forced through a high-pressure homogenizer maintained at similar temperatures to ensure that the molten state of the lipid is preserved throughout the process [163]. However the use of high temperatures may lead to the degradation of API molecules and/or change the physicochemical properties of an API and/or those of the solid lipid used [126]. Therefore it is vital that the thermal stability of an API be investigated and established prior to attempting to incorporate the molecule into nanoparticles using HHPH. In addition, the potential effects of exposing an API to relatively high temperatures on the crystalline and polymorphic nature of the chemical entity are an essential part of pre-formulation studies.

Another important aspect needing consideration prior to the development and optimization of EFV-loaded SLN/NLC is the solubility of the molecule in the lipids used. The usefulness of SLN and/or NLC as API carrier systems is usually dependent on the LC and the EE of the nanoparticles for a particular API [166], yet a major factor affecting the LC and EE of SLN and/or NLC for an API is the solubility of an API in the molten lipid [127,163,222]. Thus an adequate LC and EE can be achieved only when the solubility of an API in the molten lipid is relatively high [127,163,222]. Consequently it is important to evaluate the solubility of the API

in different solid and liquid lipids, with the primary aim of selecting a solid and/or liquid lipid combination with the best solubilizing potential for the API.

Furthermore, the production of NLC involves mixing lipid molecules that are spatially different, *viz*. solid and liquid lipids, and invariably results in the melting point of the solid lipid decreasing [170,223,416]. Nevertheless, NLC must remain solid at room and body temperatures and therefore as a general rule the melting point of the solid lipid to be used should be higher than 40°C [170,223,416] following combination with the liquid lipid. In addition the solid lipid should be miscible with the liquid lipid to permit the formation of imperfections in the crystal structure of the solid lipid [233,417]. Therefore the impact of a liquid lipid on the polymorphic nature of the solid lipid must also form part of pre-formulation studies.

5.2 MATERIALS AND METHODS

5.2.1 Materials

The following sections provide a list of all the lipids used in solubility studies. An exhaustive description of the lipids selected and deemed suitable for use in formulation development and optimization studies of SLN and NLC is given in § 6.2.1, Chapter 6. All solid and liquid lipids used in these studies have GRAS (Generally Regarded as Safe) status and have been shown to be suitable for oral use. EFV was donated by Aspen® Pharmacare (§ 3.3.3.1). The physicochemical properties, stability, clinical pharmacology and pharmacokinetics of EFV were described in Chapter 1 and will not be repeated in this Chapter. HPLC grade water was prepared as described in Chapter 3 (§ 3.3.3.1).

5.2.1.1 Solid lipids

Gelucire® 43/01 (glyceryl esters of saturated fatty acids), Compritol® 888 (glyceryl behenate) and Precirol® ATO 5 (glyceryl distearate) were donated by Gattefossé SAS (Gattefossé SAS, Saint-Priest Cedex, France). Glyceryl monostearate was purchased from Aspen® Pharmacare (Port Elizabeth, Eastern Cape, South Africa).

5.2.1.2 Liquid lipids

Lauroglycol™ 90 (propylene glycol monolaurate type II), Lauroglycol™ FCC (propylene glycol monolaurate type I), Capryol™ PGMC (propylene glycol monocaprylate type I), Labrafac™ Lipophile WL1349 (medium chain triglycerides), Geloil™ SC (soya bean oil and glyceryl distearate polyglyceryl-3 dioleate), Labrasol® (caprylocaproyl macrogol-8 glycerides), Labrafac™ PG (propylene glycol dicaprylocaprate), Labrafil® M1944CS (oleoyl macrogol-6 glycerides), Transcutol® HP (diethylene glycol monoethyl ether), Capryol™ 90 (propylene glycol monocaprylate type II), Labrafil® M2125CS (linoleoyl macrogol-6 glycerides) were donated by Gattefossé SAS (Gattefossé SAS, Saint-Priest Cedex, France).

5.2.2 Methods

5.2.2.1 Characterization of EFV

5.2.2.1.1 TGA characterization

The thermal stability of EFV was investigated using a Perkin-Elmer® FT-IR thermogravimetric analyzer (Perkin-Elmer® Ltd, Connecticut, USA). An aliquot of 1.743 mg EFV was weighed prior to analysis. The sample was heated between 30 and 650°C at a heating rate of 10°C/min. The TGA system was constantly purged with liquid nitrogen at a flow rate of 20 ml/min, and data generated were manipulated using Pyris™ Manger Software (Perkin-Elmer® Ltd, Connecticut, USA).

5.2.2.1.2 FT-IR characterization

The characteristic structural bands of EFV were investigated using a Perkin-Elmer® Precisely FT-IR spectrometer Spectrum 100 (Perkin-Elmer® Pty Ltd, Beaconsfield, England). The bands are shown in Figure 1.3 (§ 1.2.10).

5.2.2.1.3 DSC characterization

The melting point of EFV was determined using a Model Q100 differential scanning calorimetry (DSC) fitted with a RCS (90) refrigerated cooling system (TA instruments, Lukens Drive New Castle, DE, USA). An aliquot of 3.721 g of EFV [229] was weighed directly into a standard 40 µl aluminum open pan. The DSC scan was generated by heating the sample from 22°C to 250°C and then cooling for one cycle to 22°C at heating and cooling rates of 10°C/min. The system was purged with liquid nitrogen at a flow rate of 100 ml/min, and the resultant data were analyzed using the TA Universal Analysis 2000 for Windows software (TA instruments, Lukens Drive New Castle, DE, USA). The DSC data for EFV were generated prior to and following exposure to a temperature of 70°C for one hour in order to establish whether thermal exposure had an effect on physicochemical properties of the molecule.

5.2.2.1.4 WAXS characterization

Wide-angle X-ray scattering (WAXS) patterns of EFV were recorded using a Model D8 Discover X-ray diffractometer (Bruker, Billeria, MA, USA) that was equipped with a PSD LynxEye detector coupled to a copper anode (Cu-Kα radiation, λ = 1.5405 Å, 30 kV) fitted with a nickel filter. Samples were placed on a zero background (511) silicon wafer embedded in a generic sample holder. The data were recorded at room temperature (22°C) using a 2θ range between 10˚ and 100˚, a scanning rate of 1˚ min^{-1}, a filter time constant of 2.0 s per step and a slit width of 6.0 mm. The data were fitted using evaluation (Eva) curve-fitting software (Bruker, Billeria, MA, USA). All samples used for WAXS analysis were identical to those used for DSC studies in order to ensure ease of data comparison and characterization.

5.2.2.2 Screening of lipids

5.2.2.2.1 Selection of solid lipids

The solubility of EFV in different solid lipids was determined visually by dissolving increasing amounts of the API in a fixed amount of molten lipid [223]. Initially 0.1 g EFV and 1.0 g of the solid lipid were accurately weighed using a Model PA 2102 Ohaus® top-loading analytical balance (Ohaus® Corp. Pine Brook, NJ USA) and transferred into a glass test tube (Pyrex® Laboratory Glassware, England). The sample was then exposed to heat for one hour using a LABOTEC® shaking water bath (Laboratory Thermal Equipment, Greenfield NR. Oldham) set at the temperature and speed of 70°C and 100 rpm respectively. The disappearance of EFV crystals in the molten dispersion was visually observed and was used as an indication of the solubility of EFV in the lipid. Following dissolution an additional 0.1 g aliquot of EFV was added until saturation was observed and no additional EFV was able to dissolve in the molten lipid after shaking for 24 hours at 70°C.

5.2.2.2.2 Selection of liquid lipids

The saturation solubility of EFV in different liquid lipids was determined in a manner similar to that described in § 5.2.2.2.1.

5.2.2.2.3 Selection of a binary mixture of solid and liquid lipid

The solid and liquid lipids with the greatest solubilizing potential for EFV as identified from the studies described in § 5.2.2.2.1 and 5.2.2.2.2, were mixed in various ratios to determine a binary mixture of solid and liquid lipid material that would be suitable for use for the manufacture of NLC. The miscibility of the two components was evaluated using a total lipid mixture of 1.0 g in the following ratios of solid lipid : liquid lipid : 95:5, 90:10, 85:15, 80:20, 75:25, 70:30, 60:40, 50:50 and 40:60. Samples were weighed directly into a glass test tube and placed into a LABOTEC® shaking water bath (Laboratory Thermal Equipment, Greenfield NR. Oldham) for one hour with the temperature and speed set to 70°C and 100 rpm respectively. The samples

were allowed to cool to room temperature (22°C) for 24 hours prior to analysis. The miscibility of the two lipids was evaluated by smearing a small sample of the dried mixture onto hydrophilic filter paper (Whatman® 110 diameter filter papers, Whatman® International Ltd, Maidstone, England) prior to visual inspection for the presence of oil droplets. A miscible binary mixture of lipids for which EFV potentially exhibited the highest solubility was selected for formulation of NLC, and the melting point was determined using DSC to confirm that it was > 40°C.

5.2.2.3 Polymorphism and crystallinity of bulk lipids

Polymorphic modifications of solid lipid matrices may affect the incorporation of an API into SLN and/or NLC [417,418]. It has been suggested that the degree of crystallization and polymorphic transitions of solid lipids following exposure to heat, such as for example during HHPH, may influence API incorporation and release rate from SLN and/or NLC which would have a subsequent impact on the ultimate quality of the product [126,127,176]. The production of SLN and/or NLC using HHPH requires the solid lipid to melt prior to dissolving an API in the lipid. The API-containing lipid melt is dispersed in a hot surfactant solution to yield a pre-emulsion. Homogenization of the pre-emulsion gives rise to a hot o/w nano-emulsion that on cooling results in recrystallization of the solid lipids with subsequent *in situ* formation of nanoparticles [417] (§ 2.4.1.1). Consequently analysis of SLN and/or NLC using DSC for the determination of the impact of additional melting processes on the properties of solid lipid(s) is essential. Therefore prior to homogenization of the pre-emulsion, the lipid would have been melted during API dissolution, necessitating a second DSC scan of the bulk lipid(s) during characterization of the bulk material [417]. However the use of DSC to characterize bulk lipids following exposure to heat, and which mimics the API dissolution stage of manufacture, would require only a single DSC scan corresponding to the analysis of SLN and/or NLC [233]. DSC in conjunction with WAXS was therefore used to characterize the polymorphic modifications of the bulk lipids.

5.2.2.3.1 DSC characterization

DSC characterization of the lipids was performed using the system described in § 5.2.2.1.3. DSC scans of bulk solid lipid and binary mixtures of solid and liquid lipid were generated by heating samples from 22°C to 250°C and subsequently cooling to 22°C at heating and cooling rates of 10°C/min. The mass analyzed was 3-5 mg, and all samples were analyzed prior to and after exposure to a temperature of 70°C for one hour.

5.2.2.3.2 WAXS characterization

WAXS patterns of bulk solid lipid and binary mixtures of solid and liquid lipids were generated using the system described in § 5.2.2.1.4. All samples were analyzed prior to and following exposure to a temperature of 70°C for one hour. The samples were similar to those used to generate DSC data so as to simplify assessment and analysis of data. The scattering angles observed from WAXS diffraction patterns were transformed into short spacing using Bragg's equation (Equation 5.1) [419] so as to generate information about lipid modifications.

$$d = \frac{\lambda}{sin\ 2\theta} \qquad \textbf{\textit{Equation 5.1}}$$

Where

d = inter-atomic distance
λ = wavelength of an X-ray beam
θ = the angle of incidence of the beam

5.2.2.4 Interaction of bulk lipids with EFV

Potential physical interactions between lipid excipients and EFV were investigated using FT-IR, DSC and WAXS using the equipment described in § 5.2.2.1.2, 5.2.2.1.3 and 5.2.2.1.4. Binary mixtures of solid lipid and EFV in addition to a ternary mixture of the solid lipid, liquid lipid and EFV were analyzed prior to and following exposure to a temperature of 70°C for one hour.

5.3 RESULTS AND DISCUSSION

5.3.1 Characterization of EFV

5.3.1.1 TGA characterization

TGA is used to measure changes in the physicochemical properties of materials as a function of increasing temperature at a constant rate [420,421]. The loss in weight of EFV and the artificial derivative of the TGA profile for the molecule was recorded as a function of increasing temperature and correlated to the thermal stability of the compound. These data are shown in Figures 5.1 and 5.2.

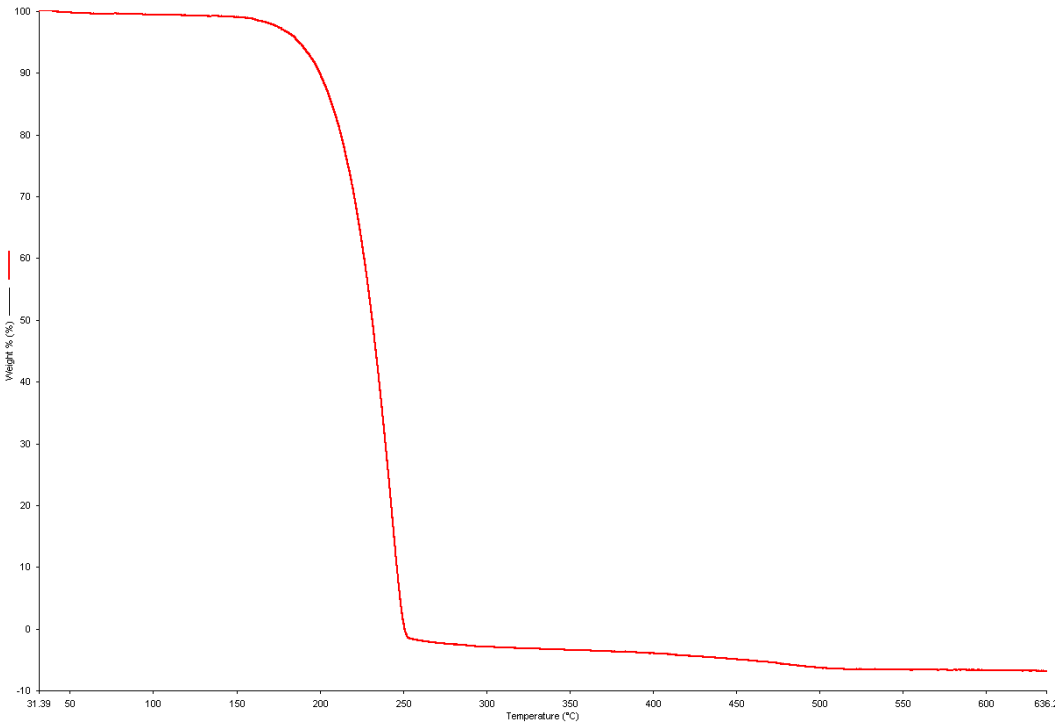

Figure 5.1: *TGA curve for EFV generated at a heating rate of 10°C/min*

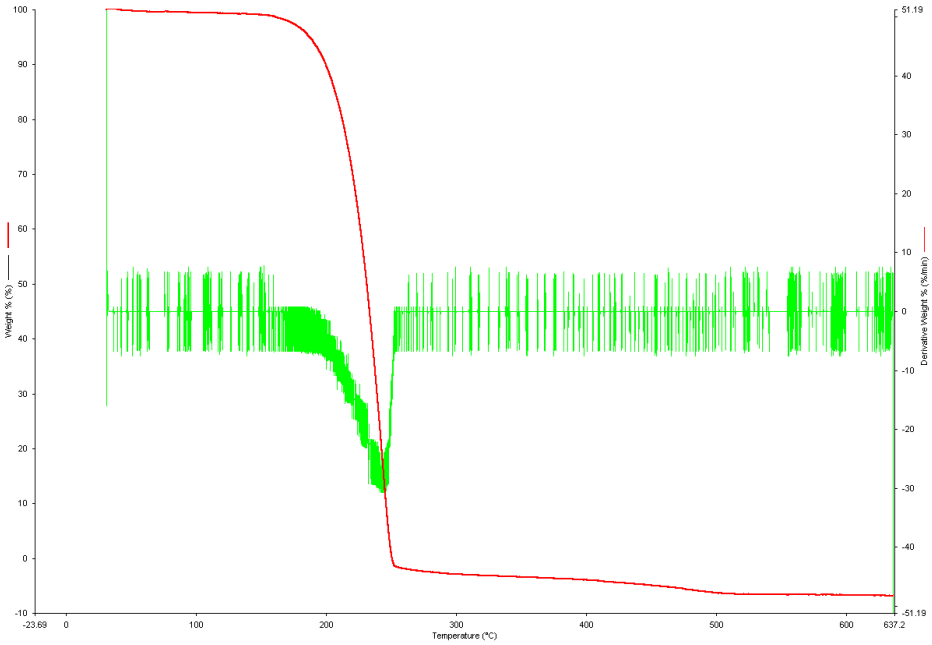

Figure 5.2: *TGA curve for EFV (red) and the artificial derivative generated following heating at a rate of 10°C/min*

These data clearly indicate that the weight of EFV remains constant when it is exposed to heat up to a temperature of approximately 200°C after which thermal degradation of the molecule, that is in the molten state, occurs leading to 100% weight loss. These results are in agreement with previously reported data [422]. It is evident that EFV is thermostable at temperatures ranging between 70 and 80°C, and therefore the molecule is likely to be stable during solubility studies and manufacture of SLN and/or NLC using HHPH.

5.3.1.2 DSC characterization

The melting behavior, crystalline and polymorphic nature of anhydrous EFV prior to and following exposure to a temperature of 70°C for one hour was evaluated using DSC. The molecule was exposed to heat for one hour to mimic the length of time over which the molecule was expected to be exposed to heat during the manufacture of the nanoparticles. The DSC data generated in these studies are shown in Figure 5.3 and are summarized in Table 5.1. Data showing the difference between the onset and melting temperature, or the width of the peak

(WP) can be used to determine lattice defects in crystalline materials [223,233] are also summarized in Table 5.1.

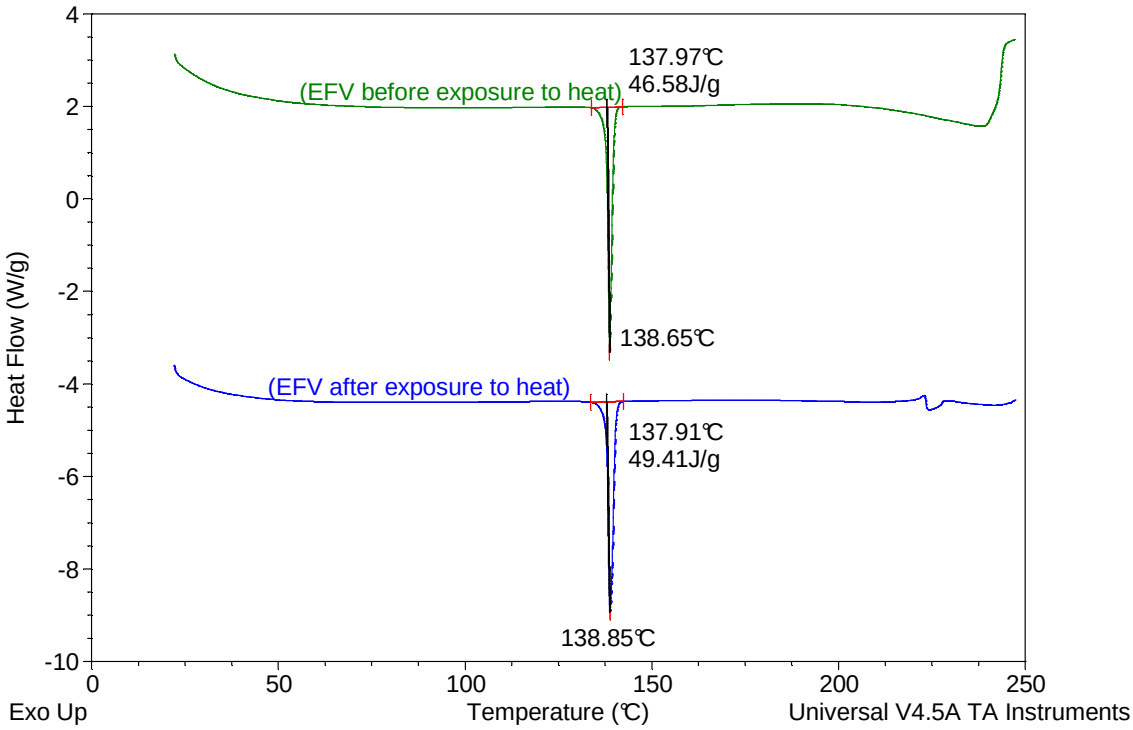

Figure 5.3: *DSC thermograms for EFV prior to and following exposure to a temperature of 70°C for one hour*

Table 5.1: *DSC parameters for EFV prior to and following exposure to a temperature of 70°C for one hour*

Efavirenz	Thermal event	Onset (°C)	MP (°C)	Enthalpy (J/g)	WP (°C)
Prior to heating	Endothermic	137.97	138.65	46.58	0.68
After heating	Endothermic	137.91	138.85	49.41	0.94

The DSC data for EFV reveal the presence of a sharp single melting endotherm at 138.65°C (enthalpy = 46.58 J/g) and 138.85°C (enthalpy = 49.41 J/g) respectively. These data clearly indicate that EFV exists as a single polymorph and that the polymorphic nature of the molecule does not change following exposure to a temperature of 70°C for one hour. The sharp nature of the peak and its narrow WP of 0.68 observed prior to exposure to heat reveal that EFV is a highly crystalline material. Following exposure to heat the WP increases to 0.94, indicating that

heating EFV may disrupt the crystal structure of the molecule to some extent. Nevertheless the peak observed in the thermogram is sharp, thus revealing a lack of a significant change in the crystalline nature of the molecule following exposure to a temperature of 70°C. WAXS data were used to further interpret the DSC data that had been generated.

5.3.1.3 WAXS characterization

Confirmation of the DSC data reported in § 5.3.1.2 was undertaken using data derived from WAXS studies and the resultant diffractograms are shown in Figure 5.4.

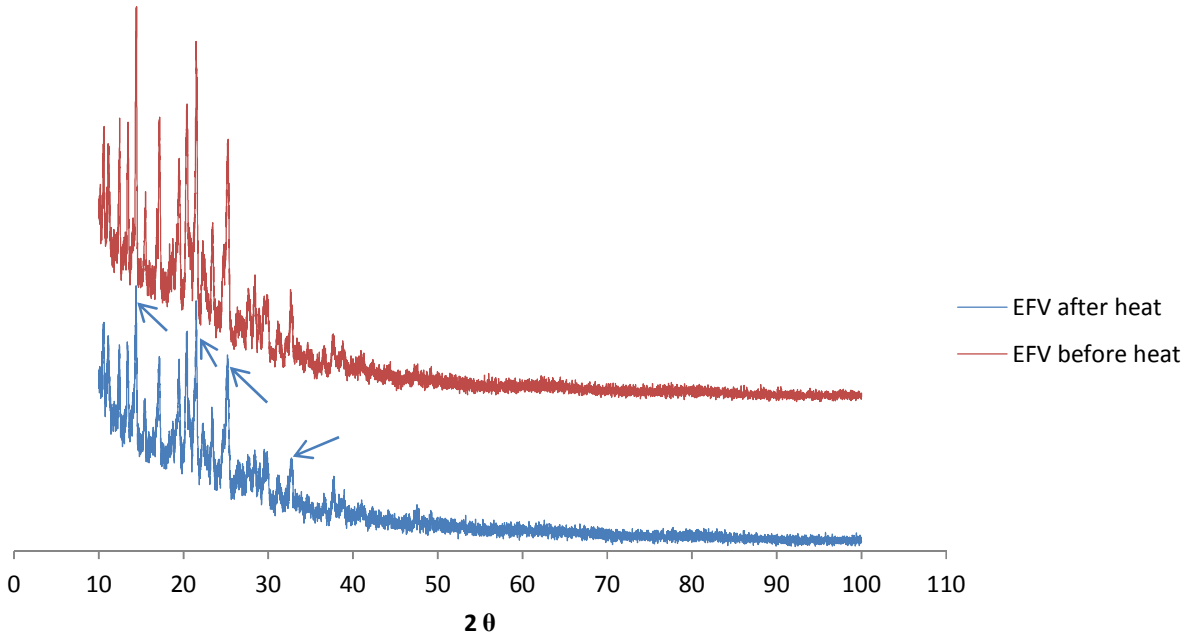

Figure 5.4: *WAXS patterns for EFV prior to (red) and following (blue) exposure to a temperature of 70°C for one hour*

The WAXS profiles for EFV prior to and following exposure to heat show the presence of similar diffraction bands characteristic of the crystalline form of the molecule. The data confirm that EFV retains a crystalline state following exposure to 70°C for one hour. However there is a decrease in peak intensity of the WAXS diffraction patterns for EFV following exposure to heat

(indicated by arrows) that may be attributed to a decrease in the degree of crystallinity of EFV. This finding is in agreement with that observed with DSC data that revealed slight disruption in the crystalline nature of EFV following exposure to a temperature of 70°C for one hour.

5.3.2 Screening of lipids

5.3.2.1 Selection of a solid lipid

The solubility of EFV in various solid lipids was determined with the primary aim of selecting a solid lipid with the best solubilizing potential for EFV. The resultant data are shown in Figure 5.5.

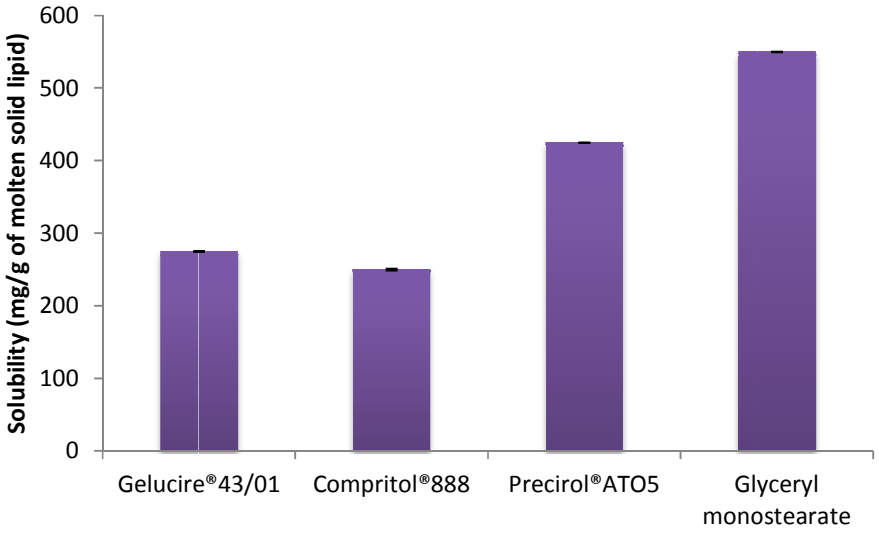

Figure 5.5: *The solubility of EFV in 1.0 g of various solid lipids at 70°C (n=3)*

These data reveal that EFV is soluble to some degree in the solid lipids investigated, but glyceryl monostearate (GM) exhibited the best-solubilizing potential for the molecule. The presence of mono- and diglycerides in a lipid matrix has been shown to promote API solubilization [127], which is consistent with the results observed in these studies. GM and Precirol® ATO 5 (glyceryl distearate) exhibited a solubilizing potential for EFV that was better than that observed for Gelucire® (glyceryl esters) and Compritol® (glyceryl behenate). Therefore GM was selected as

the solid lipid for use in formulation development and optimization studies of EFV-loaded SLN and NLC.

5.3.2.2 Selection of a liquid lipid

In contrast to SLN, the primary difference in structure of NLC is the formation of a nano-structured lipid matrix system capable of incorporating and maintaining a relatively large payload of API [162,166]. Therefore the structural matrix of NLC requires the addition of a liquid lipid that results in the formation of a less ordered lipid matrix with imperfections that can ultimately accommodate greater quantities of API [162,166]. It was therefore necessary to select a suitable liquid lipid for use in the formulation and manufacture of EFV-loaded NLC. The solubility of EFV in various liquid lipids was investigated in order to select a liquid lipid with the best solubilizing potential for the molecule. These data are shown in Figure 5.5.

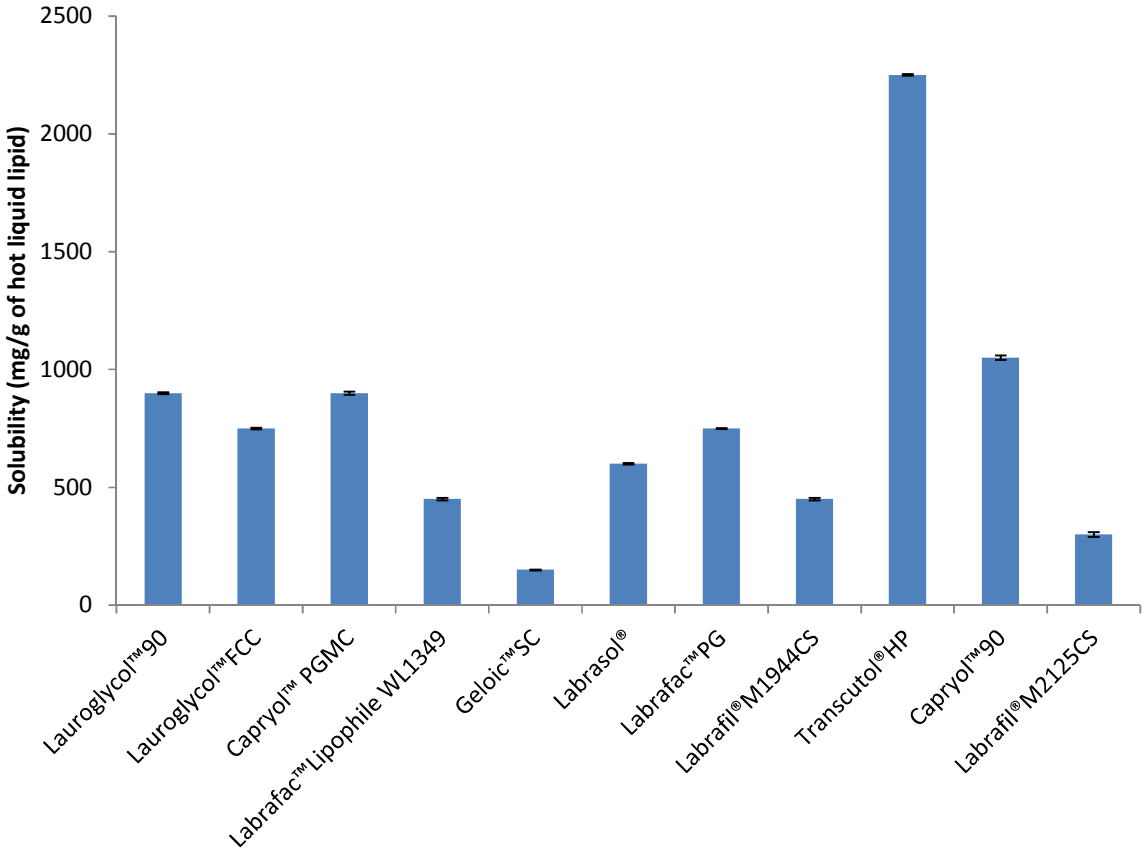

Figure 5.6: *Solubility of EFV in 1.0 g of various liquid lipids at a temperature of 70°C (n=3)*

These data reveal that EFV is highly soluble in Transcutol® HP (THP), which is a combination of diethylene glycol monoethyl ethers [423]. Consequently THP was selected as the liquid lipid for use in formulation development and optimization studies of EFV-loaded NLC.

5.3.2.3 Determination of a solid and liquid lipid binary mixture ratio

The primary aim of these studies was to establish the best composition of a binary mixture of GM and THP for the formulation and manufacture of EFV-loaded NLC. The lipids were mixed in various ratios and exposed to a temperature of 70°C for one hour and then allowed to cool to room temperature (22°C). An aliquot of each sample was smeared onto hydrophilic filter paper

(Whatman® 110 diameter filter papers, Whatman® International Ltd, Maidstone, England) to assess the miscibility of the lipids by visual observation. The presence of liquid lipid droplets on the filter paper was a clear indication of poor miscibility of the lipids, and any binary mixture in which droplets were observed was deemed unsuitable for use. The data generated in these studies are summarized in Table 5.2.

Table 5.2: *Visual observation data for assessment of miscibility of binary mixtures of GM and THP*

GM : THP	Visual observation
95:5	No oil droplets observed on filter paper
90:10	No oil droplets observed on filter paper
85:15	No oil droplets observed on filter paper
80:20	No oil droplets observed on filter paper
75:25	No oil droplets observed on filter paper
70:30	No oil droplets observed on filter paper
60:40	Oil droplets observed on filter paper
50:50	Oil droplets observed on filter paper
40:60	Oil droplets observed on filter paper

When formulating NLC it is considered ideal to incorporate a relatively large amount of oil into a solid lipid to improve the solubility of the API and subsequently increase the loading capacity of the NLC for that API [170,223,416]. However the lipids must be miscible at the concentrations used [170,223,416], and the binary mixture must exhibit a melting point > 40°C [170,223,416]. The results generated in these studies reveal the absence of THP droplets on the filter paper following addition to GM up to a concentration of 30% w/w. However, the presence of THP droplets on the filter paper was observed when ≥ 40% w/w of the liquid lipid was added, providing evidence that THP and GM are immiscible when relatively high amounts of the liquid lipid are added to solid material. Consequently, a binary mixture of GM and THP (70:30) was considered the most suitable combination for the formulation and manufacture of EFV-loaded NLC. This binary mixture commenced melting at 49.32°C, which is relatively high compared to 40°C.

5.3.3 Characterization of raw material

5.3.3.1 Glyceryl monostearate (GM)

5.3.3.1.1 FT-IR characterization

The FT-IR profiles generated for GM prior to and following exposure to heat are shown in Figure 5.7 and the relevant band assignments of the principal peaks are summarized in Table 5.3.

Table 5.3: *IR frequency bands for GM*

Frequency (cm^{-1})	Vibrational Assignments
3384	-OH group
2950-2910	C-H stretching
1733	ester carbonyl group

The FTIR spectrum of GM showed characteristic peaks for the –OH group at 3384 cm^{-1}, C-H stretch at 2950-2910 cm^{-1} and an ester carbonyl group at 1733 cm^{-1}. These band assignments are characteristic of GM [98]. Following exposure to heat, the major peaks (circled) of GM did not change, indicating that no vibrational energy changes of chemical bonds were observed as shown in Figure 5.7.

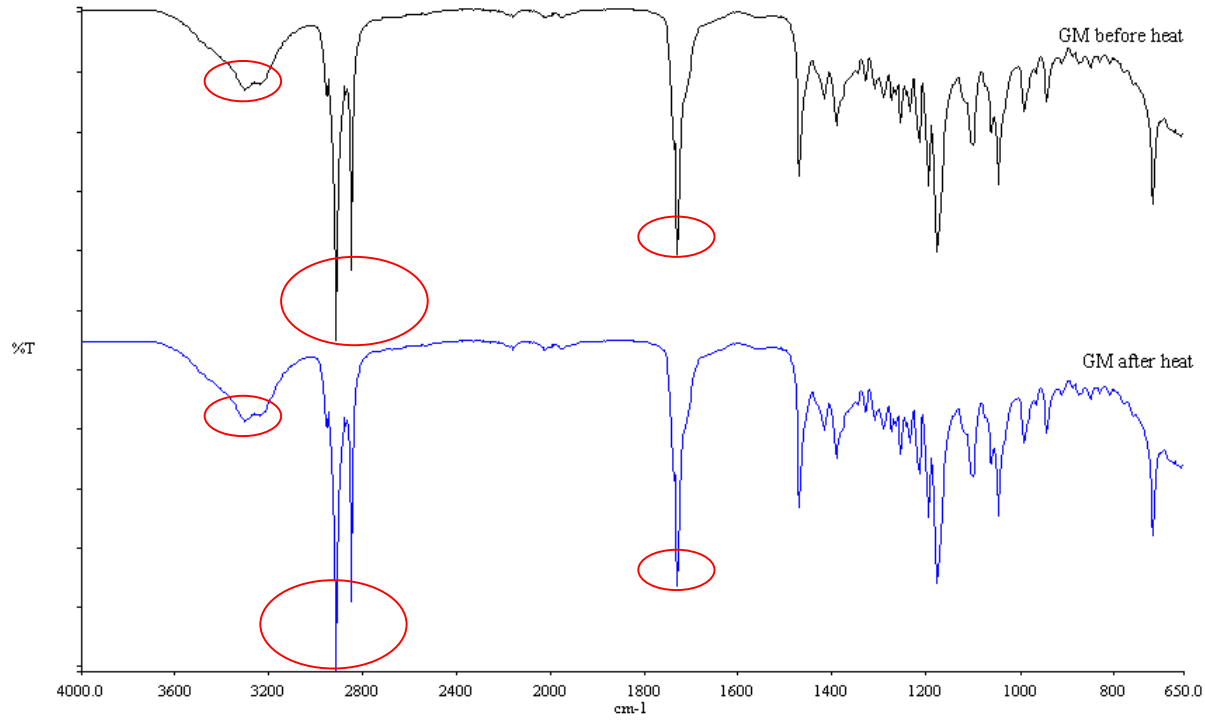

Figure 5.7: *FT-IR spectrum of GM prior to and following exposure to a temperature of 70°C for one hour.*

5.3.3.1.2 DSC characterization

The DSC thermograms of GM prior to and following exposure to a temperature of 70°C for one hour are shown in Figure 5.8, and the melting events observed are summarized in Table 5.3. The thermogram generated prior to heating (run 1) reveals the presence of a single peak at an onset temperature and melting point of 55.03°C and 61.12°C respectively. This is consistent with the β'-modification of GM [424] and is confirmation that the solid lipid exists as a single polymorphic form prior to exposure to heat. In addition the data reveal that the melting enthalpy for the initial study was 224.3 J/g. This value is relatively high compared to those obtained following exposure to DSC analysis for a second time (73.91 J/g) and first run following exposure to heat (87.20 J/g). This indicates that GM is in a highly crystalline state prior to exposure to heat.

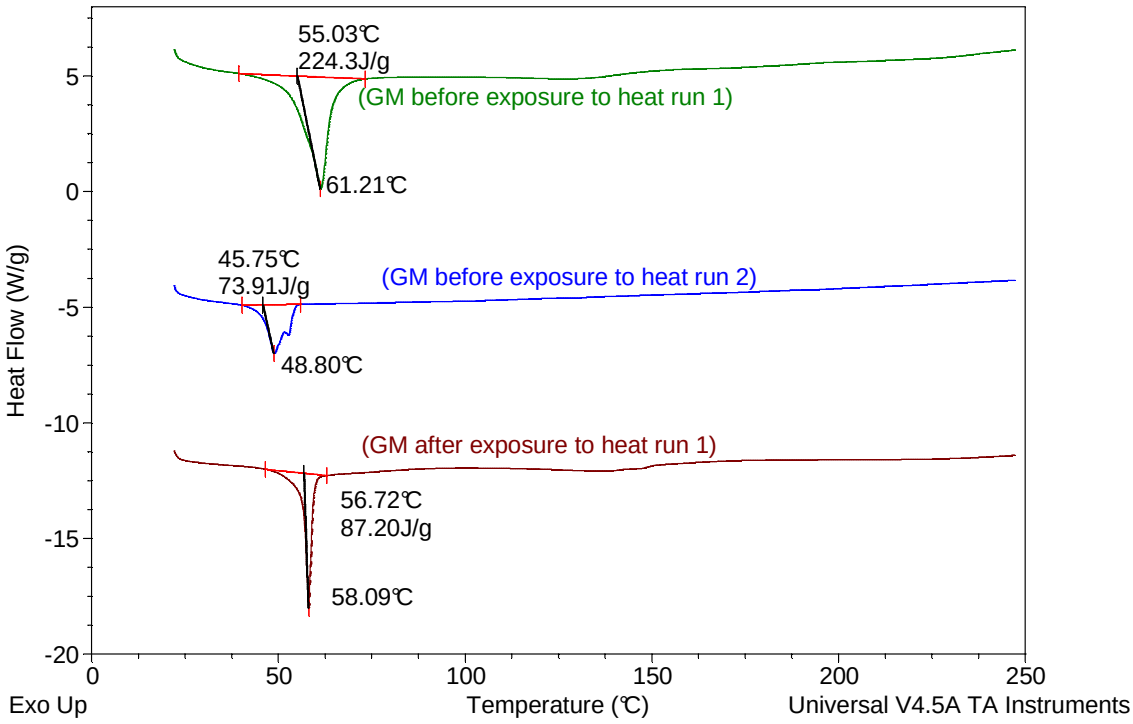

Figure 5.8: *DSC thermograms of glyceryl monostearate generated prior to and following exposure to a temperature of 70°C for one hour*

Table 5.4: *DSC parameters for glyceryl monostearate prior to and following exposure to a temperature of 70°C for one hour*

Glyceryl monostearate	Thermal event	Onset (°C)	MP (°C)	Enthalpy (J/g)	WP (°C)
Prior to heating run 1	Endothermic	55.03	61.21	224.3	6.18
Prior to heating run 2	Endothermic	45.75	48.80	73.91	3.05
After heating	Endothermic	56.72	58.09	87.20	1.37

The thermogram generated following a second DSC scan of the same sample of GM (run 2) reveals the presence of two peaks, with the onset temperature of the major peak reduced from 55.03 to 45.75°C. The presence of two peaks may be attributed to the presence of β' and α-modifications of GM [417]. Therefore it is clear that GM recrystallizes to form two polymorphic forms following exposure to heat. It is also evident that the melting enthalpy of the thermogram following a second DSC run (73.91 J/g) was lower than that observed when the sample was subjected to a single DSC run (224.3 J/g), which may be due to the fact that following an isothermal phase at 22°C for approximately 10 minutes, the molten lipid had not yet been fully recrystallized.

Exposure of GM to a temperature of 70°C for one hour prior to DSC analysis revealed a single endotherm peak with an onset temperature and melting point of 56.72°C and 58.09°C respectively, revealing the presence of a single polymorphic form for GM. This can be attributed to complete α-modification of the compound. In addition the low enthalpy of 87.20 J/g suggests a less crystalline lattice structure of GM in comparison to that observed for GM prior to exposure to heat (224.3 J/g), implying the presence of an α-modification of the material. Although DSC is a useful analytical tool for investigating the polymorphic nature of solid lipids, WAXS should also be used to ensure that the data obtained using DSC are corroborated and are reliable.

5.3.3.1.3 WAXS characterization

The WAXS diffraction patterns of glyceryl monostearate prior to and following exposure to a temperature of 70°C for one hour are shown in Figure 5.9.

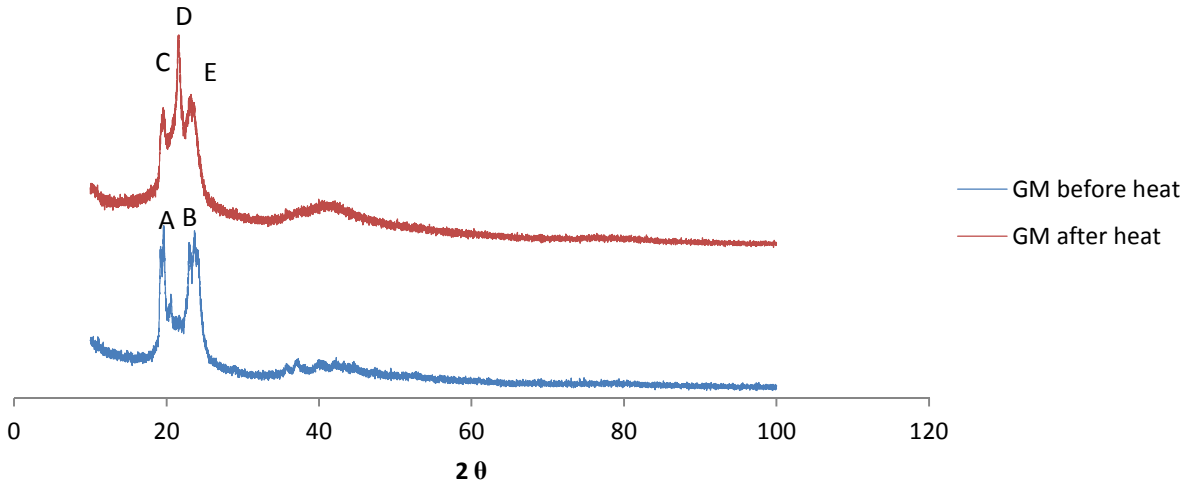

Figure 5.9: *WAXS patterns of glyceryl monostearate generated prior to (blue) and following (red) exposure to a temperature of 70°C for one hour*

WAXS was used to investigate the lamellar arrangement of the lipid molecule and the crystallinity of fatty acid chains in the acylglycerols of GM. GM is a mixture of mono-, di- and triacylglycerols (§ 6.2.1.1.). Due to differences in chain length of the fatty acids in the acylglycerols (palmitic and stearic acids) and three hydroxyl groups of glycerol, a β'-modification occurs [417].

The difference observed in the WAXS of GM prior to and following exposure to a temperature of 70°C is clearly shown in Figure 5.8. Exposure of GM to heat leads to an increase in the intensity of peak A, that is a consequence of a drastic decrease in the crystallinity of side chains. The increase in peak intensity and decrease in side chain crystallinity suggests that heating of the lipid creates defects in the lamellar structure of the lipid that may possibly lead to polymorphic transitions. The diffraction patterns reveal scattering peaks around peak A that permits the identification of lipid modifications [417]. Generally lipid modifications can be identified using four criteria from WAXS diffraction patterns when plotting intensity *versus* scattering vectors [417,425]. These include (i) modification with a single scattering reflex of the lipid side chain of

the glycerol at a Bragg distance of 0.415 nm confirming an α-modification [417,425], (ii) modification with two reflexes at Bragg distances of 0.389 nm and 0.420 nm confirming a β'-modification [417,425], (iii) a β_i-modification identified by the presence of three reflexes at Bragg distances of 0.389, 0.420 and 0.460 nm, and (iv) a modification which does not meet these criteria confirms the presents of a β-modification [417,425]. The Bragg spacing distances were calculated using Equation 5.1 and used to identify the polymorphic modifications of glyceryl monostearate prior to and following exposure to a temperature of 70°C for one hour.

GM shows two scattering reflections identified as A and B prior to heating, corresponding to Bragg distances of 0.420 and 0.385 nm respectively. This is indicative of a highly crystalline β'-modification form and is consistent with the DSC data observed. WAXS patterns of GM generated following heating reveal the presence of three scattering reflections identified as C, D and E, corresponding to Bragg distances of 0.420, 0.461 and 0.398 nm respectively, and which are indicative of the presence of a β_i-modification. However DSC data reveal the presence of a single polymorph following exposure of GM to heat. Although WAXS was able to detect the presence of two additional scattering reflections it should be noted that the scattering reflection D, located at a Bragg spacing of 0.420 nm, was significantly greater in intensity than those observed for B and C. This is consistent with the presence of the less crystalline α-modification form in the lipid lattice following exposure to heat. DSC and WAXS reveal that exposing GM to heat results in a change in the crystalline nature of the lipid and ultimately the polymorphic form in which it exists. WAXS was used to confirm the lipid modifications determined on the basis of melting temperature and melting enthalpy following DSC analysis.

5.3.3.2 Glyceryl monostearate (GM) and Transcutol® HP (THP)

FT-IR, DSC and WAXS were used to investigate potential interactions, if any, between GM and THP, and to establish whether incorporation of a liquid lipid in GM had an influence on the polymorphic and crystalline nature of the solid lipid. A binary mixture of GM and THP at a ratio of 70:30 was exposed to a temperature of 70°C for one hour prior to cooling to room temperature (22°C) for analysis. The FT-IR, DSC and WAXS data for GM following exposure to a temperature of 70°C for one hour were used as reference data. DSC and WAXS data for the

binary mixture prior to exposure to heat was used to establish the melting behavior and diffraction patterns of GM and therefore these could not be used as reference data for this study.

5.3.3.2.1 FT-IR characterization

The FT-IR spectrum of GM and that of a binary mixture of GM and THP following exposure to a temperature of 70°C for one hour are shown in Figure 5.10. It is clearly evident that both spectra show bands characteristic for GM (circled), and that the incorporation of THP into GM did not result in the generation of additional peaks, confirming the lack of an interaction between the liquid and solid lipid. However a marked reduction in the intensity of the peaks was observed following the addition of THP, indicating the impact on molecular vibrations of GM by THP. DSC was consequently used to further investigate the effect of THP addition on the crystallinity and polymorphic nature of GM.

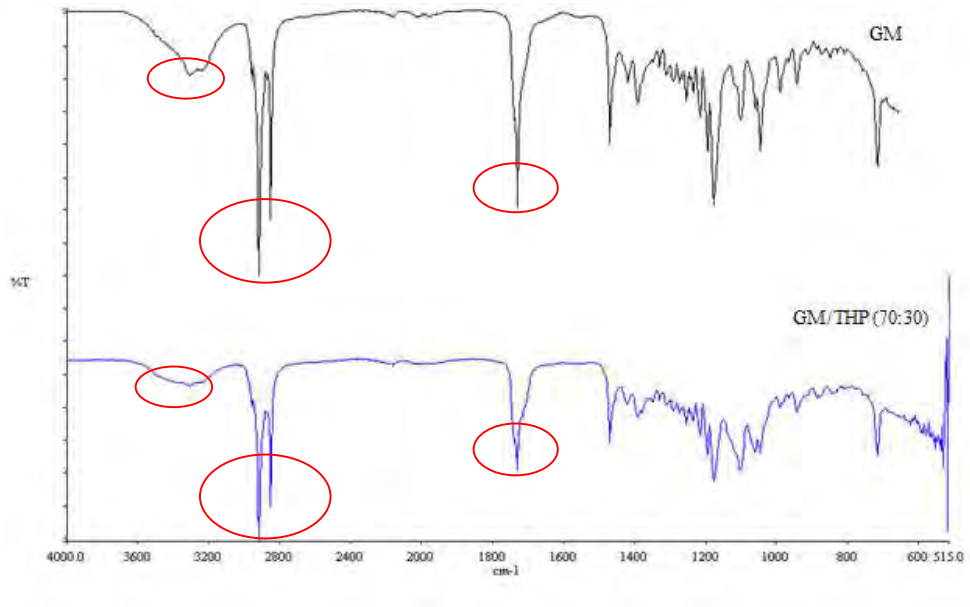

Figure 5.10: *FT-IR spectra for GM and a binary mixture of GM and THP generated following exposure to a temperature of 70°C for one hour*

5.3.3.2.2 DSC characterization

The DSC thermogram generated for GM and for a binary mixture of GM and THP following exposure of both samples to a temperature of 70°C for one hour is shown in Figure 5.11. The corresponding DSC parameters generated from the respective thermograms are summarized in Table 5.4.

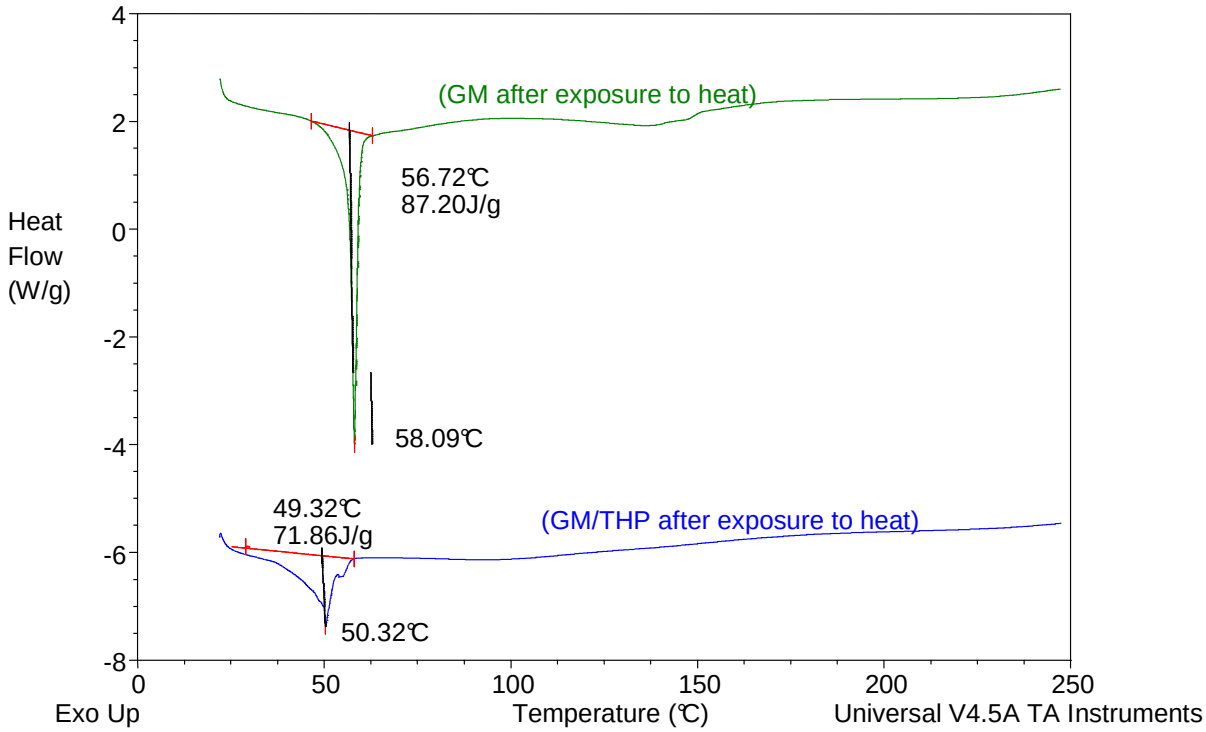

Figure 5.11: *DSC thermograms of GM and of a binary mixture of GM and THP generated following exposure to a temperature of 70°C for one hour*

Table 5.5: *DSC parameters for GM and of a binary mixture of GM and THP (70:30) generated following exposure to a temperature of 70°C for one hour*

Material	Thermal event	Onset (°C)	MP (°C)	Enthalpy (J/g)	WP (°C)
GM after heating	Endothermic	56.72	58.09	87.20	1.37
GM/THP (70:30) after heating	Endothermic	49.32	50.32	71.86	1.00

The data reported in § 5.3.3.1.2 revealed that GM existed in a highly crystalline β-modification form prior to heating, and following exposure to heat the polymorphic nature of GM changed to the less crystalline α-modification. The DSC thermogram of a binary mixture of GM and THP following exposure to a temperature of 70°C for one hour revealed the presence of two discrete peaks that are indicative of the co-existence of two polymorphic forms of GM. The melting onset of 49.32°C observed for the major peak corresponds to the presence of the less crystalline α-modification and the minor peak is representative of the more crystalline β'-modification. The inclusion of THP into GM appears to create imperfections within the solid lipid matrix that consequently results in the melting point depression from 58.09 to 50.32°C. The resultant binary mixture is also less crystalline in nature than GM alone, as confirmed by the decrease in enthalpy from 87.20 J/g to 71.86 J/g. The addition of THP to GM also favors the transformation of GM from the β- to α- polymorphic modification, and the presence of a minor peak suggests that both the α- and β'-polymorphic modifications co-exist in the resultant solid lipid matrix, with the β'-form present in a relatively smaller amount, as can be seen from the intensities of the two peaks.

5.3.3.2.3 WAXS characterization

The WAXS patterns for the binary mixture of GM and THP (70:30) generated following exposure of the lipid mixture to a temperature of 70°C for one hour is shown in Figure 5.12. The WAXS profile for GM generated prior to heating was used as a reference diffractogram.

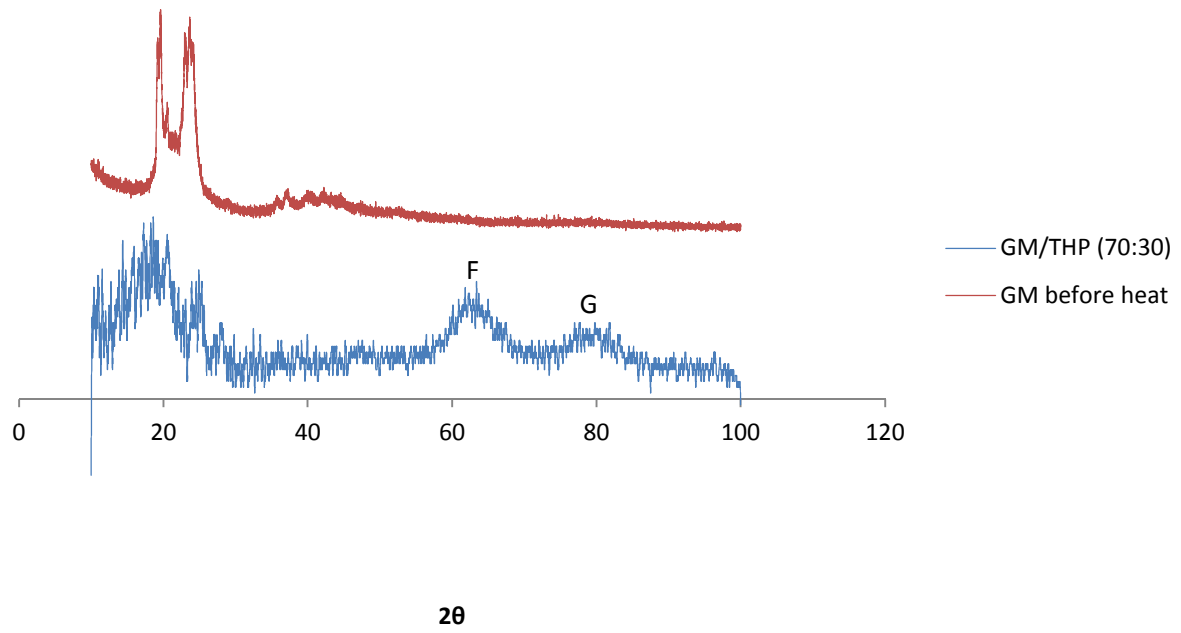

Figure 5.12: *WAXS patterns for a binary mixture of GM and THP (70:30) (blue) generated following exposure of the lipid mixture to a temperature of 70°C for one hour*

Two scattering reflections were observed for GM prior to heating, which corresponded to Bragg distances of 0.420 and 0.385 respectively (§ 5.3.3.1.3). This is indicative of the presence of a highly crystalline β'-modification of the material. However the lipid binary mixture of GM and THP (70:30) following exposure to heat produced similar Bragg distances, in addition to two reflections F and G in the region 2θ = 60-85, suggesting that the lipid mixture produced occurs in the β polymorphic form. However DSC data revealed the co-existence of the α- and β'-polymorphic modifications. This is likely to be the case, although WAXS did not detect the α-polymorphic form, which may be attributed to low intensity of the polymorphic form.

5.3.4 Interactions of lipids with EFV

FT-IR, DSC and WAXS were also used to evaluate potential interactions between EFV and the lipids to be used in the NLC formulation

5.3.4.1 GM and EFV

5.3.4.1.1 FT-IR characterization

The FT-IR spectrum of EFV and that of a binary mixture of EFV and GM prior to heating is shown in Figure 5.13.

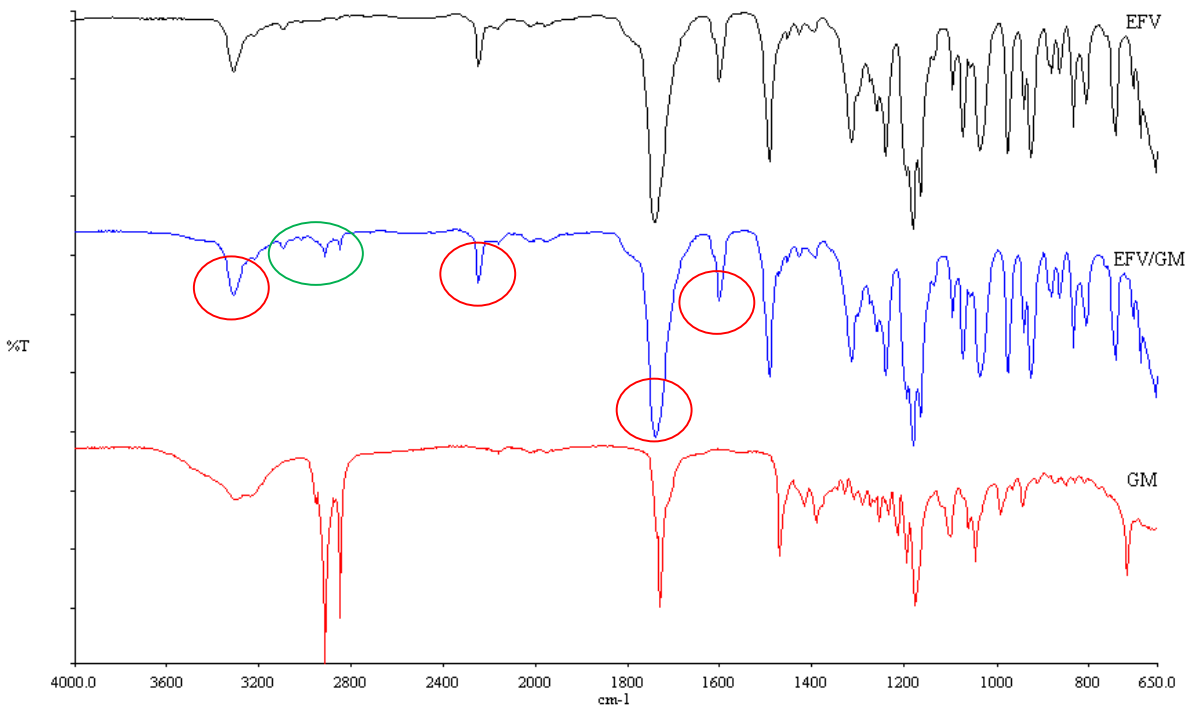

Figure 5.13: *FT-IR spectra of EFV, GM and a binary mixture (1:1) generated prior to heating*

These data show that there are additional peaks for GM in the binary mixture that occur at a frequency between 2950 and 2910 cm^{-1}(circled in green), corresponding to a C-H stretch. However the spectrum of the binary mixture also reveals frequency bands characteristic of EFV

(circled in red), confirming the absence of any interaction between EFV and GM in this binary mixture.

5.3.4.1.2 DSC characterization

The DSC thermogram generated for the binary mixture of EFV and GM prior to and following exposure to a temperature of 70°C for one hour is shown in Figure 5.14 and the corresponding DSC parameters are summarized in Table 5.6.

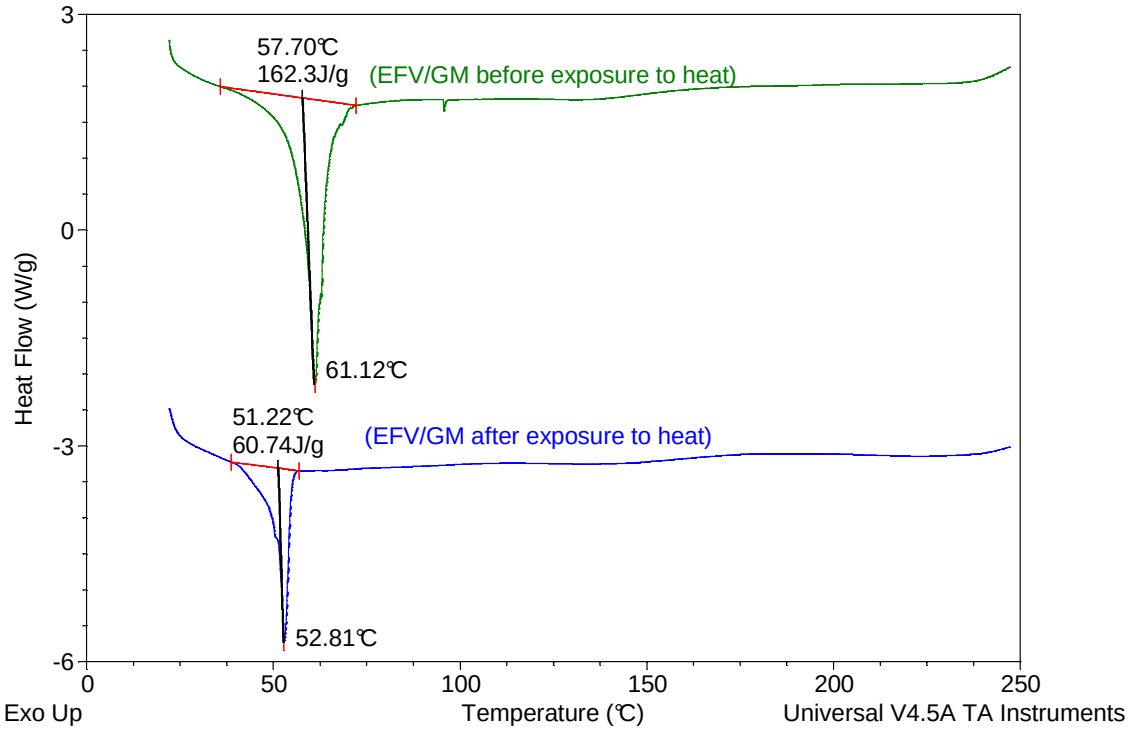

Figure 5.14: *DSC thermogram for a binary mixture of EFV and GM (1:1) prior to and following exposure to a temperature of 70°C for one hour*

Table 5.6: *DSC parameters of a binary mixture of EFV and GM (1:1) prior to and following exposure to a temperature of 70°C for one hour*

EFV and GM	Thermal event	Onset (°C)	MP (°C)	Enthalpy (J/g)	WP (°C)
Prior to heating	Endothermic	57.70	61.12	162.3	3.42
After heating	Endothermic	51.22	52.81	60.74	1.59

The DSC thermograms for the binary mixture of EFV and GM (1:1) prior to and following exposure to heat reveal the presence of a single peak, which is a result of melting of GM. There is clearly no evidence of an interaction between EFV and the solid lipid. The absence of a peak due to the presence of EFV in each thermogram indicates that EFV was probably completely dissolved in GM as the molecule is highly lipophilic and therefore exhibits a high degree of solubility in GM. The DSC thermogram for the binary mixture of EFV and GM following exposure to heat revealed a peak with an onset temperature of 51.22°C and an enthalpy of 60.74 J/g, which is a characteristic of the less crystalline α-modification of GM compared to the more crystalline β-modification observed prior to exposure to heat, with an enthalpy of 162.3 J/g. The absence of a peak consistent with the melting of EFV in the thermogram indicates that the EFV was completely dissolved and occurs as a molecular dispersion in the GM and therefore could not be detected with DSC analysis.

5.3.4.1.3 WAXS characterization

The WAXS patterns of a binary mixture of GM and EFV obtained prior to and following exposure to a temperature of 70°C for one hour are shown in Figure 5.15. The WAXS pattern for EFV following heating was used as a reference diffractogram to distinguish diffraction bands for EFV from those of the solid lipid matrix. These are shown in Figure 5.15. The diffraction patterns of the binary mixture before and after heating show a number of reflections consistent with the reflections observed for EFV, which is an indication of a lack of complete dissolution of EFV in GM at the ratios used in these studies. EFV remained in a crystalline state following exposure to a temperature of 70°C for one hour. However the intensities of the peaks for EFV in the binary mixture following exposure to heat are significantly lower than those observed prior to

exposure of the mixture to heat, which is consistent with the DSC data generated, and supports the notion that EFV dissolves in the molten lipid matrix.

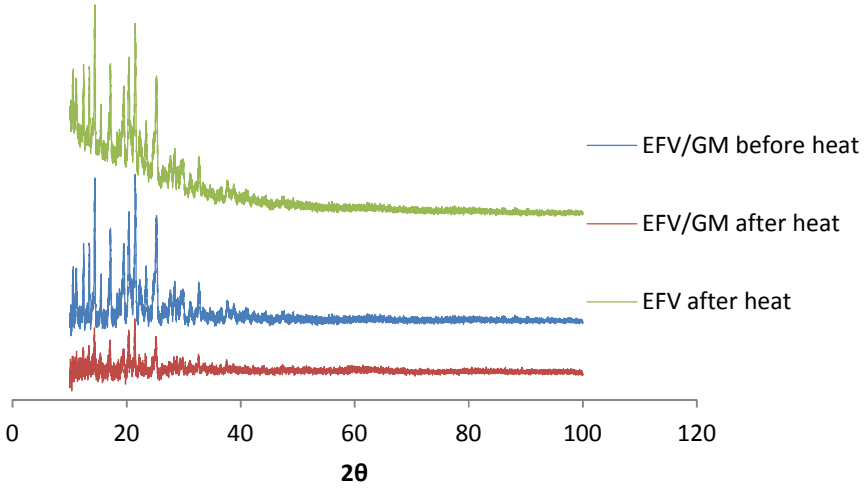

Figure 5.15: *WAXS patterns of a binary mixture of GM and EFV (1:1) generated prior to(blue) and following exposure (red) to a temperature of 70°C for one hour*

5.3.4.2 GM, THP and EFV

5.3.4.2.1 FT-IR characterization

The FT-IR spectrum generated for EFV and GM prior to exposure to heat and that of a ternary mixture of EFV, GM and THP following exposure to a temperature of 70°C for one hour is shown in Figure 5.16. Evaluation of the FT-IR spectrum for the ternary mixture reveals the presence of peaks (circled) that are the same as those observed for GM, confirming that neither THP nor EFV interacts with the crystalline structure of the solid lipid. However, the absence of peaks representing molecular vibrations for EFV is most probably the result of EFV occurring as a molecular dispersion in the binary mixture.

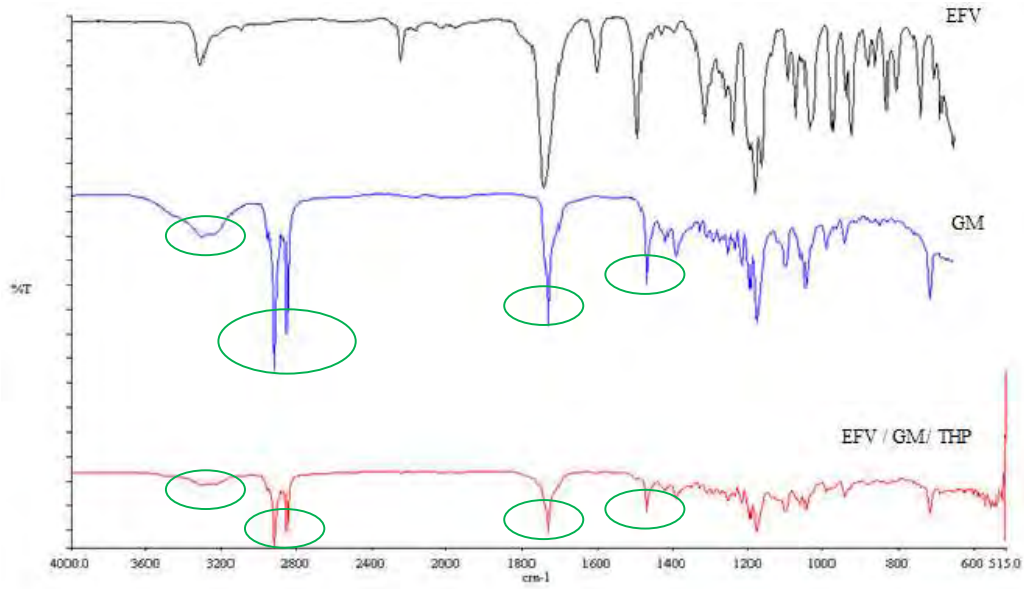

Figure 5.16: *FT-IR profiles of EFV and GM prior to exposure to heat and for a ternary mixture of EFV, GM and THP following exposure to a temperature of 70°C for one hour*

5.3.4.2.2 DSC characterization

The DSC thermogram generated for the ternary mixture of EFV, GM and THP prior to and following exposure to a temperature of 70°C for one hour is shown in Figure 5.17. The corresponding DSC parameters are summarized in Table 5.7.

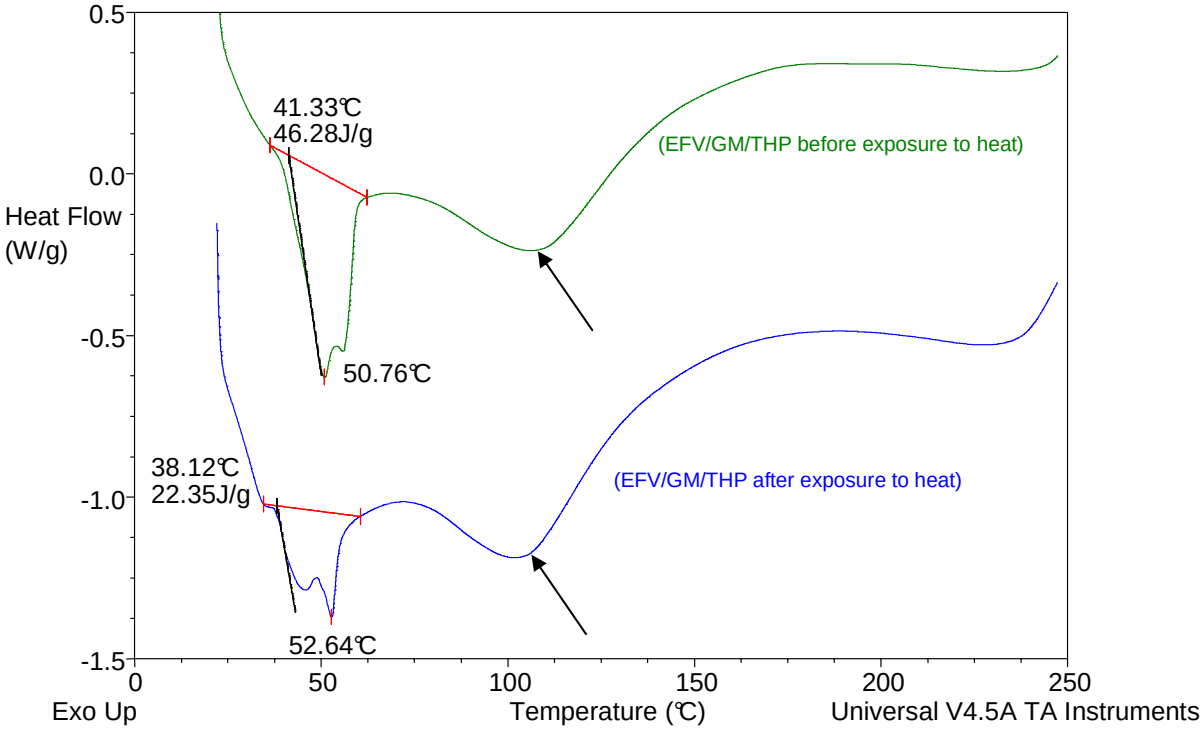

Figure 5.17: *DSC thermogram for a ternary mixture of EFV, GM and THP prior to and following exposure to a temperature of 70°C for one hour*

Table 5.7: *DSC parameters for a ternary mixture of EFV, GM and THP prior to and following exposure to a temperature of 70°C for one hour*

EFV/GM/THP	Thermal event	Onset (°C)	MP (°C)	Enthalpy (J/g)	WP (°C)
Prior to heating	Endothermic	41.33	50.76	46.28	9.43
After heating	Endothermic	38.12	52.64	22.35	14.52

The DSC thermogram generated for the ternary mixture prior to and following exposure to heat clearly shows the presence of separate endothermic events consistent with those observed for GM and EFV. However, the melting event for EFV (identified with an arrow) in the ternary mixture that was exposed to heat was relatively small compared to that observed for the ternary mixture prior to exposure to heat, which is indicative of the relatively high solubility of EFV in the molten lipid mixture. However the presence of the peak for EFV in both thermograms is also indicative of the existence of EFV in a crystalline state, which is most probably a result of

exceeding the saturation solubility of the molecule in the lipids, since 20% w/w of EFV was used in these studies. The sample analyzed following exposure to heat exhibited an enthalpy of 22.35 J/g, which is much lower than that of 46.28 J/g observed for the sample analyzed prior to exposure to heat, indicating that heat exposure of the sample results in the formation of a less crystalline lattice allowing for further dissolution of EFV in the binary mixture.

5.3.4.2.3 WAXS characterization

The WAXS pattern generated for the ternary mixture of EFV, GM and THP following exposure of the mixture to a temperature of 70°C for one hour, in addition to the WAXS pattern for EFV generated prior to exposure to heat, are shown in Figure 5.18.

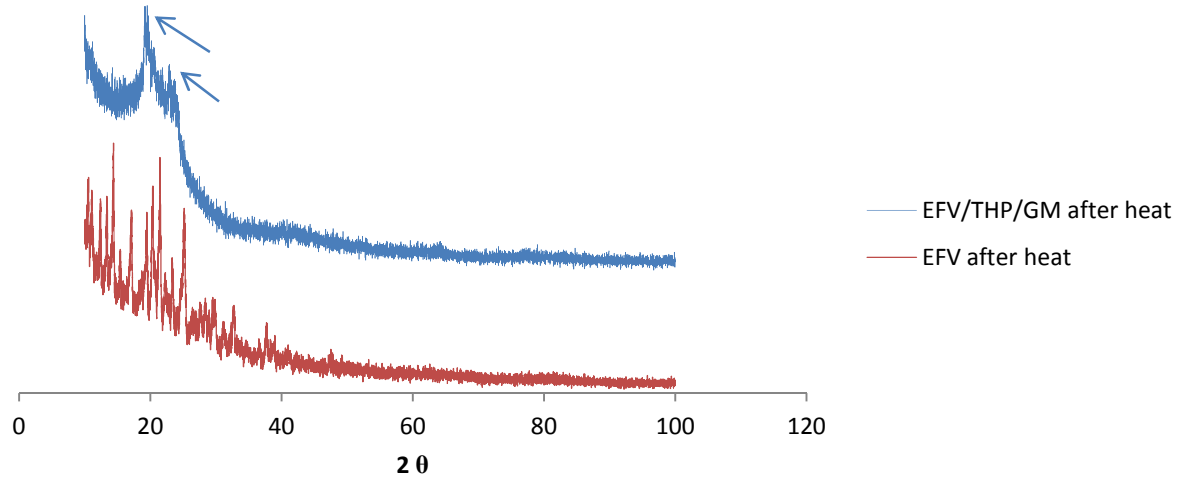

Figure 5.18: *WAXS pattern of the ternary mixture of EFV, GM and THP following exposure of the mixture to a temperature of 70°C for one hour (blue)*

The WAXS diffraction patterns observed for the ternary mixture revealed diffraction patterns matching those of EFV alone, as shown by the arrows. These data are consistent with those observed for DSC analysis results, and it can therefore be concluded that EFV is not completely dissolved in the mixture and also exists in the crystalline form as the saturation solubility of EFV was exceeded through use of a 20% w/w component for EFV in these studies.

5.4 CONCLUSIONS

The pre-formulation studies undertaken reveal that EFV is thermostable when exposed to temperatures of up to approximately 200°C. Therefore a hot high-pressure homogenization (HHPH) manufacturing procedure can be used to manufacture EFV-loaded SLN and/or NLC. In addition, exposure of EFV to temperatures of approximately 70°C for one hour revealed only very slight disruptions in the crystallinity of EFV, without any changes to the polymorphic nature of the molecule, confirming that the HHPH would be suitable for the manufacture of the nanoparticles.

EFV was relatively soluble in most of the solid and liquid lipids evaluated, however glyceryl monostearate (GM) and Transcutol® HP (THP) exhibited the best-solubilizing potential for EFV. The lipids were therefore suitable for use for the formulation and manufacture of EFV-loaded SLN and/or NLC. GM exists in the stable β-modification prior to exposure to heat, however the polymorphic form is altered to the α-modification following exposure to a temperature of 70°C for one hour. The best ratio for GM and THP for the manufacture of EFV-NLC was 70:30. At this ratio the two lipids are miscible and were assumed to have the greatest solubilizing potential for EFV. DSC analysis revealed that the lipid samples had an onset of melting that is higher than the recommended temperature of 40°C.

The addition of THP to GM resulted in a change to the polymorphic nature of the solid lipid from the β-polymorphic form to one in which the α- and β'-polymorphic modifications coexist. Furthermore the addition of a relatively large amount of EFV of 20% w/w to the binary mixture of GM and THP revealed that some of the API existed in the crystalline state within the mixture and it was evident that potential interactions between EFV and the lipids did not occur.

Theoretically the relatively high solubility of EFV in THP in comparison to GM suggests that NLC are likely to have a higher LC and EE for EFV than SLN. In addition, the co-existence of the α- and β'-polymorphic modifications of the solid lipid matrix suggests that that expulsion of

EFV on prolonged storage is less likely to occur if EFV is incorporated into NLC rather than SLN. It was deemed appropriate to develop and optimize SLN and NLC carrier systems for EFV in order to establish which approach would provide the best potential to control the release of EFV.

CHAPTER 6

FORMULATION DEVELOPMENT AND CHARACTERIZATION OF EFV-LOADED SLN AND NLC

6.1 INTRODUCTION

The formulation of SLN and NLC dispersions requires the use of one or more emulsifying agents, lipids and water to impart stability to the system (Chapter 2). The selection of a suitable surfactant is usually dependent on the intended purpose of the SLN or NLC. The primary objective of these studies was to develop SLN and/or NLC which may have the potential to deliver and control the release of EFV to the CNS. Therefore it was vital to select a surfactant or combination of surfactants with the potential to aid the delivery of SLN and/or NLC to the brain. Tween®80 or polysorbate-80 has been shown to aid the delivery of drug-loaded nanoparticles to the brain [164].

The mechanism by which the surfactant assists in the delivery of nanocarriers to the brain is largely unknown. Kreuter [426] postulated that the nanoparticles coated with either polysorbate 20, 40, 60 or 80 have the ability to adsorb apolipoprotein E (Apo E) from the systemic circulation, thereby facilitating interaction with low-density lipoprotein (LDL) receptors on the cerebral endothelium and subsequent internalization by the endothelial cells and delivery across the blood brain barrier (BBB) through endocytosis or transcytosis. Once inside the CNS the nanoparticles release API into brain structures via diffusion [427]. Therefore on the basis of published data polysorbate-80 was selected as the surfactant for use in the formulation of EFV-loaded SLN and NLC. GM and THP were selected and used as the solid and liquid lipid respectively as described in Chapter 5.

6.2 MATERIALS AND METHODS

6.2.1 Materials

6.2.1.1 Glyceryl monostearate

Glyceryl monostearate (GM) ($C_{12}H_{42}O_2$, MW = 358.6) (Aspen® Pharmacare Port Elizabeth, South Africa) is a solid lipid consisting of 40-55% monoacylglycerols, 30-45% of diacylglycerols and 5-15% triacylglycerols [428]. It is usually prepared by reacting glycerin with triglycerides from animal and vegetable sources or by reacting glycerol with stearoyl chloride. GM is generally regarded as safe (GRAS) as it is non-toxic and non-irritant. The lipid is widely used as an emulsifier in food, cosmetics and oral and topical pharmaceutical formulations [428].

GM is characteristically waxy and has a melting range of 54 to 64°C. The hydroxyl and saponification value of GM is 194-237 mg KOH/g and 158-177 mg KOH/g respectively [428]. It has a hydrophilic-lipophilic balance (HLB) value of 3.8 and is soluble in hot ethanol, hot acetone, ether, chloroform, mineral oil and fixed oils. It is practically insoluble in water [428]. GM can be used as an emollient, emulsifying agent, stabilizing agent, solubilizing agent, lubricant, and for sustaining the release of an API [428]. GM should be stored in a tightly closed container in a cool, dry place, and should be protected from light [428].

6.2.1.2 Transcutol® HP

Transcutol® HP (THP) (Gattefossé SAS, Saint-Priest Cedex, France) consists of highly purified diethylene glycol monoethyl ether. THP is an excellent solvent for hydrophilic API [423] and therefore can be used as a hydrophilic co-solvent in self-emulsifying lipid formulations [423]. Toxicological studies have shown that THP is safe [423] and the compound is suitable for incorporation into oral dosage forms.

6.2.1.3 Tween®80

Tween®80 ($C_{64}H_{124}O_{26}$, MW = 1310) (Aspen® Pharmacare Port Elizabeth, South Africa) is a proprietary name for polysorbate 80. It consists of a series of partial fatty acid esters of sorbitol and its anhydrides copolymerized with approximately 20, 5 or 4 moles of ethylene oxide for each mole of sorbitol and anhydride [428]. The preparation of Tween® 80 is a three-step process [428]. Initially sorbital is dehydrated to form sorbitan which is then partially esterified using a fatty acid, e.g. oleic acid or stearic acid, to yield a hexitan ester. Ethylene oxide is chemically added in the presence of a catalyst to produce polysorbate 80 [428]. The surfactant is a yellow liquid at 25°C, with a characteristic odor and a somewhat bitter taste. It feels warm to the touch [428].

Tween®80 is soluble in ethanol and water, but insoluble in mineral and vegetable oils [428]. The acid and hydroxyl value of Tween®80 is 2% and 65-80 mg KOH/g respectively. It has an HLB value of 15 and a saponification value ranging between 45 and 55 mg KOH/g. The molecule is stable in the presence of electrolytes and weak acids/bases [428]. Saponification occurs with the addition of strong acids and bases. Tween®80 should be stored in a well-closed container in a cool and dry place, protected from light. It forms peroxides when stored for protracted periods of time [428].

Tween®80 has GRAS status and is generally regarded as non-toxic and non-irritating. Consequently it can be used as a dispersing, emulsifying, solubilizing, suspending and/or wetting agent in a variety of food, cosmetic and pharmaceutical preparations [428]. Occasional reports of hypersensitivity to polysorbates in general, and their association with serious side effects, including death in some cases, has resulted in a limit for the acceptable daily intake of Tween®80, calculated as a function of total polysorbate esters is 2.5 g/kg of body weight [428,429].

6.2.1.4 Water

HPLC grade water was prepared as described in Chapter 3 (§ 3.3.3.1).

6.2.2 Methods

6.2.2.1. Formulation development

6.2.2.1.1. Box-Behnken Design (BBD)

A non-rotatable BBD was used to investigate the impact of four variables, formulation and process variables on the Critical Quality Attributes (CQA) of SLN and NLC. The input variables were EFV content (X_1), homogenization pressure (X_2), Tween®80 content (X_3) and number of homogenization cycles (X_4). The total lipid concentration in the formulation was kept constant at 5% w/w. Twenty nine (29) experimental runs were generated using Design Expert® 8.0.2 statistical software (Stat-Ease Inc., Minneapolis, MN, USA). The number of experiments performed for the formulation process using BBD may be established using Equation 6.1. The assignment of the actual and coded factors and their respective ranges are listed in Table 6.1.

$$N = 2k(k-1) + C_o \qquad \textit{Equation 6.1}$$

Where

N =number of experiments
k = number of factors
C_o = number of central points

Table 6.1: *Levels of input variables and responses monitored for BBD*

	Levels: Actual [Coded]		
Input Factor	**Low**	**Medium**	**High**
$X_{1=}$ EFV (%)	5	10	15
	[-1]	[0]	[+1]
$X_{2=}$Homogenization pressure (rpm, x 1000)	0.5	1	1.5
	[-1]	[0]	[+1]
$X_{3=}$ Tween® 80 (%)	1	3	5
	[-1]	[0]	[+1]
$X_{4=}$ Homogenization cycles	1	3	5
	[-1]	[0]	[+1]

The CQA that were monitored included ZP (Y_1), PS (Y_2), PDI (Y_3), visual assessment (Y_4) and release rate (RR) after 24 hours (Y_5). Preliminary studies revealed that the variables investigated did not have a significant effect on the EE and LC of EFV in SLN and NLC, since it is a highly

lipophilic compound (§ 1.2.4). Therefore the LC and EE were not considered critical responses and were removed from the BBD. However the responses were monitored during stability studies on the optimum formulations.

6.2.2.2 Production of EFV formulations

A discontinuous hot high-pressure homogenization technique (Figure 2.7, § 2.4.1.1) was used for the production of EFV-loaded SLN and NLC. The representative formulation and corresponding instrumental variables used in the manufacture of the nanocarriers are summarized in Table 6.2. A total of 5% w/w lipids was used for all formulations and a 70:30 ratio of GM to THP was used for the production of NLC. The batch size was 100 mL.

Table 6.2: *Formulae for SLN and NLC formulations developed and tested in optimization studies*

Run	EFV (%)	Homogenization pressure (bar)	Tween 80 (%)	Homogenization cycles
1	15	1000	3	5
2	10	1000	3	3
3	5	1000	3	5
4	15	1500	3	3
5	15	500	3	3
6	15	1000	5	3
7	10	1000	5	1
8	5	1000	5	3
9	10	1000	1	1
10	10	1000	3	3
11	10	1500	3	1
12	10	1000	3	3
13	5	1000	3	1
14	10	1500	5	3
15	5	1000	1	3
16	15	1000	3	1
17	10	1000	1	5
18	15	1000	1	3
19	5	500	3	3
20	10	500	3	5
21	10	500	3	1
22	10	1000	3	3
23	10	1000	3	3
24	10	1500	3	5
25	5	1500	3	3
26	10	500	1	3
27	10	500	5	3
28	10	1500	1	3
29	10	1000	5	5

The lipid phase containing EFV was briefly heated to approximately 70°C. An aqueous phase containing Tween®80 was heated to the same temperature prior to dispersion in the molten lipid phase using a Model T 18 Ultra-Turrax® BS2 homogenizer (Janke & Kunkel GmbH and Co KG, Staufen, Germany) at 1000 rpm for one minute to produce a pre-emulsion. The resultant hot pre-emulsion was then homogenized using an APV 2000 high-pressure homogenizer (West Sussex, England) at a predetermined pressure and number of homogenization cycles. The nanoemulsion was filled into glass vials and allowed to cool to room temperature (22°C) to allow subsequent recrystallization and formation of EFV-loaded SLN or NLC *in situ*. All batches were characterized on the day of manufacture.

6.2.2.3 Characterization of SLN and NLC

6.2.2.3.1 Particle size analysis

The mean PS and PDI of the nanoparticles were measured using a Model Nano-ZS Zetasizer (Malvern Instruments Ltd, Worcestershire, UK) with the instrument set to PCS mode. Approximately 30 µL of an aqueous dispersion of SLN/NLC was diluted with 10 mL of HPLC-grade water prior to analysis. The sample was then placed in a 10 x 10 x 45 mm polystyrene cell and all measurements were performed in replicate (n = 10) at a scattering angle and temperature of 90° and 25°C respectively. The analysis of PC data was achieved using Mie theory, with the real and imaginary refractive indices set at 1.456 and 0.01 respectively.

6.2.2.3.2 Zeta Potential (ZP)

The ZP of the nanocarriers was measured using a Model Nano-ZS Zetasizer (Malvern Instruments Ltd, Worcestershire, UK) with the equipment set in the Laser Doppler Anemometry (LDA) mode. The sample was prepared as described in § 6.2.2.3.1 and placed into folded capillary cells. All measurements (n = 10) were performed at an applied field strength of 20 V/cm and the Helmholtz-Smoluchowsky equation (Equation 2.2, § 2.6.3) was used *in situ* to calculate the ZP value of each sample.

6.2.2.3.3 Imaging analysis

6.2.2.3.3.1 Transmission electron microscopy (TEM)

TEM was used to investigate the shape and surface morphology of the nanoparticles in the original aqueous dispersions. A drop of the aqueous SLN/NLC dispersion was placed onto a copper grid with a carbon film. The excess liquid was removed using hydrophilic filter paper (Whatman® 110 diameter filter papers, Whatman® International Ltd, Maidstone, England) and

the sample was allowed to dry at room temperature (22°C) for 24 hours. The sample was visualized using a Zeiss Libra® 120 TEM (Zeiss, GmbH, Germany).

6.2.2.3.3.2 Scanning electron microscopy (SEM)

SEM was used to evaluate the shape and surface morphology of SLN/NLC. Prior to analysis aqueous dispersions of SLN/NLC were lyophilized without a cryoprotectant using a Vacutec freeze drier (Labconco® Corp, Kansas City, Missouri, USA). Following lyophilization the powdered sample was mounted onto a carbon stub and sputter-coated with gold under vacuum for 15 minutes using a sputter-coater (Balzers Union Ltd, Balzers, Lichtenstein). The sample was visualized using a Model TS 5136 LM Vega® Tescan SEM (Tescan, Vega LMU, Czechoslovakia Republic) at a voltage of 20 kV.

6.2.2.3.4 Crystallography and polymorphism

6.2.2.3.4.1 DSC characterization

The degree of crystallinity and polymorphism of the nanocarriers was determined using a Model Q100 DSC fitted with a RCS (90) refrigerated cooling system (TA instruments, Lukens Drive New Castle, DE, USA). Prior to analysis the liquid nanoemulsion was lyophilized without cryoprotectant (§ 6.2.2.3.3.2). Samples of SLN and/or NLC weighing between 3 and 5 mg were weighed directly into a standard 40 µl aluminum open pan. DSC curves were generated by heating the sample from 22°C to 250°C and successive cooling to 22°C at heating and cooling rates of 10°C/min. A nitrogen flow rate of 100 ml/min was used, and the resultant data were analyzed using TA Universal Analysis 2000 for Windows software (TA instruments, Lukens Drive New Castle, DE, USA).

6.2.2.3.4.2 FT-IR characterization

The crystalline and polymorphic nature of SLN/NLC was also investigated using FT-IR as a complementary analytical tool to DSC. Lyophilized samples of the nanoparticles were mounted onto a diamond crystal using an applied force of approximately 100 N. The FT-IR spectrum was generated using a Precisely FT-IR Spectrum 100 spectrometer (Perkin-Elmer® Pty Ltd, Beaconsfield, England) in a scan range of between 4000 and 650 cm^{-1} at a resolution of 4 cm^{-1}.

6.2.2.3.5 Loading capacity (LC) and encapsulation efficiency (EE)

The LC and EE of the SLN and NLC for EFV was investigated using the RP-HPLC-UV method developed and validated as described in Chapter 3 following filtration of the aqueous dispersion using Centrisart® filter tubes (Satorius AG, Goettingen, Germany). The filter tubes consisted of a filter membrane with a molecular cut-off of 300 KDa at the base of the sample recovery chamber. Approximately 2 mL of the aqueous dispersion of the SLN/NLC was placed into the outer chamber of the tube after which the sample recovery chamber was fitted. The unit was allowed to equilibrate to room temperature (22°C) for 5 minutes and centrifuged at 1500 rpm for 10 minutes using a Model HN-SII IEC centrifuge (Damon, Needham HTS, MA, USA). The amount of EFV in the aqueous filtrate was determined using RP-HPLC, and the LC and EE of EFV in the SLN or NLC was calculated using Equations 2.4 and 2.5 as described Chapter 2, § 2.5.5.

6.2.2.3.6 In Vitro release

The *in vitro* release of EFV from SLN and NLC aqueous dispersions was investigated using a Sotax™ CE 7 USP Apparatus 4 (Sotax™ AG, Binningerstrasse, Allshwil, Switzerland) equipped with 22.6 mm diameter cells and operated in a closed loop mode at 37°C. A 5 mm diameter ruby bead was placed at the base of the 22.6 mm sample cell and approximately 2 g of 1 mm diameter glass beads were added to fill the base of the conical part of the sample holder to ensure that the

liquid sample was retained in the cell. Approximately 6 mL of the aqueous dispersion of SLN or NLC was placed into the chamber and a 25 mm diameter glass fiber filter with a pore size of 0.7 µm (Macherey-Nagel, Germany) was fitted to the top of the chamber prior to sealing the unit. The dissolution medium was 2000 ml of a 1% sodium lauryl sulphate (SLS) solution in distilled water maintained at 37°C, and was pumped through each cell at a rate of 8.8 mL/min. An aliquot of 1.25 mL of the dissolution medium was withdrawn at specified time intervals and was replaced with fresh medium of similar volume to maintain sink conditions throughout the study period. The *in vitro* release studies were performed in triplicate and the amount of EFV released from the nanoparticles was estimated using RP-HPLC-UV, developed and validated as described in Chapter 3.

6.2.2.3.7 Robustness of in vitro release

The robustness of the *in vitro* release method was evaluated by changing the flow rate [242,430] and composition of the dissolution medium using preliminary SLN formulations. The dissolution medium used was 2000 mL of SLS in distilled water. The flow rate and the amount of SLS in the dissolution medium were varied between 8.8 and 16.6 mL/min as well as 1 and 3% w/v respectively, and the studies were conducted in triplicate.

6.2.2.3.8 Comparison of release profiles

The *in vitro* release profiles of EFV from nanoparticle formulations can be compared using the difference (f_1) and similarity (f_2) factors first described by Moore and Flanner in 1996 [431]. The f_1 reflects the cumulative difference between the reference product and test release profiles at all-time points. It is therefore a measure of the relative error between the two curves at all-time points. An f_1 value of between 0 and 15 is indicative of statistical similarity between the profiles [432]. The f_2 is a logarithmic transformation of the sum-squared error of differences between the test and reference products over all-time points. The f_2 value may lie between 0 and 100, however the closer the value to 100 the more similar the profiles are [432,433]. The FDA

recommends the use of f_2 only as it has been shown to be more sensitive in identifying large differences between two profiles at any particular time point [432]. Consequently the f_2 factor was used to compare the release profiles of EFV in these studies. The f_2 factor can be calculated using Equation 6.5

$$f_2 = 50^* \log \{[1+ (\frac{1}{n}) \sum_{t=1} n(R_t\text{-}T_t)^2]^{-0.5} *100\} \qquad \textbf{\textit{Equation 6.5}}$$

Where

R_t = cumulative percentage API release for the reference product
T_t = cumulative percentage API release for the test product
n = number of time points

6.2.2.4 Kinetics and mechanism of EFV release

The use of mathematical modelling to predict the kinetics and mechanism of release of an API from drug delivery systems is gaining attention in academia and the industry [434]. The mathematical theories of modelling are based on real phenomena such as diffusion, dissolution, swelling, erosion, precipitation and/or degradation [434,435] and are of great benefit in identification of the underlying mechanisms that may control the release of an API from a particular dosage form, and therefore allow for improvement of therapy [436,437]. In addition the quantitative prediction of the effects of formulation and processing parameters on the kinetics of API release with the use of mathematical theories is possible and feasible [438]. Therefore computer-generated simulations can be applied to identify the required composition for a formulation, and the process parameters required to produce that formulation in order to define an explicit and preferred profile for API release [434,435].

Generally the release of an API from lipid-based nanoparticles is governed by one or more of three different mechanisms, *viz*. diffusion, erosion, and swelling [439]. It has been suggested that erosion and swelling are the predominant mechanisms of release of carbohydrates and proteins from lipid-based nanocarriers [439]. API release from lipid-based carriers such as SLN and/or NLC exhibit mathematical models that describe diffusion controlled release mechanisms

[166,439]. The kinetics and mechanism of release of EFV from SLN and NLC were evaluated using zero-order, first-order kinetics and the Higuchi models.

6.2.2.4.1 Zero order release model

The zero-order release model can be used to describe the release of an API from a pharmaceutical dosage form that does not disintegrate, or when API release is slow [433]. The model can be applied to modified release dosage forms such as transdermal systems, tablet matrices containing hydrophobic molecules, coated systems and osmotic systems [433]. The model holds true when a drug device releases the same amount of API per unit time, and therefore is able to release the API in a controlled manner [433]. The zero-order release model is mathematically described using Equation 6.2.

$$Q_t = Q_0 + K_0 t \qquad \textbf{Equation 6.2}$$

Where

Q_t = amount of API dissolved in time t,
Q_0 = initial amount of API in the solution, and,
K_0 = zero order release constant

6.2.2.4.2 First-order release model

The release of hydrophilic molecules from porous matrices usually follows a first-order release mechanism [440]. The release of an API from these matrices is proportional to the amount of API remaining in the device and release of the molecule diminishes over time. A plot of the logarithm of the amount of API released *versus* time usually yields a straight line [433,440]. The first order release model is mathematically described using Equation 6.3.

$$\log Q_t = \log Q_0 + \frac{K_1 t}{2.303}$$ ***Equation 6.3***

Where

Q_t = amount of API dissolved in time *t*,
Q_0 = initial amount of API in the solution, and,
K_1 = first order release constant

6.2.2.4.3 Higuchi release model

In 1963 Higuchi [439] developed a mathematical model that can be used to describe the release of an API from spherical devices. The mathematical relationship for the Higuchi release model is shown in Equation 6.4.

$$\frac{M_t}{A} = \sqrt{D(C_0 - C_s)C_s t}$$ ***Equation 6.4***

Where

M_t = cumulative absolute amount of API released at time *t*
A = surface area of the film exposed to the release medium
D = API diffusivity in the carrier material
C_0 = initial API concentration
C_s = solubility of the API in the carrier material

When the Higuchi equation is applied to controlled delivery systems, a number of assumptions are made. These include that the initial amount of API in the system must be higher than the saturation solubility of the API as this provides the basis for an applied pseudo-steady state approach to rationalization. The second assumption is that the geometry of the device should be thin such that edge effects are negligible and the size of the particles must be smaller than the thickness of the film and the matrix does not swell or dissolve. Finally the diffusivity of the API should not be dependent on time or position, and should be constant whilst perfect sink conditions are maintained throughout the entire experimental process [434]. The release of an API from a dosage form is said to follow the Higuchi model when a linear relationship is generated by plotting the cumulative % API released *versus* the square root of time [434].

6.2.2.5 Determination of best fit model

To determine the mathematical model that best fitted EFV release data generated from EFV-loaded SLN and NLC, best fit linear regression plots of the cumulative % EFV released *versus* time (zero order model), natural logarithm of cumulative % EFV remaining in the matrix *versus* time (first order model) and cumulative % EFV released *versus* square root of time (Higuchi model) were generated. The determination coefficient (R^2) was used as an indicator of the best kinetic model that explained the release of EFV from the colloidal systems.

6.2.2.4.7 Stability studies

The stability of aqueous dispersions of nanoparticles was initially evaluated using visual observation following storage at room temperature (22°C) for two weeks. The objective was to generate preliminary information that could be used to ascertain whether the formulations remain stable over a relatively long period of time. The aqueous dispersions of SLN or NLC were assessed visually in the presence of light. The formulations that showed signs of cracking, creaming or flocculation were given a value of 0 to indicate a lack of stability, while those that were considered stable, and with the potential to remain stable for a relatively long period of time, were assigned a value of 1.

The stability of the optimized SLN and NLC formulation was evaluated using Binder® KBF-240 climatic chambers (Binder GmbH® Ltd, Munchen, Germany). Accelerated and short-term stability studies were undertaken at 40°C/75% RH and 25°C/60% RH respectively. The formulations were packed into 100 g glass ointment jars with closures that fitted tightly and were assessed at 1, 2, 4 and 8 weeks following storage. At each time the formulation was evaluated and not returned to the stability chamber. The formulations were assessed in terms of the parameters that are considered benchmarks for stability of colloidal systems. These include zeta potential, particle size, polydispersity index, encapsulation efficiency and loading capacity. The

stability protocol conducted over two months was used to perform short term and accelerated stability studies for optimized SLN and NLC formulations.

6.2.2.5 Data Analysis

The data generated from the responses monitored were analyzed using Design Expert® statistical software Version 8.0.2 (Stat-Ease Inc., Minneapolis, MN, USA). Fisher's test for Analysis of Variance (ANOVA) was used to determine whether significant differences existed among the means of the factors under investigation. A backward, stepwise elimination technique was also used to achieve model responses that could be used to navigate the design space.

6.3 RESULTS AND DISCUSSION

6.3.1 Formulation Development

The development of EFV-loaded SLN and NLC formulations was initiated using RSM, specifically with a Box-Behnken Design (BBD). The use of BBD was intended to determine the effects of different process and formulation parameters on the Critical Quality Attributes (CQA) of the nanoparticles. The process parameters investigated were the number of homogenization cycles and pressure. PS, PDI, ZP, visual assessment (VA) and EFV released at 24 hours (RR), LC, EE, polymorphism, shape and surface morphology were the CQA of the nanoparticles. In addition three mathematical models were used to fit *in vitro* release data to determine the most likely mechanism of EFV release from SLN and NLC [433]. To assess the effect of storage temperature and humidity on the formulations and to ensure that the nanoparticles produced were of good quality, stability studies were performed on optimized batches of SLN and NLC over a period of 8 weeks.

The BBD is an efficient optimization method and does not contain a combination of experiments for which all factors are simultaneously at their highest or lowest levels [332]. The BBD also avoids the need to generate data under extreme experimental conditions. Therefore it is suitable

for use when the elimination of unsatisfactory data is necessary [332]. A BBD was used to optimize EFV-loaded SLN and NLC. However, for the purpose of this discussion, only response surface plots of SLN are discussed in detail, while those for NLC are included in Appendix IV. The complete design matrix for the responses is summarized in Table 6.3.

Table 6.3: *Responses observed for Box Behnken design experiments for SLN formulations*

Runs	**Response variables**				
	Y_1 (ZP) mV	**Y_2 (PS) nm**	**Y_3 (PDI)**	**Y_4 (VA)**	**Y_5 (RR) %**
EFV-SLN 001	-41.8	74.08	0.628	0	85.5
EFV-SLN 002	-37.9	116.4	0.615	1	83.4
EFV-SLN 003	-43	75.57	0.488	1	84.1
EFV-SLN 004	-39.9	95.92	0.424	0	80.1
EFV-SLN 005	-34.8	317.9	0.631	0	54.5
EFV-SLN 006	-38.2	390.3	0.719	0	55.2
EFV-SLN 007	-35.5	635.5	0.855	1	37.5
EFV-SLN 008	-33.7	118.7	0.527	1	80.3
EFV-SLN 009	-46.3	185.7	0.439	0	76.8
EFV-SLN 010	-39.2	116.8	0.586	1	83.6
EFV-SLN 011	-40.5	616.3	0.937	1	41.5
EFV-SLN 012	-38.6	114.9	0.614	1	82.5
EFV-SLN 013	-38.8	476.4	0.785	1	52.2
EFV-SLN 014	-40.2	67.42	0.618	1	91.5
EFV-SLN 015	-51.6	116.7	0.674	0	78.8
EFV-SLN 016	-42.6	653.8	0.928	0	41.9
EFV-SLN 017	-44.8	71.43	0.565	0	83.1
EFV-SLN 018	-51.1	125.9	0.623	0	79
EFV-SLN 019	-44.1	254.6	0.83	1	72.2
EFV-SLN 020	-38.9	100.9	0.594	1	82.6
EFV-SLN 021	-38.6	684	0.824	1	33.7
EFV-SLN 022	-41.7	120.2	0.642	1	82.6
EFV-SLN 023	-43.3	103.5	0.567	1	81.5
EFV-SLN 024	-31.5	42.19	0.444	1	94.1
EFV-SLN 025	-34.6	89.29	0.496	1	83
EFV-SLN 026	-48.9	127.1	0.727	0	79.6
EFV-SLN 027	-37.3	101.1	0.707	1	83.7
EFV-SLN 028	-47.3	106.4	0.533	0	85.2
EFV-SLN 029	-37.5	51.55	0.502	1	93.4

6.3.1.1 Model fitting and statistical analysis

ANOVA and the Regression Coefficient (R^2) were used to statistically analyze the data reported in Table 6.3. In addition normal plots of residuals, studentized residuals, Box-Cox plots, contour and 3-dimensional plots were used to describe these data graphically. The model(s) that best

described the data were selected for use in the optimization process. Results were analyzed and used to establish experimental parameters to achieve target performance levels. The data were fitted to linear, two factorial, quadratic and cubic models, and the results reveal that the correlation between process variables and formulation responses was best described by four quadratic polynomial models and one linear model.

6.3.1.2 Model fit equations and their regression coefficients

The data summarized in Table 6.3 indicate that the PS and PDI of the SLN formulations ranged between 42 and 684 nm, and 0.424 and 0.937 respectively. The ZP of the nanoparticles ranged between -51.6 mV and -31.5 mV. The EFV released ranged between 33.7 and 94.1% and the VA score between 0 and 1. Five center point experiments were performed to determine the level of experimental error and the reproducibility of the data in the overall design matrix. The sequential model sum of squares was used to select the best fit model based on selection of the highest order polynomial in which the additional terms were significant and the model was not aliased. The final models selected for ZP (Y_1), PS (Y_2), PDI (Y_3), VA (Y_4) and RR after 24 hours (Y_5) in terms of coded factors are shown in Equations 6.6-6.10.

Zeta potential (Y_1) = $-40.14-0.22X_1+0.72X_2+5.63X_3+0.40X_4-3.65X_1X_2-1.25X_1X_3+1.25X_1X_4-1.13X_2X_3+2.32X_2X_4-0.88X_3X_4-0.81X_1^2+1.39X_2^2-3.08X_3^2+0.99X_4^2$ ***Equation 6.6***

1/Particle size (Y_2) = $+9.581E-003-6.957E-004X_1+2.915E-003X_2+2.933E-004X_3+6.673E-003X_4+3.408E-003X_2X_4+2.303E-003X_3X_4-2.368E-003X_1^2$ ***Equation 6.7***

Polydispersity index (Y_3) = $+0.64+0.013X_1-0.072X_2+0.031X_3-0.13X_4$ ***Equation 6.8***

Visual stability (Y_4) = $+1.00-0.42X_1+0.000X_2+0.42X_3+0.000X_4+0.000X_1X_2-0.25X_1X_3+0.000X_1X_4+0.000X_2X_3+0.000X_2X_4+0.000X_3X_4-0.42X_1^2-0.042X_2^2-0.42X_3^2-0.042X_4^2$ ***Equation 6.9***

Release Rate (Y_5) = $+82.72-4.53X_1+5.76X_2-3.41X_3+19.93X_4+3.70X_1X_2-6.33X_1X_3+2.93X_1X_4+0.55X_2X_3+0.92X_2X_4+12.40X_3X_4-7.57X_1^2-3.21X_2^2+2.09X_3^2-12.62X_4^2$ ***Equation 6.10***

The polynomial equations consist of coefficients for the intercept, first-order main effects, interaction terms and higher-order effects. The sign and magnitude of the main effects signify the relative influence of each factor on the response which is the average result of changing one factor at a time from low to high values. However at a given set of factor levels the higher-order polynomials yield results representative of the net effect of all coefficient terms in the polynomial. A negative sign in all equations denotes an antagonistic effect and a positive sign indicates a synergistic effect of the input variables on the responses. The interaction terms such as X_1X_2, X_1X_3, and X_1X_4 are indicative of response changes when two formulation factors are changed simultaneously. Finally the second degree terms, *viz*. X_1^2, X_2^2, X_3^2, and X_4^2 are incorporated in order to investigate non-linearity in the model [441-444].

The correlation coefficient, R^2 and the standard deviation values were used to evaluate the quality of the models. The closer the R^2 value is to one and the smaller the standard deviation the more accurate the response predicted by the model. Good correlation between experimental and predicted responses is indicated by an R^2 value of > 0.9 [441,443]. The model correlation coefficients and standard deviations are summarized in Table 6.4.

Table 6.4: *Correlation coefficients and standard deviations of response models*

Response factor	**Response surface model**					
	SD	**R^2**	**Adj R^2**	**Pred R^2**	**Adeq Prec**	**C.V (%)**
Y_1	2.87	0.8360	0.6720	0.1790	7.940	7.04
Y_2	1.745E-003	0.9215	0.8953	0.8516	24.803	20.29
Y_3	0.11	0.4912	0.4064	0.2107	8.881	17.04
Y_4	0.17	0.9390	0.8779	0.6485	13.433	27.79
Y_5	7.31	0.9129	0.8258	0.4996	12.555	9.89

The R^2 values for Equations 6.6-6.10 were 0.8630, 0.9215, 0.4912, 0.9390 and 0.9129 respectively, indicating that 83.6%, 92.15%, 49.12%, 93.90% and 91.29% of the total variation in Y_1, Y_2, Y_3, Y_4, and Y_5, can be attributed to the experimental variables under investigation. In addition the R^2 value of 0.8360 obtained for Equation 6.6 was considered moderate to validate the fit. The R^2 values for Y_2, Y_4 and Y_5 of 0.9215, 0.939 and 0.9192 were considered high,

indicating a good correlation between the predicted and experimental responses, and the R^2 value of 0.4912 for Y_3 was inappropriate and could not be used to validate the model fit for PDI.

The low standard deviations of 2.87, 1.745E-003, 0.11 and 0.17 for Y_1, Y_2, Y_3, and Y_4, indicate that the predicted values for the observed responses would be more accurate and closer to the actual values than the predicted value for EFV release (Y_5) as it has a significantly higher standard deviation of 7.31. Apart from the predicted R^2 value observed for Y_3 all other R^2 values were not in reasonable agreement with their respective adjusted R^2 values, indicating a possible large block effect or a problem with the models [445]. However adequate precision measures the signal to noise ratio and high values > 4 indicate adequate signal [445]. All adequate precision values generated for the observed responses were > 4, indicating the applicability of the models in navigating the design space. In addition the relatively low percentage for the coefficient of variation values indicates better precision and reliability of the experiments [445]. Model adequacy was further justified and confirmed by Analysis of Variance.

6.3.1.3 Analysis of Variance (ANOVA)

The significance of the response surface models was investigated and the model F-value and the Prob > F values were used to determine model significance at a 0.05 level of significance.

6.3.1.3.1 Response surface quadratic model for zeta potential (Y_1)

The ANOVA data for the quadratic model for ZP (Y_1) are summarized in Table 6.5. These data showed a model F-value of 5.10, indicating that the model was significant. In this model, Tween®80 content (X_3), the linear combination of EFV amount and homogenization pressure (X_1X_2) and the quadratic effect of Tween®80 content (X_3^2) were significant terms. These results revealed that the significant factors affecting response Y_1 were the synergistic linear contribution of X_3. However the same response Y_1 was affected antagonistically by the interaction effect of X_1X_2 and the quadratic effect of X_3^2, as summarized in Equation 6.6.

Table 6.5: *ANOVA analysis for the quadratic model for zeta potential*

Source	Sum of squares	Degrees of freedom (df)	Mean square	F value	Prob > F
Model	**587.46**	**14**	**41.96**	**5.10**	**0.0022**
X_1	0.56	1	0.56	0.068	0.7974
X_2	6.16	1	6.16	0.75	0.4014
X_3	**380.81**	**1**	**380.81**	**46.27**	**< 0.0001**
X_4	1.92	1	1.92	0.23	0.6366
X_1X_2	**53.29**	**1**	**53.29**	**6.47**	**0.0234**
X_1X_3	6.25	1	6.25	0.76	0.3982
X_1X_4	6.25	1	6.25	0.76	0.3982
X_2X_3	5.06	1	5.06	0.62	0.4460
X_2X_4	21.62	1	21.62	2.63	0.1274
X_3X_4	3.06	1	3.06	0.37	0.5516
X_1^2	4.25	1	4.25	0.52	0.4844
X_2^2	12.55	1	12.55	1.52	0.2373
X_3^2	**61.70**	**1**	**61.70**	**7.50**	**0.0160**
X_4^2	6.37	1	6.37	0.77	0.3939
Residual	115.23	14	8.23	-	-

The adequacy of the model can also be investigated by examining residuals. The studentized residuals are used to measure the number of standard deviations that separate the actual and predicted values [446,447]. A normal probability plot of residuals is used to evaluate the data generated, and a linear trend in the plot confirms a normal distribution and character of the residuals [446,448,449]. A scatter plot of the studentized residuals and predicted responses can be used to determine the adequacy of the model. The plot should generally show random scatter, which suggests that the variance of the original observations is constant for all response values [446,448,449]. A funnel-shaped pattern is obtained if the variance of the response depends on the mean level of *Y* [446,448,449]. Therefore investigation of the adequacy of a model usually gives an indication as to whether or not any transformation of the response variable of interest may be necessary [446,448,449]. The transformation of data may be required in order to enhance the applicability and usefulness of the applied statistical test method, and these data are usually presented using the Box-Cox plot [368] (Figure 6.1). The blue line in the plot in Figure 6.1 points to the current transformation of the model. The red lines indicate a 95% confidence interval and the 95% confidence interval includes 1.0 (blue line), which indicates that the data are approximately in the best possible region of the parabola [369-371].

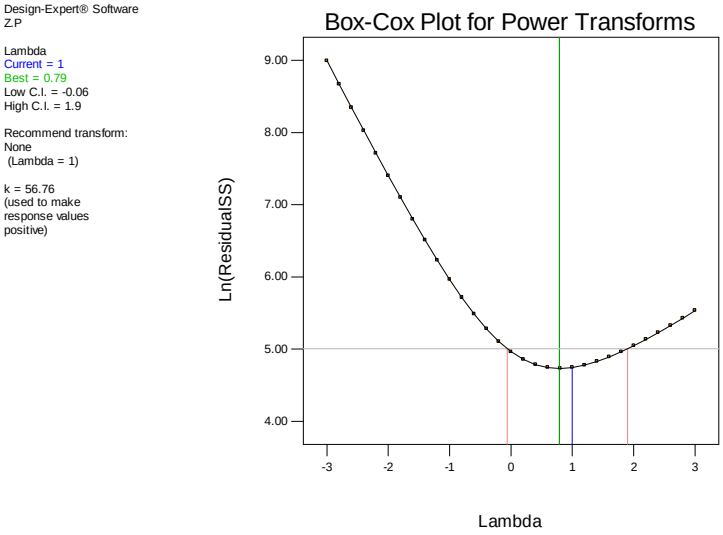

Figure 6.1: *Box-Cox plot for power transformation for zeta potential*

The normal probability and the studentized residuals plots for Y_1 are shown in Figures 6.2 and 6.3 respectively. The normal probability plot shows that the residuals were linear as they fall in a straight line. However the studentized residuals plot shows that the data were generally scattered, indicating that transformation of data was not required

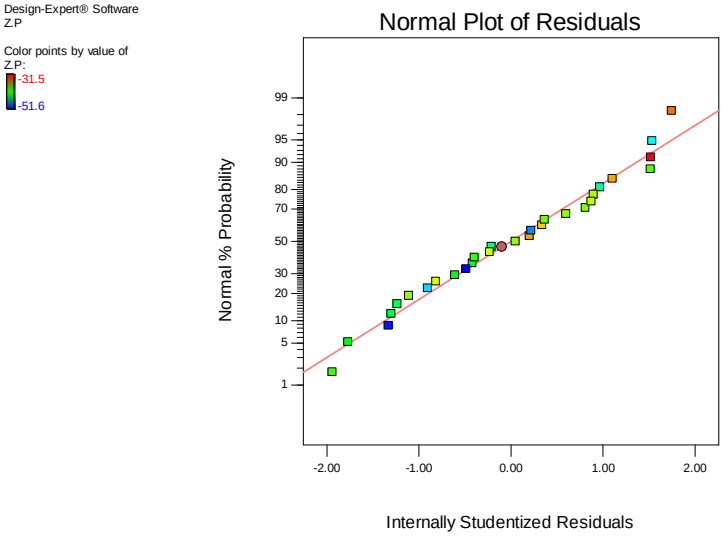

Figure 6.2: *Normal probability plot of residuals for zeta potential*

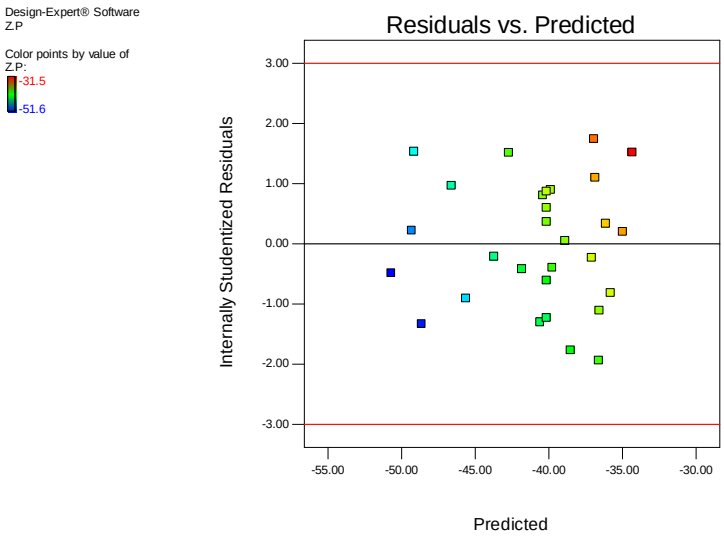

Figure 6.3: *Plot of studentized residuals versus predicted responses for zeta potential*

6.3.1.3.2 Response surface quadratic model for particle size (Y_2)

Analysis of the quadratic model for PS generated a ratio of the maximum to minimum response value of 16.2124. Usually a ratio > 10 is indicative of a need to perform model transformation. The need to transform the model was confirmed by the Box-Cox plot (Figure 6.4). These data reveal the blue line was outside the 95% confidence interval, indicating that the model was not in the optimum region of the parabola. Consequently, the model was inversely transformed using model reduction by backward elimination in order to improve the fit of the model and thus permit navigation of the design space.

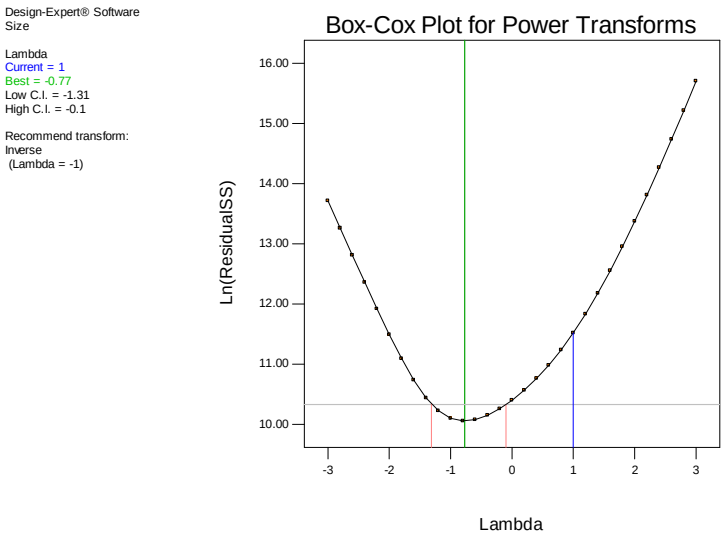

Figure 6.4: *Box-Cox plot for power transformation for particle size (before inverse transformation)*

The ANOVA data generated for the quadratic model for PS following transformation are summarized in Table 6.6. The model F-value of 35.20 indicates that the model was significant. Consequently the significant model terms affecting response Y_2 were homogenization pressure (X_2), number of homogenization cycles (X_4), their linear combination (X_2X_4), the linear combination of Tween®80 content and number of homogenization cycles (X_3X_4) and the quadratic effect of EFV amount (X_1^2). Synergistically the model was affected by the linear contribution of X_2 and X_4 and the interaction effects of X_2X_4 and X_3X_4, however the quadratic effect of X_1^2 was antagonistic, as shown in Equation 6.7.

Table 6.6: *ANOVA analysis for the inversely transformed quadratic model for particle size*

Source	Sum of squares	Degrees of freedom (df)	Mean square	F value	Prob > F
Model	**7.502E-004**	**7**	**1.072E-004**	**35.20**	**< 0.0001**
X_1	5.808E-006	1	5.808E-006	1.91	0.1818
X_2	**1.019E-004**	**1**	**1.019E-004**	**33.48**	**< 0.0001**
X_3	1.032E-006	1	1.032E-006	0.34	0.5666
X_4	**5.343E-004**	**1**	**5.343E-004**	**175.48**	**< 0.0001**
X_2X_4	**4.645E-005**	**1**	**4.645E-005**	**15.26**	**0.0008**
X_3X_4	**2.121E-005**	**1**	**2.121E-005**	**6.97**	**0.0153**
X_1^2	**3.945E-005**	**1**	**3.945E-005**	**12.96**	**0.0017**
Residual	6.394E-005	21	3.045E-006	-	-

The normal probability, studentized residuals and Box-Cox plots for Y_2 are shown in Figures 6.5, 6.6 and 6.7 respectively. The normal probability and studentized residual plots reveal a linear distribution and scatter of data, confirming a lack of significant problems with the normality of the data following transformation of the model. The Box-Cox plot generated following inverse transformation of the data using backward elimination includes the blue line within the confidence interval, confirming that the data were in the optimum region of the parabola and model adequacy.

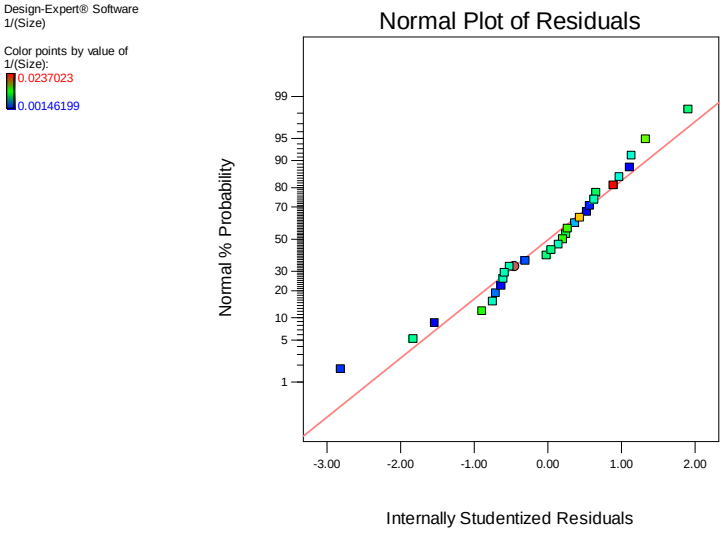

Figure 6.5: *Normal probability plot of residuals for particle size after inverse transformation*

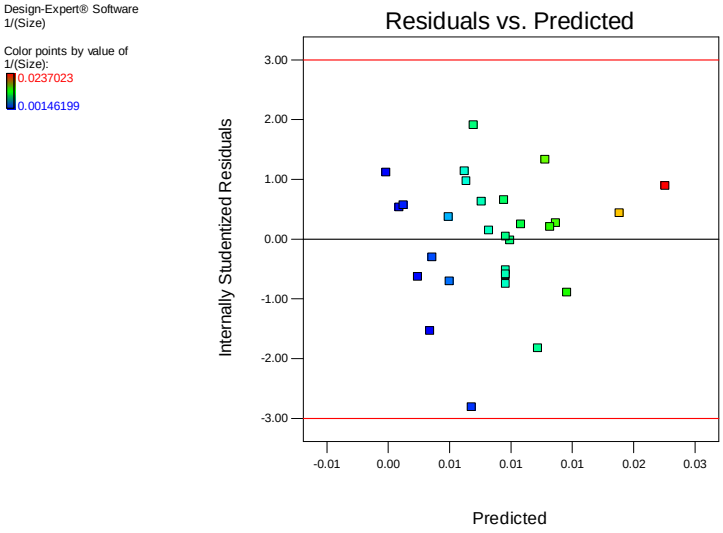

Figure 6.6: *Plot of studentized residuals versus predicted responses for particle size after inverse transformation*

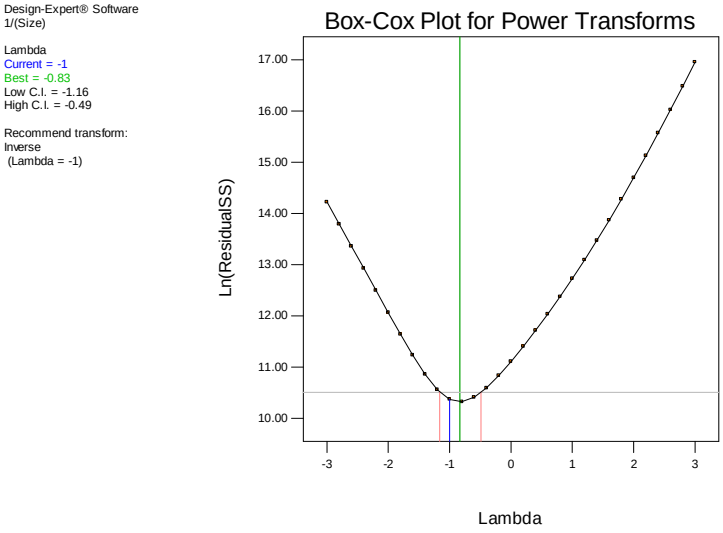

Figure 6.7: *Box-Cox plot for power transformation for particle size (after inverse transformation)*

6.3.1.3.3 Response surface linear model for polydispersity index (Y_3)

The ANOVA data for the linear model for PDI are summarized in Table 6.7. The model F-value of 5.79 indicates that the model was significant and the significant model terms affecting

response Y_3 were the antagonistic linear contribution effects of homogenization pressure (X_2) and number of homogenization cycles (X_4) as described in Equation 6.8.

Table 6.7: *ANOVA analysis for the linear model for polydispersity index*

Source	Sum of squares	Degrees of freedom (df)	Mean square	F value	Prob > F
Model	**0.27**	**4**	**0.069**	**5.79**	**0.0021**
X_1	1.951E-003	1	1.951E-003	0.16	0.6885
X_2	**0.062**	**1**	**0.062**	**5.22**	**0.0315**
X_3	0.011	1	0.011	0.95	0.3400
X_4	**0.20**	**1**	**0.20**	**16.84**	**0.0004**
Residual	0.28	24	0.012	-	-

The normal probability, studentized residuals and Box-Cox plots for Y_3 are shown in Figures 6.8, 6.9 and 6.10 respectively. The normal probability and studentized residual plots reveal a linear distribution and scatter of the data, confirming a lack of problems with the normality of the data. However the minimum PDI value falls out of the linearity range. Inspection of the Box-Cox plot reveals that the data are in the optimum region of the parabola, confirming that the model generated for PDI was adequate and that no further transformation was necessary.

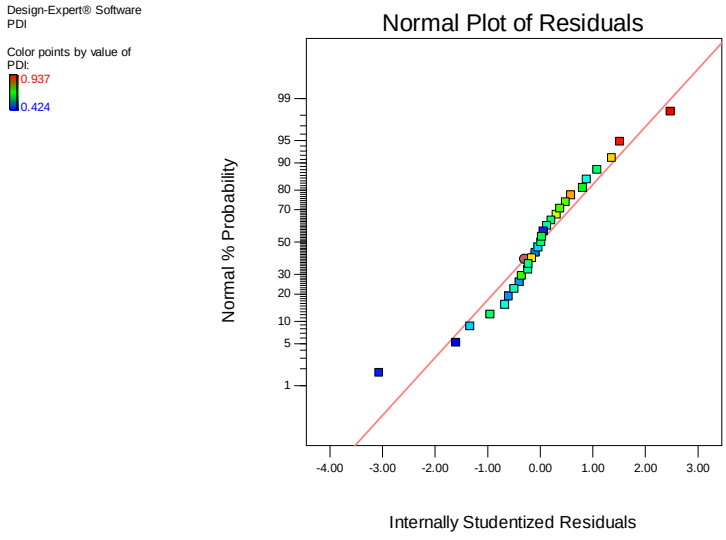

Figure 6.8: *Normal probability plot of residuals for polydispersity index*

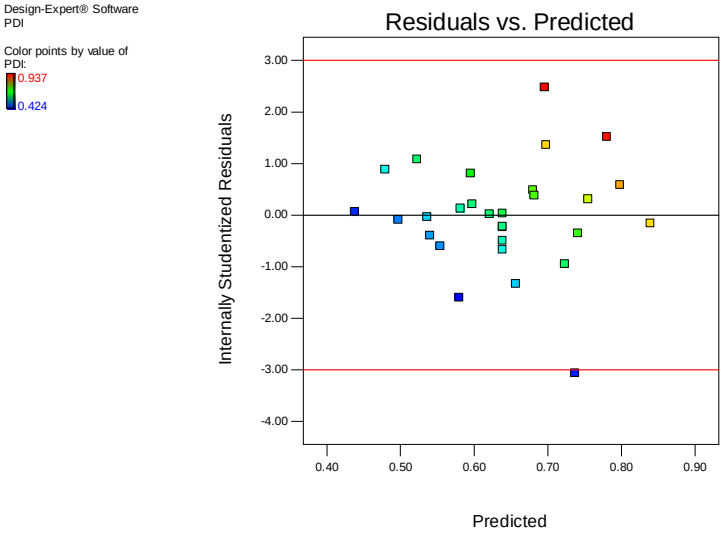

Figure 6.9: *Plot of studentized residuals versus predicted responses for polydispersity index*

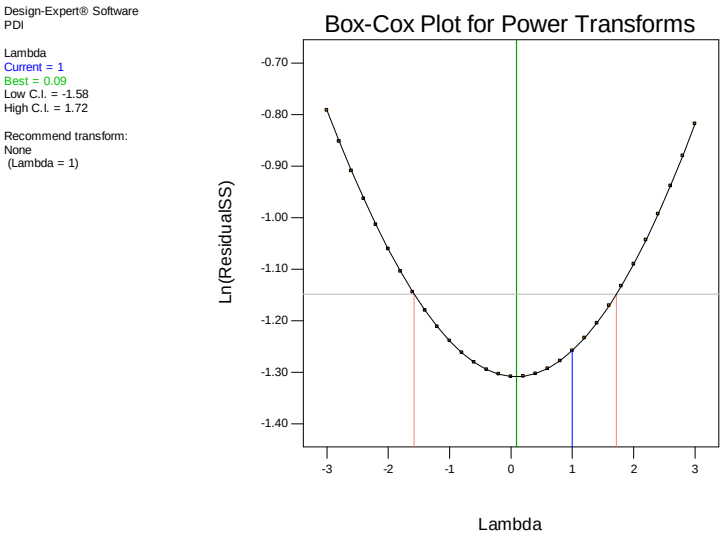

Figure 6.10: *Box-Cox plot for power transformation for polydispersity index*

6.3.1.3.4 Response surface quadratic model for visual assessment (Y_4)

The ANOVA data for the quadratic model for visual assessment are summarized in Table 6.8. The model F-value of 15.39 implies that the model was significant. The significant model terms affecting response Y_4 were the antagonistic linear contribution, interaction and quadratic effects

of amount of EFV (X_1), amount of EFV and Tween®80 content (X_1X_3) and amount of EFV (X_1^2) respectively. However the response was also affected by the synergistic linear contribution of X_3 in addition to the quadratic contribution of X_3^2 (Equation 6.9)

Table 6.8: *ANOVA analysis for the quadratic model for visual assessment*

Source	Sum of squares	Degrees of freedom (df)	Mean square	F value	Prob > F
Model	**6.41**	**14**	**0.46**	**15.39**	**< 0.0001**
X_1	**2.08**	**1**	**2.08**	**70.00**	**< 0.0001**
X_2	0.000	1	0.000	0.000	1.0000
X_3	**2.08**	**1**	**2.08**	**70.00**	**< 0.0001**
X_4	0.000	1	0.000	0.000	1.0000
X_1X_2	0.000	1	0.000	0.000	1.0000
X_1X_3	**0.25**	**1**	**0.25**	**8.40**	**0.0117**
X_1X_4	0.000	1	0.000	0.000	1.0000
X_2X_3	0.000	1	0.000	0.000	1.0000
X_2X_4	0.000	1	0.000	0.000	1.0000
X_3X_4	0.000	1	0.000	0.000	1.0000
X_1^2	**1.13**	**1**	**1.13**	**37.84**	**< 0.0001**
X_2^2	0.011	1	0.011	0.38	0.5483
X_3^2	**1.13**	**1**	**1.13**	**37.84**	**< 0.0001**
X_4^2	0.011	1	0.011	0.38	0.5483
Residual	0.42	14	0.030	-	-

The normal probability, studentized residuals and Box-Cox plots for Y_4 are shown in Figures 6.11, 6.12 and 6.13 respectively. The normal probability and studentized residual plots reveal a clustered distribution and scatter of data at the minimum (zero) and maximum (one) responses as these were the only two response parameter values used. The Box-Cox plot reveals that the data were not in the optimum region of the parabola and that transformation of the data was required. The natural logarithm transformation could not be applied since the smallest response value is 0 and the constant K for 0 is ≤ 0. However the Adequate Precision of 13.433 that was generated was indicative of a good signal indicating that the model could be used to navigate the design space.

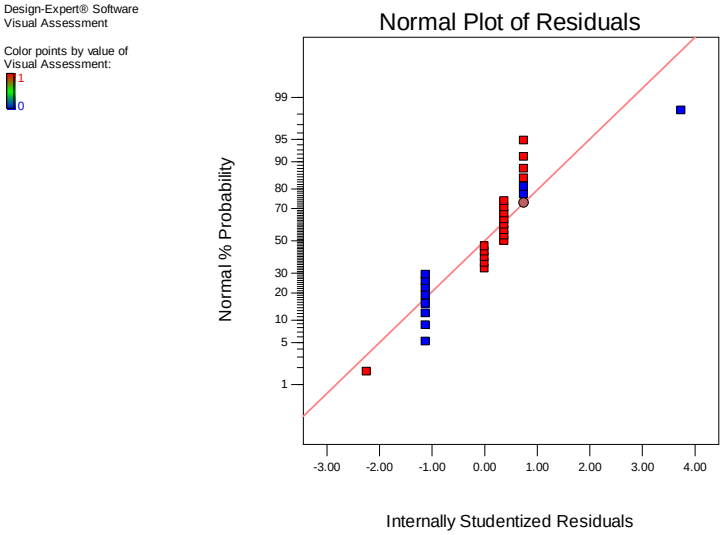

Figure 6.11: *Normal probability plot of residuals for visual assessment*

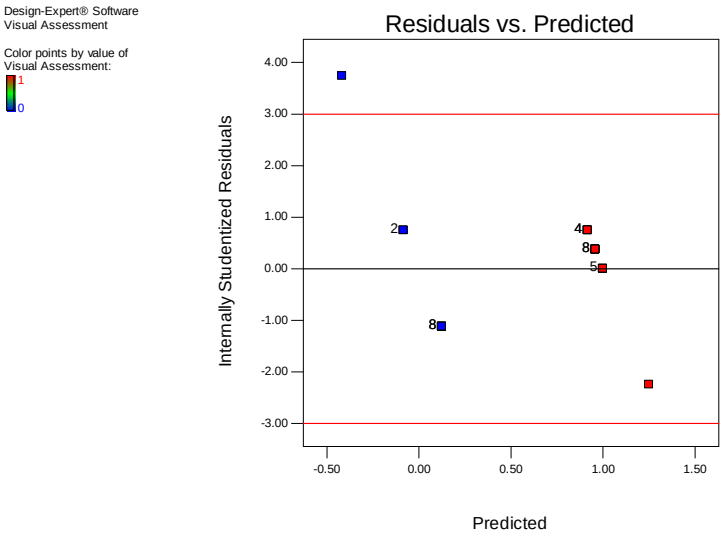

Figure 6.12: *Plot of studentized residuals versus predicted responses for visual assessment*

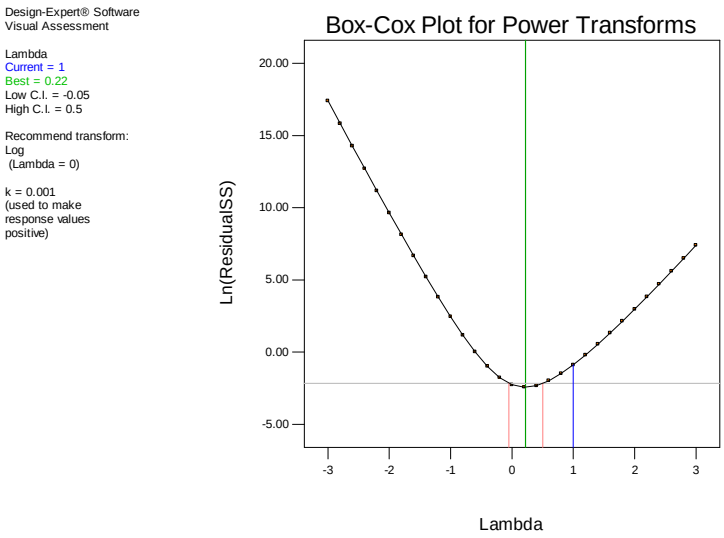

Figure 6.13: *Box-Cox plot for power transformation for visual assessment*

6.3.1.3.5 Response surface quadratic model release rate after 24 hours (Y_5)

The ANOVA data for the quadratic model for EFV release (RR) from the nanoparticles over 24 hours are summarized in Table 6.9. The model F-value of 10.48 indicates that the model was significant. The significant model terms affecting response Y_5 were the antagonistic linear contribution effects of amount of EFV (X_1) and the quadratic contributions of X_1^2 and number of homogenization cycles (X_4^2). However Y_5 was also synergistically affected by the linear contribution effects of homogenization pressure (X_2) and X_4 and the interaction effect of Tween®80 content and number of homogenization cycles (X_3X_4) as shown in Equation 6.10.

Table 6.9: *ANOVA analysis for the quadratic model for release rate*

Source	Sum of squares	Degrees of freedom (df)	Mean square	F value	Prob > F
Model	**7832.72**	**14**	**559.48**	**10.48**	**< 0.0001**
X_1	**246.61**	**1**	**246.61**	**4.62**	**0.0496**
X_2	397.90	1	397.90	7.45	0.0163
X_3	139.40	1	139.40	2.61	0.1284
X_4	**4768.05**	**1**	**4768.05**	**89.31**	**< 0.0001**
X_1X_2	54.76	1	54.76	1.03	0.3284
X_1X_3	160.02	1	160.02	3.00	0.1054
X_1X_4	34.22	1	34.22	0.64	0.4367
X_2X_3	1.21	1	1.21	0.023	0.8825
X_2X_4	3.42	1	3.42	0.064	0.8038
X_3X_4	**615.04**	**1**	**615.04**	**11.52**	**0.0044**
X_1^2	**371.95**	**1**	**371.95**	**6.97**	**0.0194**
X_2^2	66.84	1	66.84	1.25	0.2820
X_3^2	28.33	1	28.33	0.53	0.4783
X_4^2	**1033.48**	**1**	**1033.48**	**19.36**	**0.0006**
Residual	747.46	14	53.39	-	-

The normal probability, studentized residual and Box-Cox plots for Y_5 are shown in Figures 6.14, 6.15 and 6.16, respectively. The normal probability and studentized residual plots reveal a linear distribution and scatter of the data, confirming that the data were normal. The Box-Cox plot reveals that the data did not require any model transformation, indicating that the model was adequate and could be used to navigate the design space.

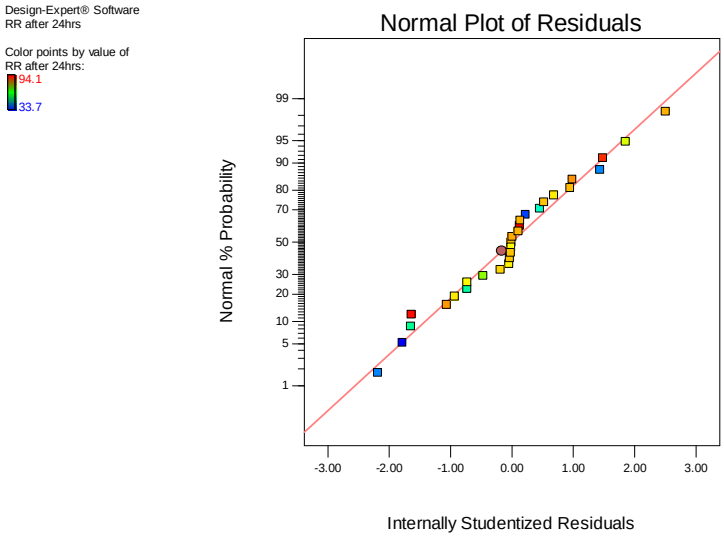

Figure 6.14: *Normal probability plot of residuals for release rate*

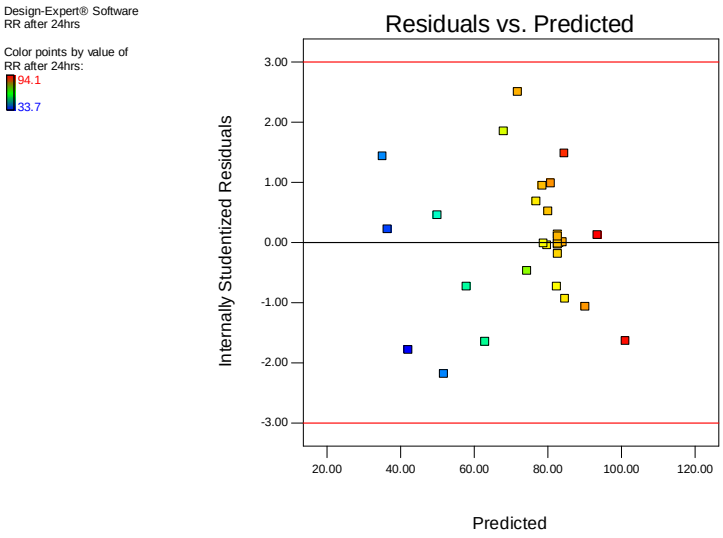

Figure 6.15: *Plot of studentized residuals versus predicted responses for release rate*

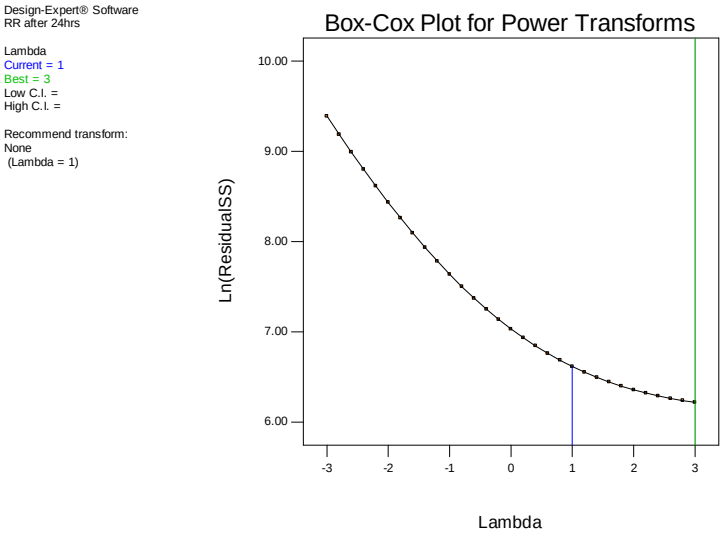

Figure 6.16: *Box-Cox plot for power transformation for release rate*

6.3.1.4 Process and Formulation Variable effects on CQA

A response surface is a graphical representation in one dimension (one factor of interest) or a surface in two or three dimensions (two factors of interest) when a response variable is plotted as a function of one or more factors [450]. One-factor contour and 3-dimensional surface plots are used to facilitate the examination of effect(s) of experimental factors on the responses monitored. These graphical representations can be obtained using Design Expert® software and are able to illustrate the responses of different experimental values and facilitate the identification of major interactions between variables [451]. When using 3-D and contour plots one variable must be set at an arbitrary value and the response surface plotted using two additional variables displayed on the X and Y-axes. Therefore the response surface generated will be a function of the selected value for the variable held constant and is likely to differ depending on the actual value used [452].

6.3.1.4.1 Zeta potential

The ZP is a measure of the overall charge at the surface of particles that have been dispersed in a particular medium. Particles tend to repel one another if the colloidal systems have high positive or negative values for the zeta potential. Consequently systems with ZP values of ± 30 mV are considered stable if dispersed in a liquid as a colloidal dispersion [453]. The ZP values generated for all formulations under investigation ranged between -31.5 and -51.6 mV. The concentration of Tween®80 (X_3) was the most significant variable affecting the ZP of the SLN and produced a synergistic effect with an F value of 46.27, as summarized in Table 6.5. The F-values for the antagonistic effects of X_1X_2 and X_3^2 were 6.47 and 7.50 respectively.

A contour and a 3-D surface plot revealing the effect of Tween®80 (X_3) on the ZP of the nanoparticles are shown in Figures 6.17 and 6.18 respectively. The surface plots show that stable formulations exhibiting relatively high negative ZP values were obtained at relatively low surfactant concentrations. The use of high concentrations of Tween®80 resulted in a decrease in the ZP and hence the stability of the SLN dispersions. The negative impact of increasing

Tween®80 concentration on the zeta potential could be explained by the solubilizing and partitioning phenomena. High concentrations of surfactant in the aqueous phase may lead to preferential partitioning of the API from the lipid phase into the aqueous phase. The preferential partitioning of the API to the aqueous phase may lead to a decrease in the magnitude of the charge at the surface of the particles that ultimately compromises the stability of the dispersions [454,455].

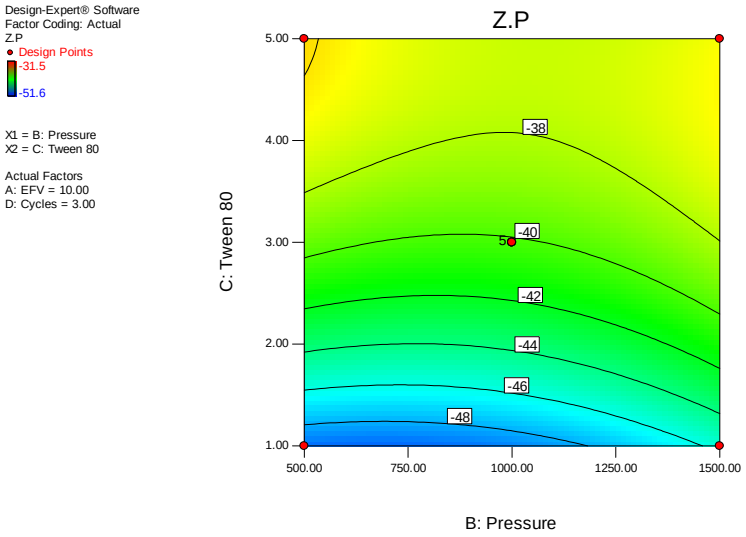

Figure 6.17: *Contour plot showing the effect of Tween®80 and homogenization pressure on zeta potential*

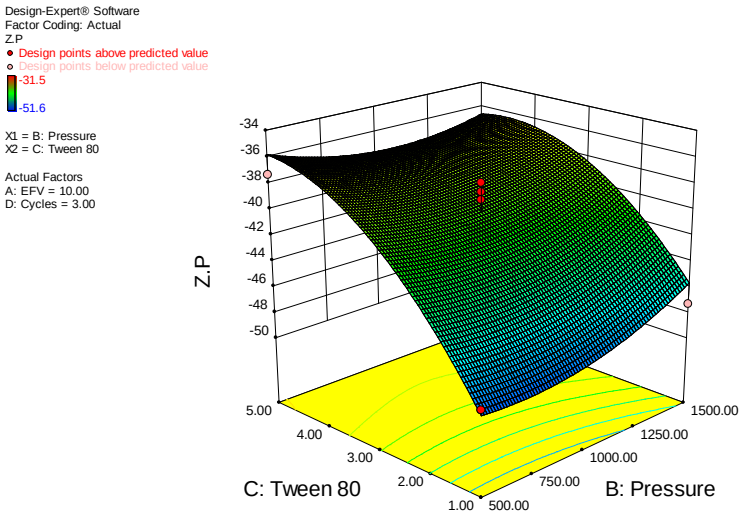

Figure 6.18: *3-D surface plot showing the effect of Tween®80 and homogenization pressure on zeta potential*

6.3.1.4.2 Particle size

The mean PS of EFV-loaded SLN was between 42.19 and 684 nm. The number of homogenization cycles (X_4) produced the largest F-value of 153.24, indicating that this parameter had the most significant impact on the size of the nanoparticles produced compared to the other variables investigated. However homogenization pressure (X_2) and a combination of homogenization pressure and homogenization cycles (X_2X_4) produced F-values of 29.24 and 13.32 respectively, which indicate that these parameters had an intermediate yet significant impact on the size of SLN.

A combination of Tween®80 and homogenization cycles (X_3X_4) and the quadratic effect of amount of EFV (X_1^2) had the least significant impact on the size of the nanoparticles as each parameter reflected relatively low F-values of 6.08 and 8.45 respectively. The contour and 3-D surface plot showing the effect of number of homogenization cycles on the particle size are shown in Figures 6.19 and 6.20 respectively. These data reveal that an inverse relationship exists between the number of homogenization cycles and the PS of the nanoparticles. The surface plots also reveal that relatively small SLN are produced if the homogenization pressure is relatively high and the number of homogenization cycles is kept constant. These results are consistent with previous findings that reported a reduction in mean PS and PDI values with an increase in homogenization pressure up to 1500 bar and using between 3 and 7 homogenization cycles [204,216]. The desired mean particle size can therefore be produced by a manipulation of the combined effects of homogenization pressure and the number of homogenization cycles used to manufacture the particles.

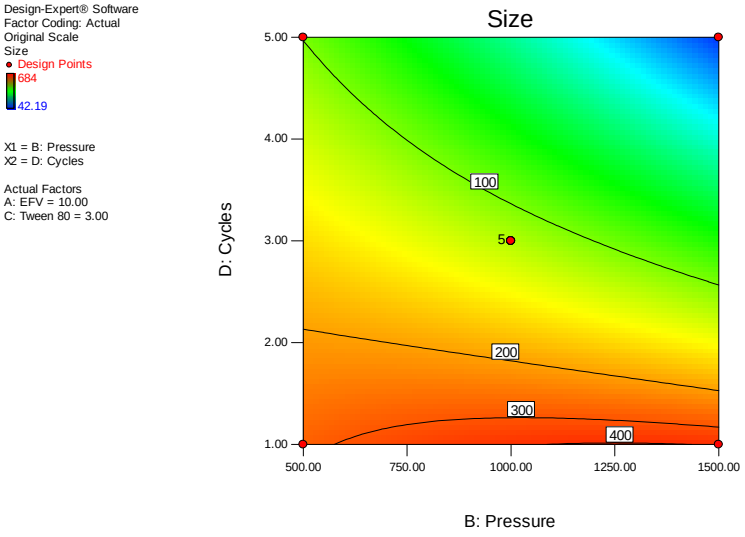

Figure 6.19: *Contour plot showing the effect of homogenization cycles and pressure on particle size*

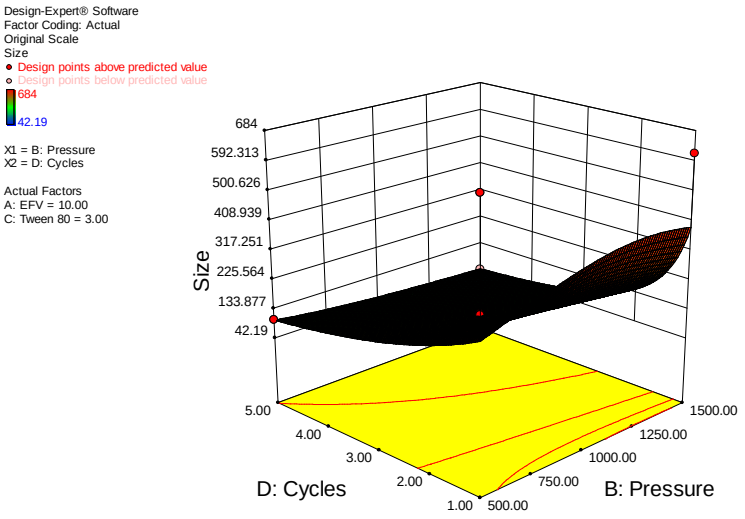

Figure 6.20: *3-D surface plot showing the effect of homogenization cycles and pressure on particle size*

6.3.1.4.3 Polydispersity index (PDI)

The PDI is a measure of the width of the distribution of particle sizes, and well-formulated colloidal systems generally exhibit narrow particle size distributions characterized by low values for PDI [210,218]. The PDI values generated for all formulations were between 0.424 and 0.937.

The largest F-value of 16.84 was observed with the number of homogenization cycles (X_4) used. However the homogenization pressure also had a significant effect on the PDI, indicated by an F-value of 5.22 as listed in Table 6.7. The one-factor plot of the effect of homogenization cycles and the contour plot showing the effect of homogenization pressure on PDI for the linear model are shown in Figures 6.21 and 6.22 respectively. These data show an inverse relationship between the homogenization pressure and the number of homogenization cycles and the PDI. Therefore similar to mean PS the desired PDI can be obtained by manipulation of the homogenization pressure and the number of homogenization cycles.

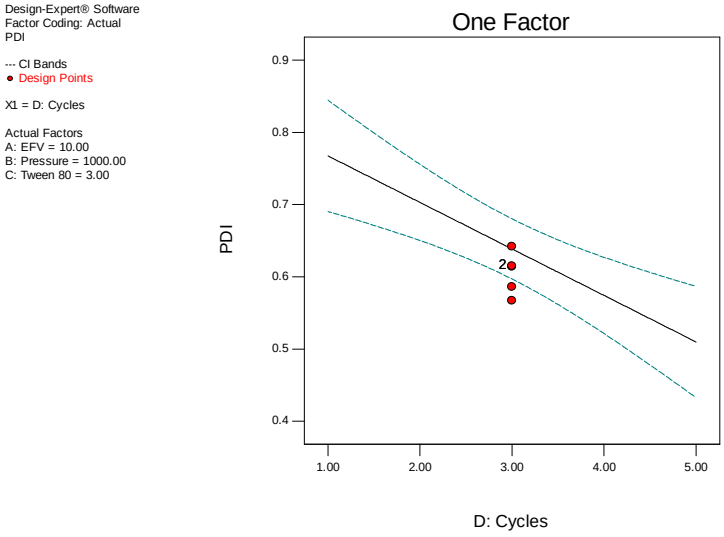

Figure 6.21: *Effect of number of homogenization cycles on polydispersity index*

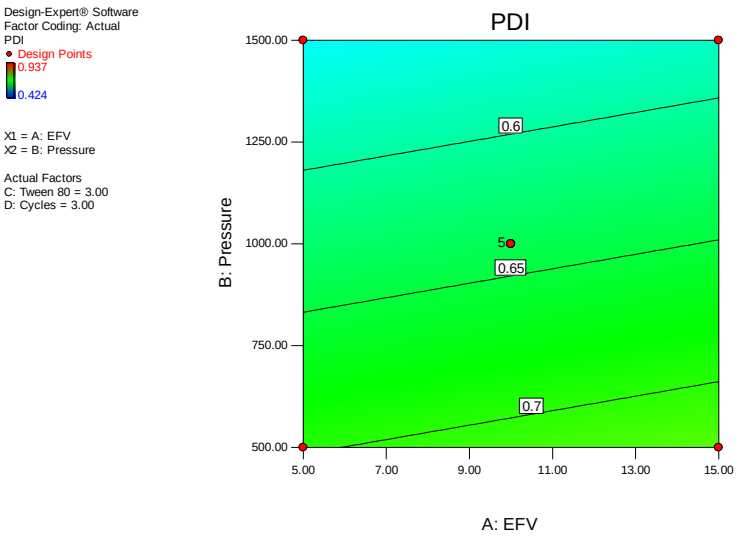

Figure 6.22: *Contour plot showing the effect of homogenization pressure and amount of EFV on polydispersity index*

6.3.1.4.4 Visual assessment

A major parameter governing the physical and chemical stability of SLN is the ability of the SLN to remain dispersed and a homogenous product over time [210,456]. Instability may lead to the breakdown of SLN emulsions and are manifested as flocculation, sedimentation and/or creaming and cracking [210,456]. The significant variables that were evaluated to assess the visual appearance of the SLN following storage at room temperature (22°C) for two weeks were the amount of EFV (X_1), Tween®80 (X_3), their quadratic effects (X_1^2 and X_3^2) and the effect of their combined interaction (X_1X_3). The largest F-value of 70 was observed for both linear contributing variables of X_1 and X_3. Their quadratic contributions had similar yet intermediate significance, with an F-value of 37.84. The interaction factor X_1X_3 had the least significant effect, with an F-value of 8.40.

However the contour and 3-D plot of X_1X_3 shown in Figures 6.23 and 6.24 respectively show a curvature in the response surface indicating the response increases and subsequently reduces as the concentration of Tween®80 and the amount of EFV in the formulation were increased. The

surface plots reveal that the SLN formulation was most stable when Tween®80 and EFV were used in combination at a relatively low concentration of 3% w/w and 10% w/w, respectively. This is in agreement with previous findings that the use of relatively high concentrations of API leads to an increase in the size of nanoparticles [125], increasing the probability of coalescence and formulation instability. However the use of relatively high surfactant/lipid ratios has been shown to produce smaller particles [215], decreasing the likelihood of coalescence and therefore enhancing the stability of formulations.

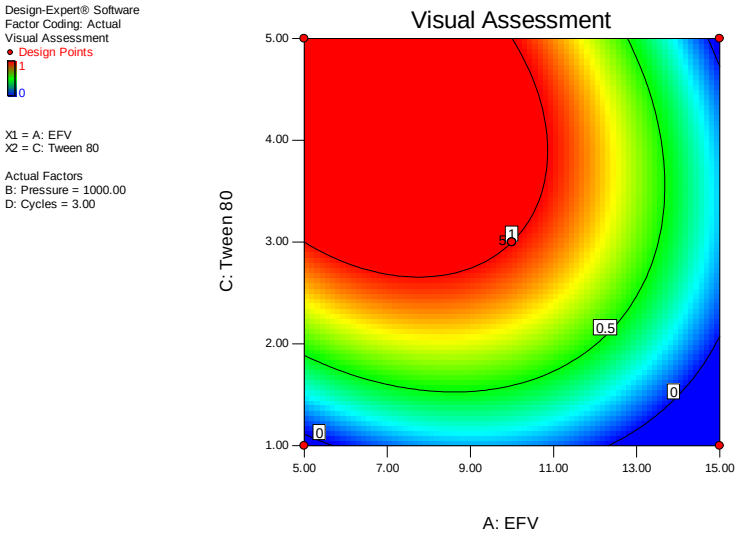

Figure 6.23: *Contour plot showing the effect of Tween® 80 and amount of EFV on visual appearance*

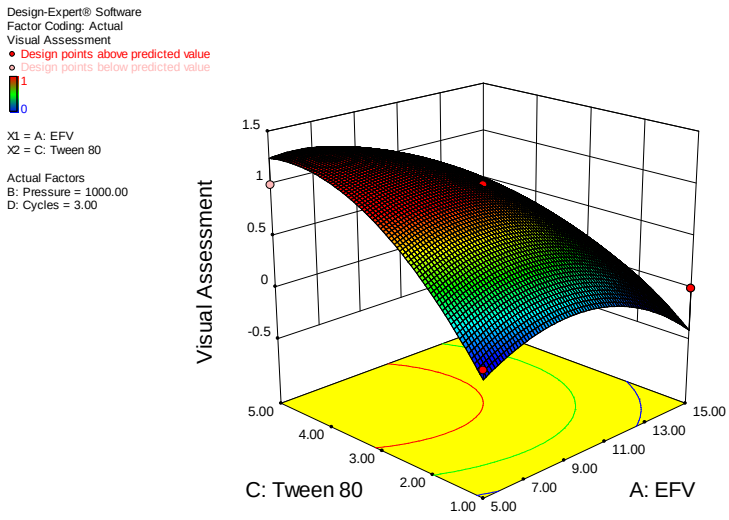

Figure 6.24: *3-D surface plot showing the effect of Tween® 80 and amount of EFV on visual appearance*

6.3.1.4.5 Cumulative percent released

The amount of EFV released from the SLN over a 24 hour test period was between 33.7 and 94.1%. The variables considered significant in evaluating the release of EFV from the SLN formulations were concentration of EFV (X_1), number of homogenization cycles (X_4), their quadratic effects (X_1^2 and X_4^2) and the interactive effect of Tween®80 and number of homogenization cycles (X_3X_4). The largest F-value of 89.31 was observed for the linear effect of number of homogenization cycles, indicating that this parameter had the most significant effect on the cumulative percent released from SLN. The effects of the quadratic contribution of number of homogenization cycles (X_4^2) and the interactive effect of Tween®80 and number of homogenization cycles (X_3X_4) were also significant, albeit to a lesser extent as these parameters produced F-values of 19.36 and 11.52 respectively. However the amount of EFV (X_1) in the formulation and its quadratic contribution (X_1^2) had the least effect on EFV release from the nanoparticles, with F-values of 4.62 and 6.97 respectively. The contour and 3-D surface plots of X_3X_4 are shown in Figures 6.25 and 6.26 respectively.

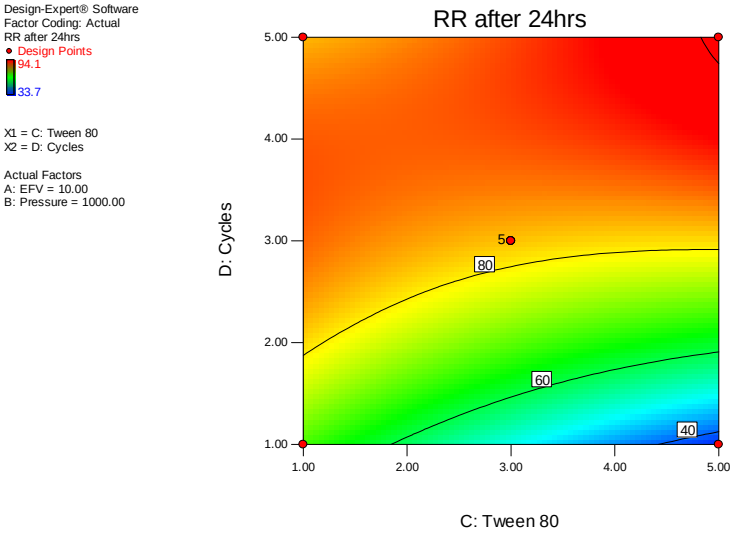

Figure 6.25: *Contour plot showing the effect of homogenization cycles and Tween® on EFV release*

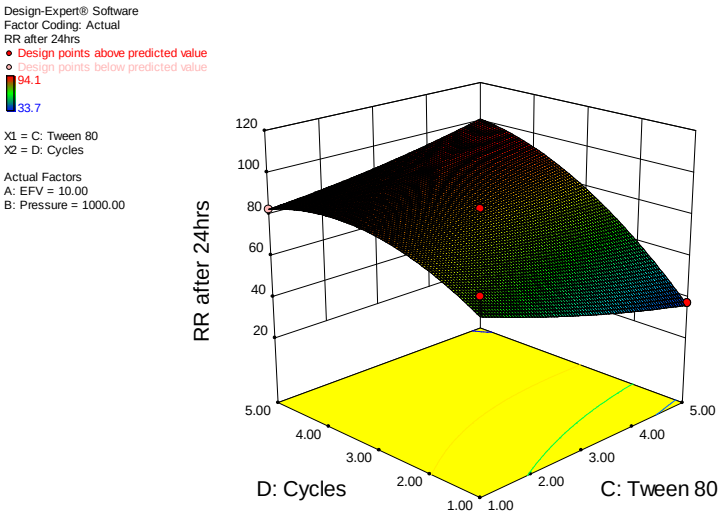

Figure 6.26: *3-D surface plot showing the effect of homogenization cycles and Tween® on EFV release*

The surface plots show that the amount of EFV released from SLN increases with an increase in the number of homogenization cycles used. In addition, when the number of homogenization cycles is kept constant an increase in the concentration of Tween®80 leads to a decrease in the release of EFV. These significant variables, i.e. number of homogenization cycles and concentration of Tween®80, also had a major impact on the size of the nanoparticles as discussed

in § 6.3.1.4.2. Previous studies have shown that the size of SLN can affect *in vitro* release of an API from nanoparticles [168]. It follows that small particles release API at a faster rate due to the small path length through which the API must diffuse and the relatively large surface area associated with small particles that permits better contact between the particles and the release medium [168].

6.3.2 Formulation Optimization

A major objective of these studies was to produce stable EFV-loaded SLN or NLC capable of controlling or sustaining the release of EFV. The ZP (Y_1), PDI (Y_3) and VA (Y_4) of the formulation were considered as the critical parameters for assessing the stability of the nanoparticle dispersions. Therefore numerical optimization was undertaken using Design Expert® software with the aim of selecting an optimum formulation composition and process parameters that would lead to the development of an SLN or NLC formulation with optimal stability and with the potential to control or sustain the release of EFV. Although there are various methods for optimizing process and formulation parameters the use of a numerical optimization technique presents a comprehensive and current description of the most effective method for continuous optimization [457,458]. Numerical optimization locates a point that maximizes the desirability function while the characteristics of a target can be modified by adjusting the importance of that target [459]. The desired target for each process variable and responses Y_1, Y_3, Y_4 and Y_5 were selected and are summarized in Table 6.10.

Table 6.10: *Predicted values for process variables and respective formulation responses*

Process variables				**Formulation responses**				**Desirability**
X_1	X_2	X_3	X_4	Y_1	Y_3	Y_4	Y_5	
10%	1100 bar	2.89%	3	-30	0.424	1	94.1%	0.909

The desirability for the model generated was found to be 0.909, therefore the optimal conditions were considered to be in the desirability zone. The optimal EFV-loaded SLN formulation was manufactured and the process parameters for the manufacture are summarized in Table 6.11

Table 6.11: *Optimized conditions for the manufacture of EFV-loaded SLN*

Process variable	Optimized condition
X_1 **(EFV)**	10%
X_2 **(Homogenization pressure)**	1100 bar
X_3 **(Tween® 80)**	3.0%
X_4 **(Homogenization cycles)**	3

The responses generated using the SLN formulation developed and manufactured using the optimum formulation and process parameters are summarized in Table 6.12, in addition to the experimental and predicted responses with their corresponding percentage prediction errors

Table 6.12 *Experimental and predicted response with percent prediction errors for the optimized formulation*

Response	Experimental value	Predicted value	% prediction error
Y_1	-32.5±4.99	-30	7.69
Y_3	0.382±0.054	0.424	-10.99
Y_4	1	1	0
Y_5	91.5±0.671	94.1	-2.84

The low value of the calculated percentage prediction error indicates the robustness of the mathematical model used. In addition the high predictive ability of RSM is also demonstrated, suggesting the efficiency of RSM as a tool for process optimization [373].

6.3.3 Kinetics and mechanism of EFV release

To determine the kinetics and mechanism of EFV release from SLN, *in vitro* release data from all 29 formulations and the optimized formulation (EFV-SLN-OPT) were fitted to three different mathematical models. The data generated from these studies are summarized in Table 6.13. Using the R^2 value as a good fit criterion it was established that EFV release from the formulations was best described by the First-order and Higuchi models, although some of the zero order models also had R^2 values > 0.90. The models described EFV release for all but two formulations viz. EFV-SLN 001 and EFV-SLN 026, with values of > 0.90 for the regression

coefficient. Therefore the release of EFV from SLN was proportional to the amount of API remaining in the nanocarriers and diminished over time.

Table 6.13: *Summary of EFV release kinetics for BBD formulations*

Formulation	R^2			Mechanism
	Zero order	First order	Higuchi	
EFV-SLN 001	0.7676	0.8935	0.8242	First order
EFV-SLN 002	0.8945	0.9490	0.9418	First order
EFV-SLN 003	0.9160	0.9690	0.9637	First order
EFV-SLN 004	0.9034	0.9461	0.9328	First order
EFV-SLN 005	0.9761	0.9835	0.9817	First order
EFV-SLN 006	0.9247	0.9573	0.9798	Higuchi
EFV-SLN 007	0.9280	0.9503	0.9814	Higuchi
EFV-SLN 008	0.8446	0.9346	0.9241	First order
EFV-SLN 009	0.9444	0.9649	0.9553	First order
EFV-SLN 010	0.8346	0.9295	0.9249	First order
EFV-SLN 011	0.9378	0.9585	0.9808	Higuchi
EFV-SLN 012	0.8399	0.9310	0.9312	Higuchi
EFV-SLN 013	0.9579	0.9821	0.9917	Higuchi
EFV-SLN 014	0.9392	0.9848	0.9776	First order
EFV-SLN 015	0.8929	0.9594	0.9456	First order
EFV-SLN 016	0.8582	0.8986	0.9368	Higuchi
EFV-SLN 017	0.9629	0.9690	0.9842	Higuchi
EFV-SLN 018	0.8859	0.9535	0.9627	Higuchi
EFV-SLN 019	0.8607	0.9277	0.9537	Higuchi
EFV-SLN 020	0.8893	0.9656	0.9574	First order
EFV-SLN 021	0.9011	0.9208	0.9522	Higuchi
EFV-SLN 022	0.8987	0.9654	0.9747	Higuchi
EFV-SLN 023	0.8557	0.9309	0.9311	Higuchi
EFV-SLN 024	0.9338	0.9636	0.9644	Higuchi
EFV-SLN 025	0.9307	0.9749	0.9716	First order
EFV-SLN 026	0.6901	0.8339	0.8178	First order
EFV-SLN 027	0.8687	0.9433	0.9352	First order
EFV-SLN 028	0.9834	0.9841	0.9832	First order
EFV-SLN 029	0.9101	0.9471	0.9378	First order
EFV-SLN-OPT	0.8894	0.9667	0.9107	First order

6.3.4 Characterization of optimized SLN and NLC

6.3.4.1 Particle size and size distribution

The stability of SLN and NLC dispersions is dependent on a number of factors including PS and PDI [176,210], therefore it essential that these two CQA are adequately monitored. The mean PS and PDI of EFV-loaded SLN was 59.00 ± 23.16 nm and 0.382 ± 0.054 respectively, measured on the day of manufacture. Similarly values of 34.73 ± 0.7709 nm and 0.394 ± 0.027 for mean PS

and PDI of EFV-loaded NLC were measured on the day of manufacture. It is clear that both SLN and NLC formulation were in the nanometer range, with particle size distributions that are considered acceptable.

However the PDI value observed for EFV-NLC was higher than that of the SLN. The substitution of 30% solid lipid with THP decreased the amount of mono-, di- and acyl-glycerols in the formulation, which tends to broaden the size distribution of NLC [417]. Therefore when the amount of EFV in SLN and NLC is the same, it is invariable that EFV-loaded NLC would exhibit a larger particle size than EFV-SLN because of the fluidity of THP in the lipid matrix that leads to the expansion of the solid lipid core. However the size of the nanoparticles may be significantly affected by process variables such as homogenization pressure and number of homogenization cycles as highlighted in § 6.3.1.3.2. Different process parameters were used for the manufacture of SLN and NLC, the consequence of which are the differences in PS and PDI values that were observed.

6.3.4.2 Zeta potential

The optimized EFV-loaded SLN and NLC had a ZP of -32.5 ± 4.99 mV and -22.4 ± 3.72 mV measured on the day of manufacture using HPLC grade water as the dispersion medium. The negative dimension for the ZP is due to the incorporation of Tween®80 in the formulation. The surfactant is non-ionic and therefore does not ionize, but molecular polarization and adsorption of the surfactant molecule onto the charged water molecules may lead to the formation of an electric double layer similar to that of an ionic surfactant [223,460].

The ZP of EFV-NLC was not as high as that of SLN and was therefore lower than the value that implies adequate stability of these systems (-30 mV). This may be attributed to a shift in the shear plane of the NLC due to the incorporation of liquid lipid into the solid lipid core [223,461] and the formulation is considered unstable. However, it should be acknowledged that reference to 30 mV in order to imply stability applies to colloidal systems that have been stabilized using

electrostatic interactions only. Tween®80 imparts steric stability to the nanoparticles in addition to electrostatic repulsion [223,461], consequently the ZP of NLC is adequate for the purpose of providing stability to nanoparticles.

6.3.4.3 Loading capacity (LC) and Encapsulation efficiency (EE)

The LC and EE values of the optimized SLN for EFV as determined on the day of manufacture were 9.68 ± 1.77 and 96.77 ± 0.45% respectively. Similarly, 9.995 ± 0.67%, and 99.93 ± 0.413% were the LC and EE for NLC. The SLN exhibited relatively low LC and EE values for EFV compared to those observed for NLC formulations, which may be due to the relatively high solubility of EFV in liquid lipid compared to the solubility observed for the solid lipid alone. It has been previously shown that high LC and EE values can be observed when the solubility of an API is increased in the lipid used [127,462]. Furthermore, the addition of THP to GM may increase the complexity of the internal solid lipid structure and this disordered molecular arrangement creates additional voids for entrapping the API [162,166]. Regardless of the relatively small differences in the magnitude of the values for LC and EE for both SLN and NLC, the EFV payload observed in these studies was considered adequate.

6.3.4.4 Polymorphism and crystallinity

6.3.4.4.1 DSC characterization

DSC was used to evaluate the polymorphism of optimized EFV-loaded SLN and NLC, and the data generated are depicted in Figures 6.27 and 6.28 respectively.

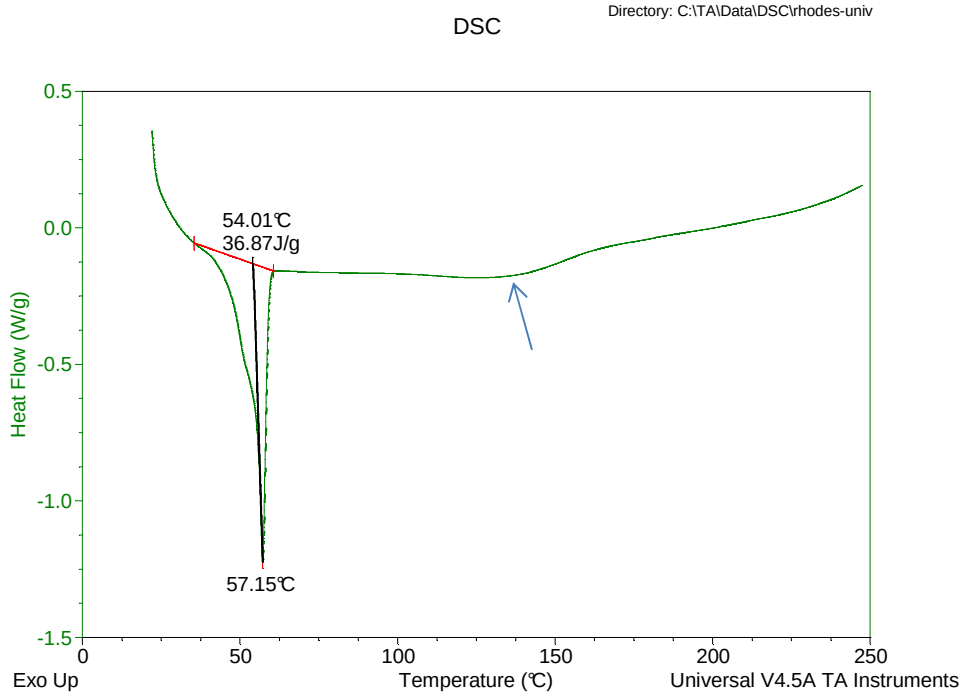

Figure 6.27: *DSC thermogram for optimized EFV-loaded SLN*

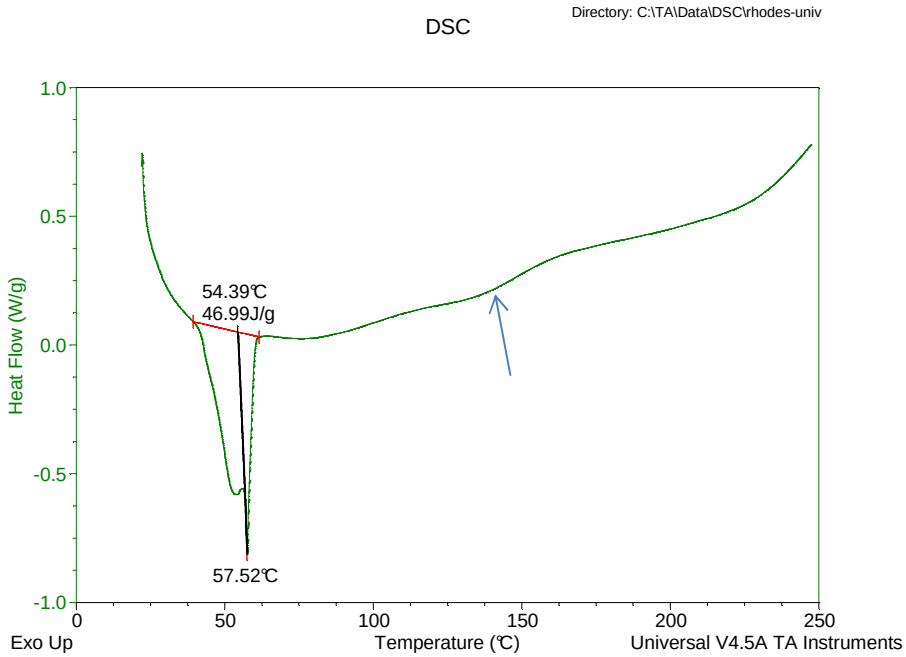

Figure 6.28: *DSC thermogram for optimized EFV-loaded NLC*

The DSC thermogram generated for EFV-loaded SLN revealed the presence of a single endothermic event and the absence of a peak for EFV around 138°C (indicated by an arrow). This indicates the existence of a single polymorphic form of the solid lipid and that EFV is molecularly dispersed in the SLN. The onset temperature and melting at 54.01°C and 57.15°C respectively are consistent with the presence of the α-polymorphic form of GM as reported in § 5.3.3.1.2. Similarly the DSC thermogram for EFV-loaded NLC revealed that EFV was molecularly dispersed in the NLC. However, the thermogram revealed the presence of two endothermic events implying the co-existence of α- and β'-polymorphic forms. In contrast to the results reported in § 5.3.3.2.2 the β'-polymorphic form is more dominant than the α-modification in the NLC as can be clearly observed from the intensities of the two peaks. This could be attributed to a change in the lattice structure of the lipid mixture due to the incorporation of EFV and Tween® 80 in the binary mixture of the lipid used for the formulation of EFV-loaded NLC.

6.3.4.4.2 FT-IR characterization

FT-IR was used to assess the crystalline nature of the optimized EFV-loaded SLN and NLC, and spectra generated are depicted in Figures 6.29 and 6.30 respectively. These data also show the FT-IR profile of GM that was generated following exposure to heat for comparative purposes and to facilitate data interpretation.

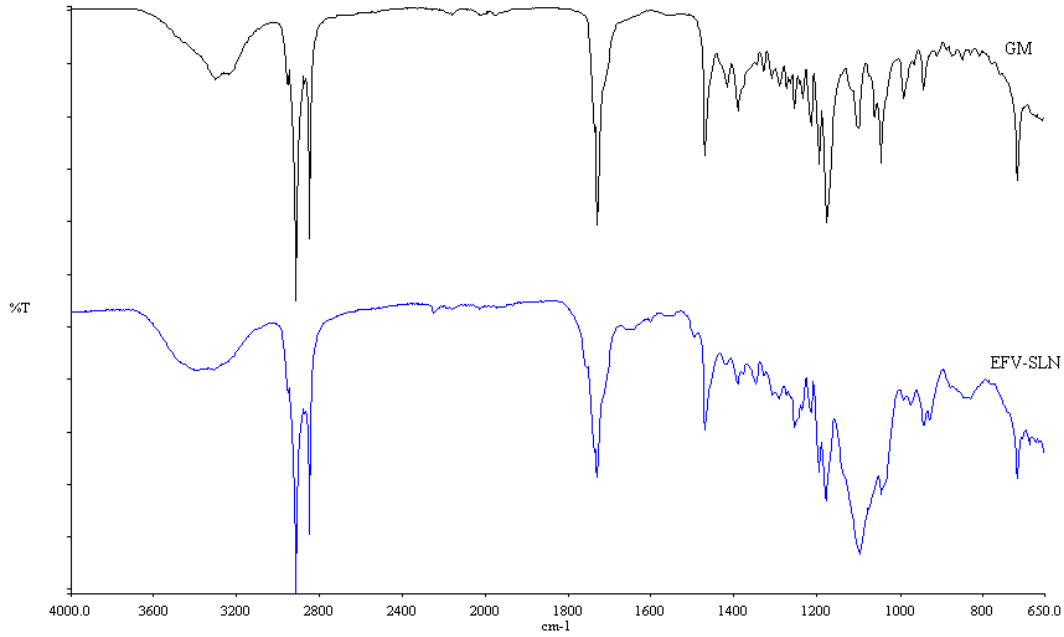

Figure 6.29: *FT-IR profiles of optimized EFV-loaded SLN and glyceryl monostearate following exposure to heat*

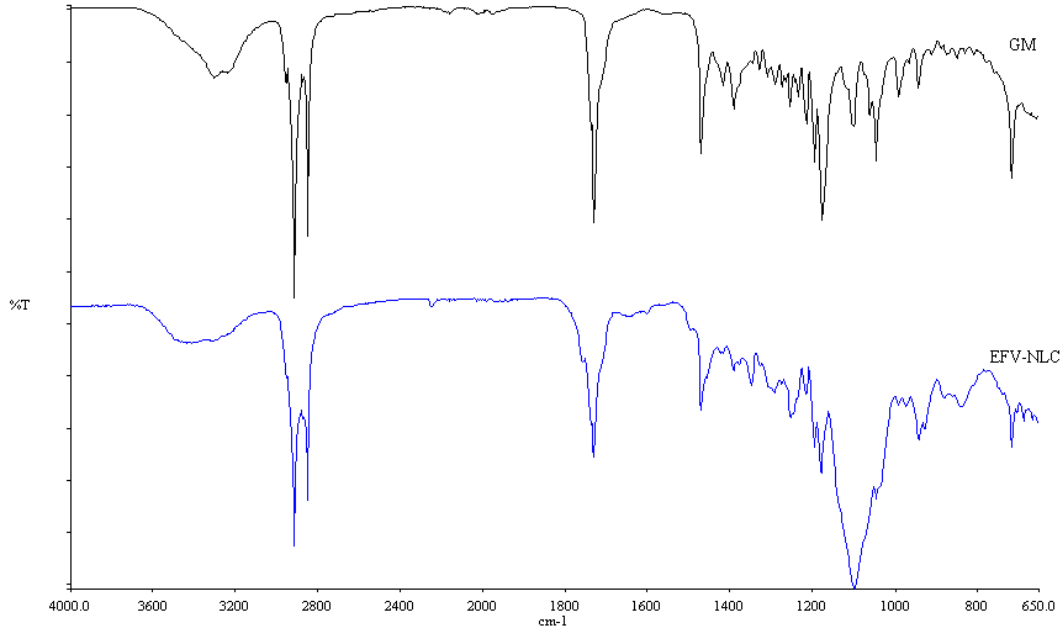

Figure 6.30: *FT-IR profiles of optimized EFV-loaded NLC and glyceryl monostearate after exposure to heat*

The FT-IR profiles for the colloidal systems reveal the presence of the characteristic bands of the solid lipid material, GM. However, the characteristic bands which are consistent with molecular

vibrations of EFV were not observed for both SLN and NLC, confirming the DSC results suggesting that EFV was molecularly dispersed in the nanoparticles. The band intensity of SLN looks similar to that of GM, suggesting that the crystalline nature of the lipid did not change to any great extent. However the NLC band intensity is low, which may indicate the amorphous nature of the carriers due to the presence of THP.

6.3.4.5 Shape and surface morphology

6.3.4.5.1 Scanning electron microscopy

The shape and surface morphology of the optimized EFV-SLN and EFV-NLC following lyophilization were evaluated using SEM. These data are shown in Figures 6.31 and 6.32 respectively.

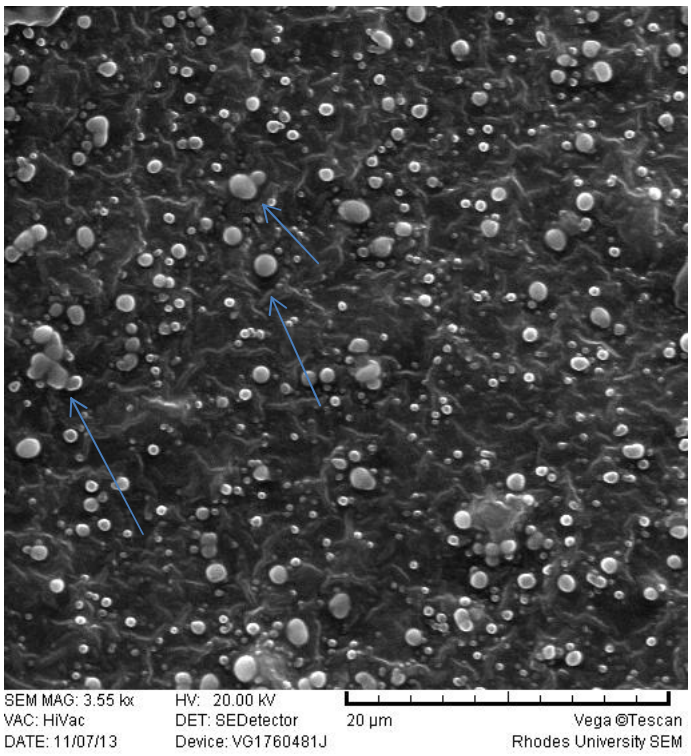

Figure 6.31: *SEM micrograph of the optimized EFV-loaded SLN*

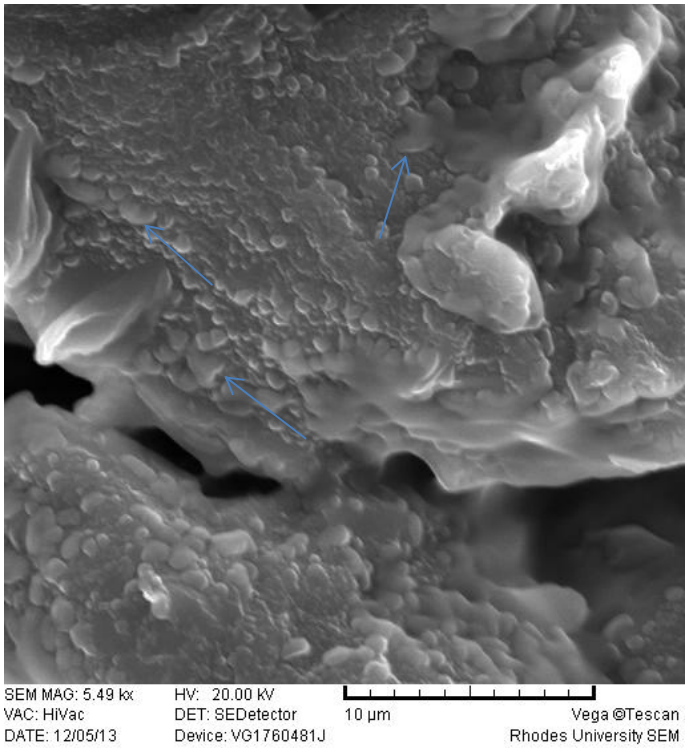

Figure 6.32: *SEM micrograph of the optimized EFV-loaded NLC*

EFV-loaded SLN and NLC appeared smooth and somewhat spherical. However, the surface of the NLC appeared to be smoother than that of the SLN, possibly due to the presence of THP in the solid lipid matrix. It can be concluded that the inclusion of THP in the lipid phase to produce NLC imparted some variation to the surface morphology of the particles. It should also be noted that close inspection of the SEM micrographs reveals the presence of microparticles, as indicated by arrows. These observations differ with the PCS data described in § 6.3.4.1. It has been suggested that lyophilization of aqueous dispersions of SLN or NLC may promote aggregation of nanoparticles, especially when freeze drying is undertaken without the use of a cryoprotectant [220,221]. The aggregates may appear as microparticles when visualized with SEM.

6.3.4.5.2 Transmission electron microscopy

TEM was also used to investigate the morphology of the optimized EFV-loaded SLN and NLC products in the original aqueous dispersion and the data generated are shown in Figures 6.33 and 6.34 respectively.

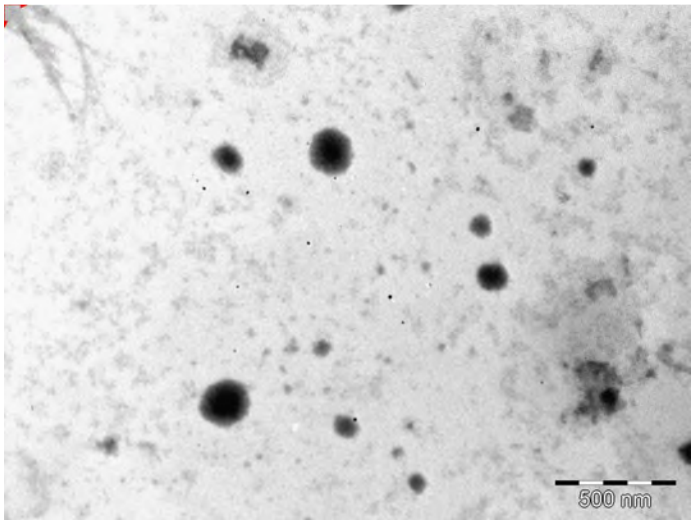

Figure 6.33: *TEM micrograph of the optimized EFV-loaded SLN*

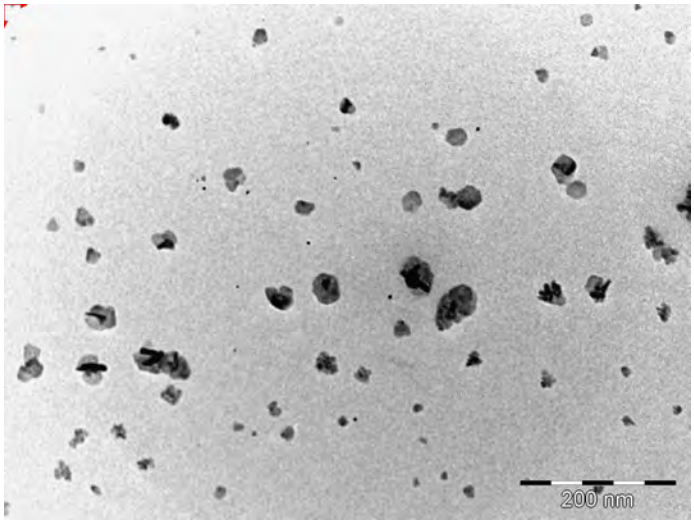

Figure 6.34: *TEM micrograph of the optimized EFV-loaded NLC*

The EFV-SLN particles are mainly present as discrete entities compared to EFV-NLC particles. The SLN particles appear to be larger than the NLC particles, which is consistent with the lower PS and higher PDI observed for NLC reported in § 6.3.4.1. Microparticles were not observed in TEM images. The preparation of samples for TEM analysis does not involve freeze-drying, supporting the notion that lyophilization may lead to the formation of microparticles.

The shape of the SLN and/or NLC particles may be determined by the purity of the lipid used. Chemically pure and homogenous lipids usually produce nanoparticles that are cuboidal [125]. Similarly spherical particles are usually observed with the use of lipids that are chemically polydispersed [125,223,232]. Therefore it was expected that EFV-loaded SLN would be cuboidal compared to the more spherical NLC observed. However the inclusion of a surfactant in the formulation of SLN has the potential to distort the crystal structure of pure lipids leading to a change of morphology of the nanoparticles from cuboidal to spherical [125]. Therefore the SLN and NLC produced in these experiments were generally spherical.

6.3.4.6 In vitro release

6.3.4.6.1 Selection of dissolution medium and flow rate

The *in vitro* release profiles for EFV-loaded SLN generated as a function of SLS concentration and dissolution medium flow rate are shown in Figures 6.35 and 6.36 respectively.

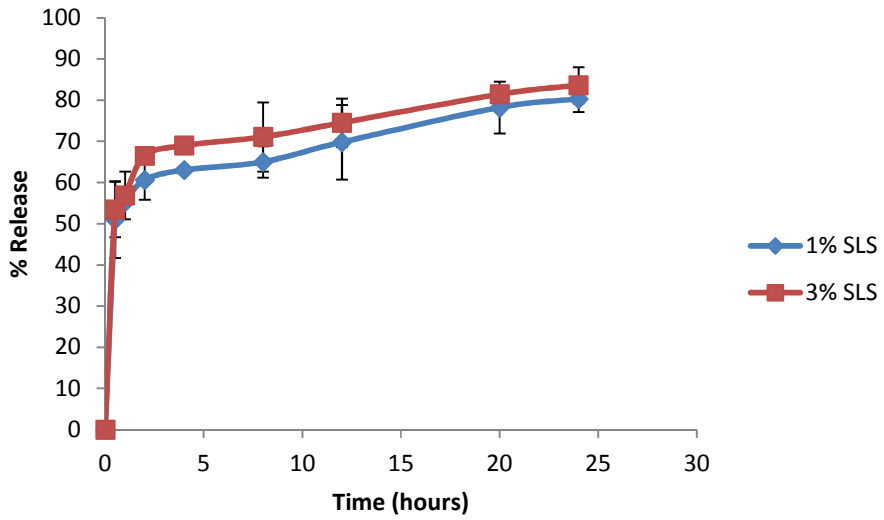

Figure 6.35: *Effect of SLS concentration on EFV release from EFV-SLN at a flow rate of 8.8 ml/min (n=3)*

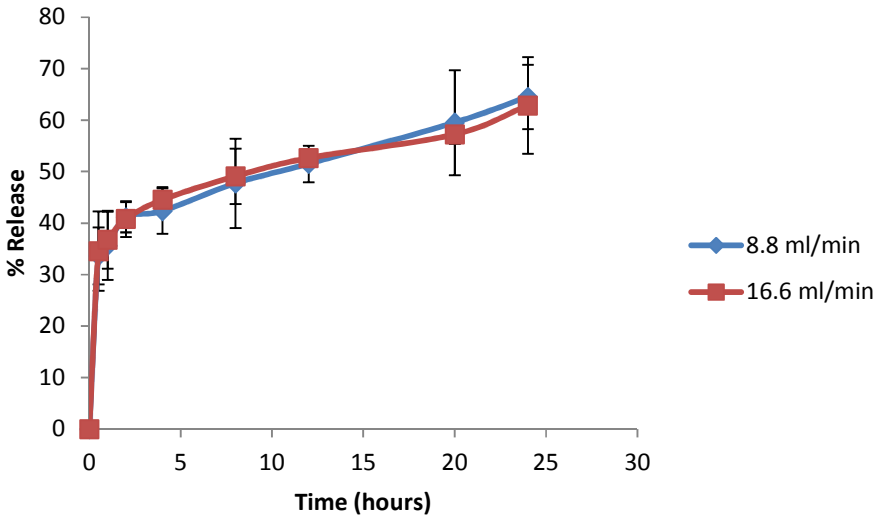

Figure 6.36: *Effect of flow rate on EFV release from f EFV-SLN in 1% SLS (n=3)*

The data plotted in Figures 6.35 and 6.36 have f_2 values of 90.5 and 96.8 respectively, indicating that the use of relatively high concentration of SLS in the dissolution medium and high flow rates did not have an effect on the rate and extent of EFV release from the nanoparticles. Therefore a dissolution medium containing 1% w/w SLS was used to assess the *in vitro* release characteristics of EFV from SLN and NLC at a flow rate of 8.8 ml/min.

6.3.4.6.2 Comparison of EFV release from SLN and NLC

The *in vitro* release profile of EFV from the optimized formulations for SLN and NLC are shown in Figure 6.37

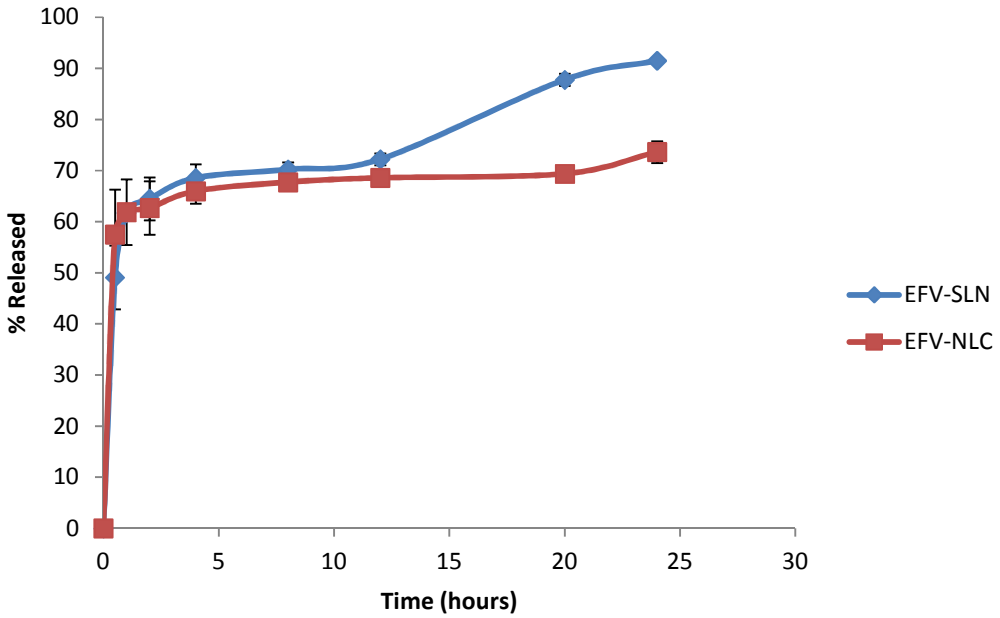

Figure 6.37: *In vitro release profile of EFV from the optimized SLN and NLC formulations (n=3)*

These data show that the cumulative amount EFV released over a 24 hour period was higher from SLN (91.5 ± 3.423%) than from NLC (73.6 ± 4.34%), possibly due to the high degree of solubility of EFV in the lipid matrix of the NLC and the complex architecture of the lipid matrix that reduces the expulsion of EFV from the carrier into the dissolution medium. The SLN appear to release EFV readily as the solid matrix is more crystalline and well-ordered, allowing the drug to escape rather easily.

The data plotted in Figures 6.37 reveal that EFV release from the SLN and NLC is biphasic with burst release occurring initially followed by slower and more sustained release. These are in agreement with SLN and NLC type I (§ 2.2). The initial burst release was observed between 0 and 3 hours. The initial burst release suggests the presence of an EFV-rich region in the exterior lipid layer of the nanoparticles. The presence of high EFV levels in the exterior lipid has been shown to be due to the addition of surfactant directly into the aqueous phase and the use of HHPH for production method. These process issues apparently lead to the formation of a

surfactant-lipid boundary layer enriched with API [127,166]. Following initial burst release the nanoparticles released EFV in a sustained manner, which can be attributed to the shear stress of agitation during dissolution testing, ultimately diminishing the surfactant layer on the surface of the nanoparticles leading to a sustained release of EFV from the decomposition of the integrated lipid core structure [462,463].

Fitting of EFV release data to mathematical models revealed that the release of EFV from SLN followed overall first order release kinetics, exhibiting an R^2 value of 0.9667 and implying that release of EFV from SLN is proportional to the amount of EFV remaining in the nanoparticles and diminishes over time. However, EFV release from the NLC followed Higuchi release with an R^2 value of 0.9236, implying a diffusion-controlled release from the NLC after the initial burst.

6.3.5 Stability testing

Stability testing of pharmaceutical products involves using a set of procedures that ultimately aim to ensure that quality, efficacy and safety of drug products is assured [464]. The assessment of stability is considered a pre-requisite to obtaining approval for licensing of a pharmaceutical product [464,465]. The stability of a formulation in a specific container indicates that the product retains physical, chemical, microbiological and toxicological integrity, and is within specification [464,465]. Consequently, the extent to which product specifications are retained throughout a period of storage and use, and the extent to which properties and characteristics are similar to those observed at the time of packing are the goal of stability studies [464,465]. Therefore stability testing can be used to evaluate the effect of environmental factors on the quality of the API and/or formulated product. Data generated from stability studies can be used to predict the shelf life of a product and to establish the storage conditions for labelling [464,465]. Stability testing is a vital requirement for regulatory approval of any API or product [464,465].

The World Health Organization (WHO) [466], the International Conference on Harmonization (ICH) [467] and Food and Drug Administration (FDA) [468] have published general guidelines pertaining to the assessment of stability of API and/or API products. These guidelines were used to design a stability study protocol that included the selection of batches, the number of batches, container closure system, sampling frequency, test storage conditions, test specifications, product specifications, test procedure and statistical evaluation of stability data [466-468].

6.3.5.1 Zeta potential

The ZP of EFV-loaded SLN and NLC following storage at 25°C/60% RH and 40°C/75% RH is shown in Figures 6.38and 6.39 respectively.

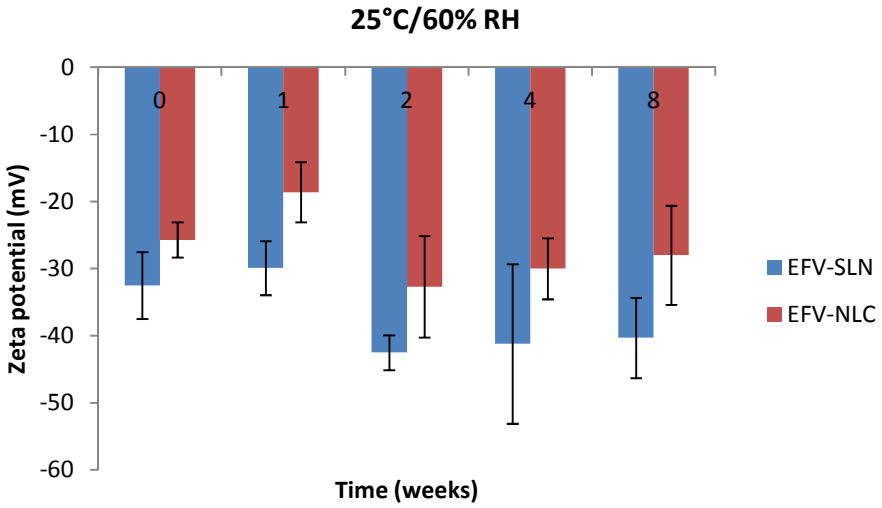

Figure 6.38: *Zeta potential of SLN and NLC following storage conditions at 25°C/60% RH*

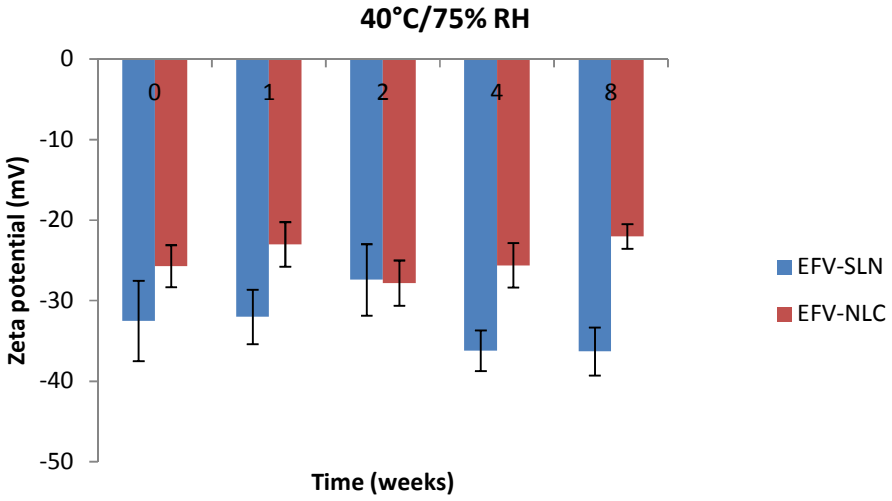

Figure 6.39: *Zeta potential of SLN and NLC following storage at 40°C/75% RH*

The ZP of the optimized EFV-loaded SLN and NLC stored at 25°C/60% RH ranged between -29.9 and -42.5 mV and -18.6 and -32.7 mV respectively. Similarly the ZP for the optimized EFV-loaded SLN and NLC stored at 40°C/75% RH ranged between -27.4 and -36.3 mV and -22.0 and -27.8 mV, respectively. The ZP for SLN indicates good physical stability of the nanoparticles (≤ -30 mV) following storage at 25°C/60% and 40°C/75% for a period of 8 weeks. However although the values for NLC under similar storage conditions were lower the stability of the nanoparticles could be inferred since the polysorbate surfactant provides stability through both electrostatic and steric hindrance mechanisms.

The ZP for all formulations generally decreased from the day of manufacture up to 1 and 2 weeks of storage, and then the ZP became constant for up to 8 weeks. The increase in stability of the formulations could be attributed to the use of HHPH that leads to the formation of a surfactant-rich interface [127,166] on the surface of the particles. The increase in ZP after 1 to 2 weeks of storage may be attributed to the immediate crystalline re-orientation of the formulations after exposure to the storage conditions, resulting in changes in the surface charges of the particles. In addition different sides of a crystal can acquire a different charge density, as is the case with aluminum silicates such as bentonite [469]. Long β crystals can be formed during 1-

dimensional crystal growth, ultimately resulting in modification of the surface ratio of differently charged crystal sides and consequently changes and/or variations in the ZP [469]. The constant ZP observed thereafter suggests no alteration to the surface properties of the particles of the SLN and NLC for the 8 week duration of storage.

Storage of the nanoparticles at 40°C/75% RH led to a faster increase (less stable) in the ZP than for samples stored at 25°C/60%. Following 8 weeks of storage, the ZP for SLN at 25°C was -40.3 mV and that for SLN stored at 40°C was -36.3 mV. In addition the ZP for NLC was -28 mV and -22 mV following storage at 25°C and 40°C for 8 weeks respectively. Generally the ZP increased with an increase in energy input which has been reported to lead to changes in the crystalline structure of lipids [231]. This crystal re-orientation can ultimately lead to changes of charge on the surface of the particle and consequently a change in the ZP [226]. However Riddick [470] defined the agglomeration threshold in dispersions with a ZP range of -20 to -11 mV. This is similar to the data generated in these studies as no agglomeration of formulations was observed following storage for 8 weeks.

6.3.5.2 Particle size and size distribution

The PS and PDI of the nanoparticles generated following storage at 25°C/60% RH and 40°C/75% RH are shown in Figures 6.40 and 6.41 respectively.

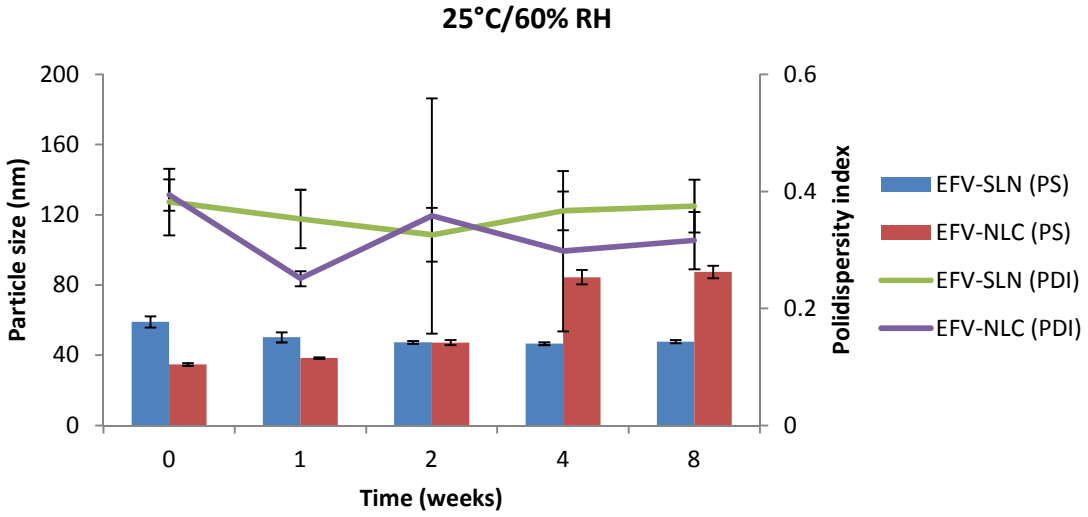

Figure 6.40: *Particle size and size distribution of SLN and NLC following storage at25°C/60% RH*

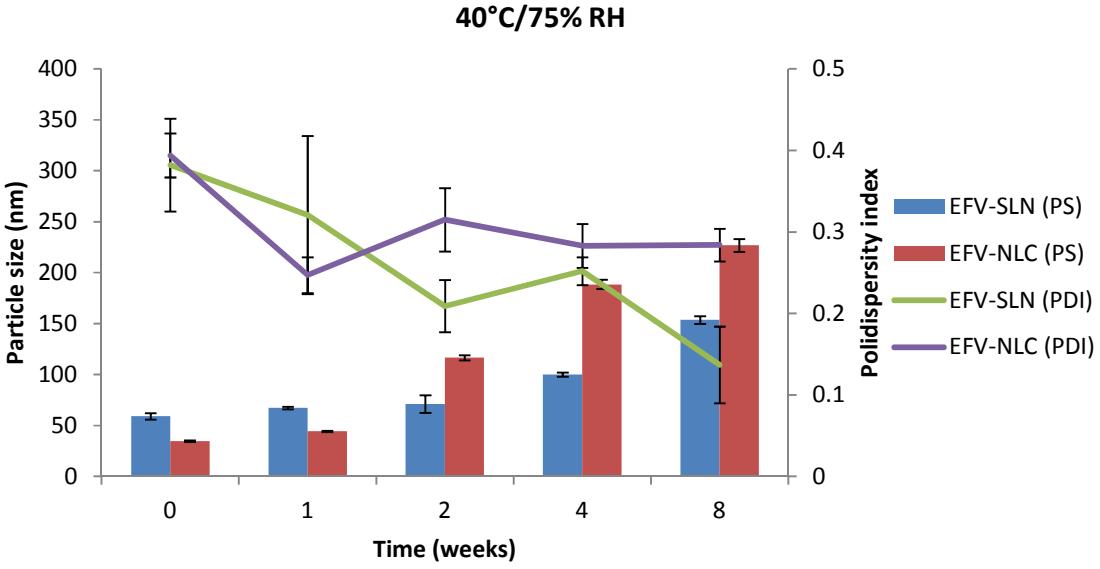

Figure 6.41: *Particle size and size distribution of SLN and NLC following storage at 40°C/75% RH*

The PS for optimized EFV-loaded SLN and NLC stored at 25°C/60% RH ranged between -46.64 and 59.0 nm and between 34.73 and 87.47 nm respectively, and the PS for the optimized EFV-loaded SLN and NLC stored at 40°C/75% RH ranged between 59.0 and 153.7 nm and between 34.73 and 226.9 nm, respectively. In general the PS of SLN and NLC increased during the 8

week storage period apart from the EFV-loaded SLN stored at 25°C, which maintained a constant size. Particle growth was slower when the nanoparticles were stored at 25°C than at 40°C. The high temperature (40°C) increased the kinetic energy of the system, leading to increased collision between particles, the consequence of which is aggregation and an increase in the size of the particles [162,163,226]. In addition a high level of the film emulsifier (microviscosity) has been shown to avert fusion of film layers after particle collision [226]. Microviscosity is a temperature-dependent factor and decreases with an increase in temperature leading to particle destabilization [210,226].

The increase in particle growth can be correlated with the decrease in the ZP reported in § 6.3.5.1. It was observed that the rate of particle growth for NLC under both storage conditions was higher than that observed for SLN, which can be attributed to the increased viscosity of the NLC due to the presence of liquid lipid in the formulation [162]. However PCS data reveal that the size of all particles remained within the nanometer range following storage for 8 weeks. In addition the low and constant PDI values observed for all formulations reveal that the SLN and NLC particles were physically stable in terms of PS and PDI at these storage conditions for at least 8 weeks.

6.3.5.3 Encapsulation efficiency and Loading capacity

The EE and LC generated for the optimized EFV-loaded SLN and NLC following storage at 25°C/60% RH and 40°C/75% RH are shown in Figures 6.42 and 6.43 respectively.

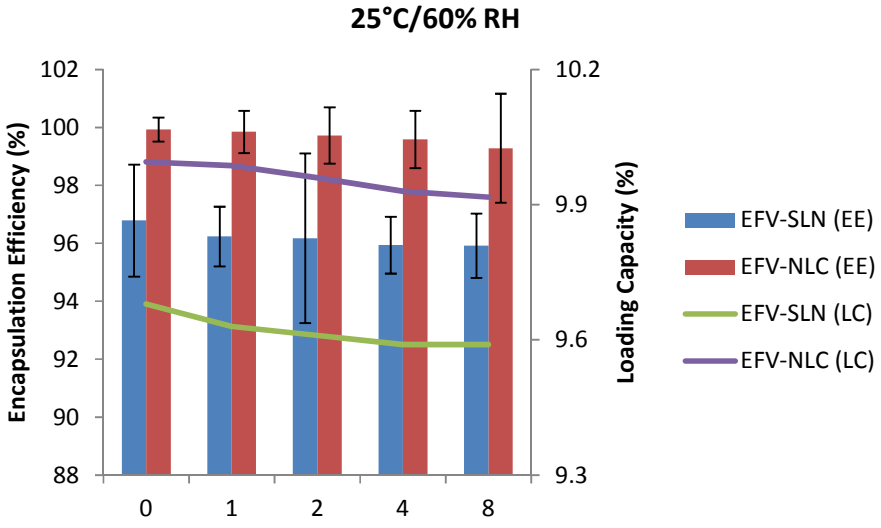

Figure 6.42: *Encapsulation efficiency and loading capacity of SLN and NLC following storage at 25°C/60% RH*

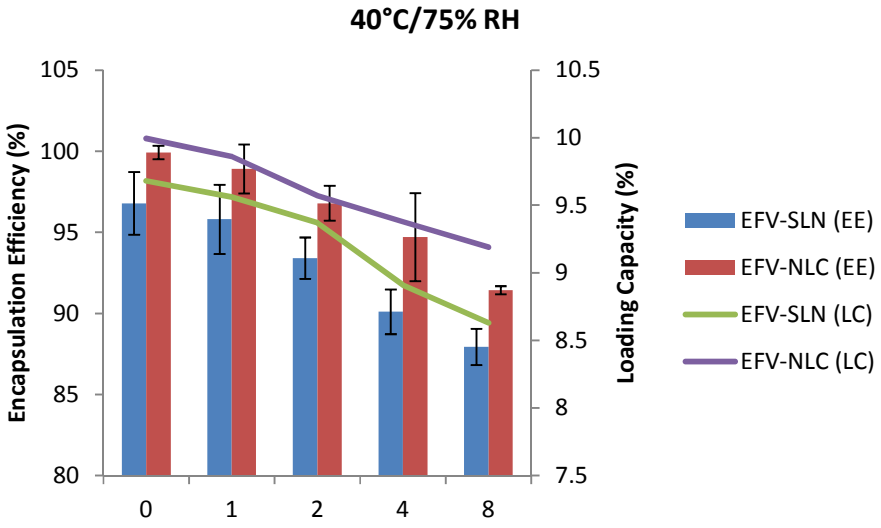

Figure 6.43: *Encapsulation efficiency and loading capacity of SLN and NLC following storage at 40°C/75% RH*

The EE for the optimized EFV-loaded SLN and NLC stored at 25°C/60% RH ranged between 96.79 and 95.92% and between 99.93 and 98.81% respectively. The corresponding LC for SLN and NLC ranged between 9.68 and 9.59% and between 9.99 and 9.88% respectively. The EE for the optimized EFV-loaded SLN and NLC stored at 40°C/75% RH ranged between 96.79 and 87.94% and 99.93 and 91.44% respectively. The corresponding LC for SLN and NLC ranged

between 9.68 and 8.63% and 9.99 and 9.19% respectively. Generally the NLC exhibited higher EE than the SLN over the 8 week period. EFV expulsion was also lower for NLC than that observed for SLN particles. This phenomenon could be attributed to the inclusion of liquid lipid in the solid lipid leading to a disturbance in the crystal structure of the solid lipid and the creation of imperfections in the crystal lattice that in turn creates additional space to accommodate EFV, thereby improving EE and reducing API expulsion [162,166].

The degree of crystallinity of SLN and NLC was calculated from the ratio of SLN and NLC enthalpy to that of bulk lipid [165]. The degree of crystallinity generated for SLN and NLC were 67% and 65% respectively. The NLC had a slightly lower degree of crystallinity than SLN, implying a relatively high degree of imperfection in the crystal lattice of the NLC allowing for increased inclusion of EFV.

The amount of EFV entrapped in SLN and NLC remained constant over the 8 week storage period at 25°C. However at higher temperatures (40°C) the EE and LC of the nanocarriers revealed a significant decrease that can be correlated to the polymorphic state of the lipid. Following production of particles using HHPH the lipid in SLN is present in the α polymorphic form and that of the NLC co-exists in α- and β' forms (§ 6.3.4.4.1). The input of high temperatures such as 40°C facilitates the conversion of lipids to different polymorphic forms during storage, thus leading to increased EFV expulsion. Freitas and Müller [231] have reported the transformation of SLN from β' forms accompanied by gel formation following the input of kinetic energy on storage at 50°C. In addition Das *et al.*, [131] reported a decrease in EE values of SLN and NLC stored at 25°C compared to those stored at between 2 and 8°C.

6.4 CONCLUSIONS

The hot high-pressure homogenization technique was successfully used for the manufacture of EFV-loaded SLN and NLC. Tween®80 was used as the surfactant to stabilize the lipid nanocarriers with the primary aim of enhancing the potential for delivery of EFV to the brain. A Box-Behnken Design (BBD) was used to deduce the optimum operating production conditions, *viz.* 1100 bar for 3 cycles for the SLN and 1500 bar for 5 cycles for NLC. EFV-loaded SLN were selected for the discussion of the optimization approach so as to avoid monotony and redundancy.

The concentration of Tween®80 was the most significant factor affecting the ZP of EFV-loaded SLN. In addition the most stable SLN formulation was produced when low concentrations of surfactant were used. The negative impact of increasing Tween®80 on the ZP could be explained by partition phenomena. High concentrations of surfactant in the aqueous phase might lead to an increase in the partitioning of EFV from the lipid phase into the aqueous phase. The increase in EFV partitioning results in greater amounts of EFV in the external aqueous phase and ultimately reduces the stability of the formulations [454,455].

The number of homogenization cycles was the most significant factor affecting the PS of the SLN, and relatively small particles were produced when the homogenization pressure was increased to relatively high values. These results are consistent with previous findings that reported a reduction in the mean PS and PDI values with an increase in homogenization pressure up to 1500 bar and number of cycles of 3 to 7 [204,216]. Therefore the desired mean PS can be obtained through the identification and manipulation of homogenization pressure and number of homogenization cycles.

The number of homogenization cycles was also significant and affected the PDI of the nanoparticles. An inverse relationship was observed between PDI and the number of homogenization cycles, albeit homogenization pressure also played a crucial role. Similarly the desired PDI could be produced by using an appropriate homogenization pressure and number of homogenization cycles.

The number of homogenization cycles was also significant and affected the cumulative percentage EFV released from SLN. The amount of EFV released from the SLN increased with an increase in number of homogenization cycles as smaller particles are produced. Previous findings have shown that the size and morphology of SLN affect the *in vitro* release of EFV [168]. The release of EFV from smaller particles was faster than from large particles and this can be attributed to a small diffusion path length through which EFV diffuses. In addition the large surface area of the small particles assists in improving interfacial contact between the particles and dissolution medium increasing EFV release.

Tween®80 and the amount of EFV in the formulation were the most significant formulation variables that influenced the quality of nanoparticle dispersions by visual assessment after the formulations were kept at room temperature (22°C) for two weeks. The optimum formulation stability without signs of creaming, sedimentation or coalescence was observed when Tween®80 and EFV were used in combination at the concentrations of 3% w/w and 10% w/w respectively. These data are in agreement with published data indicating that high concentrations of API lead to an increase in the size of particles [125] and therefore increase the probability of particle coalescence and ultimately formulation instability. The use of high surfactant/lipid ratios has also been shown to produce smaller particles [215], reducing the likelihood of particle coalescence and formulation instability.

The size of the optimized SLN and NLC formulations was in the nano range. In addition the nanocarriers had an excellent loading capacity for EFV, with an encapsulation efficiency > 90%.

However SLN had a lower EE and LC than NLC. This is a result of the higher solubility of EFV in the liquid lipid since effective entrapment has been shown to occur when the solubility of API in lipids is high [127,462]. The addition of Transcutol® HP to glyceryl monostearate increased the solubility of EFV in the lipid phase, resulting in high LC and EE of the NLC for EFV.

The optimized SLN and NLC exhibited biphasic release patterns, with burst release during the initial 0-3 hours followed by sustained release. The release of EFV from the optimized SLN and NLC followed first-order and Higuchi release kinetics, respectively, suggesting that NLC would be the most suitable carriers for EFV with the potential to sustain or control the release of EFV. Both systems exhibited excellent stability in terms of ZP, PS, PI, LC and EE following storage at 25°C/60% RH for eight weeks. However the delivery systems were relatively unstable when stored at 40°C/75% RH. Consequently improved physical stability of EFV-loaded SLN and NLC can ultimately be exploited to produce carrier systems that sustain release of EFV into brain tissue so as to reduce or limit the incidence of adverse psychiatric effects and potentially alleviate complications such as ADC in patients with HIV/AIDS, thereby improving their quality of life.

CHAPTER 7

CONCLUSIONS

EFV has been an important addition for the treatment of HIV for 14 years and has significantly contributed to the emergence and evolution of HAART due to its efficacy and once-a-day dosing requirement. In addition EFV reaches therapeutic levels in the CNS and may therefore be useful for the management of HIV and related complications in the CNS. The lack of EFV dosage forms for children < 3 years of age or weighing < 13 kg has made treatment options for HIV/ TB co-infected children of this age and weight category difficult, due to interactions between nevirapine and TB therapy. In addition aqueous solutions of EFV for the oral management of HIV in adult and/ or paediatric patients are not readily available as EFV causes a strong burning sensation when delivered from an aqueous vehicle in liquid formulations. The molecule is also susceptible to photodegradation and requires special packaging when packaging liquid dosage forms. Despite the potent activity of EFV in the management of HIV/AIDS and its potential use in managing HIV/AIDS-related complications such as ADC, the concentration of EFV in brain tissue exceeds therapeutic concentrations, leading to psychiatric effects such as severe depression and suicidal ideation. Consequently there is no choice but to discontinue treatment with this potent, durable and relatively simple addition to HAART. It is therefore imperative that research and development for innovative delivery systems for EFV be undertaken to address some or all of these unmet clinical needs.

SLN and NLC are innovative solid lipid carriers that have been developed as alternative delivery technologies to colloidal systems such as emulsions, liposomes and polymeric nanoparticles. They offer a number of advantages in comparison to other colloidal carriers, including protecting the API and reducing potential degradation, facilitating targeting, reducing potential side effects in addition to controlling API release *in vivo.* Consequently an objective of these studies was to investigate the feasibility of developing EFV-loaded SLN and/or NLC that would have the potential to sustain release of EFV to brain tissue so as to reduce or limit the incidence of adverse

psychiatric effects and alleviate AIDS-related complications such as ADC in patients with HIV/AIDS to ultimately improve their quality of life.

SLN and NLC consist of a matrix of biocompatible lipid(s) that are solid at room and body temperatures, stabilized using one or more surfactants and that have a mean particle size ranging between 10 and 1000 nm. The morphology of SLN and NLC is dependent on the method of API incorporation into the lipid matrix. Factors such as solubility of the API in the lipid(s), miscibility of the API with the molten lipid, physicochemical properties of lipid matrix and API, polymorphic nature of the lipid material, in addition to the production process may affect the incorporation of API into the lipid matrix. Although there are different methods of producing SLN and/or NLC the feasibility of encapsulating EFV into colloidal carriers was explored using a hot high-pressure homogenization approach.

Various techniques are used for the characterization of SLN and/or NLC. Photon correlation spectroscopy (PCS) was used to measure the PS and PDI of the colloidal systems manufactured in these studies. Although PCS can be used to determine PS and PDI of SLN and NLC, this technique cannot provide information pertaining to the shape and surface morphology of the nanoparticles. Data relating to the topographical profile of the SLN and NLC produced were generated using transmission electron microscopy (TEM) and scanning electron microscopy (SEM). The zeta potential, which is a predictor of the stability of colloidal dispersions, was determined using Laser Doppler Anemometry (LDA). The crystallization and polymorphic transitions of SLN and NLC were investigated using Differential Scanning Calorimetry (DSC) and Fourier Transform Infrared Spectroscopy (FT-IR). FT-IR was used to investigate EFV-lipid interactions of bulk materials. The loading capacity (LC), encapsulation efficiency (EE) and *in vitro* release (RR) of EFV from SLN and NLC were established using a reversed-phase high performance liquid chromatography (RP-HPLC) method developed and validated in these studies.

RP-HPLC is an effective and dependable analytical tool that can be used for the *in vitro* analysis of formulations such as SLN and NLC, which are complex matrices due to their lipid nature.

Prior to initiating pre-formulation and formulation development studies of EFV-loaded SLN and/or NLC, Response Surface Methodology (RSM) using a Central Composite Design (CCD) was used for the development and validation of RP-HPLC methods using different detectors *viz.* ultraviolet (UV) and electrochemical (EC) detectors. Consequently a suitable RP-HPLC was developed and validated for the quantitative analysis of EFV in pharmaceutical formulations for application in *in vitro* dissolution testing. The HPLC-UV method was simple, precise, accurate and sensitive compared to the HPLC-ECD method for the analysis of EFV and specifically for the determination of LC, EE and EFV release from the colloidal systems. Separation between the internal standard, LRT and EFV was achieved under isocratic conditions using a Nova-Pak® C_{18}, 4 µm (150 mm x 3.9 mm i.d.) cartridge column with a mobile phase consisting of 31.5 mM phosphate buffer (pH 4.5): acetonitrile (50:50 v/v). The flow rate and the injection volume were 1.0 mL/min and 20 µL respectively. The temperature of the analytical column was set at 30°C. A photodiode array detector set at a λ_{max} of 246.24 nm was used to monitor the eluent and the total run time for the analysis was 10 minutes. The method was validated according to international guidelines and was found to be simple, precise, accurate, selective and suitable for the routine analysis of EFV-loaded SLN and/or NLC. In addition solutions of EFV in mobile phase and/or diluents were found to be stable over three days at 4°C.

Prior to commencing formulation and product development studies of EFV-loaded SLN and NLC, pre-formulation studies were undertaken aimed at investigating the thermal stability of EFV and characterization of the bulk excipients in order to facilitate the selection of suitable lipids for use in the manufacture of EFV-loaded SLN and/or NLC. Hot high-pressure homogenization (HHPH) was selected as the method of production of EFV-loaded SLN and NLC. HHPH would necessarily require exposure of EFV to temperatures of approximately 70°C, therefore an investigation was undertaken of the thermal stability of EFV in addition to its crystalline and polymorphic state preceding and following exposure to heat. Thermogravimetric analysis (TGA) was used to establish the thermal stability of EFV, while DSC and WAXS were used to establish the crystalline and polymorphic nature of EFV prior to and following exposure to a temperature of 70°C for one hour. TGA data revealed that EFV is thermostable up to a temperature of approximately 200°C, thereby confirming the use of HHPH for the manufacture of EFV-loaded SLN and/or NLC. DSC and WAXS data revealed that a temperature of 70°C

would not disrupt the crystallinity of EFV to any great extent and no change in the polymorphic form of EFV was observed, further confirming the suitability of HHPH for the production of lipid nanocarriers.

The selection of lipid materials for use in the formulation of SLN and NLC was achieved by investigating the solubility of EFV in various solid and liquid lipids at 70°C to select the solid lipid and solid/liquid lipid binary mixture with the best solubilizing potential for EFV i.e. a miscible mixture with the highest ratio of liquid to solid lipid. This was necessary since one of the factors affecting the LC of an API in a lipid, and ultimately the EE of a system, is the solubility of the API in the molten lipid. Consequently a high LC is achieved only if EFV has a high solubility in the molten lipid. Solubility studies revealed that EFV was highly soluble in solid and liquid lipids, specifically glyceryl monostearate (GM) and Transcutol® HP (THP), and these were selected for use in the formulation and manufacture of SLN and NLC.

The production process for SLN and/or NLC by HHPH may influence polymorphic modification(s) of the lipid matrices from which the lipid nanocarriers are produced. The degree of crystallization and polymorphic transitions of lipids following exposure to heat during HHPH also influences API incorporation, release and product quality. Consequently DSC and WAXS were used to investigate the polymorphic and crystalline state of bulk lipid materials. In addition, the state and interaction potential of bulk lipids with EFV prior to and following exposure to 70°C for one hour was investigated. The data generated reveal that GM exists in a stable β-modification prior to exposure to heat, and exists in the α-polymorphic modification following exposure to 70°C for one hour. It is therefore likely that SLN produced from GM would exist in the α-polymorphic modification of the lipid. The DSC, WAXS and FT-IR profiles of a binary mixture of GM and EFV obtained prior to and following exposure to 70°C for one hour revealed the absence of any interaction between EFV and the solid lipid.

The production of NLC requires that the mixture of solid and liquid lipids be solid at room and body temperature, implying that binary mixtures should possess a melting temperature onset > 40°C. Consequently the miscibility of GM and THP was investigated using different proportions of the solid and liquid lipids, using a filter paper test to determine the miscibility of the different

solid and liquid lipid blends. DSC was used to monitor the melting behavior of the most suitable lipid binary mixture that would ultimately be used for the formulation of EFV-loaded NLC.

The optimum ratio of glyceryl monostearate and Transcutol® HP used for the manufacture of NLC was 70:30 solid: liquid lipid. The binary mixture was miscible and had an onset melting point > 40°C. The addition of Transcutol® HP to glyceryl monostearate revealed the co-existence of α- and β'-polymorphic modifications, implying the existence of these modifications in NLC produced from the optimum lipid combination. High EFV concentrations of 20% w/w in the lipid binary mixture were also shown to exist in the crystalline state. In addition the FT-IR profiles of the binary mixtures of lipid and EFV revealed the absence of any interaction between EFV and the lipids selected for the production of the nanocarriers.

EFV has a significantly higher solubility in Transcutol® HP than in glyceryl monostearate. NLC are therefore most likely to have a higher LC and EE than SLN. In addition the existence of both the α- and β'-polymorphic modifications in the binary mixture of lipids implies that EFV expulsion on prolonged storage is less likely to occur from NLC than from SLN. Despite the advantages of NLC over SLN, formulation development and optimization studies for SLN and NLC were undertaken to identify the best delivery approach for EFV in respect of stability and that exhibited an appropriate LC and EE for the molecule.

Tween®80 was used for formulation development and optimization of SLN and NLC. A RSM approach in conjunction with a Box-Behnken Design (BBD) was used to establish the effects of different process and formulation variables such as number of homogenization cycles, pressure, amount of EFV and Tween®80 on formulation responses *viz.* PS, PDI, ZP, VA and EFV released after 24 hours. In addition the LC, EE, degree of crystallinity, lipid modification, shape and surface morphology of the optimized batches of SLN and NLC were investigated to ensure that a product of desirable quality had been produced. The ZP of the nanocarriers was measured in HPLC grade water and for the optimized SLN ranged from -29.9 to -42.5 mV and -27.4 to -36.3 mV following storage for 8 weeks at 25°C/60% RH and 40°C/75% RH respectively. The ZP for the optimized NLC ranged from -18.6 to -32.7 mV and -22.0 to -27.8 mV following storage for 8

weeks at 25°C/60% RH and 40°C/75% RH respectively. Following assessment after 8 weeks at 25°C/60% and 40°C/75% the ZP for EFV-SLN indicated good physical stability (≤ -30 mV). However zeta potential values for NLC were > -30 mV and are generally considered to be too low for a solely electrostatic stabilized technology. However the negative charge observed will further enhance the physical stability and steric stabilization by Tween®80. In addition the agglomeration threshold in dispersions is defined at a zeta potential range of -20 to -11 mV, which is similar to the data generated in these studies. None of the formulations were seen to agglomerate following storage for 8 weeks.

The FT-IR profiles for the colloidal systems revealed characteristic bands for the solid lipid glyceryl monostearate. The characteristic bands consistent with molecular vibrations for EFV were not observed in SLN and NLC, indicating that EFV was molecularly dispersed in the SLN and NLC. The band intensity for SLN was similar to that for GM, indicating that the crystalline nature of GM did not change. However the band intensity for the NLC was relatively low, which may indicate the amorphous nature of the carriers due to the presence of THP.

The DSC thermogram for EFV-loaded SLN revealed the presence of a single endothermic event and the absence of a peak for EFV, indicating the existence of a single polymorphic form and that EFV was molecularly dispersed in the SLN. Similarly the DSC thermogram for EFV-loaded NLC revealed that EFV was molecularly dispersed in the SLN. However the thermogram revealed the presence of two endothermic events, implying that the α- and β'-polymorphic forms co-exist, with the β'-polymorphic form being more dominant than the α-modification.

The nanocarriers had excellent loading capacity for EFV, with an encapsulation efficiency > 90%. However the SLN exhibited a lower EE and LC for EFV than the NLC. This is most probably to be a result of the higher solubility of EFV in the liquid lipids since effective entrapment has been shown to occur when the solubility of the API in lipids is high. The addition of Transcutol® HP increased the complexity of the internal lipid structure of the NLC, and EFV

expulsion during storage for 8 weeks was also lower in NLC than in SLN. This can be attributed to the inclusion of the liquid to the solid lipid. Such inclusion can lead to crystal order disturbances creating imperfections in the crystal lattice, in turn creating additional space for accommodating EFV molecules, thereby improving EE and reducing EFV expulsion. The NLC had a slightly lower degree of crystallinity than SLN, indicating a greater incidence of imperfections in the crystal lattice of NLC, allowing for additional space to accommodate greater amounts of EFV. The amount of EFV in SLN and NLC remained fairly constant over the 8 week storage period at 25°C/60% RH. However at conditions of higher temperature and humidity (40°C/75% RH) the EE of the nanocarriers decreased and the observation can be correlated to the polymorphic state of the lipid. The high temperatures precipitate transformation of the lipids to different polymorphic forms on storage, leading to an increase in EFV expulsion.

The particle size of SLN and NLC increased over the storage period, apart from the EFV-loaded SLN stored at 25°C, which were fairly constant in size. The particle growth was slower when the nanoparticles were stored at 25°C, as at higher temperatures (40°C) the kinetic energy of the system increases and may lead to an increase in the number of collisions between the particles. Subsequently aggregation occurs and an increase in size is observed. In addition, a high level of film emulsifier (microviscosity) has been shown to prevent fusion of film layers following particle collision. Microviscosity is a temperature-dependent factor and decreases with an increase in temperature, leading to particle destabilization. Under both storage conditions it was observed that the rate of particle growth for NLC was higher than that for the SLN, which can be attributed to the increased viscosity of the surface components of the NLC due to the presence of liquid lipid in the formulation. PCS data revealed that the size of all particles remained within the nanometer range following storage for 8 weeks, and the low and constant PDI values observed for all formulations revealed that SLN and NLC were physically stable in terms of PS and PDI at these storage conditions for at least 8 weeks.

This research has shown the feasibility of using HHPH to manufacture EFV-loaded SLN and NLC. Tween®80 was used to stabilize the lipid nanocarriers so as to enhance the potential for

targeted delivery of EFV to the brain. The optimized colloidal systems exhibited biphasic release patterns, with burst release after the initial 0-3 hours followed by sustained release over 24 hours when fitted to kinetic models. Mathematical modelling revealed that EFV release from the optimized EFV-SLN formulation followed first order kinetics, whereas for the EFV-NLC release of EFV followed the Higuchi model. The colloidal systems had excellent stability in terms of ZP, PS, PDI, LC and EE when stored for 8 weeks at 25°C/60% RH in comparison to that observed following storage at 40°C/75% RH. Optimum storage conditions can therefore improve the physical stability of EFV-loaded SLN and NLC, which can ultimately be exploited as carrier systems that sustain release into brain tissue.

The *in vitro* release profiles of EFV-loaded lipid carriers show that these systems can be used to sustain API release. However these colloidal systems require further investigation using *in vitro* differential protein adsorption patterns to establish their potential to deliver EFV to the brain. In addition *in vitro* data may be used as a platform for conducting *in vivo* studies to ultimately confirm that SLN and NLC can deliver EFV to the CNS. Should *in vivo* studies confirm the presence of EFV in the CNS, the use of SLN and NLC in suspension formulations for the administration of EFV for sustained release may be possible. This approach is likely to improve the management of HIV as it may be possible to limit the incidence of adverse psychiatric effects and potentially alleviate AIDS-related complications such as ADC in patients with HIV/AIDS, thereby improving their quality of life.

APPENDIX I

BATCH PRODUCTION RECORDS

Note that only the production records for the optimized batches EFV-SLN-OPT and EFV-NLC-OPT are included here. The batch production records for all other formulations manufactured and assessed during formulation development and optimization studies are available on request. All formulations manufactured and assessed during formulation development and optimization studies were manufactured using Good Manufacturing Practice (GMP).

RHODES UNIVERSITY, FACULTY OF PHARMACY

GRAHAMSTOWN, 6140, SOUTH AFRICA

BATCH PRODUCTION RECORD

Product name: EFV-loaded SLN **Page 1 of 5**

Batch ID: EFV-SLN-OPT **Batch size: 100 g**

MANUFACTURING APPROVALS

Batch record issued by_____ **Date**_____

Master record issued by_____ **Date**_____

RHODES UNIVERSITY, FACULTY OF PHARMACY

GRAHAMSTOWN, 6140, SOUTH AFRICA

BATCH PRODUCTION RECORD

Product name: EFV-loaded SLN **Page 2 of 5**

Batch ID: EFV-SLN-OPT **Batch size: 100 g**

Item	Material	Quantity (% w/w)	Amount/batch (g)	Amount dispensed (g)	Dispensed by	Checked by
1	EFV	0.50	0.50	0.53		
2	Glyceryl monostearate	4.50	4.50	4.54		
3	Tween® 80	3.00	3.00	3.02		
4	Aqua	92.00	92.00	92.21		

RHODES UNIVERSITY, FACULTY OF PHARMACY

GRAHAMSTOWN, 6140, SOUTH AFRICA

BATCH PRODUCTION RECORD

Product name: EFV-loaded SLN **Page 3 of 5**

Batch ID: EFV-SLN-OPT **Batch size: 100 g**

EQUIPMENT VERIFICATION			
Description	**Type**	**Verified by**	**Confirmed by**
High speed homogenizer	Model T 18 Ultra-Turrax®		
High-pressure homogenizer	APV 2000		

RHODES UNIVERSITY, FACULTY OF PHARMACY

GRAHAMSTOWN, 6140, SOUTH AFRICA

BATCH PRODUCTION RECORD

Product name: EFV-loaded SLN **Page 4 of 5**

Batch ID: EFV-SLN-OPT **Batch size: 100 g**

MANUFACTURING PROCEDURE				
Step	**Procedure**	**Time**	**Done by**	**Checked by**
1	Weigh all the materials.			
2	Heat water (item 4) to 70°C in a beaker and disperse Tween® 80 (item 3) into the hot water until a clear solution is obtained. Maintain the temperature of the resultant aqueous phase at 70°C.			
3	Heat glyceryl monostearate (item 2) at 70°C until a clear melt is obtained. Disperse EFV (item 1) in the lipid melt and maintain at 70°C.			
4	Disperse the heated aqueous phase in the molten lipid phase using high speed stirring at 1000 rpm to form a pre-emulsion.			
5	Homogenize the pre-emulsion at 70°C using the high-pressure homogenizer by applying three homogenization cycles at 1100 bar.			
6	Fill and seal the hot o/w nanoemulsion immediately in a glass vial and allow the product to cool to room temperature (22ºC).			
7	Store all samples at room temperature for at least 24 hours prior to characterization.			

RHODES UNIVERSITY, FACULTY OF PHARMACY

GRAHAMSTOWN, 6140, SOUTH AFRICA

BATCH PRODUCTION RECORD

Product name: EFV-loaded SLN

Batch ID: EFV-SLN-OPT **Batch size: 100 g**

SIGNATURE AND INITIAL REFERENCE			
Full name (Print)	**Signature**	**Initials**	**Date**

RHODES UNIVERSITY, FACULTY OF PHARMACY

GRAHAMSTOWN, 6140, SOUTH AFRICA

BATCH PRODUCTION RECORD

Product name: EFV-loaded NLC

Batch ID: EFV-NLC-OPT **Batch size: 100 g**

MANUFACTURING APPROVALS

Batch record issued by_____ **Date**_____

Master record issued by_____ **Date**_____

RHODES UNIVERSITY, FACULTY OF PHARMACY

GRAHAMSTOWN, 6140, SOUTH AFRICA

BATCH PRODUCTION RECORD

Product name: EFV-loaded NLC **Page 2 of 5**

Batch ID: EFV-NLC-OPT **Batch size: 100 g**

Item	Material	Quantity (% w/w)	Amount/batch (g)	Amount dispensed (g)	Dispensed by	Checked by
1	EFV	0.50	0.50	0.51		
2	Glyceryl monostearate	3.15	3.15	3.17		
3	Transcutol® HP	1.35	1.35	1.34		
4	Tween® 80	4.00	4.00	3.98		
5	Aqua	91.00	91.00	91.34		

RHODES UNIVERSITY, FACULTY OF PHARMACY

GRAHAMSTOWN, 6140, SOUTH AFRICA

BATCH PRODUCTION RECORD

Product name: EFV-loaded NLC

Batch ID: EFV-NLC-OPT **Batch size: 100 g**

EQUIPMENT VERIFICATION			
Description	**Type**	**Verified by**	**Confirmed by**
High speed homogenizer	Model T 18 Ultra-Turrax®		
High-pressure homogenizer	APV 2000		

RHODES UNIVERSITY, FACULTY OF PHARMACY

GRAHAMSTOWN, 6140, SOUTH AFRICA

BATCH PRODUCTION RECORD

Product name: EFV-loaded NLC **Page 4 of 5**

Batch ID: EFV-NLC-OPT **Batch size: 100 g**

MANUFACTURING PROCEDURE				
Step	**Procedure**	**Time**	**Done by**	**Checked by**
1	Weigh all the materials.			
2	Heat water (item 5) to 70°C in a beaker and disperse Tween® 80 (item 4) into the hot water until a clear solution is obtained. Maintain the temperature of the resultant aqueous phase at 70°C.			
3	Heat glyceryl monostearate (item 2) and Transcutol® HP (item 3) together at 70°C until a clear melt is obtained. Disperse EFV (item 1) in the lipid melt and maintain at 70°C.			
4	Disperse the heated aqueous phase in the molten lipid phase using high speed stirring at 1000 rpm to form a pre-emulsion.			
5	Homogenize the pre-emulsion at 70°C using the high-pressure homogenizer by applying five homogenization cycles at 1500 bar.			
6	Fill and seal the hot o/w nanoemulsion immediately in a glass vial and allow the product to cool to room temperature (22ºC).			
7	Store all samples at room temperature for at least 24 hours prior to characterization.			

RHODES UNIVERSITY, FACULTY OF PHARMACY

GRAHAMSTOWN, 6140, SOUTH AFRICA

BATCH PRODUCTION RECORD

Product name: EFV-loaded NLC **Page 5 of 5**

Batch ID: EFV-NLC-OPT **Batch size: 100 g**

SIGNATURE AND INITIAL REFERENCE			
Full name (Print)	**Signature**	**Initials**	**Date**

APPENDIX II

SLN PRODUCTION REPORTS

All SLN formulations manufactured and assessed during formulation development and optimization studies were manufactured using Good Manufacturing Practice (GMP).

RHODES UNIVERSITY, FACULTY OF PHARMACY

GRAHAMSTOWN, 6140, SOUTH AFRICA

SLN BATCH SUMMARY REPORT

Formulator: **Pedzisai Makoni**
Product: **EFV-loaded SLN**
Batch I.D: **EFV-SLN 001**
Batch size: **100 g**
Date of manufacture: **10 October 2013**

Formula:

Item	Material	Quantity (% w/w)	Amount/batch (g)
1	EFV	0.75	0.75
2	Glyceryl monostearate	4.25	4.25
3	Tween® 80	3.00	3.00
4	Aqua	92.00	92.00

Production equipment used:
High speed homogenization: One minute at 1000 rpm at 70°C
Hot high-pressure homogenization: Five homogenization cycles at 1000 bar at 70°C

Evaluated parameters and *in vitro* dissolution profile:

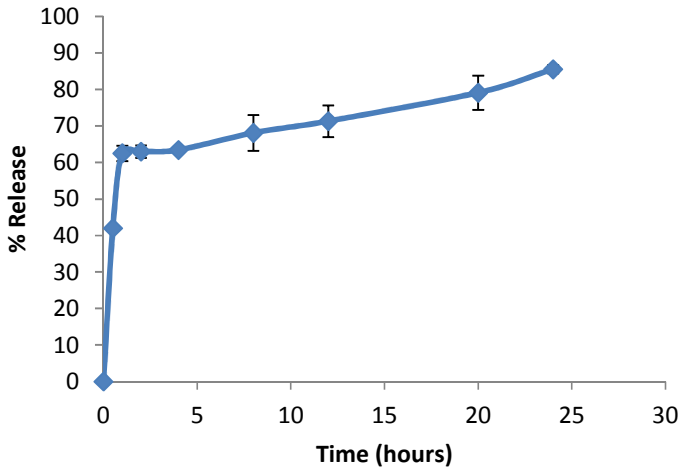

ZP: -41.8±3.72 mV
PS: 74.08±4.739 nm
PDI: 0.628±0.094

Comments:
- Formulation was unstable and not homogenous on visual assessment after two weeks at room temperature (22°C).

RHODES UNIVERSITY, FACULTY OF PHARMACY

GRAHAMSTOWN, 6140, SOUTH AFRICA

SLN BATCH SUMMARY REPORT

Formulator: **Pedzisai Makoni**
Product: **EFV-loaded SLN**
Batch I.D: **EFV-SLN 002**
Batch size: **100 g**
Date of manufacture: **10 October 2013**

Formula:

Item	Material	Quantity (% w/w)	Amount/batch (g)
1	EFV	0.50	0.50
2	Glyceryl monostearate	4.50	4.50
3	Tween® 80	3.00	3.00
4	Aqua	92.00	92.00

Production equipment used:
High speed homogenization: One minute at 1000 rpm at 70°C
Hot high-pressure homogenization: Three homogenization cycles at 1000 bar at 70°C

Evaluated parameters and *in vitro* dissolution profile:

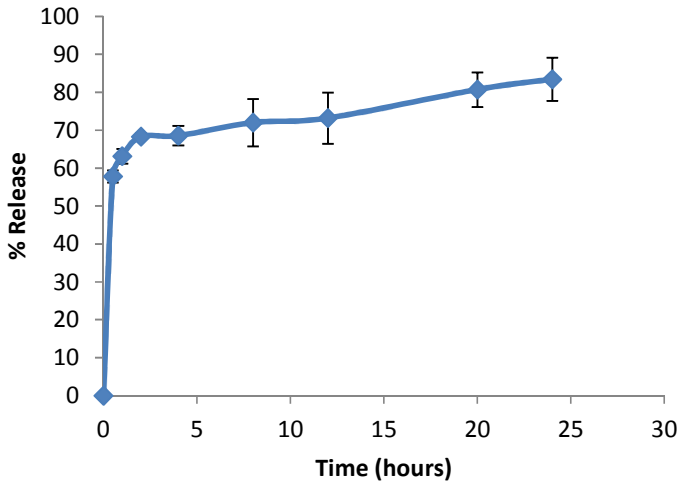

ZP: -37.9±5.68 mV
PS: 116.4±35.83 nm
PDI: 0.615±0.191

Comments:
- Formulation was stable and homogenous on visual assessment after two weeks at room temperature (22°C).

RHODES UNIVERSITY, FACULTY OF PHARMACY

GRAHAMSTOWN, 6140, SOUTH AFRICA

SLN BATCH SUMMARY REPORT

Formulator: **Pedzisai Makoni**
Product: **EFV-loaded SLN**
Batch I.D: **EFV-SLN 003**
Batch size: **100 g**
Date of manufacture: **10 October 2013**

Formula:

Item	Material	Quantity (% w/w)	Amount/batch (g)
1	EFV	0.25	0.25
2	Glyceryl monostearate	4.75	4.75
3	Tween® 80	3.00	3.00
4	Aqua	92.00	92.00

Production equipment used:
High speed homogenization: One minute at 1000 rpm at 70°C
Hot high-pressure homogenization: Five homogenization cycles at 1000 bar at 70°C

Evaluated parameters and *in vitro* dissolution profile:

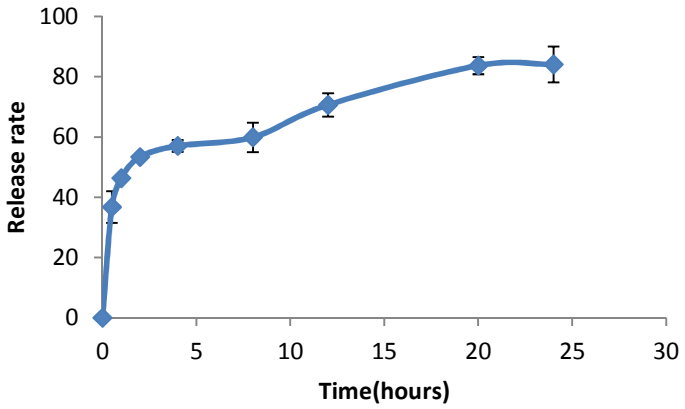

ZP: -43.0±5.11 mV
PS: 75.57±20.51 nm
PDI: 0.488±0.08

Comments:
- Formulation was stable and homogenous on visual assessment after two weeks at room temperature (22°C).

RHODES UNIVERSITY, FACULTY OF PHARMACY

GRAHAMSTOWN, 6140, SOUTH AFRICA

SLN BATCH SUMMARY REPORT

Formulator: **Pedzisai Makoni**
Product: **EFV-loaded SLN**
Batch I.D: **EFV-SLN 004**
Batch size: **100 g**
Date of manufacture: **11 October 2013**

Formula:

Item	Material	Quantity (% w/w)	Amount/batch (g)
1	EFV	0.75	0.75
2	Glyceryl monostearate	4.25	4.25
3	Tween® 80	3.00	3.00
4	Aqua	92.00	92.00

Production equipment used:
High speed homogenization: One minute at 1000 rpm at 70°C
Hot high-pressure homogenization: Three homogenization cycles at 1500 bar at 70°C

Evaluated parameters and *in vitro* dissolution profile:

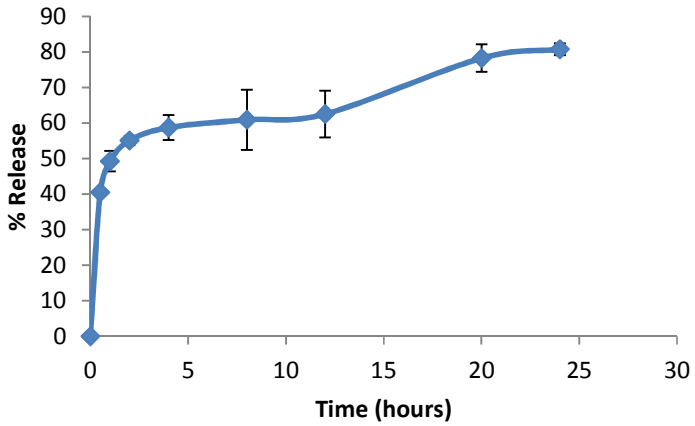

ZP: -39.9±3.17 mV
PS: 95.92±38.67 nm
PDI: 0.424±0.071

Comments:
- Formulation was unstable and not homogenous on visual assessment after two weeks at room temperature (22°C).

RHODES UNIVERSITY, FACULTY OF PHARMACY

GRAHAMSTOWN, 6140, SOUTH AFRICA

SLN BATCH SUMMARY REPORT

Formulator: **Pedzisai Makoni**
Product: **EFV-loaded SLN**
Batch I.D: **EFV-SLN 005**
Batch size: **100 g**
Date of manufacture: **11 October 2013**

Formula:

Item	Material	Quantity (% w/w)	Amount/batch (g)
1	EFV	0.75	0.75
2	Glyceryl monostearate	4.25	4.25
3	Tween® 80	3.00	3.00
4	Aqua	92.00	92.00

Production equipment used:
High speed homogenization: One minute at 1000 rpm at 70°C
Hot high-pressure homogenization: Three homogenization cycles at 500 bar at 70°C

Evaluated parameters and *in vitro* dissolution profile:

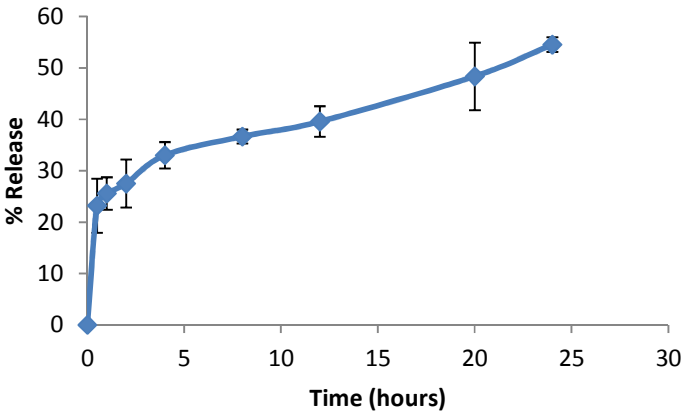

ZP: -34.8±11.0 mV
PS: 317.9±20.34 nm
PDI: 0.631±0.109

Comments:
- Formulation was unstable and not homogenous on visual assessment after two weeks at room temperature (22°C).

RHODES UNIVERSITY, FACULTY OF PHARMACY

GRAHAMSTOWN, 6140, SOUTH AFRICA

SLN BATCH SUMMARY REPORT

Formulator: **Pedzisai Makoni**
Product: **EFV-loaded SLN**
Batch I.D: **EFV-SLN 006**
Batch size: **100 g**
Date of manufacture: **11 October 2013**

Formula:

Item	Material	Quantity (% w/w)	Amount/batch (g)
1	EFV	0.75	0.75
2	Glyceryl monostearate	4.25	4.25
3	Tween® 80	5.00	5.00
4	Aqua	90.00	90.00

Production equipment used:
High speed homogenization: One minute at 1000 rpm at 70°C
Hot high-pressure homogenization: Three homogenization cycles at 1000 bar at 70°C

Evaluated parameters and *in vitro* dissolution profile:

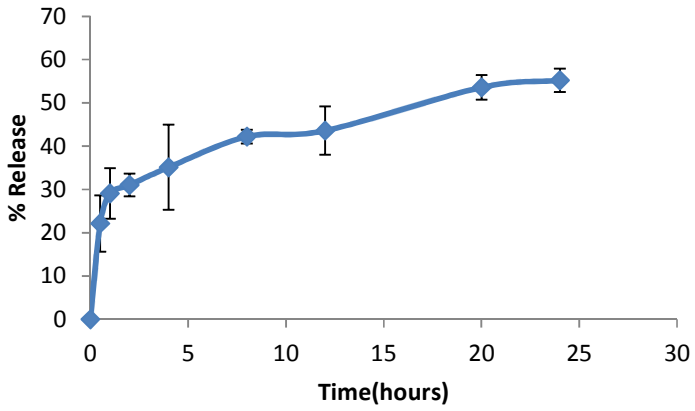

ZP: -38.2±3.21 mV
PS: 390.3±131.3 nm
PDI: 0.719±0.182
Comments:
- Formulation was unstable and not homogenous on visual assessment after two weeks at room temperature (22°C).

RHODES UNIVERSITY, FACULTY OF PHARMACY

GRAHAMSTOWN, 6140, SOUTH AFRICA

SLN BATCH SUMMARY REPORT

Formulator: **Pedzisai Makoni**
Product: **EFV-loaded SLN**
Batch I.D: **EFV-SLN 007**
Batch size: **100 g**
Date of manufacture: **12 October 2013**

Formula:

Item	Material	Quantity (% w/w)	Amount/batch (g)
1	EFV	0.50	0.50
2	Glyceryl monostearate	4.50	4.50
3	Tween® 80	5.00	5.00
4	Aqua	90.00	90.00

Production equipment used:
High speed homogenization: One minute at 1000 rpm at 70°C
Hot high-pressure homogenization: One homogenization cycle at 1000 bar at 70°C

Evaluated parameters and *in vitro* dissolution profile:

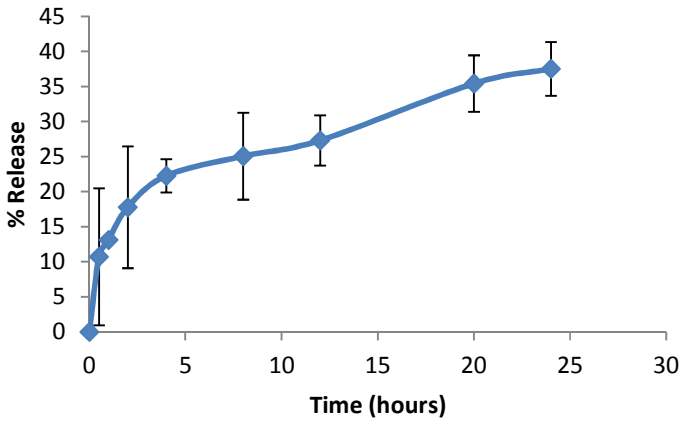

ZP: -35.5±3.98 mV
PS: 635.5±146.9 nm
PDI: 0.855±0.102

Comments:
- Formulation was stable and homogenous on visual assessment after two weeks at room temperature (22°C).

RHODES UNIVERSITY, FACULTY OF PHARMACY

GRAHAMSTOWN, 6140, SOUTH AFRICA

SLN BATCH SUMMARY REPORT

Formulator: **Pedzisai Makoni**
Product: **EFV-loaded SLN**
Batch I.D: **EFV-SLN 008**
Batch size: **100 g**
Date of manufacture: **12 October 2013**

Formula:

Item	Material	Quantity (% w/w)	Amount/batch (g)
1	EFV	0.25	0.25
2	Glyceryl monostearate	4.75	4.75
3	Tween® 80	5.00	5.00
4	Aqua	90.00	90.00

Production equipment used:
High speed homogenization: One minute at 1000 rpm at 70°C
Hot high-pressure homogenization: Three homogenization cycles at 1000 bar at 70°C

Evaluated parameters and *in vitro* dissolution profile:

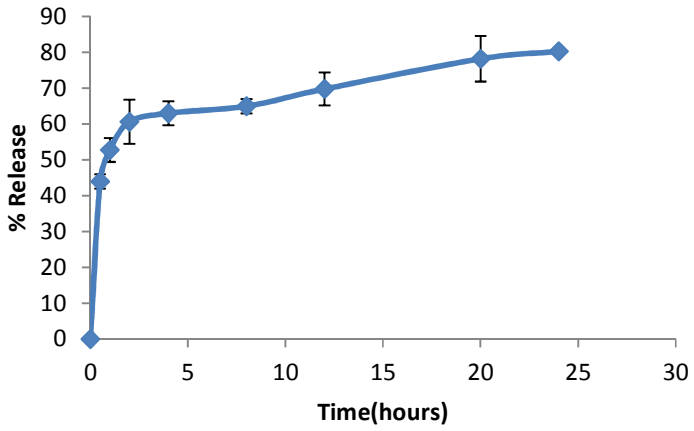

ZP: -33.7±6.35 mV
PS: 118.7±8.545 nm
PDI: 0.527±0.119

Comments:
- Formulation was stable and homogenous on visual assessment after two weeks at room temperature (22°C).

RHODES UNIVERSITY, FACULTY OF PHARMACY

GRAHAMSTOWN, 6140, SOUTH AFRICA

SLN BATCH SUMMARY REPORT

Formulator: **Pedzisai Makoni**
Product: **EFV-loaded SLN**
Batch I.D: **EFV-SLN 009**
Batch size: **100 g**
Date of manufacture: **12 October 2013**

Formula:

Item	Material	Quantity (% w/w)	Amount/batch (g)
1	EFV	0.50	0.50
2	Glyceryl monostearate	4.50	4.50
3	Tween® 80	1.00	1.00
4	Aqua	94.00	94.00

Production equipment used:
High speed homogenization: One minute at 1000 rpm at 70°C
Hot high-pressure homogenization: One homogenization cycle at 1000 bar at 70°C

Evaluated parameters and *in vitro* dissolution profile:

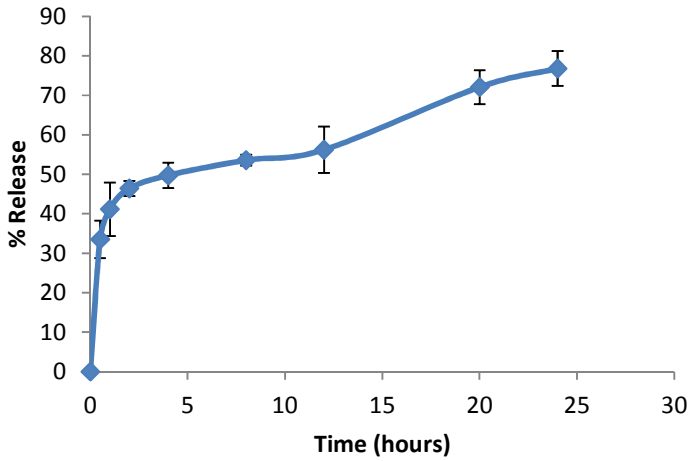

ZP: -46.3±4.56 mV
PS: 185.7±30.13 nm
PDI: 0.439±0.06

Comments:
- Formulation was unstable and not homogenous on visual assessment after two weeks at room temperature (22°C).

RHODES UNIVERSITY, FACULTY OF PHARMACY

GRAHAMSTOWN, 6140, SOUTH AFRICA

SLN BATCH SUMMARY REPORT

Formulator: **Pedzisai Makoni**
Product: **EFV-loaded SLN**
Batch I.D: **EFV-SLN 010**
Batch size: **100 g**
Date of manufacture: **13 October 2013**

Formula:

Item	Material	Quantity (% w/w)	Amount/batch (g)
1	EFV	0.50	0.50
2	Glyceryl monostearate	4.50	4.50
3	Tween® 80	3.00	3.00
4	Aqua	92.00	92.00

Production equipment used:
High speed homogenization: One minute at 1000 rpm at 70°C
Hot high-pressure homogenization: Three homogenization cycles at 1000 bar at 70°C

Evaluated parameters and *in vitro* dissolution profile:

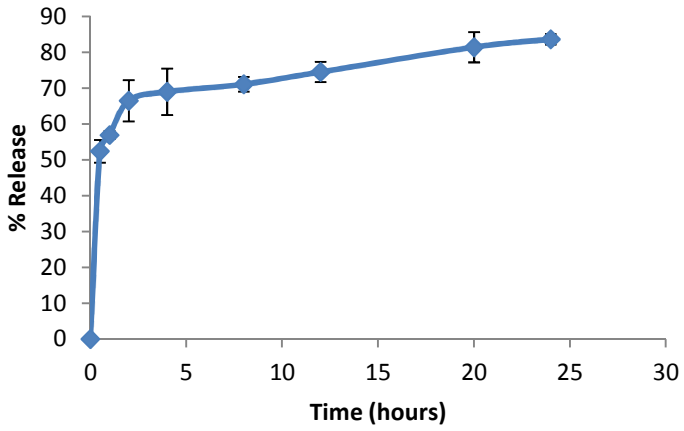

ZP: -39.2±4.19 mV
PS: 116.8±46.81 nm
PDI: 0.586±0.121

Comments:
- Formulation was stable and homogenous on visual assessment after two weeks at room temperature (22°C).

RHODES UNIVERSITY, FACULTY OF PHARMACY

GRAHAMSTOWN, 6140, SOUTH AFRICA

SLN BATCH SUMMARY REPORT

Formulator: **Pedzisai Makoni**
Product: **EFV-loaded SLN**
Batch I.D: **EFV-SLN 011**
Batch size: **100 g**
Date of manufacture: **13 October 2013**

Formula:

Item	Material	Quantity (% w/w)	Amount/batch (g)
1	EFV	0.50	0.50
2	Glyceryl monostearate	4.50	4.50
3	Tween® 80	3.00	3.00
4	Aqua	92.00	92.00

Production equipment used:
High speed homogenization: One minute at 1000 rpm at 70°C
Hot high-pressure homogenization: One homogenization cycle at 1500 bar at 70°C

Evaluated parameters and *in vitro* dissolution profile:

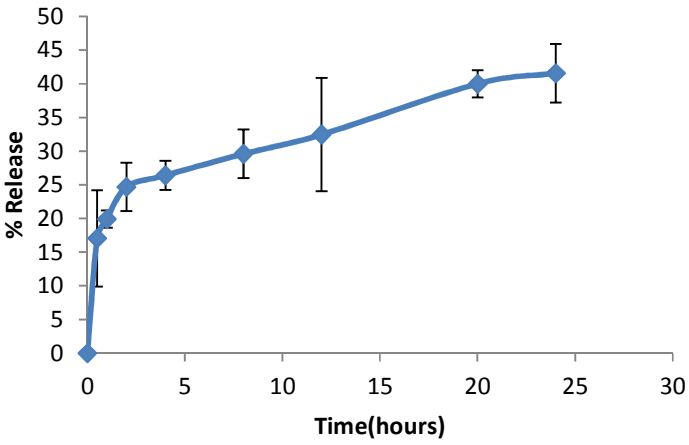

ZP: -40.5±9.08 mV
PS: 616.3±279.4 nm
PDI: 0.937±0.077

Comments:
- Formulation was stable and homogenous on visual assessment after two weeks at room temperature (22°C).

RHODES UNIVERSITY, FACULTY OF PHARMACY

GRAHAMSTOWN, 6140, SOUTH AFRICA

SLN BATCH SUMMARY REPORT

Formulator: **Pedzisai Makoni**
Product: **EFV-loaded SLN**
Batch I.D: **EFV-SLN 012**
Batch size: **100 g**
Date of manufacture: **13 October 2013**

Formula:

Item	Material	Quantity (% w/w)	Amount/batch (g)
1	EFV	0.50	0.50
2	Glyceryl monostearate	4.50	4.50
3	Tween® 80	3.00	3.00
4	Aqua	92.00	92.00

Production equipment used:
High speed homogenization: One minute at 1000 rpm at 70°C
Hot high-pressure homogenization: Three homogenization cycles at 1000 bar at 70°C

Evaluated parameters and *in vitro* dissolution profile:

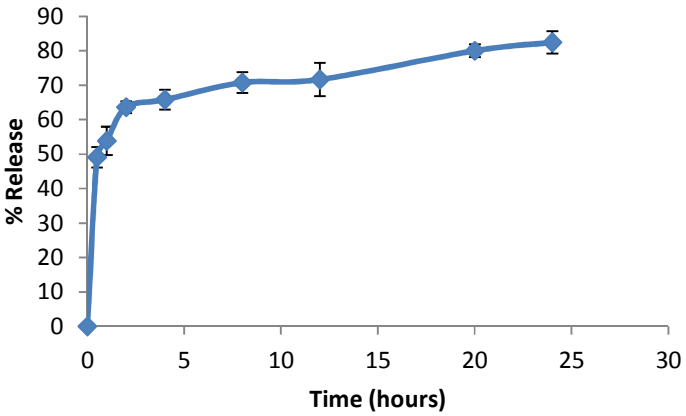

ZP: -38.6±3.65 mV
PS: 114.9±46.17 nm
PDI: 0.614±0.212

Comments:
- Formulation was stable and homogenous on visual assessment after two weeks at room temperature (22°C).

RHODES UNIVERSITY, FACULTY OF PHARMACY

GRAHAMSTOWN, 6140, SOUTH AFRICA

SLN BATCH SUMMARY REPORT

Formulator: **Pedzisai Makoni**
Product: **EFV-loaded SLN**
Batch I.D: **EFV-SLN 013**
Batch size: **100 g**
Date of manufacture: **14 October 2013**

Formula:

Item	Material	Quantity (% w/w)	Amount/batch (g)
1	EFV	0.25	0.25
2	Glyceryl monostearate	4.75	4.75
3	Tween® 80	3.00	3.00
4	Aqua	92.00	92.00

Production equipment used:
High speed homogenization: One minute at 1000 rpm at 70°C
Hot high-pressure homogenization: One homogenization cycle at 1000 bar at 70°C

Evaluated parameters and *in vitro* dissolution profile:

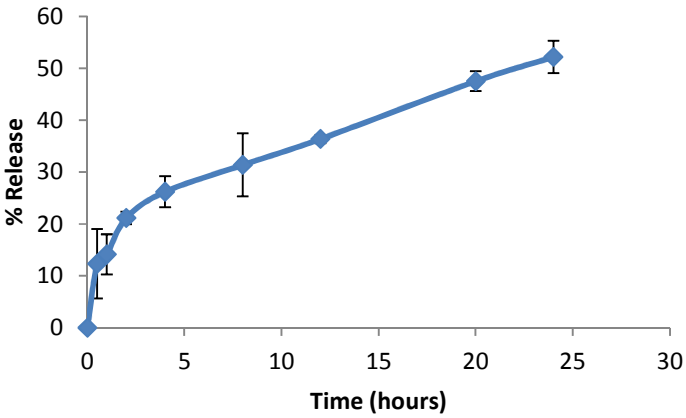

ZP: -38.3±4.90 mV
PS: 476.4±31.69 nm
PDI: 0.785±0.127

Comments:
- Formulation was stable and homogenous on visual assessment after two weeks at room temperature (22°C).

RHODES UNIVERSITY, FACULTY OF PHARMACY

GRAHAMSTOWN, 6140, SOUTH AFRICA

SLN BATCH SUMMARY REPORT

Formulator: **Pedzisai Makoni**
Product: **EFV-loaded SLN**
Batch I.D: **EFV-SLN 014**
Batch size: **100 g**
Date of manufacture: **14 October 2013**

Formula:

Item	Material	Quantity (% w/w)	Amount/batch (g)
1	EFV	0.50	0.50
2	Glyceryl monostearate	4.50	4.50
3	Tween® 80	5.00	5.00
4	Aqua	90.00	90.00

Production equipment used:
High speed homogenization: One minute at 1000 rpm at 70°C
Hot high-pressure homogenization: Three homogenization cycles at 1500 bar at 70°C

Evaluated parameters and *in vitro* dissolution profile:

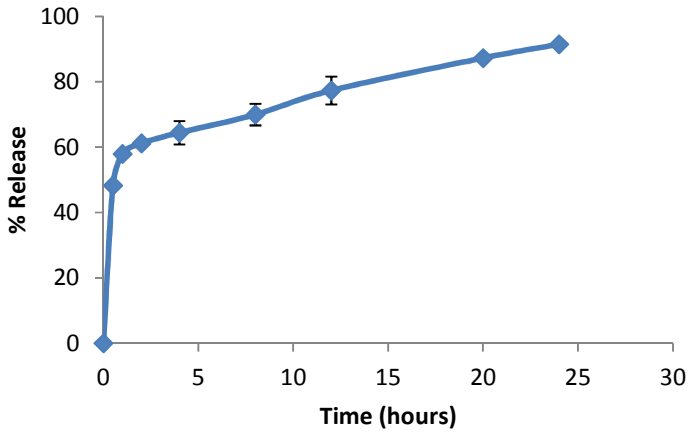

ZP: -40.2±5.03 mV
PS: 67.42±4.274 nm
PDI: 0.618±0.095
Comments:
- Formulation was stable and homogenous on visual assessment after two weeks at room temperature (22°C).

RHODES UNIVERSITY, FACULTY OF PHARMACY

GRAHAMSTOWN, 6140, SOUTH AFRICA

SLN BATCH SUMMARY REPORT

Formulator: **Pedzisai Makoni**
Product: **EFV-loaded SLN**
Batch I.D: **EFV-SLN 015**
Batch size: **100 g**
Date of manufacture: **14 October 2013**

Formula:

Item	Material	Quantity (% w/w)	Amount/batch (g)
1	EFV	0.25	0.25
2	Glyceryl monostearate	4.75	4.75
3	Tween® 80	1.00	1.00
4	Aqua	94.00	94.00

Production equipment used:
High speed homogenization: One minute at 1000 rpm at 70°C
Hot high-pressure homogenization: Three homogenization cycles at 1000 bar at 70°C

Evaluated parameters and *in vitro* dissolution profile:

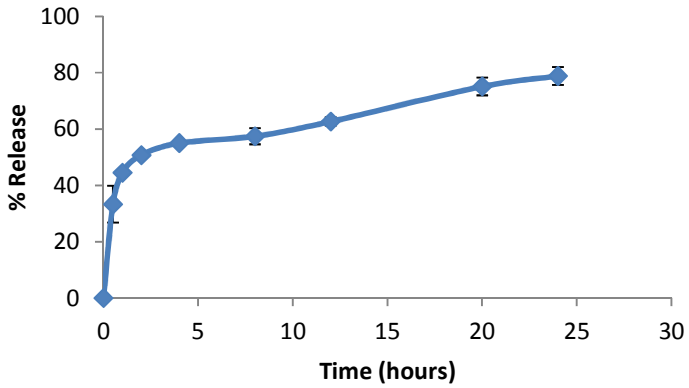

ZP: -51.6±6.78 mV
PS: 116.7±7.821 nm
PDI: 0.674±0.154

Comments:
- Formulation was unstable and not homogenous on visual assessment after two weeks at room temperature (22°C).

RHODES UNIVERSITY, FACULTY OF PHARMACY

GRAHAMSTOWN, 6140, SOUTH AFRICA

SLN BATCH SUMMARY REPORT

Formulator: **Pedzisai Makoni**
Product: **EFV-loaded SLN**
Batch I.D: **EFV-SLN 016**
Batch size: **100 g**
Date of manufacture: **15 October 2013**

Formula:

Item	Material	Quantity (% w/w)	Amount/batch (g)
1	EFV	0.75	0.75
2	Glyceryl monostearate	4.25	4.25
3	Tween® 80	3.00	3.00
4	Aqua	92.00	92.00

Production equipment used:
High speed homogenization: One minute at 1000 rpm at 70°C
Hot high-pressure homogenization: One homogenization cycle at 1000 bar at 70°C

Evaluated parameters and *in vitro* dissolution profile:

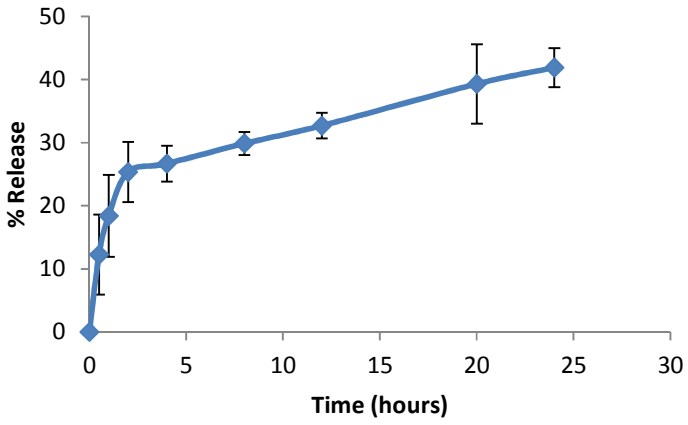

ZP: -42.6±6.57 mV
PS: 653.8±341.6 nm
PDI: 0.928±0.109

Comments:
- Formulation was unstable and not homogenous on visual assessment after two weeks at room temperature (22°C).

RHODES UNIVERSITY, FACULTY OF PHARMACY

GRAHAMSTOWN, 6140, SOUTH AFRICA

SLN BATCH SUMMARY REPORT

Formulator: **Pedzisai Makoni**
Product: **EFV-loaded SLN**
Batch I.D: **EFV-SLN 017**
Batch size: **100 g**
Date of manufacture: **15 October 2013**

Formula:

Item	Material	Quantity (% w/w)	Amount/batch (g)
1	EFV	0.50	0.50
2	Glyceryl monostearate	4.50	4.50
3	Tween® 80	1.00	1.00
4	Aqua	94.00	94.00

Production equipment used:
High speed homogenization: One minute at 1000 rpm at 70°C
Hot high-pressure homogenization: Five homogenization cycles at 1000 bar at 70°C

Evaluated parameters and *in vitro* dissolution profile:

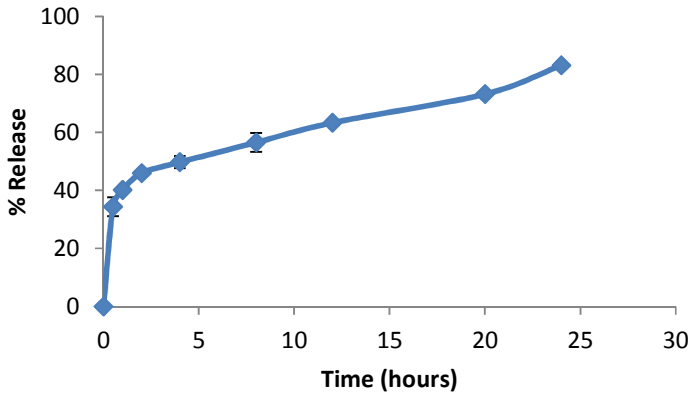

ZP: -44.8±4.85 mV
PS: 71.43±1.776 nm
PDI: 0.565±0.074

Comments:
- Formulation was unstable and not homogenous on visual assessment after two weeks at room temperature (22°C).

RHODES UNIVERSITY, FACULTY OF PHARMACY

GRAHAMSTOWN, 6140, SOUTH AFRICA

SLN BATCH SUMMARY REPORT

Formulator: **Pedzisai Makoni**
Product: **EFV-loaded SLN**
Batch I.D: **EFV-SLN 018**
Batch size: **100 g**
Date of manufacture: **15 October 2013**

Formula:

Item	Material	Quantity (% w/w)	Amount/batch (g)
1	EFV	0.75	0.75
2	Glyceryl monostearate	4.25	4.25
3	Tween® 80	1.00	1.00
4	Aqua	94.00	94.00

Production equipment used:
High speed homogenization: One minute at 1000 rpm at 70°C
Hot high-pressure homogenization: Three homogenization cycles at 1000 bar at 70°C

Evaluated parameters and *in vitro* dissolution profile:

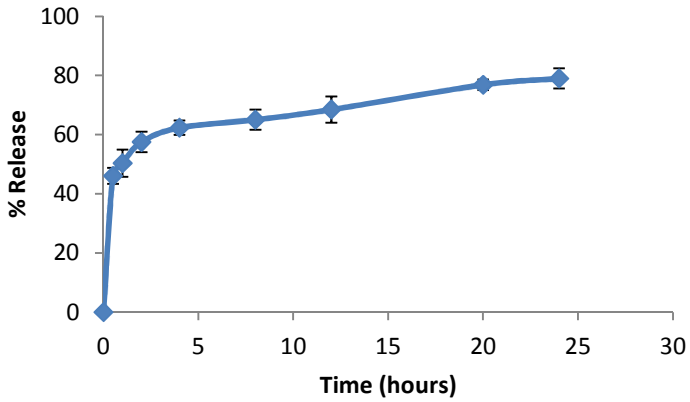

ZP: -51.1±4.10 mV
PS: 125.9±43.66 nm
PDI: 0.623±0.099

Comments:
- Formulation was unstable and not homogenous on visual assessment after two weeks at room temperature (22°C).

RHODES UNIVERSITY, FACULTY OF PHARMACY

GRAHAMSTOWN, 6140, SOUTH AFRICA

SLN BATCH SUMMARY REPORT

Formulator: **Pedzisai Makoni**
Product: **EFV-loaded SLN**
Batch I.D: **EFV-SLN 019**
Batch size: **100 g**
Date of manufacture: **16 October 2013**

Formula:

Item	Material	Quantity (% w/w)	Amount/batch (g)
1	EFV	0.25	0.25
2	Glyceryl monostearate	4.75	4.75
3	Tween® 80	3.00	3.00
4	Aqua	92.00	92.00

Production equipment used:
High speed homogenization: One minute at 1000 rpm at 70°C
Hot high-pressure homogenization: Three homogenization cycles at 500 bar at 70°C

Evaluated parameters and *in vitro* dissolution profile:

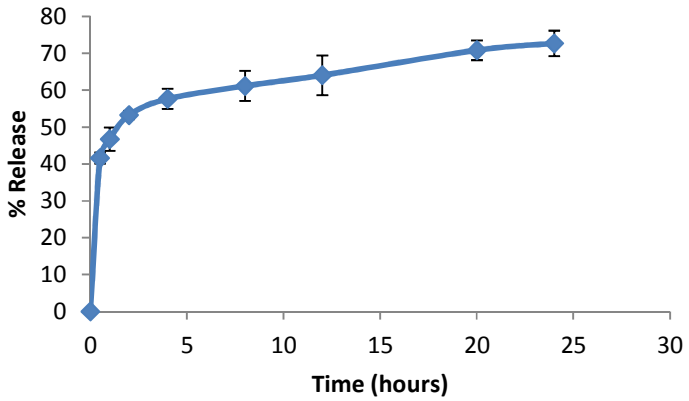

ZP: -44.1±6.28 mV
PS: 245.6±55.31 nm
PDI: 0.830±0.170

Comments:
- Formulation was stable and homogenous on visual assessment after two weeks at room temperature (22°C).

RHODES UNIVERSITY, FACULTY OF PHARMACY

GRAHAMSTOWN, 6140, SOUTH AFRICA

SLN BATCH SUMMARY REPORT

Formulator: **Pedzisai Makoni**
Product: **EFV-loaded SLN**
Batch I.D: **EFV-SLN 020**
Batch size: **100 g**
Date of manufacture: **16 October 2013**

Formula:

Item	Material	Quantity (% w/w)	Amount/batch (g)
1	EFV	0.50	0.50
2	Glyceryl monostearate	4.50	4.50
3	Tween® 80	3.00	3.00
4	Aqua	92.00	92.00

Production equipment used:
High speed homogenization: One minute at 1000 rpm at 70°C
Hot high-pressure homogenization: Five homogenization cycles at 500 bar at 70°C

Evaluated parameters and *in vitro* dissolution profile:

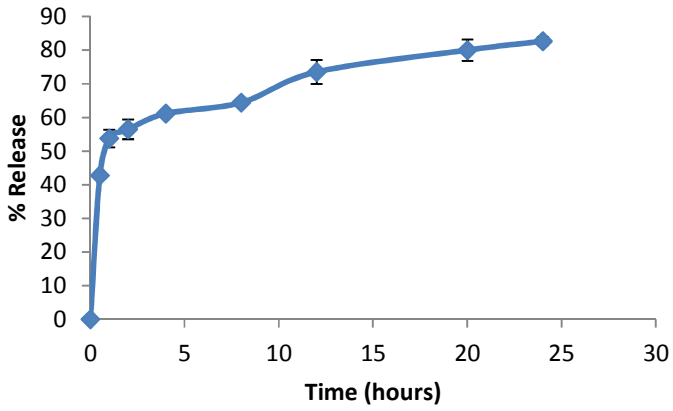

ZP: -38.9±2.66 mV
PS: 100.6±3.856 nm
PDI: 0.594±0.035
Comments:
- Formulation was stable and homogenous on visual assessment after two weeks at room temperature (22°C).

RHODES UNIVERSITY, FACULTY OF PHARMACY

GRAHAMSTOWN, 6140, SOUTH AFRICA

SLN BATCH SUMMARY REPORT

Formulator: **Pedzisai Makoni**
Product: **EFV-loaded SLN**
Batch I.D: **EFV-SLN 021**
Batch size: **100 g**
Date of manufacture: **16 October 2013**

Formula:

Item	Material	Quantity (% w/w)	Amount/batch (g)
1	EFV	0.50	0.50
2	Glyceryl monostearate	4.50	4.50
3	Tween® 80	3.00	3.00
4	Aqua	92.00	92.00

Production equipment used:
High speed homogenization: One minute at 1000 rpm at 70°C
Hot high-pressure homogenization: One homogenization cycle at 500 bar at 70°C

Evaluated parameters and *in vitro* dissolution profile:

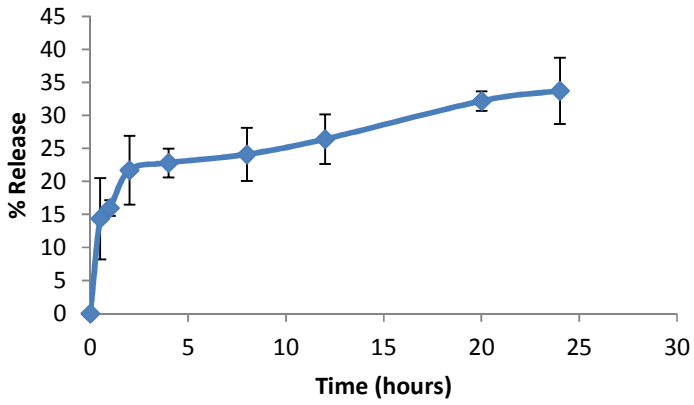

ZP: -38.6±6.40 mV
PS: 684.0±139.6 nm
PDI: 0.824±0.160

Comments:
- Formulation was stable and homogenous on visual assessment after two weeks at room temperature (22°C).

RHODES UNIVERSITY, FACULTY OF PHARMACY

GRAHAMSTOWN, 6140, SOUTH AFRICA

SLN BATCH SUMMARY REPORT

Formulator: **Pedzisai Makoni**
Product: **EFV-loaded SLN**
Batch I.D: **EFV-SLN 022**
Batch size: **100 g**
Date of manufacture: **17 October 2013**

Formula:

Item	Material	Quantity (% w/w)	Amount/batch (g)
1	EFV	0.50	0.50
2	Glyceryl monostearate	4.50	4.50
3	Tween® 80	3.00	3.00
4	Aqua	92.00	92.00

Production equipment used:
High speed homogenization: One minute at 1000 rpm at 70°C
Hot high-pressure homogenization: Three homogenization cycles at 1000 bar at 70°C

Evaluated parameters and *in vitro* dissolution profile:

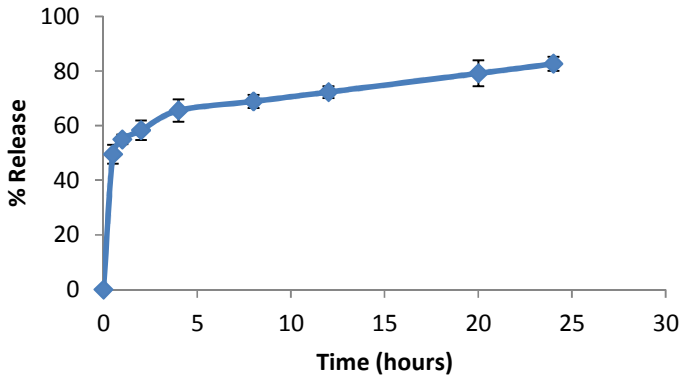

ZP: -41.7±8.81 mV
PS: 120.2±30.24 nm
PDI: 0.642±0.153

Comments:
- Formulation was stable and homogenous on visual assessment after two weeks at room temperature (22°C).

RHODES UNIVERSITY, FACULTY OF PHARMACY

GRAHAMSTOWN, 6140, SOUTH AFRICA

SLN BATCH SUMMARY REPORT

Formulator: **Pedzisai Makoni**
Product: **EFV-loaded SLN**
Batch I.D: **EFV-SLN 023**
Batch size: **100 g**
Date of manufacture: **17 October 2013**

Formula:

Item	Material	Quantity (% w/w)	Amount/batch (g)
1	EFV	0.50	0.50
2	Glyceryl monostearate	4.50	4.50
3	Tween® 80	3.00	3.00
4	Aqua	92.00	92.00

Production equipment used:
High speed homogenization: One minute at 1000 rpm at 70°C
Hot high-pressure homogenization: Three homogenization cycles at 1000 bar at 70°C

Evaluated parameters and *in vitro* dissolution profile:

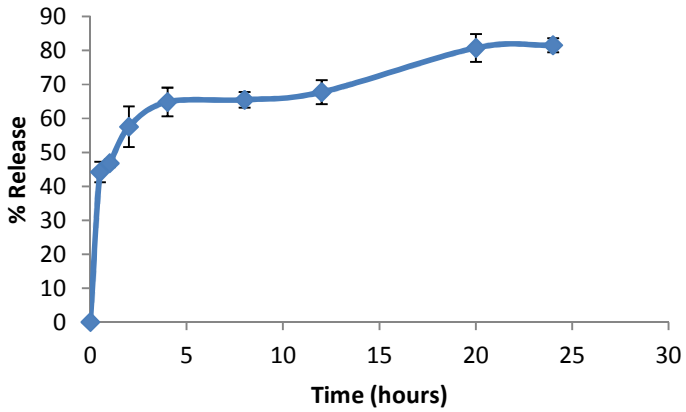

ZP: -43.3±11.6 mV
PS: 103.5±25.17 nm
PDI: 0.567±0.122

Comments:
- Formulation was stable and homogenous on visual assessment after two weeks at room temperature (22°C).

RHODES UNIVERSITY, FACULTY OF PHARMACY

GRAHAMSTOWN, 6140, SOUTH AFRICA

SLN BATCH SUMMARY REPORT

Formulator: **Pedzisai Makoni**
Product: **EFV-loaded SLN**
Batch I.D: **EFV-SLN 024**
Batch size: **100 g**
Date of manufacture: **17 October 2013**

Formula:

Item	Material	Quantity (% w/w)	Amount/batch (g)
1	EFV	0.50	0.50
2	Glyceryl monostearate	4.50	4.50
3	Tween® 80	3.00	3.00
4	Aqua	92.00	92.00

Production equipment used:
High speed homogenization: One minute at 1000 rpm at 70°C
Hot high-pressure homogenization: Five homogenization cycles at 1500 bar at 70°C

Evaluated parameters and *in vitro* dissolution profile:

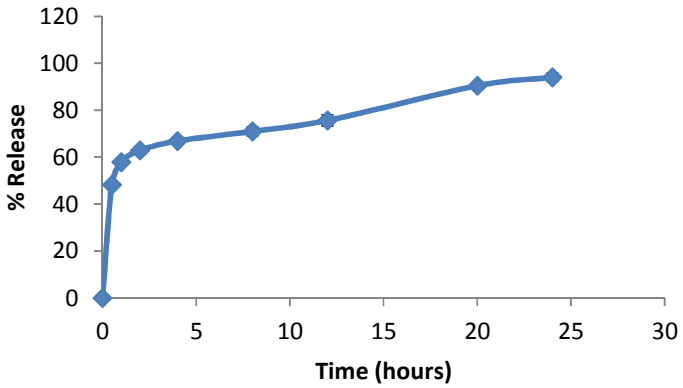

ZP: -31.5±5.79 mV
PS: 42.19±1.358 nm
PDI: 0.5670.444±0.018

Comments:
- Formulation was stable and homogenous on visual assessment after two weeks at room temperature (22°C).

RHODES UNIVERSITY, FACULTY OF PHARMACY

GRAHAMSTOWN, 6140, SOUTH AFRICA

SLN BATCH SUMMARY REPORT

Formulator: **Pedzisai Makoni**
Product: **EFV-loaded SLN**
Batch I.D: **EFV-SLN 025**
Batch size: **100 g**
Date of manufacture: **18 October 2013**

Formula:

Item	Material	Quantity (% w/w)	Amount/batch (g)
1	EFV	0.25	0.25
2	Glyceryl monostearate	4.75	4.75
3	Tween® 80	3.00	3.00
4	Aqua	92.00	92.00

Production equipment used:
High speed homogenization: One minute at 1000 rpm at 70°C
Hot high-pressure homogenization: Three homogenization cycles at 1500 bar at 70°C

Evaluated parameters and *in vitro* dissolution profile:

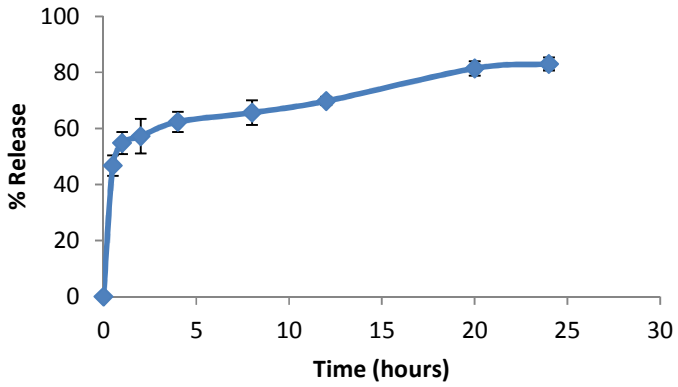

ZP: -34.6±6.21 mV
PS: 89.29±25.98 nm
PDI: 0.496±0.185

Comments:
- Formulation was stable and homogenous on visual assessment after two weeks at room temperature (22°C).

RHODES UNIVERSITY, FACULTY OF PHARMACY

GRAHAMSTOWN, 6140, SOUTH AFRICA

SLN BATCH SUMMARY REPORT

Formulator: **Pedzisai Makoni**
Product: **EFV-loaded SLN**
Batch I.D: **EFV-SLN 026**
Batch size: **100 g**
Date of manufacture: **18 October 2013**

Formula:

Item	Material	Quantity (% w/w)	Amount/batch (g)
1	EFV	0.50	0.50
2	Glyceryl monostearate	4.50	4.50
3	Tween® 80	1.00	1.00
4	Aqua	92.00	92.00

Production equipment used:
High speed homogenization: One minute at 1000 rpm at 70°C
Hot high-pressure homogenization: Three homogenization cycles at 500 bar at 70°C

Evaluated parameters and *in vitro* dissolution profile:

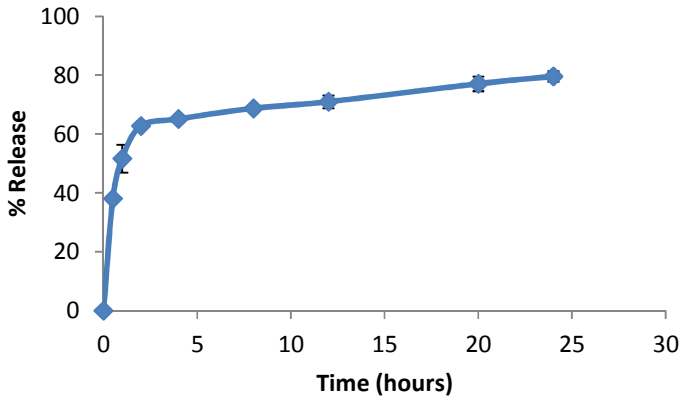

ZP: -48.9±3.99 mV
PS: 127.1±8.775 nm
PDI: 0.727±0.144

Comments:
- Formulation was unstable and not homogenous on visual assessment after two weeks at room temperature (22°C).

RHODES UNIVERSITY, FACULTY OF PHARMACY

GRAHAMSTOWN, 6140, SOUTH AFRICA

SLN BATCH SUMMARY REPORT

Formulator: **Pedzisai Makoni**
Product: **EFV-loaded SLN**
Batch I.D: **EFV-SLN 027**
Batch size: **100 g**
Date of manufacture: **18 October 2013**

Formula:

Item	Material	Quantity (% w/w)	Amount/batch (g)
1	EFV	0.50	0.50
2	Glyceryl monostearate	4.50	4.50
3	Tween® 80	5.00	5.00
4	Aqua	90.00	90.00

Production equipment used:
High speed homogenization: One minute at 1000 rpm at 70°C
Hot high-pressure homogenization: Three homogenization cycles at 500 bar at 70°C

Evaluated parameters and *in vitro* dissolution profile:

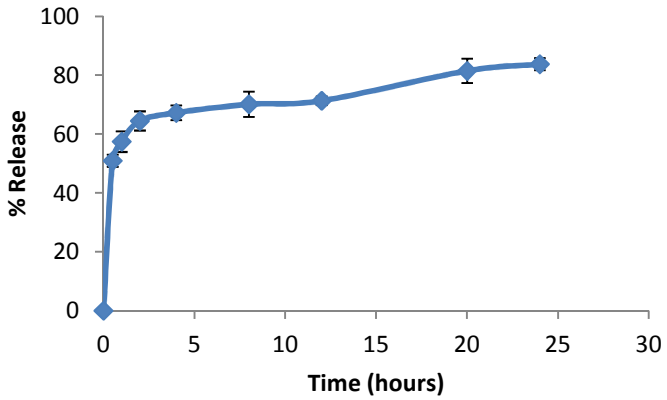

ZP: -37.3±3.10 mV
PS: 101.1±5.712 nm
PDI: 0.707±0.111

Comments:
- Formulation was stable and homogenous on visual assessment after two weeks at room temperature (22°C).

RHODES UNIVERSITY, FACULTY OF PHARMACY

GRAHAMSTOWN, 6140, SOUTH AFRICA

SLN BATCH SUMMARY REPORT

Formulator: **Pedzisai Makoni**
Product: **EFV-loaded SLN**
Batch I.D: **EFV-SLN 028**
Batch size: **100 g**
Date of manufacture: **19 October 2013**

Formula:

Item	Material	Quantity (% w/w)	Amount/batch (g)
1	EFV	0.50	0.50
2	Glyceryl monostearate	4.50	4.50
3	Tween® 80	1.00	1.00
4	Aqua	94.00	94.00

Production equipment used:
High speed homogenization: One minute at 1000 rpm at 70°C
Hot high-pressure homogenization: Three homogenization cycles at 1500 bar at 70°C

Evaluated parameters and *in vitro* dissolution profile:

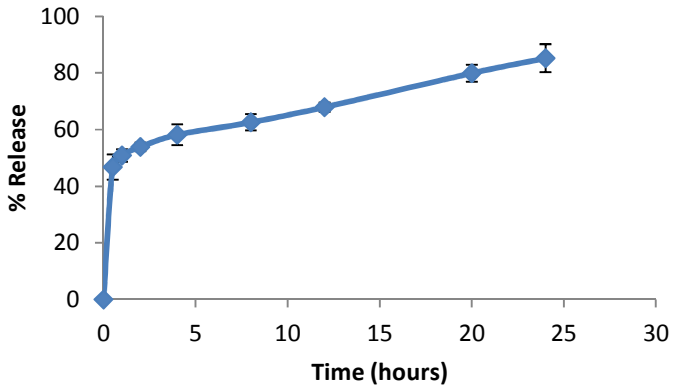

ZP: -47.3±4.43 mV
PS: 106.4±45.89 nm
PDI: 0.533±0.089

Comments:
- Formulation was unstable and not homogenous on visual assessment after two weeks at room temperature (22°C).

RHODES UNIVERSITY, FACULTY OF PHARMACY

GRAHAMSTOWN, 6140, SOUTH AFRICA

SLN BATCH SUMMARY REPORT

Formulator: **Pedzisai Makoni**
Product: **EFV-loaded SLN**
Batch I.D: **EFV-SLN 029**
Batch size: **100 g**
Date of manufacture: **19 October 2013**

Formula:

Item	Material	Quantity (% w/w)	Amount/batch (g)
1	EFV	0.50	0.50
2	Glyceryl monostearate	4.50	4.50
3	Tween® 80	5.00	5.00
4	Aqua	90.00	90.00

Production equipment used:
High speed homogenization: One minute at 1000 rpm at 70°C
Hot high-pressure homogenization: Five homogenization cycles at 1000 bar at 70°C

Evaluated parameters and *in vitro* dissolution profile:

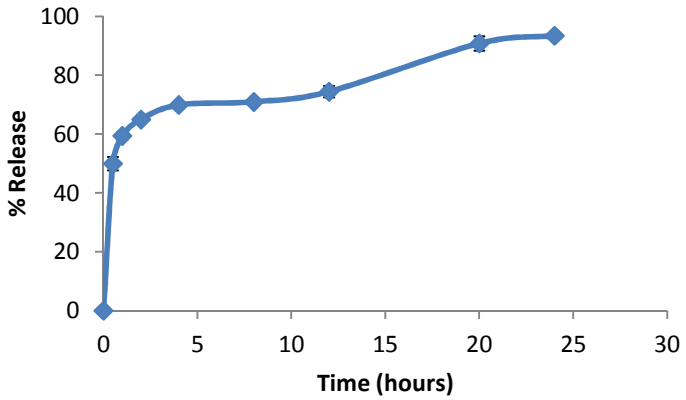

ZP: -37.5±3.08 mV
PS: 51.55±1.193 nm
PDI: 0.502±0.032
Comments:
- Formulation was stable and homogenous on visual assessment after two weeks at room temperature (22°C).

APPENDIX III

NLC PRODUCTION REPORTS

All NLC formulations manufactured and assessed during formulation development and optimization studies were manufactured using Good Manufacturing Practice (GMP).

RHODES UNIVERSITY, FACULTY OF PHARMACY

GRAHAMSTOWN, 6140, SOUTH AFRICA

NLC BATCH SUMMARY REPORT

Formulator: **Pedzisai Makoni**
Product: **EFV-loaded NLC**
Batch I.D: **EFV-NLC 001**
Batch size: **100 g**
Date of manufacture: **25 October 2013**

Formula:

Item	Material	Quantity (% w/w)	Amount/batch (g)
1	EFV	0.75	0.75
2	Glyceryl monostearate	2.975	2.975
3	Transcutol® HP	1.275	1.275
4	Tween® 80	3.00	3.00
5	Aqua	92.00	92.00

Production equipment used:
High speed homogenization: One minute at 1000 rpm at 70°C
Hot high-pressure homogenization: Five homogenization cycles at 1000 bar at 70°C

Evaluated parameters:

ZP:-22.4±4.96 mV
PS: 55.85±3.843 nm
PDI: 0.456±0.091
Comments:
- Formulation was unstable and not homogenous on visual assessment after two weeks at room temperature (22°C).

NLC BATCH SUMMARY REPORT

Formulator: **Pedzisai Makoni**
Product: **EFV-loaded NLC**
Batch I.D: **EFV-NLC 002**
Batch size: **100 g**
Date of manufacture: **25 October 2013**

Formula:

Item	Material	Quantity (% w/w)	Amount/batch (g)
1	EFV	0.50	0.50
2	Glyceryl monostearate	3.15	3.15
3	Transcutol® HP	1.35	1.35
4	Tween® 80	3.00	3.00
5	Aqua	92.00	92.00

Production equipment used:
High speed homogenization: One minute at 1000 rpm at 70°C
Hot high-pressure homogenization: Three homogenization cycles at 1000 bar at 70°C

Evaluated parameters:

ZP: -30.5±6.29 mV
PS: 65.3±129.4 nm
PDI: 0.551±0.174
Comments:
- Formulation was stable and homogenous on visual assessment after two weeks at room temperature (22°C).

RHODES UNIVERSITY, FACULTY OF PHARMACY

GRAHAMSTOWN, 6140, SOUTH AFRICA

NLC BATCH SUMMARY REPORT

Formulator: **Pedzisai Makoni**
Product: **EFV-loaded NLC**
Batch I.D: **EFV-NLC 003**
Batch size: **100 g**
Date of manufacture: **25 October 2013**

Formula:

Item	Material	Quantity (% w/w)	Amount/batch (g)
1	EFV	0.25	0.25
2	Glyceryl monostearate	3.325	3.325
3	Transcutol® HP	1.425	1.425
4	Tween® 80	3.00	3.00
5	Aqua	92.00	92.00

Production equipment used:
High speed homogenization: One minute at 1000 rpm at 70°C
Hot high-pressure homogenization: Five homogenization cycles at 1000 bar at 70°C

Evaluated parameters:

ZP: -30.9±3.69 mV
PS: 67.13±13.10 nm
PDI: 0.621±0.163
Comments:
- Formulation was stable and homogenous on visual assessment after two weeks at room temperature (22°C).

RHODES UNIVERSITY, FACULTY OF PHARMACY

GRAHAMSTOWN, 6140, SOUTH AFRICA

NLC BATCH SUMMARY REPORT

Formulator: **Pedzisai Makoni**
Product: **EFV-loaded NLC**
Batch I.D: **EFV-NLC 004**
Batch size: **100 g**
Date of manufacture: **26 October 2013**

Formula:

Item	Material	Quantity (% w/w)	Amount/batch (g)
1	EFV	0.75	0.75
2	Glyceryl monostearate	2.975	2.975
3	Transcutol® HP	1.275	1.275
4	Tween® 80	3.00	3.00
5	Aqua	92.00	92.00

Production equipment used:
High speed homogenization: One minute at 1000 rpm at 70°C
Hot high-pressure homogenization: Three homogenization cycles at 1500 bar at 70°C

Evaluated parameters:

ZP: -27.3±3.52 mV
PS: 66.42±10.62 nm
PDI: 0.475±0.059
Comments:
- Formulation was unstable and not homogenous on visual assessment after two weeks at room temperature (22°C).

RHODES UNIVERSITY, FACULTY OF PHARMACY

GRAHAMSTOWN, 6140, SOUTH AFRICA

NLC BATCH SUMMARY REPORT

Formulator: **Pedzisai Makoni**
Product: **EFV-loaded NLC**
Batch I.D: **EFV-NLC 005**
Batch size: **100 g**
Date of manufacture: **26 October 2013**

Formula:

Item	Material	Quantity (% w/w)	Amount/batch (g)
1	EFV	0.75	0.75
2	Glyceryl monostearate	2.975	2.975
3	Transcutol® HP	1.275	1.275
4	Tween® 80	3.00	3.00
5	Aqua	92.00	92.00

Production equipment used:
High speed homogenization: One minute at 1000 rpm at 70°C
Hot high-pressure homogenization: Three homogenization cycles at 500 bar at 70°C

Evaluated parameters:

ZP: -34.3±3.06 mV
PS: 97.3±23.22 nm
PDI: 0.435±0.079
Comments:
- Formulation was unstable and not homogenous on visual assessment after two weeks at room temperature (22°C).

RHODES UNIVERSITY, FACULTY OF PHARMACY

GRAHAMSTOWN, 6140, SOUTH AFRICA

NLC BATCH SUMMARY REPORT

Formulator: **Pedzisai Makoni**
Product: **EFV-loaded NLC**
Batch I.D: **EFV-NLC 006**
Batch size: **100 g**
Date of manufacture: **26 October 2013**

Formula:

Item	Material	Quantity (% w/w)	Amount/batch (g)
1	EFV	0.75	0.75
2	Glyceryl monostearate	2.975	2.975
3	Transcutol® HP	1.275	1.275
4	Tween® 80	5.00	5.00
5	Aqua	90.00	90.00

Production equipment used:
High speed homogenization: One minute at 1000 rpm at 70°C
Hot high-pressure homogenization: Three homogenization cycles at 1000 bar at 70°C

Evaluated parameters:

ZP: -29.3±4.72 mV
PS: 70.57±290.7 nm
PDI: 0.516±0.161
Comments:
- Formulation was stable and homogenous on visual assessment after two weeks at room temperature (22°C).

RHODES UNIVERSITY, FACULTY OF PHARMACY

GRAHAMSTOWN, 6140, SOUTH AFRICA

NLC BATCH SUMMARY REPORT

Formulator: **Pedzisai Makoni**
Product: **EFV-loaded NLC**
Batch I.D: **EFV-NLC 007**
Batch size: **100 g**
Date of manufacture: **27 October 2013**

Formula:

Item	Material	Quantity (% w/w)	Amount/batch (g)
1	EFV	0.50	0.50
2	Glyceryl monostearate	3.15	3.15
3	Transcutol® HP	1.35	1.35
4	Tween® 80	5.00	5.00
5	Aqua	90.00	90.00

Production equipment used:
High speed homogenization: One minute at 1000 rpm at 70°C
Hot high-pressure homogenization: One homogenization cycle at 1000 bar at 70°C

Evaluated parameters:

ZP: -27.3±4.63 mV
PS: 584.2±31.13 nm
PDI: 0.772±0.129
Comments:
- Formulation was stable and homogenous on visual assessment after two weeks at room temperature (22°C).

RHODES UNIVERSITY, FACULTY OF PHARMACY

GRAHAMSTOWN, 6140, SOUTH AFRICA

NLC BATCH SUMMARY REPORT

Formulator: **Pedzisai Makoni**
Product: **EFV-loaded NLC**
Batch I.D: **EFV-NLC 008**
Batch size: **100 g**
Date of manufacture: **27 October 2013**

Formula:

Item	Material	Quantity (% w/w)	Amount/batch (g)
1	EFV	0.25	0.25
2	Glyceryl monostearate	3.325	3.325
3	Transcutol® HP	1.425	1.425
4	Tween® 80	5.00	5.00
5	Aqua	90.00	90.00

Production equipment used:
High speed homogenization: One minute at 1000 rpm at 70°C
Hot high-pressure homogenization: Three homogenization cycles at 1000 bar at 70°C

Evaluated parameters:

ZP: -29.5±3.98 mV
PS: 98.56±480.3 nm
PDI: 0.544±0.241
Comments:
- Formulation was stable and homogenous on visual assessment after two weeks at room temperature (22°C).

RHODES UNIVERSITY, FACULTY OF PHARMACY

GRAHAMSTOWN, 6140, SOUTH AFRICA

NLC BATCH SUMMARY REPORT

Formulator: **Pedzisai Makoni**
Product: **EFV-loaded NLC**
Batch I.D: **EFV-NLC 009**
Batch size: **100 g**
Date of manufacture: **27 October 2013**

Formula:

Item	Material	Quantity (% w/w)	Amount/batch (g)
1	EFV	0.50	0.50
2	Glyceryl monostearate	3.15	3.15
3	Transcutol® HP	1.35	1.35
4	Tween® 80	1.00	1.00
5	Aqua	94.00	94.00

Production equipment used:
High speed homogenization: One minute at 1000 rpm at 70°C
Hot high-pressure homogenization: One homogenization cycle at 1000 bar at 70°C

Evaluated parameters:

ZP: -41.5±8.96 mV
PS: 2902±1.387 nm
PDI: 0.641±0.042
Comments:
- Formulation was unstable and not homogenous on visual assessment after two weeks at room temperature (22°C).

RHODES UNIVERSITY, FACULTY OF PHARMACY

GRAHAMSTOWN, 6140, SOUTH AFRICA

NLC BATCH SUMMARY REPORT

Formulator: **Pedzisai Makoni**
Product: **EFV-loaded NLC**
Batch I.D: **EFV-NLC 010**
Batch size: **100 g**
Date of manufacture: **28 October 2013**

Formula:

Item	Material	Quantity (% w/w)	Amount/batch (g)
1	EFV	0.50	0.50
2	Glyceryl monostearate	3.15	3.15
3	Transcutol® HP	1.35	1.35
4	Tween® 80	3.00	3.00
5	Aqua	92.00	92.00

Production equipment used:
High speed homogenization: One minute at 1000 rpm at 70°C
Hot high-pressure homogenization: Three homogenization cycles at 1000 bar at 70°C

Evaluated parameters:

ZP: -30.9±2.88 mV
PS: 66.51±33.22 nm
PDI: 0.451±0.084
Comments:
- Formulation was stable and homogenous on visual assessment after two weeks at room temperature (22°C).

RHODES UNIVERSITY, FACULTY OF PHARMACY

GRAHAMSTOWN, 6140, SOUTH AFRICA

NLC BATCH SUMMARY REPORT

Formulator: **Pedzisai Makoni**
Product: **EFV-loaded NLC**
Batch I.D: **EFV-NLC 011**
Batch size: **100 g**
Date of manufacture: **28 October 2013**

Formula:

Item	Material	Quantity (% w/w)	Amount/batch (g)
1	EFV	0.50	0.50
2	Glyceryl monostearate	3.15	3.15
3	Transcutol® HP	1.35	1.35
4	Tween® 80	3.00	3.00
5	Aqua	92.00	92.00

Production equipment used:
High speed homogenization: One minute at 1000 rpm at 70°C
Hot high-pressure homogenization: One homogenization cycle at 1500 bar at 70°C

Evaluated parameters:

ZP: -32.4±9.08 mV
PS: 141.1±1.115 nm
PDI: 0.477±0.020
Comments:
- Formulation was unstable and not homogenous on visual assessment after two weeks at room temperature (22°C).

RHODES UNIVERSITY, FACULTY OF PHARMACY

GRAHAMSTOWN, 6140, SOUTH AFRICA

NLC BATCH SUMMARY REPORT

Formulator: **Pedzisai Makoni**
Product: **EFV-loaded NLC**
Batch I.D: **EFV-NLC 012**
Batch size: **100 g**
Date of manufacture: **28 October 2013**

Formula:

Item	Material	Quantity (% w/w)	Amount/batch (g)
1	EFV	0.50	0.50
2	Glyceryl monostearate	3.15	3.15
3	Transcutol® HP	1.35	1.35
4	Tween® 80	3.00	3.00
5	Aqua	92.00	92.00

Production equipment used:
High speed homogenization: One minute at 1000 rpm at 70°C
Hot high-pressure homogenization: Three homogenization cycles at 1000 bar at 70°C

Evaluated parameters:

ZP: -33.8±3.34 mV
PS: 66.19±163.2 nm
PDI: 0.508±0.226
Comments:
- Formulation was stable and homogenous on visual assessment after two weeks at room temperature (22°C).

RHODES UNIVERSITY, FACULTY OF PHARMACY

GRAHAMSTOWN, 6140, SOUTH AFRICA

NLC BATCH SUMMARY REPORT

Formulator: **Pedzisai Makoni**
Product: **EFV-loaded NLC**
Batch I.D: **EFV-NLC 013**
Batch size: **100 g**
Date of manufacture: **29 October 2013**

Formula:

Item	Material	Quantity (% w/w)	Amount/batch (g)
1	EFV	0.25	0.25
2	Glyceryl monostearate	3.325	3.325
3	Transcutol® HP	1.425	1.425
4	Tween® 80	3.00	3.00
5	Aqua	92.00	92.00

Production equipment used:
High speed homogenization: One minute at 1000 rpm at 70°C
Hot high-pressure homogenization: One homogenization cycle at 1000 bar at 70°C

Evaluated parameters:

ZP: -31.4±4.20 mV
PS: 513.6±20.20 nm
PDI: 0.526±0.143
Comments:
- Formulation was unstable and not homogenous on visual assessment after two weeks at room temperature (22°C).

RHODES UNIVERSITY, FACULTY OF PHARMACY

GRAHAMSTOWN, 6140, SOUTH AFRICA

NLC BATCH SUMMARY REPORT

Formulator: **Pedzisai Makoni**
Product: **EFV-loaded NLC**
Batch I.D: **EFV-NLC 014**
Batch size: **100 g**
Date of manufacture: **29 October 2013**

Formula:

Item	Material	Quantity (% w/w)	Amount/batch (g)
1	EFV	0.50	0.50
2	Glyceryl monostearate	3.15	3.15
3	Transcutol® HP	1.35	1.35
4	Tween® 80	5.00	5.00
5	Aqua	90.00	90.00

Production equipment used:
High speed homogenization: One minute at 1000 rpm at 70°C
Hot high-pressure homogenization: Three homogenization cycles at 1500 bar at 70°C

Evaluated parameters:

ZP: -31.9±3.39 mV
PS: 63.56±3.196 nm
PDI: 0.521±0.074
Comments:
- Formulation was stable and homogenous on visual assessment after two weeks at room temperature (22°C).

RHODES UNIVERSITY, FACULTY OF PHARMACY

GRAHAMSTOWN, 6140, SOUTH AFRICA

NLC BATCH SUMMARY REPORT

Formulator: **Pedzisai Makoni**
Product: **EFV-loaded NLC**
Batch I.D: **EFV-NLC 015**
Batch size: **100 g**
Date of manufacture: **29 October 2013**

Formula:

Item	Material	Quantity (% w/w)	Amount/batch (g)
1	EFV	0.25	0.25
2	Glyceryl monostearate	3.325	3.325
3	Transcutol® HP	1.425	1.425
4	Tween® 80	1.00	1.00
5	Aqua	94.00	94.00

Production equipment used:
High speed homogenization: One minute at 1000 rpm at 70°C
Hot high-pressure homogenization: Three homogenization cycles at 1000 bar at 70°C

Evaluated parameters:

ZP: -39.6±3.00 mV
PS: 1518±278.5 nm
PDI: 0.535±0.161
Comments:
- Formulation was unstable and not homogenous on visual assessment after two weeks at room temperature (22°C).

RHODES UNIVERSITY, FACULTY OF PHARMACY

GRAHAMSTOWN, 6140, SOUTH AFRICA

NLC BATCH SUMMARY REPORT

Formulator: **Pedzisai Makoni**
Product: **EFV-loaded NLC**
Batch I.D: **EFV-NLC 016**
Batch size: **100 g**
Date of manufacture: **30 October 2013**

Formula:

Item	Material	Quantity (% w/w)	Amount/batch (g)
1	EFV	0.75	0.75
2	Glyceryl monostearate	2.975	2.975
3	Transcutol® HP	1.275	1.275
4	Tween® 80	3.00	3.00
5	Aqua	92.00	92.00

Production equipment used:
High speed homogenization: One minute at 1000 rpm at 70°C
Hot high-pressure homogenization: One homogenization cycle at 1000 bar at 70°C

Evaluated parameters:

ZP: -31.1±4.26 mV
PS: 433.5±18.39 nm
PDI: 0.746±0.068
Comments:
- Formulation was unstable and not homogenous on visual assessment after two weeks at room temperature (22°C).

RHODES UNIVERSITY, FACULTY OF PHARMACY

GRAHAMSTOWN, 6140, SOUTH AFRICA

NLC BATCH SUMMARY REPORT

Formulator: **Pedzisai Makoni**
Product: **EFV-loaded NLC**
Batch I.D: **EFV-NLC 017**
Batch size: **100 g**
Date of manufacture: **30 October 2013**

Formula:

Item	Material	Quantity (% w/w)	Amount/batch (g)
1	EFV	0.50	0.50
2	Glyceryl monostearate	3.15	3.15
3	Transcutol® HP	1.35	1.35
4	Tween® 80	1.00	1.00
5	Aqua	94.00	94.00

Production equipment used:
High speed homogenization: One minute at 1000 rpm at 70°C
Hot high-pressure homogenization: Five homogenization cycles at 1000 bar at 70°C

Evaluated parameters:

ZP: -41.2±4.10 mV
PS: 68.1±2.931 nm
PDI: 0.505±0.043
Comments:
- Formulation was unstable and not homogenous on visual assessment after two weeks at room temperature (22°C).

RHODES UNIVERSITY, FACULTY OF PHARMACY

GRAHAMSTOWN, 6140, SOUTH AFRICA

NLC BATCH SUMMARY REPORT

Formulator: **Pedzisai Makoni**
Product: **EFV-loaded NLC**
Batch I.D: **EFV-NLC 018**
Batch size: **100 g**
Date of manufacture: **30 October 2013**

Formula:

Item	Material	Quantity (% w/w)	Amount/batch (g)
1	EFV	0.75	0.75
2	Glyceryl monostearate	2.975	2.975
3	Transcutol® HP	1.275	1.275
4	Tween® 80	1.00	1.00
5	Aqua	94.00	94.00

Production equipment used:
High speed homogenization: One minute at 1000 rpm at 70°C
Hot high-pressure homogenization: Three homogenization cycles at 1000 bar at 70°C

Evaluated parameters:

ZP: -49.1±5.78 mV
PS: 80.42±3.064 nm
PDI: 0.460±0.052
Comments:
- Formulation was unstable and not homogenous on visual assessment after two weeks at room temperature (22°C).

RHODES UNIVERSITY, FACULTY OF PHARMACY

GRAHAMSTOWN, 6140, SOUTH AFRICA

NLC BATCH SUMMARY REPORT

Formulator: **Pedzisai Makoni**
Product: **EFV-loaded NLC**
Batch I.D: **EFV-NLC 019**
Batch size: **100 g**
Date of manufacture: **31 October 2013**

Formula:

Item	Material	Quantity (% w/w)	Amount/batch (g)
1	EFV	0.25	0.25
2	Glyceryl monostearate	3.325	3.325
3	Transcutol® HP	1.425	1.425
4	Tween® 80	3.00	3.00
5	Aqua	92.00	92.00

Production equipment used:
High speed homogenization: One minute at 1000 rpm at 70°C
Hot high-pressure homogenization: Three homogenization cycles at 500 bar at 70°C

Evaluated parameters:

ZP: -32.8±4.98 mV
PS: 93.99±1.577 nm
PDI: 0.456±0.049
Comments:
- Formulation was stable and homogenous on visual assessment after two weeks at room temperature (22°C).

RHODES UNIVERSITY, FACULTY OF PHARMACY

GRAHAMSTOWN, 6140, SOUTH AFRICA

NLC BATCH SUMMARY REPORT

Formulator: **Pedzisai Makoni**
Product: **EFV-loaded NLC**
Batch I.D: **EFV-NLC 020**
Batch size: **100 g**
Date of manufacture: **31 October 2013**

Formula:

Item	Material	Quantity (% w/w)	Amount/batch (g)
1	EFV	0.50	0.50
2	Glyceryl monostearate	3.15	3.15
3	Transcutol® HP	1.35	1.35
4	Tween® 80	3.00	3.00
5	Aqua	92.00	92.00

Production equipment used:
High speed homogenization: One minute at 1000 rpm at 70°C
Hot high-pressure homogenization: Five homogenization cycles at 500 bar at 70°C

Evaluated parameters:

ZP: -32.7±3.30 mV
PS: 79.21±11.45 nm
PDI: 0.472±0.053
Comments:
- Formulation was stable and homogenous on visual assessment after two weeks at room temperature (22°C).

RHODES UNIVERSITY, FACULTY OF PHARMACY

GRAHAMSTOWN, 6140, SOUTH AFRICA

NLC BATCH SUMMARY REPORT

Formulator: **Pedzisai Makoni**
Product: **EFV-loaded NLC**
Batch I.D: **EFV-NLC 021**
Batch size: **100 g**
Date of manufacture: **31 October 2013**

Formula:

Item	Material	Quantity (% w/w)	Amount/batch (g)
1	EFV	0.50	0.50
2	Glyceryl monostearate	3.15	3.15
3	Transcutol® HP	1.35	1.35
4	Tween® 80	3.00	3.00
5	Aqua	92.00	92.00

Production equipment used:
High speed homogenization: One minute at 1000 rpm at 70°C
Hot high-pressure homogenization: One homogenization cycle at 500 bar at 70°C

Evaluated parameters:

ZP: -31.6±2.32 mV
PS: 112.8±1.343 nm
PDI: 0.380±0.041
Comments:
- Formulation was unstable and not homogenous on visual assessment after two weeks at room temperature (22°C).

RHODES UNIVERSITY, FACULTY OF PHARMACY

GRAHAMSTOWN, 6140, SOUTH AFRICA

NLC BATCH SUMMARY REPORT

Formulator: **Pedzisai Makoni**
Product: **EFV-loaded NLC**
Batch I.D: **EFV-NLC 022**
Batch size: **100 g**
Date of manufacture: **1 November 2013**

Formula:

Item	Material	Quantity (% w/w)	Amount/batch (g)
1	EFV	0.50	0.50
2	Glyceryl monostearate	3.15	3.15
3	Transcutol® HP	1.35	1.35
4	Tween® 80	3.00	3.00
5	Aqua	92.00	92.00

Production equipment used:
High speed homogenization: One minute at 1000 rpm at 70°C
Hot high-pressure homogenization: Three homogenization cycles at 1000 bar at 70°C

Evaluated parameters:

ZP: -39.2±3.48 mV
PS: 66.81±27.73 nm
PDI: 0.489±0.037
Comments:
- Formulation was stable and homogenous on visual assessment after two weeks at room temperature (22°C).

RHODES UNIVERSITY, FACULTY OF PHARMACY

GRAHAMSTOWN, 6140, SOUTH AFRICA

NLC BATCH SUMMARY REPORT

Formulator: **Pedzisai Makoni**
Product: **EFV-loaded NLC**
Batch I.D: **EFV-NLC 023**
Batch size: **100 g**
Date of manufacture: **1 November 2013**

Formula:

Item	Material	Quantity (% w/w)	Amount/batch (g)
1	EFV	0.50	0.50
2	Glyceryl monostearate	3.15	3.15
3	Transcutol® HP	1.35	1.35
4	Tween® 80	3.00	3.00
5	Aqua	92.00	92.00

Production equipment used:
High speed homogenization: One minute at 1000 rpm at 70°C
Hot high-pressure homogenization: Three homogenization cycles at 1000 bar at 70°C

Evaluated parameters:

ZP: -33.9±2.52 mV
PS: 72.89±1.559 nm
PDI: 0.473±0.024
Comments:
- Formulation was stable and homogenous on visual assessment after two weeks at room temperature (22°C).

RHODES UNIVERSITY, FACULTY OF PHARMACY

GRAHAMSTOWN, 6140, SOUTH AFRICA

NLC BATCH SUMMARY REPORT

Formulator: **Pedzisai Makoni**
Product: **EFV-loaded NLC**
Batch I.D: **EFV-NLC 024**
Batch size: **100 g**
Date of manufacture: **1 November 2013**

Formula:

Item	Material	Quantity (% w/w)	Amount/batch (g)
1	EFV	0.50	0.50
2	Glyceryl monostearate	3.15	3.15
3	Transcutol® HP	1.35	1.35
4	Tween® 80	3.00	3.00
5	Aqua	92.00	92.00

Production equipment used:
High speed homogenization: One minute at 1000 rpm at 70°C
Hot high-pressure homogenization: Five homogenization cycles at 1500 bar at 70°C

Evaluated parameters:

ZP: -26.5±8.40 mV
PS: 37.19±3.859 nm
PDI: 0.421±0.053
Comments:
- Formulation was stable and homogenous on visual assessment after two weeks at room temperature (22°C).

RHODES UNIVERSITY, FACULTY OF PHARMACY

GRAHAMSTOWN, 6140, SOUTH AFRICA

NLC BATCH SUMMARY REPORT

Formulator: **Pedzisai Makoni**
Product: **EFV-loaded NLC**
Batch I.D: **EFV-NLC 025**
Batch size: **100 g**
Date of manufacture: **2 November 2013**

Formula:

Item	Material	Quantity (% w/w)	Amount/batch (g)
1	EFV	0.25	0.25
2	Glyceryl monostearate	3.325	3.325
3	Transcutol® HP	1.425	1.425
4	Tween® 80	3.00	3.00
5	Aqua	92.00	92.00

Production equipment used:
High speed homogenization: One minute at 1000 rpm at 70°C
Hot high-pressure homogenization: Three homogenization cycles at 1500 bar at 70°C

Evaluated parameters:

ZP: -28.6±3.16 mV
PS: 63.02±3.083 nm
PDI: 0.455±0.042
Comments:
- Formulation was stable and homogenous on visual assessment after two weeks at room temperature (22°C).

RHODES UNIVERSITY, FACULTY OF PHARMACY

GRAHAMSTOWN, 6140, SOUTH AFRICA

NLC BATCH SUMMARY REPORT

Formulator: **Pedzisai Makoni**
Product: **EFV-loaded NLC**
Batch I.D: **EFV-NLC 026**
Batch size: **100 g**
Date of manufacture: **2 November 2013**

Formula:

Item	Material	Quantity (% w/w)	Amount/batch (g)
1	EFV	0.50	0.50
2	Glyceryl monostearate	3.15	3.15
3	Transcutol® HP	1.35	1.35
4	Tween® 80	1.00	1.00
5	Aqua	92.00	92.00

Production equipment used:
High speed homogenization: One minute at 1000 rpm at 70°C
Hot high-pressure homogenization: Three homogenization cycles at 500 bar at 70°C

Evaluated parameters:

ZP: -34.8±3.33 mV
PS: 97.47±3.083 nm
PDI: 0.422±0.042
Comments:
- Formulation was unstable and not homogenous on visual assessment after two weeks at room temperature (22°C).

RHODES UNIVERSITY, FACULTY OF PHARMACY

GRAHAMSTOWN, 6140, SOUTH AFRICA

NLC BATCH SUMMARY REPORT

Formulator: **Pedzisai Makoni**
Product: **EFV-loaded NLC**
Batch I.D: **EFV-NLC 027**
Batch size: **100 g**
Date of manufacture: **2 November 2013**

Formula:

Item	Material	Quantity (% w/w)	Amount/batch (g)
1	EFV	0.50	0.50
2	Glyceryl monostearate	3.15	3.15
3	Transcutol®	1.35	1.35
4	Tween® 80	5.00	5.00
5	Aqua	90.00	90.00

Production equipment used:
High speed homogenization: One minute at 1000 rpm at 70°C
Hot high-pressure homogenization: Three homogenization cycles at 500 bar at 70°C

Evaluated parameters:

ZP: -25.0±5.52 mV
PS: 73.64±1.409 nm
PDI: 0.530±0.040
Comments:
- Formulation was stable and homogenous on visual assessment after two weeks at room temperature (22°C).

RHODES UNIVERSITY, FACULTY OF PHARMACY

GRAHAMSTOWN, 6140, SOUTH AFRICA

NLC BATCH SUMMARY REPORT

Formulator: **Pedzisai Makoni**
Product: **EFV-loaded NLC**
Batch I.D: **EFV-NLC 028**
Batch size: **100 g**
Date of manufacture: **3 November 2013**

Formula:

Item	Material	Quantity (% w/w)	Amount/batch (g)
1	EFV	0.50	0.50
2	Glyceryl monostearate	3.15	3.15
3	Transcutol® HP	1.35	1.35
4	Tween® 80	1.00	1.00
5	Aqua	94.00	94.00

Production equipment used:
High speed homogenization: One minute at 1000 rpm at 70°C
Hot high-pressure homogenization: Three homogenization cycles at 1500 bar at 70°C

Evaluated parameters:

ZP: -36.9±4.96 mV
PS: 69.81±1.585 nm
PDI: 0.483±0.037
Comments:
- Formulation was unstable and not homogenous on visual assessment after two weeks at room temperature (22°C).

RHODES UNIVERSITY, FACULTY OF PHARMACY

GRAHAMSTOWN, 6140, SOUTH AFRICA

NLC BATCH SUMMARY REPORT

Formulator: **Pedzisai Makoni**
Product: **EFV-loaded NLC**
Batch I.D: **EFV-NLC 029**
Batch size: **100 g**
Date of manufacture: **3 November 2013**

Formula:

Item	Material	Quantity (% w/w)	Amount/batch (g)
1	EFV	0.50	0.50
2	Glyceryl monostearate	3.15	3.15
3	Transcutol® HP	1.35	1.35
4	Tween® 80	5.00	5.00
5	Aqua	90.00	90.00

Production equipment used:
High speed homogenization: One minute at 1000 rpm at 70°C
Hot high-pressure homogenization: Five homogenization cycles at 1000 bar at 70°C

Evaluated parameters:

ZP: -24.9±2.93 mV
PS: 53.37±1.741 nm
PDI: 0.479±0.051
Comments:
- Formulation was stable and homogenous on visual assessment after two weeks at room temperature (22°C).

APPENDIX IV

NLC BOX BEHNKEN DESIGN SUMMARY

Table Ap.4.1 *Responses observed for Box Behnken design experiments for NLC formulations*

Runs	Response variables			
	Y_1 mV	Y_2 nm	Y_3	Y_4
1	-22.4	55.85	0.456	0
2	-30.5	65.3	0.551	1
3	-30.9	67.13	0.621	1
4	-27.3	66.42	0.475	0
5	-34.3	97.3	0.435	0
6	-29.3	70.57	0.516	1
7	-27.3	584.2	0.772	1
8	-29.5	98.56	0.544	1
9	-41.5	2902	0.641	0
10	-30.9	66.51	0.451	1
11	-32.4	141.1	0.477	0
12	-33.8	66.19	0.508	1
13	-31.4	513.6	0.526	0
14	-31.9	63.56	0.521	1
15	-39.6	1518	0.535	0
16	-31.1	433.5	0.746	0
17	-41.2	68.1	0.505	0
18	-49.1	80.42	0.46	0
19	-32.8	93.99	0.456	1
20	-32.7	79.21	0.472	1
21	-31.6	112.8	0.38	0
22	-39.2	66.81	0.489	1
23	-33.9	72.89	0.473	1
24	-26.5	37.19	0.421	1
25	-28.6	63.02	0.455	1
26	-34.8	97.47	0.422	0
27	-25	73.64	0.53	1
28	-36.9	69.81	0.483	0
29	-24.9	53.37	0.479	1

Model fit equations and their regression coefficients

Zeta potential (Y_1) = $-32.46-0.058X_1+0.63X_2+6.27X_3+1.39X_4$ ***Equation Ap.4.1***

(Size) [1] = $-24.30-129.19X_1-315.99X_3-360.53X_4+352.40X_1X_3+575.77X_3X_4+392.95X_3^2+313.99X_4^2$ ***Equation Ap.4.2***

Polydispersity index (Y_3) = $+0.49-4.083E-003X_1+0.011X_2+0.026X_3-0.049X_4+0.010X_1X_2+0.012\ X_1X_3 -0.096X_1X_4-0.018X_2X_3-0.037X_2X_4-0.039X_3X_4+0.017X_1^2-0.070X_2^2+0.040X_3^2+0.051X_4^2$ ***Equation Ap.4.3***

Visual stability (Y_4) = $+1.00-0.25X_1+0.000X_2+0.50X_3+0.25X_4+0.000X_1X_2+0.000X_1X_3-0.25X_1X_4 +0.000X_2X_3+0.000X_2X_4+0.000X_3X_4-0.33X_1^2-0.21X_2^2-0.21X_3^2-0.33X_4^2$ ***Equation Ap.4.4***

Table Ap.4.2 *Correlation coefficients and standard deviations of response models*

Response factor	**Response surface model**					
	SD	**R^2**	**Adj R^2**	**Pred R^2**	**Adeq Prec**	**C.V (%)**
Y_1	4.15	0.5468	0.4713	0.3200	8.883	12.79
Y_2	394.00	0.6598	0.5464	-0.1384	10.317	146.89
Y_3	0.062	0.7497	0.4993	-0.3313	6.742	12.25
Y_4	0.28	0.8490	0.6979	0.1300	7.498	50.42

A negative "Pred R-Squared" implies that the overall mean is a better predictor of your response than the current model.

ANOVA analysis for response surface quadratic model for zeta potential (Y_1)

Table Ap. 4.3. *ANOVA analysis for the quadratic model for zeta potential*

Source	**Sum of squares**	**Degrees of freedom (df)**	**Mean square**	**F value**	**Prob > F**
Model	**499.35**	**4**	**124.84**	**7.24**	**0.0006**
X_1	*0.041*	*1*	*0.041*	*2.368E-003*	*0.9616*
X_2	*4.81*	*1*	*4.81*	*0.28*	*0.6021*
X_3	***471.25***	***1***	***471.25***	***27.33***	***< 0.0001***
X_4	*23.24*	*1*	*23.24*	*1.35*	*0.2571*
Residual	413.84	24	17.24	-	-

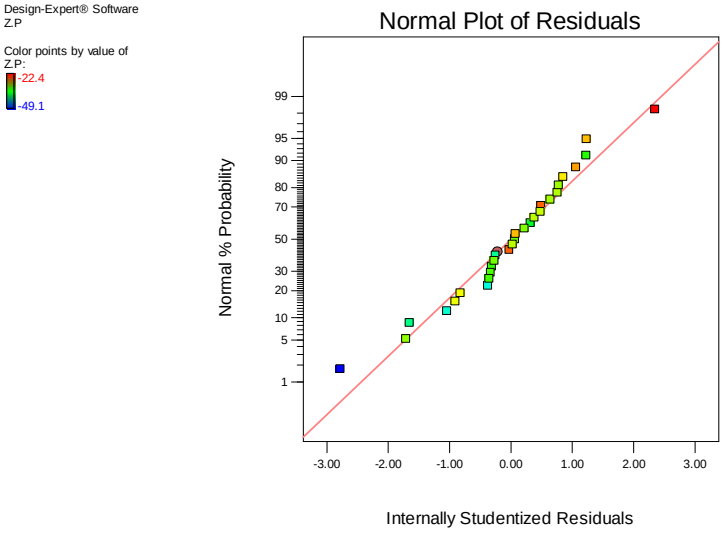

Figure Ap.4.1. *Normal probability plot of residuals for zeta potential*

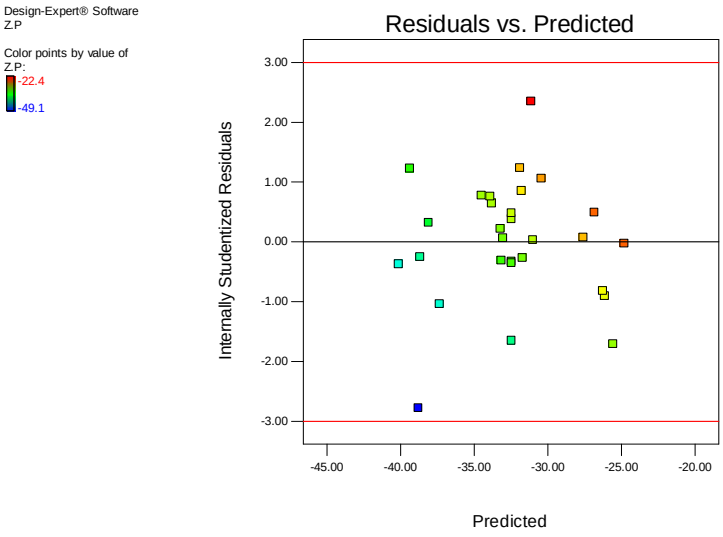

Figure Ap.4.2 *Plot of studentized residuals versus predicted responses for zeta potential*

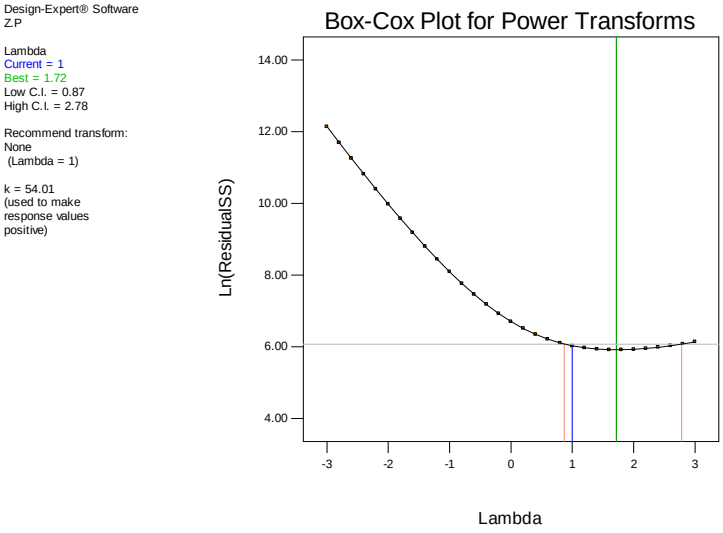

Figure Ap.4.3. *Box-Cox plot for power transformation for zeta potential*

ANOVA analysis for response surface quadratic model for particle size (Y_2)

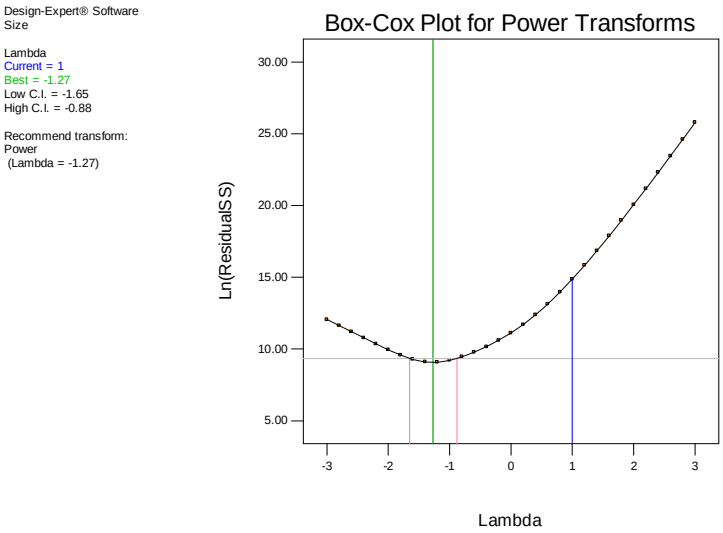

Figure Ap.4.4 *Box-Cox plot for power transformation for particle size (before power transformation)*

Table Ap.4.4 *ANOVA analysis for the power transformed quadratic model for particle size*

Source	Sum of squares	Degrees of freedom (df)	Mean square	F value	Prob > F
Model	**6.322E+006**	**7**	**9.032E+005**	**5.82**	**0.0008**
X_1	2.003E+005	1	2.003E+005	1.29	0.2688
X_3	**1.198E+006**	**1**	**1.198E+006**	**7.72**	**0.0113**
X_4	**1.560E+006**	**1**	**1.560E+006**	**10.05**	**0.0046**
X_1X_3	4.967E+005	1	4.967E+005	3.20	0.0881
X_3X_4	**1.326E+006**	**1**	**1.326E+006**	**8.54**	**0.0081**
X_3^2	**1.066E+006**	**1**	**1.066E+006**	**6.86**	**0.0160**
X_4^2	**6.805E+005**	**1**	**6.805E+005**	**4.38**	**0.0486**
Residual	3.260E+006	21	1.552E+005	-	-

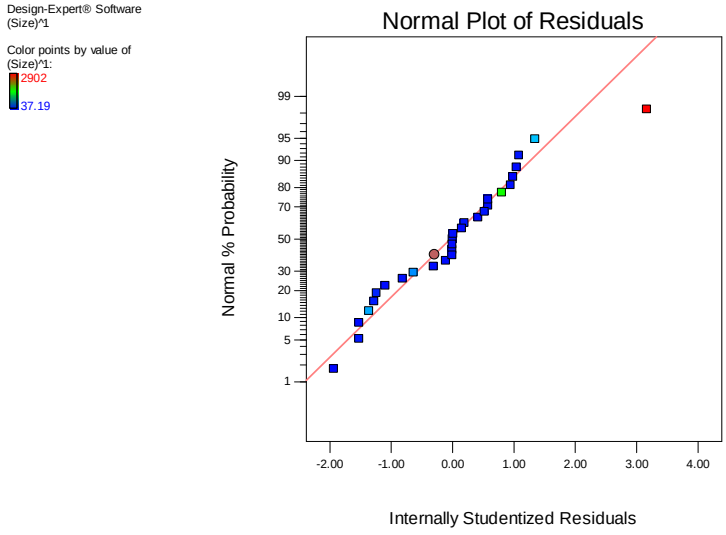

Figure Ap.4.5 *Normal probability plot of residuals for particle size after power transformation*

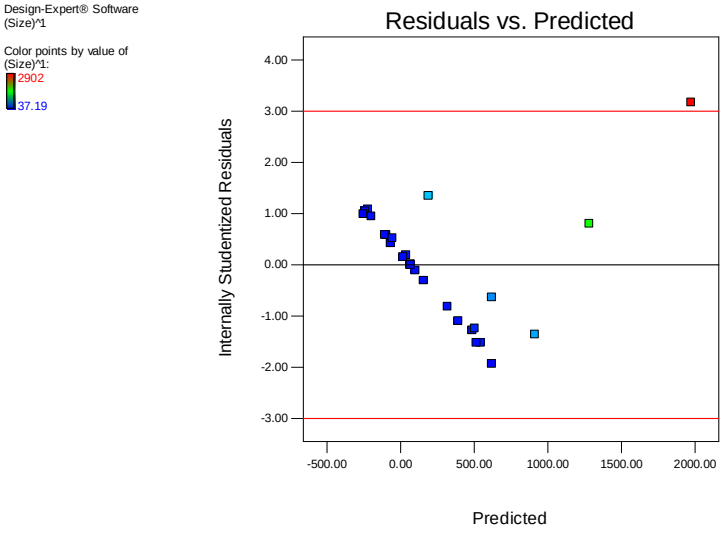

Figure Ap.4.6 *Plot of studentized residuals versus predicted responses for particle size after inverse transformation*

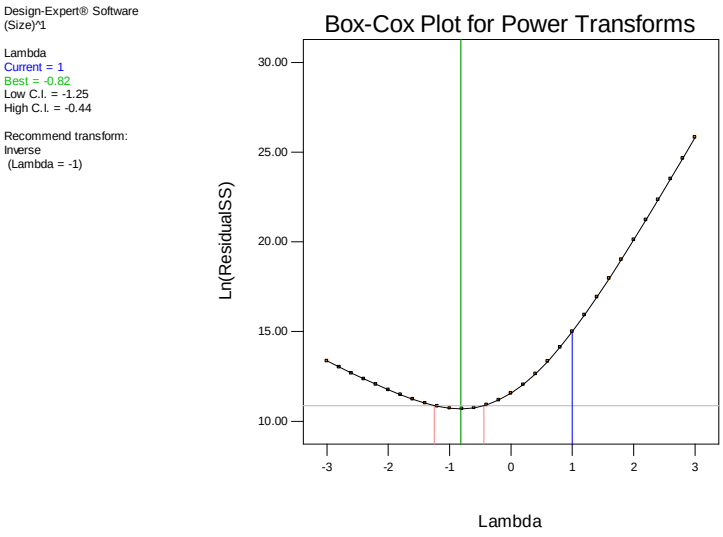

Figure Ap.4.7 *Box-Cox plot for power transformation for particle size (after power transformation)*

ANOVA analysis for response surface linear model for polydispersity index (Y_3)

Table Ap.4.5 *ANOVA analysis for the linear model for polydispersity index*

Source	Sum of squares	Degrees of freedom (df)	Mean square	F value	Prob > F
Model	**0.16**	**14**	**0.012**	**2.99**	**0.0245**
X_1	2.001E-004	1	2.001E-004	0.051	0.8242
X_2	1.564E-003	1	1.564E-003	0.40	0.5370
X_3	8.321E-003	1	8.321E-003	2.13	0.1665
X_4	**0.029**	**1**	**0.029**	**7.38**	**0.0167**
X_1X_2	4.203E-004	1	4.203E-004	0.11	0.7477
X_1X_3	5.523E-004	1	5.523E-004	0.14	0.7125
X_1X_4	**0.037**	**1**	**0.037**	**9.49**	**0.0081**
X_2X_3	1.225E-003	1	1.225E-003	0.31	0.5843
X_2X_4	5.476E-003	1	5.476E-003	1.40	0.2561
X_3X_4	6.162E-003	1	6.162E-003	1.58	0.2296
X_1^2	1.932E-003	1	1.932E-003	0.49	0.4934
X_2^2	**0.032**	**1**	**0.032**	**8.14**	**0.0128**
X_3^2	0.010	1	0.010	2.68	0.1242
X_4^2	0.017	1	0.017	4.34	0.0560
Residual	0.055	14	3.905E-003	-	-

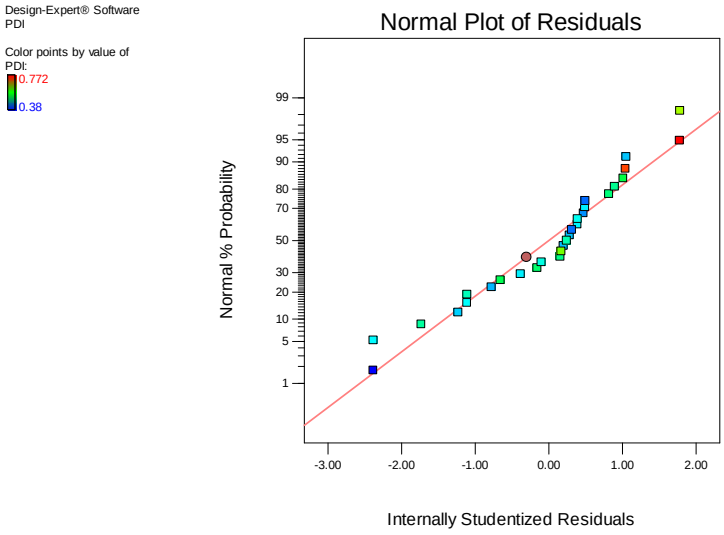

Figure Ap.4.8 *Normal probability plot of residuals for polydispersity index*

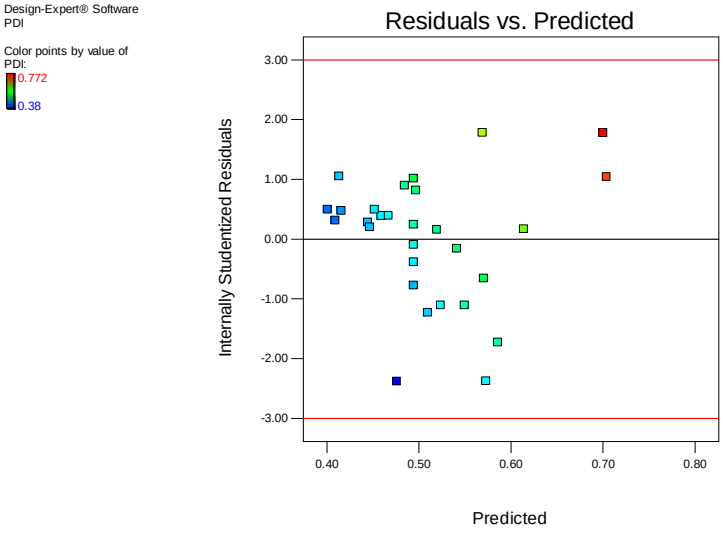

Figure Ap.4.9 *Plot of studentized residuals versus predicted responses for polydispersity index*

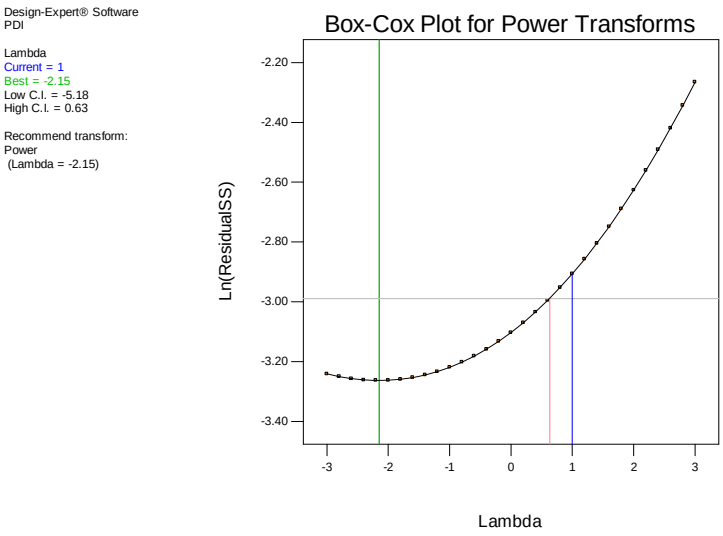

Figure Ap.4.10 *Box-Cox plot for power transformation for polydispersity index*

ANOVA analysis for response surface quadratic model for visual assessment (Y_4)

Table Ap.4.6 *ANOVA analysis for the quadratic model for visual assessment*

Source	Sum of squares	Degrees of freedom (df)	Mean square	F value	Prob > F
Model	**6.09**	**14**	**0.43**	**5.62**	**0.0013**
X_1	**0.75**	**1**	**0.75**	**9.69**	**0.0076**
X_2	0.000	1	0.000	0.000	1.0000
X_3	**3.00**	**1**	**3.00**	**38.77**	**< 0.0001**
X_4	**0.75**	**1**	**0.75**	**9.69**	**0.0076**
X_1X_2	0.000	0.75	1	0.75	9.69
X_1X_3	0.000	1	0.000	0.000	1.0000
X_1X_4	0.25	1	0.25	3.23	0.0939
X_2X_3	0.000	1	0.000	0.000	1.0000
X_2X_4	0.000	1	0.000	0.000	1.0000
X_3X_4	0.000	1	0.000	0.000	1.0000
X_1^2	0.72	1	0.72	9.31	0.0086
X_2^2	0.28	1	0.28	3.64	0.0772
X_3^2	0.28	1	0.28	3.64	0.0772
X_4^2	**0.72**	**1**	**0.72**	**9.31**	**0.0086**
Residual	1.08	14	0.077	-	-

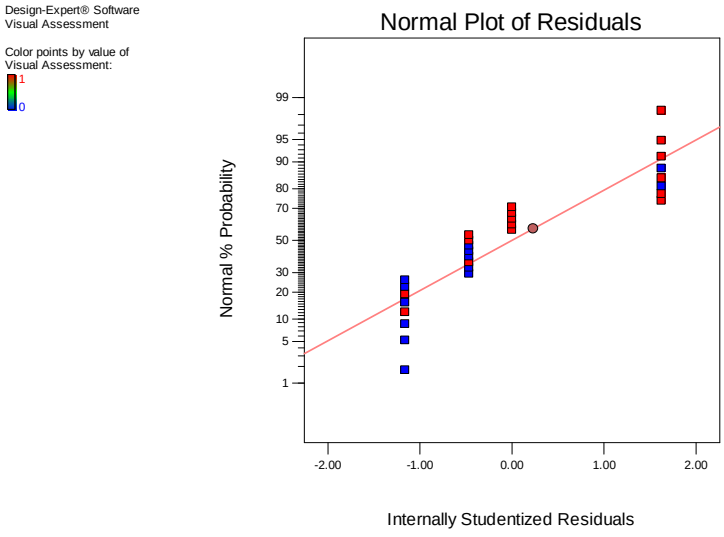

Figure Ap.4.11 *Normal probability plot of residuals for visual assessment*

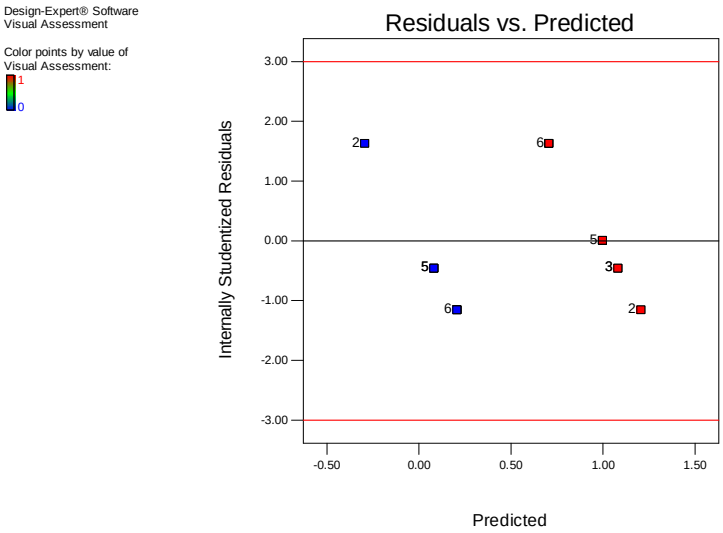

Figure Ap.4.12 *Plot of studentized residuals versus predicted responses for visual assessment*

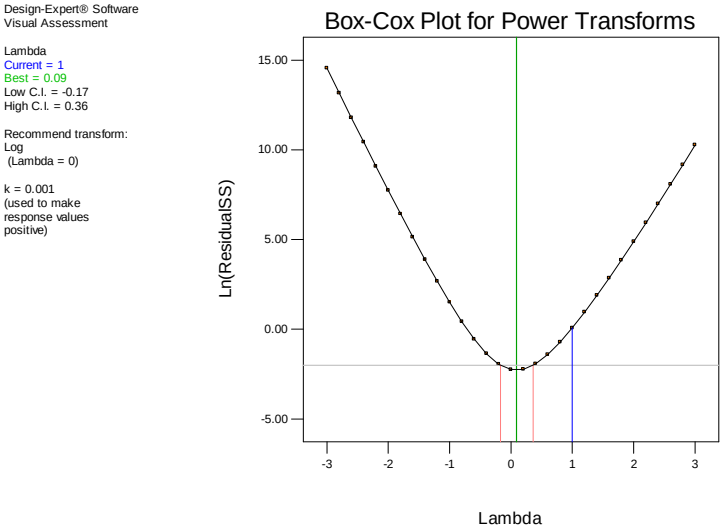

Figure Ap.4.13 *Box-Cox plot for power transformation for visual assessment*

Effects of Process Variables

Zeta potential

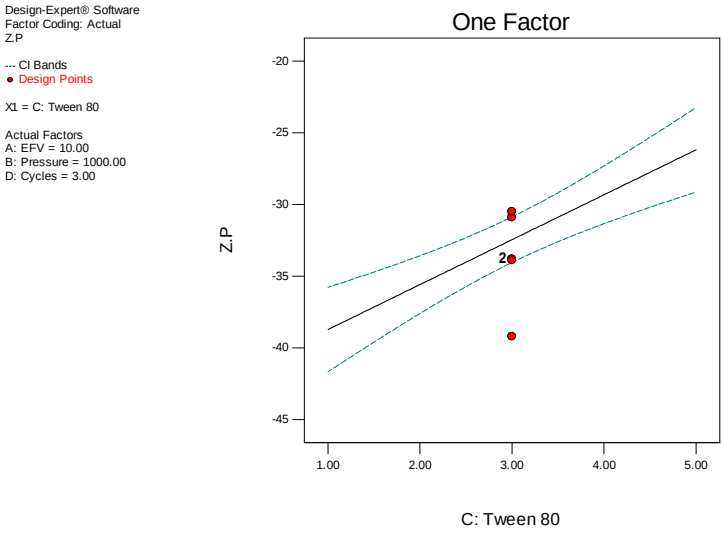

Figure Ap.4.14 *Effect of Tween® 80 on zeta potential*

Particle size

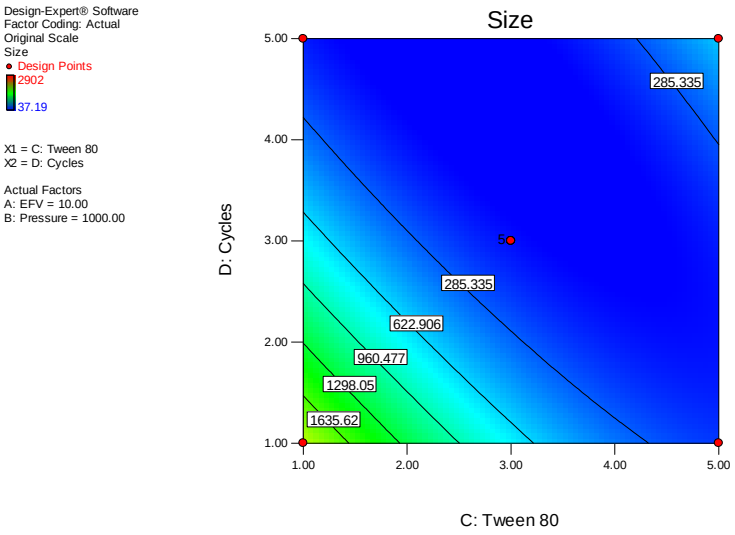

Figure Ap.4.15 *Contour plot showing the effect of homogenization cycles and Tween® 80 on particle size*

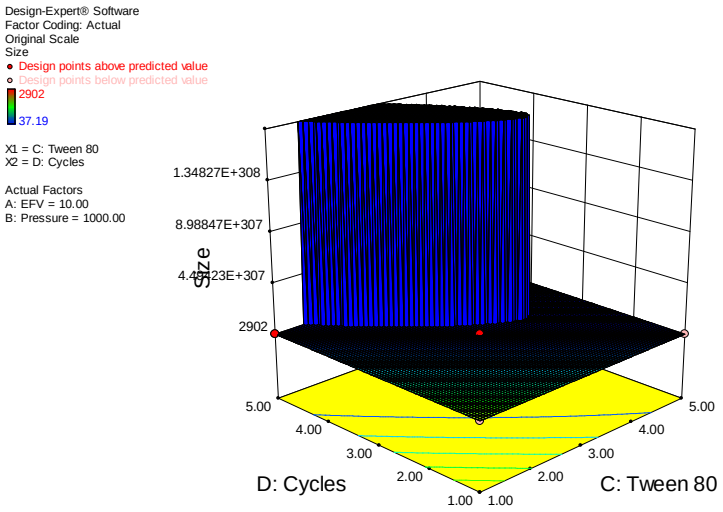

Figure Ap.4.16 *3-D surface plot showing the effect of homogenization cycles and Tween® 80 on particle size*

Polydispersity index

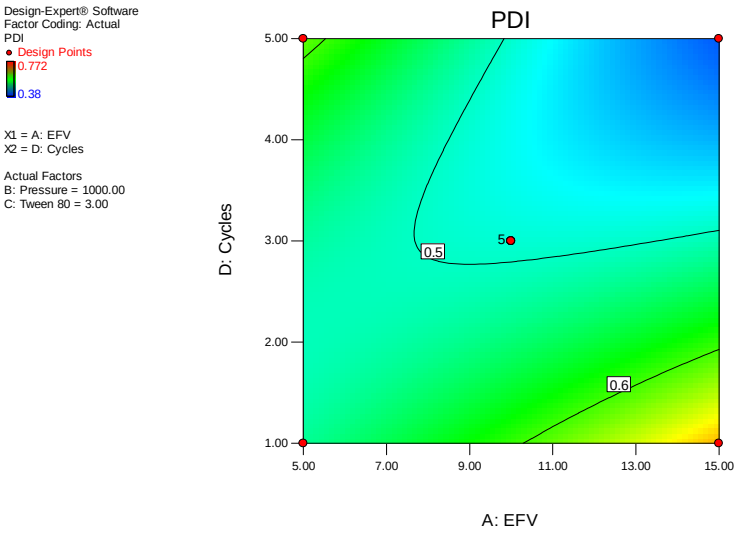

Figure Ap.4.17 *Contour plot showing the effect of homogenization cycles and amount of EFV on polydispersity index*

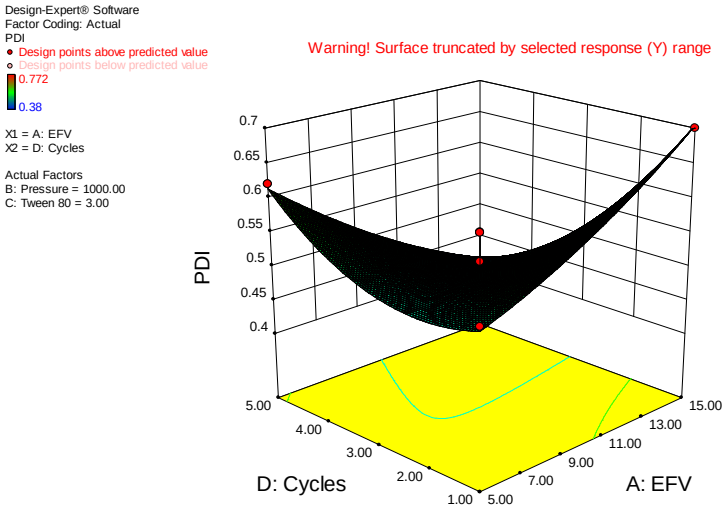

Figure Ap.4.18 *3-D surface plot showing the effect of homogenization cycles and amount of EFV on polydispersity index*

Visual assessment

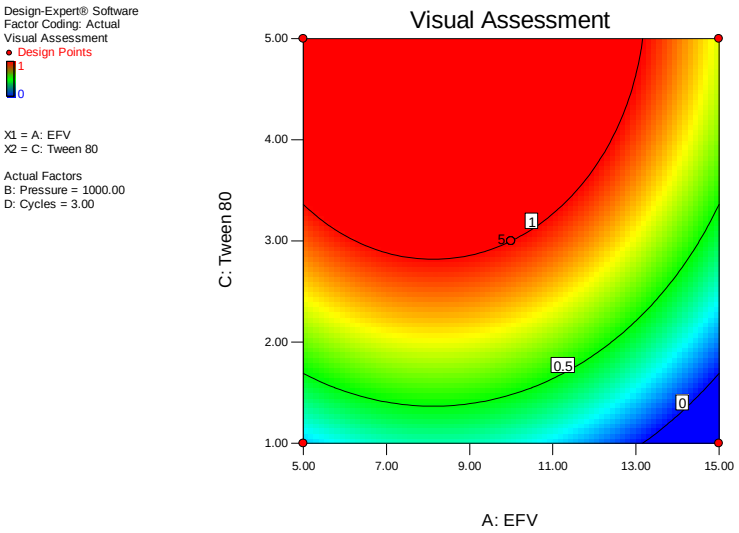

Figure Ap.4.19 *Contour plot showing the effect of Tween® 80 and amount of EFV on visual appearance*

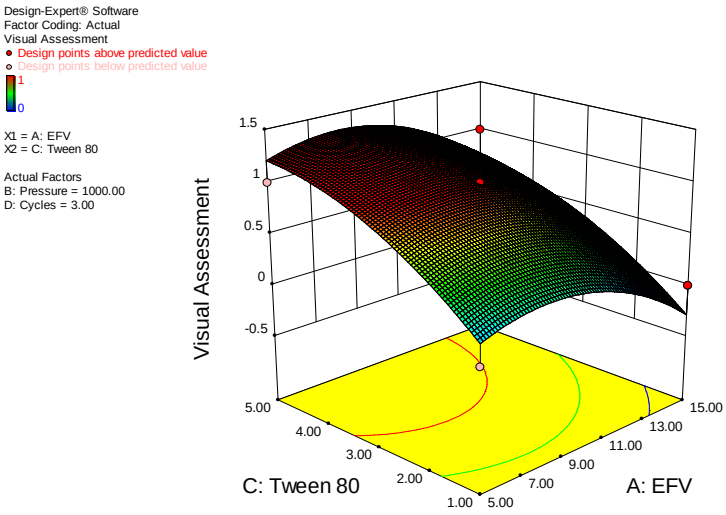

Figure Ap.4.20 *3-D surface plot showing the effect of Tween® 80 and amount of EFV on visual appearance*

Formulation Optimization

Table Ap.4.7 *Predicted values for process variables and respective formulation responses*

Process variables				Formulation responses			Desirability
X_1	X_2	X_3	X_4	Y_1	Y_3	Y_4	
10%	1499 bar	4.16%	4.51	-27.08	0.400	1	0.982

Table Ap.4.8 *Experimental and predicted response values with corresponding percentage prediction errors for the optimized formulation*

Response	Experimental value	Predicted value	% prediction error
Y_1	-25.7±2.62	-27.08	-5.37
Y_3	0.394±0.027	0.424	-7.61
Y_4	1	1	0

Table Ap.4.9 *Selected optimized formulation conditions for EFV-loaded NLC*

Process variable	Optimized condition
X_1 **(EFV)**	10%
X_2 **(Homogenization pressure)**	1500 bar
X_3 **(Tween® 80)**	4.0%
X_4 **(Homogenization cycles)**	5

REFERENCES

[1] S.Ravichandran, R.Veerasamy, S.Raman, P.N Krishnan, and R.K Agrawal, An Overview On HIV-1 Reverse Transcriptase Inhibitors, Digest Journal of Nanomaterials and Biostructures, 3 (2008) 171-187.

[2] World Heath Organisation. Global Summary of the HIV/AIDS Epidemic. http://www.who.int/hiv/data/en/. 2013. Accessed: 4/25/2013.

[3] J.C.McArthur, N.Haughey, S.Gartner, K.Conant, C.Pardo, A.Nath, and N.Sacktor, Human immunodeficiency virus-associated dementia: An evolving disease, Journal of NeuroVirology, 9 (2003) 205-221.

[4] L.K.Schrager and M.P.D'Souza, Cellular and anatomical reservoirs of HIV-1 in patients receiving potent antiretroviral combination therapy, Journal of American Medical Association, 280 (1998) 67-71.

[5] M.B.Yatvin, W.Li, M.J.Meredith, and M.A.Shenoy, Improved uptake and retention of lipophilic prodrug to improve treatment of HIV, Advanced Drug Delivery Reviews 1999, 39 (1999) 165-182.

[6] P.Portegies, AIDS dementia complex: a review, Journal of Acquired ImmuneDeficiency Syndromes, 7 (1994) S38-S49.

[7] P.Portegies, R.H.Enting, J.de Gans, P.R.Algra, M.M.Derix, J.M.Lange, and J.Goudsmit, Presentation of AIDS dementia complex: 10 years of follow-up in Amsterdam, The Netherlands., AIDS, 7 (1993) 669-675.

[8] M.Perices and D.A.Cooper, Neuropsychological investigation of patients with AIDS and ARC, Journal of Acquired Immune Deficiency Syndromes, 36 (1990) 555-564.

[9] R.Price and B.Brew, AIDS commentary:The AIDS dementia complex, Journal of Infectious Diseases, 158 (1988) 1079-1083.

[10] B.J.Brew, AIDS dementia complex, Neurologic Clinics, 17 (1999) 861-881.

[11] The Department of Health: Republic of South Africa. The South African Antiretroviral Treatment Guidelines. http://www.doh.gov.za/docs/policy/2013/ART_Treatment_Guidelines_Final_25March2013.pdf . 4/1/2013. Accessed: 11/20/2013.

[12] B.Bozal, B.Uslu, and S.A Ozkan, A Review of Electroanalytical Techniques for Determination of Anti-HIV Drugs, International Journal of Electrochemistry, (2011) 1-17.

[13] Médecins Sans Frontières. Untangling The Web of antiretroviral price reductions. http://utw.msfaccess.org/drugs/4fe29e6f850dfc2ba800000f . 7/23/2012. Accessed: 4/12/2013.

[14] Division of Clinical Pharmacology Faculty of Health Sciences University of Cape Town, South Africans Medicines Formulary, pp. 339-340, 2012.

[15] D.A.Chiappetta, C.Hocht, C.Taira, and A.Sosnik, Oral pharmacokinetics of the anti-HIV efavirenz encapsulated within polymeric micelles, Biomaterials, 32 (2011) 2379-2387.

[16] United States Pharmacopeial Convention, US Pharmacopeia, Twinbrook Parkway, Rockville, MD, USA, pp 3010, 2012.

[17] S.C.Sweetman. Martindale:The Complete Drug Reference. http://0-www.medicinescomplete.com.wam.seals.ac.za/mc/martindale/current/3463-d.htm?q=efavirenz&t=search&ss=text&p=1&hide=1 33rd. 2007. London, Pharmaceutical Press. Accessed: 4/26/2013.

[18] S.Rowe, L.Fontalbert, S.Rabel, and M.Maurin. Physical Chemical properties of efavirenz. American Association of Pharmaceutical Scientists (http://www.aapsj.org/abstracts/AM_1999/1005.htm) . 2012. DuPont Pharmaceuticals Company, Wilmington, DE. Accessed: 10/4/2012.

[19] M.B.Maurin, S.M.Rowe, K.Blom, and M.E.Pierce, Kinetics and Mechanism of Hydrolysis of Efavirenz, Pharmaceutical Research, 19 (2002) 517-521.

[20] J.Shaji and D.Jadhav, Newer Approaches To Self Emulsifying Drug Delivery System, International Journal of Pharmacy and Pharmaceutical Sciences, 2 (2010) 37-42.

[21] S.Rabel, M.Maurin, S.Rowe, and M.Hussain, Determination of the pKa and pH-solubility behavior of an ionizable cyclic carbamate, (S)-6-chloro-4-(cyclopropylethynyl)-1,4-dihydro-4-(trifluoromethyl)-2H-3,1-benzoxazin-2-one (DMP 266)., Pharm Dev Technol, 1 (1996) 91-95.

[22] R.Cristofoletti, A.Nair, B.Abrahamson, D.W.Groot, S.Kopp, P.Langgnth, J.E.Polli, V.P.Shah, and J.B.Dressman, Biowaiver Monographs for Immediate Release Solid Oral Dosage Forms: Efavirenz, J. Pharm. Sci., 102 (2012) 318-329.

[23] The World Health Organization. International Pharmacopoeia Monograph on Efavirenz, World Health Organization. http://www.who.int/medicines/areas/quality_safety/QAS_145_Efavirenz_monograph_23Aug2005.pdf , 1/7/2005. Geneva, Switzerland. Accessed: 10/4/2012.

[24] K.P.Seremeta, D.A.Chiappetta, and A.Sosnik, Poly(æ-caprolactone), Eudragit® RS 100 and poly(æ-caprolactone)/Eudragit® RS 100 blend submicron particles for the sustained release of the antiretroviral efavirenz, Colloids and Surfaces B: Biointerfaces, 102 (2013) 441-449.

[25] Z.Perold, E.Swanepoel, and M.Britis, Anomalous dissolution behaviour of a novel amorphous form of Efavirenz, Am. J. PharmTech Res, 2 (2012) 273-292.

[26] S.Mogatle. African Traditional Medicines-Antiretroviral Drug Interactions: The Effect Of African Potato (Hypoxis Hemerocallidea) On The Pharmacokinetics Of Efavirenz In Humans. Rhodes University, pp. 23-37, 2008.

[27] D.L.Pavia, G.Lampman, G.Kriz, and J.Vyvyan, Introduction to Spectroscopy, Cengage Learning, pp. 1-15, 2008.

[28] Northen Illinois University Department of Chemistry and Biochemistry. FT-IR sample preparation. http://www.niu.edu/AnalyticalLab/ftir/sample%20preparation.shtml . 2007. Accessed: 4/14/2013.

[29] R.Seiceira, C.R.Rodrigues, C.R.D.Hoffmeister, L.M.Cabral, and H.V.A.Rocha, Efavirenz Dissolution Enhancement I: Co-Micronization, Pharmaceutics, 5 (2012) 1-22.

[30] G.Ngwa, Forced Degradation as an Integral Part of HPLC Stability-Indicating Method Development, Drug Delivery Technology, 10 (2010) 1-4.

[31] M.Bakshi and S.Singh, Development of validated stability-indicating assay methods-critical review, Journal of Pharmaceutical and Biomedical Analysis, 28 (2002) 1011-1040.

[32] R.Kumar, M.Sharma, and G.R.Verma, Stability Indicating Analytical Method Development and Validation of Efavirenz Quantification by High Performance Liquid Chromatographic Technique, E-Journal of Chemistry, 8 (2011) 1498-1503.

[33] B.U.Rao and A.P.Nikalje, Stability- indicating HPLC method for the determination of efavirenz in bulk drug and in pharmaceutical dosage form, African Journal of Pharmacy and Pharmacology, 3 (2009) 643-650.

[34] T.Gadkari, P.Chandrachood, A.Ruikar, S.Tele, N.Deshpande, J.Salvekar, and S.Sonawane, Validated stability indicating LC-PDA-MS method to investigate pH rate profile and degradation kinetics of efavirenz and identification of hydrolysis product by LCMS., International Journal of Pharmacy and Pharmaceutical Sciences, 2 (2010) 169-176.

[35] A.Williams and K.T Douglas, Elimination-Addition Mechanisms of Acyl Transfer Reactions, Chemival Reviews, 75 (1975) 627-649.

[36] A.Vigroux, M.Bergon, C.Bergonzi, and P.Tisnes, A General Acid-Catalyzed Anion Breakdown Associated with an E1cB Reaction in the Hydrolysis of Aryl N-(Substituted Phenylsulfonyl)carbamates, J. Am. Chem. Soc., 116 (1994) 11787-11796.

[37] S.D.Young, S.F.Britcher, L.O.Tran, L.S.Payne, W.C.Lumma, T.A.Lyle, J.R.Huff, P.S.Anderson, D.B.Olsen, and S.S.Carroll, L-743, 726 (DMP-266): a novel, highly potent nonnucleoside inhibitor of the human immunodeficiency virus type 1 reverse nonnucleoside inhibitor of the human L-743, 726 (DMP-266): a novel, highly potent transcriptase., Antimicrob. Agents Chemother, 39 (1995) 2602-2605.

[38] A.S.Thompson, E.G.Corley, M.F.Huntington, and E.J.J.Grabowski, Use of an ephedrine alkoxide to mediate enantioselective addition of an acetylide to a prochiral ketone: asymmetric synthesis of the reverse transcriptase inhibitor L-743,726, Tetrahedron Letters, 36 (1995) 8937-8940.

[39] M.E.Pierce, R.L.Parsons, L.A.Radesca, Y.S.Lo, S.Silverman, J.R.Moore, Q.Islam, A.Choudhury, J.M.D.Fortunak, D.Nguyen, C.Luo, S.J.Morgan, W.P.Davis, P.N.Confalone, C.Y.Chen, R.D.Tillyer, L.Frey, L.Tan, F.Xu, D.Zhao, A.S.Thompson, E.G.Corley, E.J.J.Grabowski, R.Reamer, and P.J.Reider, Practical Asymmetric Synthesis of Efavirenz (DMP 266), an HIV-1 Reverse Transcriptase Inhibitor, J. Org. Chem., 63 (1998) 8536-8543.

[40] M.Patel, Jr.McHugh, B.C.Cordova, R.M.Klabe, L.T.Bacheler, S.Erickson-Viitanen, and J.D.Rodgers, Synthesis and evaluation of novel quinolinones as HIV-1 reverse transcriptase inhibitors, Bioorganic & Medicinal Chemistry Letters, 11 (2001) 1943-1945.

[41] I.Olivares, A.Mulky, P.I.Boross, J.Tozser, J.C.Kappes, C.Lopez-Galindez, and L.Menendez-Arias. HIV-1 Protease Dimer Interface Mutations that Compensate for Viral Reverse Transcriptase Instability in Infectious Virions, J Mol Biol, 372 (2007) 1-35.

[42] Pharmacare Limited. ASPEN EFAVIRENZ 600 mg (tablets). http://home.intekom.com/pharm/aspen-p/a-efavir.html . 8/10/2007. Accessed: 4/15/2013.

[43] A.Blas-Garcia, N.Apostolova, and J.V.Esplugues, Future Perspectives in NNRTI-Based Therapy: Bases for Understanding Their Toxicity, in: Y.W Tang (Ed.), In Tech, 2011, pp. 276-294.

[44] V.A.Braz, L.A.Holladay, and M.D.Barkley, Efavirenz Binding to HIV-1 Reverse Transcriptase Monomers and Dimers, Biochemistry, 49 (2010) 601-610.

[45] G.Tachedjian, K.L.Moore, S.P.Goff, and N.Sluis-Cremer, Efavirenz enhances the proteolytic processing of an HIV-1 pol polyprotein precursor and reverse transcriptase homodimer formation, FEBS Letters, 579 (2005) 379-384.

[46] S.Staszewski, J.Morales-Ramirez, K.T.Tashima, A.Rachlis, D.Skiest, J.Stanford, R.Stryker, P.Johnson, D.F.Labriola, D.Farina, D.J.Manion, and N.M.Ruiz, Efavirenz plus Zidovudine and Lamivudine, Efavirenz plus Indinavir, and Indinavir plus Zidovudine and Lamivudine in the Treatment of HIV-1 Infection in Adults, N Engl J Med, 341 (1999) 1865-1873.

[47] R.Manfredi, L.Calza, and F.Chiodo, Prospective, open-label comparative study of liver toxicity in an unselected population of HIV-infected patients treated for the first time with efavirenz or nevirapine., HIV Clinical Trials, 6 (2013) 302-311.

[48] C.F.Lacy, L.L.Armstrong, M.P.Goldman, and L.L.Lance, Drug Information Handbook, Lexi-comp,Inc, Ohio, pp. 508-509, 2005.

[49] National Institutes of Health. AIDSinfo Drug Database. http://aidsinfo.nih.gov/drugs/269/efavirenz/0/professional/#Section_5.7 . 2013. Accessed: 1/15/2013.

[50] B.Damle, R.Labadie, P.Crowner, and P.Glue, Pharmacokinetic interactions of efavirenz and voriconazole in healthy volunteers, Journal of Clinical Pharmacology, 65 (2008) 523-530.

[51] E.M.Yakiwchuk, M.M.Foisy, and C.A.Hughes, Complexity of Interactions Between Voriconazole and Antiretroviral Agents, The Annals of Pharmacotherapy, 42 (2008) 698-703.

[52] L.F.López-Cortés, R.Ruiz-Valderas, P.Viciana, A.A.González, J.Gómez-Mateos, E.León-Jimenez, M.Sarasanacenta, Y.López-Pua, and J.Pachòn, Pharmacokinetic Interactions Between Efavirenz and Rifampicin in HIV-Infected Patients with Tuberculosis, Clinical Pharmacokinetics, 41 (2002) 681-690.

[53] M.D.Shah and K.Balderson, A manic episode associated with efavirenz therapy for HIV infection, AIDS, 17 (2003) 1713-1714.

[54] A.Matteelli, M.Regazzi, P.Villani, G.De Iaco, M.Cusato, A.C.Carvalho, S.Caligaris, L.Tomasoni, M.Manfrin, S.Capone, and G.Carosi, Multiple-Dose Pharmacokinetics of Efavirenz with and without the Use of Rifampicin in HIV-Positive Patients, Current HIV Research, 5 (2007) 349-353.

[55] MayoClinic. Efavirenz, Emtricitabine, and Tenofovir (Oral Route). http://www.mayoclinic.com/health/drug-information/DR601979/DSECTION=before-using . 8/10/2012. Accessed: 4/15/2013.

[56] M.F.Chersich, M.F.Urban, F.W.D.Venter, T.Wessels, A.Krause, G.E.Gray, S.Luchters, and D.L.Viljoen, Efavirenz use during pregnancy and for women of child-bearing potential, AIDS Research and Therapy, 3 (2006) 1-6.

[57] B.S.Kappelhoff, F.van Leth, P.A.Robinson, T.R.Machregor, E.Baraldi, F.Montella, D.E.Uip, M.A.Thompson, D.B.Russel, J.M.A Lange, J.H.Beijnen, and A.D.R.Huitema, Are adverse events of nevirapine and efavirenz related to plasma concentrations?, Antivaral Therapy, 10 (2005) 489-498.

[58] F.Maggiolo, Efavirenz: a decade of clinical experience in the treatment of HIV, Journal of Antimicrobial Chemotherapy, 64 (2009) 910-928.

[59] B.G.Gazzard and on behalf of the BHIVA Treatment Guidelines Writing Group, British HIV Association guidelines for the treatment of HIV-1-infected adults with antiretroviral therapy 2008, HIV Medicine, 9 (2008) 563-608.

[60] S.A.Pereira, U.Caixas, T.Branco, I.Germano, F.Lampreia, A.L.Papoila, and E.C.Monteiro, Efavirenz concentrations in HIV-infected patients with and without viral hepatitis, British Journal of Clinical Pharmacology, 66 (2008) 551-555.

[61] J.Berenguer, J.M.Bellón, P.Miralles, E.Álvarez, I.Castillo, J.Cosín, J.C.López, C.M.Sánchez, B.Padilla, and S.Resino, Association between Exposure to Nevirapine and Reduced Liver Fibrosis Progression in Patients with HIV and Hepatitis C Virus Coinfection, Clinical Infectious Diseases, 46 (2008) 137-143.

[62] K.Tsuchiya, H.Gatanaga, N.Tachikawa, K.Teruya, Y.Kikuchi, M.Yoshino, T.Kuwahara, T.Shirasaka, S.Kimura, and S.Oka, Homozygous CYP2B6 *6 (Q172H and K262R) correlates with high plasma efavirenz concentrations in HIV-1 patients treated with standard efavirenz-containing regimens, Biochemical and Biophysical Research Communications, 319 (2004) 1322-1326.

[63] M.Bonnet, N.Bhatt, E.Baudin, C.Silva, C.Michon, A.M.Taburet, L.Ciaffi, A.Sobry, R.Bastos, E.Nunes, C.Rouzioux, I.Jani, and A.Calmy, Nevirapine versus efavirenz for patients co-infected

with HIV and tuberculosis: a randomised non-inferiority trial, The Lancet Infectious Diseases, 13 (2013) 303-312.

[64] P.Liu, G.Foster, R.Labadie, M.J Gutierez, and A.Sharma, Pharmacokinetic interaction between voriconazole and efavirenz at steady state in healthy subjects, Clinical Pharmacology & Therapeutics, 77 (2005) 40.

[65] P.Ji, B.Damle, J.Xie, S.E.Unger, D.M.Grasela, and S.Kaul, Pharmacokinetic Interaction Between Efavirenz and Carbamazepine After Multiple-Dose Administration in Healthy Subjects, The Journal of Clinical Pharmacology, 48 (2008) 948-956.

[66] J.O.Soyinka and C.O.Onyeji, Alteration of pharmacokinetics of proguanil in healthy volunteers following concurrent administration of efavirenz, European Journal of Pharmaceutical Sciences, 39 (2010) 213-218.

[67] A.Thompson, B.Silverman, L.Dzeng, and G.Treisman, Psychotropic Medications and HIV, Clinical Infectious Diseases, 42 (2006) 1305-1310.

[68] S.Mouly, K.S Lown, D.Kornhauser, J.L Joseph, W.D Fiske, I.H Benedek, and P.B Watkins, Hepatic but not intestinal CYP3A4 displays dose-dependent induction by efavirenz in humans, Clinical Pharmacology & Therapeutics, 72 (2002) 1-9.

[69] P.J.Hughes, E.Cretton-Scott, A.Teague, and T.M.Wensel, Protease Inhibitors for Patients With HIV-1 Infection, Pharmacy and Therapeutics, 36 (2002) 341-345.

[70] M.Weiner, D.Benator, C.A.Peloguin, W.Burman, A.Vernom, M.Engle, A.Khan, and Z.Zhao, Evaluation of the Drug Interaction between Rifabutin and Efavirenz in Patients with HIV Infection and Tuberculosis, Clinical Infectious Diseases, 41 (2005) 1343-1349.

[71] J.G.Gerber, S.L.Rosenkranz, C.J.Fichtenbaum, J.M.Vega, A.Yang, B.L.Alsto, S.W.Brobst, Y.Segal, and J.A.Aberg, Effect of efavirenz on the pharmacokinetics of simvastatin, atorvastatin, and pravastatin: results of AIDS Clinical Trials Group 5108 Study., Journal of Aquired Immune Deficiency Syndromes, 39 (2005) 307-312.

[72] S.Sriwiriyajan, W.Mahatthanatrakul, W.Ridtitid, and S.Jaruratanasirikul, Effect of efavirenz on the pharmacokinetics of ketoconazole in HIV-infected patients, European Journal of Clinical Pharmacology, 63 (2007) 479-483.

[73] M.Boffito, A.Rassati, H.E.Reynolds, P.G.Haggard, D.J.Back, and G.Di Perri, Undefined Duration of Opiate Withdrawal Induced by Efavirenz in Drug Users with HIV Infection and Undergoing Chronic Methadone Treatment, AIDS Research and Human Retroviruses, 18 (2002) 341-342.

[74] J.Fellay, C.Marzolini, L.Decosterd, K.P.Golay, P.Baumann, T.Buclin, A.Telenti, and C.Eap, Variations of CYP3A activity induced by antiretroviral treatment in HIV-1 infected patients, Eur J Clin Pharmacol, 60 (2005) 865-873.

[75] J.Blanch, B.Corbella, F.Garcia, E.Parellada, and J-M.Gatell, Manic Syndrome Associated with Efavirenz Overdose, Clinical Infectious Diseases, 33 (2001) 270-271.

[76] P.Lochet, H.Peyriere, A.Lotthe, J.M.Mauboussin, B.Delmas, and J.Reynes, Long-term assessment of neuropsychiatric adverse reactions associated with efavirenz, HIV Medicine, 4 (2003) 62-66.

[77] J.J.Parienti, V.Massari, D.Rey, P.Poubeau, and R.Verdon, Efavirenz to Nevirapine Switch in HIV-1–Infected Patients with Dyslipidemia: A Randomized, Controlled Study, Clinical Infectious Diseases, 45 (2007) 263-266.

[78] E.Cassol, T.Page, A.Mosam, G.Friedland, C.Jack, U.Lalloo, J.Kopetka, B.Patterson, T.Esterhuizen, and H.M.Coovadia, Therapeutic Response of HIV-1 Subtype C in African Patients Coinfected with either Mycobacterium tuberculosis or Human Herpesvirus-8, Journal of Infectious Diseases, 191 (2005) 324-332.

[79] R.Manfredi, L.Calza, and F.Chiodo, Efavirenz versus nevirapine in current clinical practice: a prospective, open-label observational study, Journal of Aquired Immune Deficiency Syndromes, 35 (2004) 492-502.

[80] The HIV-CAUSAL Collaboration, The effect of efavirenz versus nevirapine-containing regimens on immunologic, virologic and clinical outcomes in a prospective observational study, AIDS, 26 (2012) 1-16.

[81] R.M.Gulick, H.J.Ribaudo, and C.M.Shikuma, Three- vs four-drug antiretroviral regimens for the initial treatment of hiv-1 infection: A randomized controlled trial, JAMA, 296 (2006) 769-781.

[82] M.Perz-Elias, A.Moreno, D.Lopez, A.Antela, J.L.Casado, F.Dronda, C.Gutierrez, E.Navas, V.Abraira, and M.A.Rodriguez, Higher Virological Effectiveness of NNRTI-Based Antiretroviral Regimens Containing Nevirapine or Efavirenz Compared to a Triple NRTI Regimen As Initial Therapy in HIV-1-Infected Adults, HIV Clinical Trials, 6 (2005) 312-319.

[83] J.Lindberg, S.Sigurdsson, S.Lowgren, H.O.Anderson, C.Sahlberg, R.Noreen, K.Fridborg, H.Zhang, and T.Unge, Structural basis for the inhibitory efficacy of efavirenz (DMP-266), MSC194 and PNU142721 towards the HIV-1 RT K103N mutant, European Journal of Biochemistry, 269 (2002) 1670-1677.

[84] H.J.Ribaudo, D.W.Haas, C.Tierney, R.B.Kim, G.R.Wilkinson, R.M.Gulick, D.B.Clifford, C.Marzolini, C.Fletcher, K.T.Tashima, D.R.Kuritzkes, and E.P.Acosta, Pharmacogenetics of Plasma Efavirenz Exposure after Treatment Discontinuation: An Adult AIDS Clinical Trials Group Study, Clinical Infectious Diseases, 42 (2006) 401-407.

[85] P.R.Harrigan, R.S.Hogg, W.W.Y.Dong, B.Yip, B.Wynhoven, J.Woodward, C.J.Brumme, Z.L.Brumme, T.Mo, C.S.Alexander, and J.S.G.Montaner, Predictors of HIV Drug-Resistance Mutations in a Large Antiretroviral-Naive Cohort Initiating Triple Antiretroviral Therapy, Journal of Infectious Diseases, 191 (2005) 339-347.

[86] C.Csajka, C.Marzolini, K.Fattinger, L.A Decosterd, J.Fellay, A.Telenti, J.Biollaz, and T.Buclin, Population pharmacokinetics and effects of efavirenz in patients with human immunodeficiency virus infection., Clinical Pharmacology and Therapeutics, 73 (2003) 20-30.

[87] L.M.Almond, P.G.Hoggard, D.Edirisinghe, S.H.Khoo, and D.J.Back, Intracellular and plasma pharmacokinetics of efavirenz in HIV-infected individuals, Journal of Antimicrobial Chemotherapy, 56 (2005) 738-744.

[88] Bristol-Myers Squibb Pharmaceuticals Ltd. Efavirenz: Summary of Product Characteristics. http://www.medicines.org.uk/emc/history/11284/SPC/Sustiva+600+mg+Film-Coated+Tablets , 2009. Accessed: 4/22/2013.

[89] N.Dupin, M.Buffet, A.G.Marcelin, C.Lamotte, I.Gorin, Z.Ait-Arkoub, J.M.Treluyer, P.Bui, V.Calvez, and G.Peytavin, HIV and antiretroviral drug distribution in plasma and fat tissue of HIV-infected patients with lipodystrophy, AIDS, 16 (2002) 2419-2424.

[90] B.M.Best, P.P.Koopmans, S.L.Letendre, E.V.Capparelli, S.S.Rossi, D.B.Clifford, A.C.Collier, B.B.Gelman, G.Mbeo, J.A.McCutchan, D.M.Simpson, R.Haubrich, R.Ellis, and I.Grant, Efavirenz concentrations in CSF exceed IC50 for wild-type HIV, Journal of Antimicrobial Chemotherapy, 66 (2011) 354-357.

[91] N.N.Bumpus, U.M.Kent, and P.F.Hollenberg, Metabolism of Efavirenz and 8-Hydroxyefavirenz by P450 2B6 Leads to Inactivation by Two Distinct Mechanisms, Journal of Pharmacology and Experimental Therapeutics, 318 (2006) 345-351.

[92] J.A.Markwalder, D.D.Christ, A.Mutlib, B.C.Cordova, R.M.Klabe, and S.P.Seitz, Synthesis and biological activities of potential metabolites of the non-nucleoside reverse transcriptase inhibitor Efavirenz, Bioorganic & Medicinal Chemistry Letters, 11 (2001) 619-622.

[93] A.E.Mutlib, H.Chen, G.A.Nemeth, J.A.Markwalder, S.P.Seitz, L.S.Gan, and D.D.Christ, Identification and Characterization of Efavirenz Metabolites by Liquid Chromatography/Mass Spectrometry and High Field NMR: Species Differences in the Metabolism of Efavirenz, Drug Metabolism and Disposition, 27 (1999) 1319-1333.

[94] S.Rodriguez-Novoa, P.Barreiro, A.Rendón, I.Jiménez-Nacher, J.González-Lahoz, and V.Soriano, Influence of 516G>T Polymorphisms at the Gene Encoding the CYP450-2B6 Isoenzyme on Efavirenz Plasma Concentrations in HIV-Infected Subjects, Clinical Infectious Diseases, 40 (2005) 1358-1361.

[95] D.Burger, I.Van Der Heiden, C.La Porte, M.Van Der Ende, P.Groeneveld, C.Richter, P.Koopmans, F.Kroon, H.Sprenger, J.Lindemans, P.Schenk, and R.Van Schaik, Interpatient variability in the pharmacokinetics of the HIV non-nucleoside reverse transcriptase inhibitor efavirenz: the effect of gender, race, and CYP2B6 polymorphism, British Journal of Clinical Pharmacology, 61 (2006) 148-154.

[96] J.M.Molina, G.Peytavin, S.Perusat, C.Lascoux-Combes, D.Sereni, W.Rozenbaum, and G.Chene, Pharmacokinetics of emtricitabine, didanosine and efavirenz administered once-daily for the treatment of HIV-infected adults (pharmacokinetic substudy of the ANRS 091 trial)*, HIV Medicine, 5 (2004) 99-104.

[97] J.M.Molina, V.Journot, A.Furco, P.Palmer, N.De Castro, F.Raffi, P.Morlat, T.May, C.Rancinan, and G.Chene, Five-year follow up of once-daily therapy with emtricitabine, didanosine and efavirenz (Montana ANRS 091 trial)., Antiviral Therapy, 12 (2007) 417-422.

[98] A.Madhusudhan, G.B.Reddy, M.Venkatesham, and G.Veerabhadram, Design and Evaluation of Efavirenz loaded Solid Lipid Nanoparticles to Improve the Oral Bioavailability, International Journal of Pharmacy and Pharmaceutical Science Research, 2 (2012) 84-89.

[99] T.Puzantian, Central Nervous System Adverse Effects with Efavirenz: Case Report and Review, Pharmacotherapy: The Journal of Human Pharmacology and Drug Therapy, 22 (2002) 930-933.

[100] M.Beija, R.Salvayre, N.Lauth-de Viguerie, and J.D.Marty, Colloidal systems for drug delivery: from design to therapy, Trends in Biotechnology, 30 (2012) 485-496.

[101] K.Kostarelos, Rational design and engineering of delivery systems for therapeutics: biomedical exercises in colloid and surface science, Advances in Colloid and Interface Science, 106 (2003) 147-168.

[102] D.J.A.Crommelin and G.Storm, Liposomes: From the Bench to the Bed, Journal of Liposome Research, 13 (2003) 33-36.

[103] O.Ishida, K.Maruyama, H.Tanahashi, M.Iwatsuru, K.Sasaki, M.Eriguchi, and H.Yanagie, Liposomes Bearing Polyethyleneglycol-Coupled Transferrin with Intracellular Targeting Property to the Solid Tumors In Vivo, Pharm Res, 18 (2001) 1042-1048.

[104] S.T.E.P.Perret, M.I.C.H.GOLDING, and W.P.Williams, A Simple Method for the Preparation of Liposomes for Pharmaceutical Applications: Characterization of the Liposomes, Journal of Pharmacy and Pharmacology, 43 (1991) 154-161.

[105] R.R.Sawant and V.P.Torchilin, Liposomes as 'smart' pharmaceutical nanocarriers, Soft Matter, 6 (2010) 4026-4044.

[106] V.P.Torchilin, Recent advances with liposomes as pharmaceutical carriers, Nature Reviews Drug Discovery, 4 (2005) 145-160.

[107] N.Anton and T.F.Vandamme, Nano-emulsions and Micro-emulsions: Clarifications of the Critical Differences, Pharm Res, 28 (2011) 978-985.

[108] K.Burapapadh, M.Kumpugdee-Vollrath, D.Chantasart, and P.Sriamornsak, Fabrication of pectin-based nanoemulsions loaded with itraconazole for pharmaceutical application, Carbohydrate Polymers, 82 (2010) 384-393.

[109] P.Calvo, J.L.Vila-Jato, and M.J.Alonso, Comparative in vitro evaluation of several colloidal systems, nanoparticles, nanocapsules, and nanoemulsions, as ocular drug carriers, J. Pharm. Sci., 85 (1996) 530-536.

[110] N.Sadurní, C.Solans, N.Azemar, and M.J.García-Celma, Studies on the formation of O/W nano-emulsions, by low-energy emulsification methods, suitable for pharmaceutical applications, European Journal of Pharmaceutical Sciences, 26 (2005) 438-445.

[111] C.Solans, P.Izquierdo, J.Nolla, N.Azemar, and M.J.Garcia-Celma, Nano-emulsions, Current Opinion in Colloid & Interface Science, 10 (2005) 102-110.

[112] P.Calvo, A.Sánchez, J.Martínez, M.I.López, M.Calonge, J.C.Pastor, and M.J.Alonso, Polyester Nanocapsules as New Topical Ocular Delivery Systems for Cyclosporin A, Pharm Res, 13 (1996) 311-315.

[113] P.Couvreur, B.Kante, M.Roland, P.Guiot, P.BAuduin, and P.Speiser, Polycyanoacrylate nanocapsules as potential lysosomotropic carriers: preparation, morphological and sorptive properties, Journal of Pharmacy and Pharmacology, 31 (1979) 331-332.

[114] H.J.Krause and P.Rohdewald, Preparation of Gelatin Nanocapsules and Their Pharmaceutical Characterization, Pharm Res, 2 (1985) 239-243.

[115] S.Peltier, J.M.Oger, F.Lagarce, W.Couet, and J.P.Benoît, Enhanced Oral Paclitaxel Bioavailability After Administration of Paclitaxel-Loaded Lipid Nanocapsules, Pharm Res, 23 (2006) 1243-1250.

[116] H.Pinto-Alphandary, M.Aboubakar, D.Jaillard, P.Couvreur, and C.Vauthier, Visualization of Insulin-Loaded Nanocapsules: In Vitro and in Vivo Studies After Oral Administration to Rats, Pharm Res, 20 (2003) 1071-1084.

[117] C.Prego, M.Fabre, D.Torres, and M.J.Alonso, Efficacy and Mechanism of Action of Chitosan Nanocapsules for Oral Peptide Delivery, Pharm Res, 23 (2006) 549-556.

[118] J.M.Rollot, P.Couvreur, L.Roblot-Treupel, and F.Puisieux, Physicochemical and morphological characterization of polyisobutyl cyanoacrylate nanocapsules, J. Pharm. Sci., 75 (1986) 361-364.

[119] V.Bhardwaj, S.Hariharan, I.Bala, A.Lamprecht, N.Kumar, R.Panchagnula, and K.M.N.V.Ravi, Pharmaceutical Aspects of Polymeric Nanoparticles for Oral Drug Delivery, Journal of Biomedical Nanotechnology, 1 (2005) 235-258.

[120] R.C.Pinto, R.J.Neufeld, J.António, and F.Veiga, Nanoencapsulation I. Methods for preparation of drug-loaded polymeric nanoparticles, Nanomedicine: Nanotechnology, Biology and Medicine, 2 (2006) 8-21.

[121] K.S.Soppimath, T.M.Aminabhavi, A.R.Kulkarni, and W.E.Rudzinski, Biodegradable polymeric nanoparticles as drug delivery devices, Journal of Controlled Release, 70 (2001) 1-20.

[122] W.K.Yin and S.S.Feng, Effects of particle size and surface coating on cellular uptake of polymeric nanoparticles for oral delivery of anticancer drugs, Biomaterials, 26 (2005) 2713-2722.

[123] G.Zhang, A.Niu, S.Peng, M.Jiang, Y.Tu, M.Li, and C.Wu, Formation of Novel Polymeric Nanoparticles, Acc. Chem. Res., 34 (2001) 249-256.

[124] A.Bargoni, R.Cavalli, O.Caputo, A.Fundarò, M.R.Gasco, and G.P.Zara, Solid Lipid Nanoparticles in Lymph and Plasma After Duodenal Administration to Rats, Pharm Res, 15 (1998) 745-750.

[125] A.Dingler, R.P.Blum, H.Niehus, R.H.Müller, and S.Gohla, Solid lipid nanoparticles (SLN^{TM}/Lipopearls^{TM}) a pharmaceutical and cosmetic carrier for the application of vitamin E in dermal products, Journal of Microencapsulation, 16 (1999) 751-767.

[126] W.Mehnert and K.Mäder, Solid lipid nanoparticles: Production, characterization and applications, Advanced Drug Delivery Reviews, 47 (2001) 165-196.

[127] R.H.Müller, K.Mader, and S.Gohla, Solid lipid nanoparticles (SLN) for controlled drug delivery- a review of the state of the art, European Journal of Pharmaceutics and Biopharmaceutics, 50 (2000) 161-177.

[128] R.H.Müller, D.Rühl, S.Runge, K.Schulze-Forster, and W.Mehnert, Cytotoxicity of Solid Lipid Nanoparticles as a Function of the Lipid Matrix and the Surfactant, Pharm Res, 14 (1997) 458-462.

[129] K.A.Shah, A.A.Date, M.D.Joshi, and V.B.Patravale, Solid lipid nanoparticles (SLN) of tretinoin: Potential in topical delivery, International Journal of Pharmaceutics, 345 (2007) 163-171.

[130] S.Yang, J.Zhu, Y.Lu, B.Liang, and C.Yang, Body Distribution of Camptothecin Solid Lipid Nanoparticles After Oral Administration, Pharm Res, 16 (1999) 751-757.

[131] S.Das, W.K.Ng, and R.B.Tan, Are nanostructured lipid carriers (NLCs) better than solid lipid nanoparticles (SLNs): Development, characterizations and comparative evaluations of clotrimazole-loaded SLNs and NLCs?, European Journal of Pharmaceutical Sciences, 47 (2012) 139-151.

[132] C.H.Liu and C.T.Wu, Optimization of nanostructured lipid carriers for lutein delivery, Colloids and Surfaces A: Physicochemical and Engineering Aspects, 353 (2010) 149-156.

[133] D.Liu, Z.Liu, L.Wang, C.Zhang, and N.Zhang, Nanostructured lipid carriers as novel carrier for parenteral delivery of docetaxel, Colloids and Surfaces B: Biointerfaces, 85 (2011) 262-269.

[134] M.J.Tsai, P.C.Wu, Y.B.Huang, J.S.Chang, C.L.Lin, Y.H.Tsai, and J.Y.Fang, Baicalein loaded in tocol nanostructured lipid carriers (tocol NLCs) for enhanced stability and brain targeting, International Journal of Pharmaceutics, 423 (2012) 461-470.

[135] M.Zheng, M.Falkeborg, Y.Zheng, T.Yang, and X.Xu, Formulation and characterization of nanostructured lipid carriers containing a mixed lipids core, Colloids and Surfaces A: Physicochemical and Engineering Aspects, 430 (2013) 76-84.

[136] C.Vauthier and P.Couvreur, Nanomedicines: A New Approach for the Treatment of Serious Diseases, Journal of Biomedical Nanotechnology, 3 (2007) 223-234.

[137] N.Bertrand and J.C.Leroux, The journey of a drug-carrier in the body: An anatomo-physiological perspective, Journal of Controlled Release, 161 (2012) 152-163.

[138] A.Chrastina, K.A.Massey, and J.E.Schnitzer, Overcoming in vivo barriers to targeted nanodelivery, WIREs Nanomed Nanobiotechnol, 3 (2011) 421-437.

[139] H.Cabral and K.Kataoka, Multifunctional nanoassemblies of block copolymers for future cancer therapy, Science and Technology of Advanced Materials, 11 (2010) 1-9.

[140] I.A.Khalil, K.Kogure, H.Akita, and H.Harashima, Uptake Pathways and Subsequent Intracellular Trafficking in Nonviral Gene Delivery, Pharmacological Reviews, 58 (2006) 32-45.

[141] J.Wang, J.D.Byrne, M.E.Napier, and J.M.DeSimone, More Effective Nanomedicines through Particle Design, Small, 7 (2011) 1919-1931.

[142] Y.Perrie, P.M.Fredrick, and G.Gregoriadis, Liposome-mediated DNA vaccination: the effect of vesicle composition, Vaccine, 19 (2000) 3301-3310.

[143] M.G.Carstens, M.G.M.Camps, M.Henriksen-Lacey, K.Franken, T.H.M.Ottenhoff, Y.Perrie, J.A.Bouwstra, F.Ossendorp, and W.Jiskoot, Effect of vesicle size on tissue localization and immunogenicity of liposomal DNA vaccines, Vaccine, 29 (2011) 4761-4770.

[144] J.M.Harris and R.B.Chess, Effect of pegylation on pharmaceuticals., Nature Reviews Drug Discovery, 2 (2003) 214-221.

[145] J.C.Olivier, Drug Transport to Brain with Targeted Nanoparticles, Neurotherapeutics, 2 (2013) 108-119.

[146] H.Rainer, K.M.Müller, and S.Gohla, Solid lipid nanoparticles (SLN) for controlled drug delivery - a review of the state of the art, European Journal of Pharmaceutics and Biopharmaceutics, 50 (2000) 161-177.

[147] A.Samad, Y.Sultana, and M.Aqil, Liposomal Drug Delivery Systems: An Update Review, Current Drug Delivery, 4 (2007) 297-305.

[148] J.A.Custódio, L.M.Almeida, and V.Madeira, The anticancer drug tamoxifen induces changes in the physical properties of model and native membranes, Biochimica et Biophysica Acta (BBA)-Biomembranes, 1150 (1993) 123-129.

[149] H.Wiseman, M.Cannon, H.R.V.Arnstein, and B.Halliwel, Mechanism of inhibition of lipid peroxidation by tamoxifen and 4-hydroxytamoxifen introduced into liposomes: Similarity to cholesterol and ergosterol, FEBS Letters, 274 (1990) 107-110.

[150] A.R.Mohammed, V.W.Bramwell, A.G.A.Coombes, and Y.Perrie, Lyophilisation and sterilisation of liposomal vaccines to produce stable and sterile products, Methods, 40 (2006) 30-38.

[151] G.Gregoriadis, B.McCormack, M.Obrenovic, R.Saffie, B.Zadi, and Y.Perrie, Vaccine entrapment in liposomes, Methods, 19 (1999) 156-162.

[152] K.Riehemann, S.W.Schneider, T.A.Luger, B.Godin, M.Ferrari, and H.Fuchs, Nanomedicine—Challenge and Perspectives, Angew. Chem. Int. Ed, 48 (2009) 872-897.

[153] B.Godin, R.E.Serda, J.Sakamoto, P.Decuzzi, and M.Ferrari, Nanoparticles for Cancer Detection and Therapy, Nanotechnology, Wiley-VCH Verlag GmbH & Co. KGaA, 2010.

[154] V.K.Venishetty, R.Chede, R.Komuravelli, L.Adepu, R.Sistla, and P.V.Diwan, Design and evaluation of polymer coated carvedilol loaded solid lipid nanoparticles to improve the oral bioavailability: A novel strategy to avoid intraduodenal administration, Colloids and Surfaces B: Biointerfaces, 95 (2012) 1-9.

[155] V.Teeranachaideekul, R.H.Müller, and V.B.Junyaprasert, Encapsulation of ascorbyl palmitate in nanostructured lipid carriers (NLC)–Effects of formulation parameters on physicochemical stability, International Journal of Pharmaceutics, 340 (2007) 198-206.

[156] M.D.Joshi and R.H.Müller, Lipid nanoparticles for parenteral delivery of actives, European Journal of Pharmaceutics and Biopharmaceutics, 71 (2009) 161-172.

[157] J.K.Kim, J.S.Park, and C.K.Kim, Development of a binary lipid nanoparticles formulation of itraconazole for parenteral administration and controlled release, International Journal of Pharmaceutics, 383 (2010) 209-215.

[158] R.H.Müller, M.Radtke, and S.A.Wissing, Solid lipid nanoparticles (SLN) and nanostructured lipid carriers (NLC) in cosmetic and dermatological preparations, Advanced Drug Delivery Reviews, 54, Supplement (2002) S131-S155.

[159] J.Pardeike, A.Hommoss, and R.H.Müller, Lipid nanoparticles (SLN, NLC) in cosmetic and pharmaceutical dermal products, International Journal of Pharmaceutics, 366 (2009) 170-184.

[160] A.Garud, D.Singh, and N.Garud, Solid Lipid Nanoparticles (SLN): Method, Characterization and Applications, International Current PharmaceuticalJournal, 1 (2012) 384-393.

[161] EMB Chemicals Inc. Material Safety Data-Chloroform. http://www.unl.edu/cahoonlab/Chloroform%20MSDS.pdf . 2013. Accessed: 12/20/2013.

[162] F.Q.Hu, S.P.Jiang, Y.Z.Du, H.Yuan, Y.Q.Ye, and S.Zeng, Preparation and characteristics of monostearin nanostructured lipid carriers, International Journal of Pharmaceutics, 314 (2006) 83-89.

[163] S.A.Wissing, O.Kayser, and R.H.Müller, Solid lipid nanoparticles for parenteral drug delivery, Advanced Drug Delivery Reviews, 56 (2004) 1257-1272.

[164] L.I Haibin and D.Xuechen, Nanoparticles for drug delivery to central nervous system, Nanoscience, 11 (2006) 207-209.

[165] A.zur Mühlen, C.Schwarz, and W.Mehnert, Solid lipid nanoparticles (SLN) for controlled drug delivery – Drug release and release mechanism, European Journal of Pharmaceutics and Biopharmaceutics, 45 (1998) 149-155.

[166] E.B.Souto and R.H.Müller, Solid Lipid Nanoparticles and Nanostructured Lipid Carriers-Lipid Nanoparticles for Medicals and Pharmaceuticals, Nanoscience and Nanotechnology, 23 (2011) 313-328.

[167] M.Schäfer-Korting, M.Wolfgang, and H-C.Korting, Lipid nanoparticles for improved topical application of drugs for skin diseases, Advanced Drug Delivery Reviews, 59 (2007) 427-443.

[168] E.B.Souto, S.A.Wissing, C.M.Barbosa, and R.H.Müller R.H, Development of a controlled release formulation based on SLN and NLC for topical clotrimazole delivery, Internation Journal of Pharmaceutics, 278 (2004) 71-77.

[169] J.Y.Fang, C.L.Fang, C.H.Liu, and Y.H.Su, Lipid nanoparticles as vehicles for topical psoralen delivery: Solid lipid nanoparticles (SLN) versus nanostructured lipid carriers (NLC), European Journal of Pharmaceutics and Biopharmaceutics, 70 (2008) 633-640.

[170] R.H.Müller, M.Radtke, and S.A.Wissing, Nanostructured lipid matrices for improved microencapsulation of drugs, Internation Journal of Pharmaceutics, 242 (2002) 121-128.

[171] J.C.Shah, Y.S.Sadhale, and D.M.Chilukuri, Cubic phase gels as drug delivery systems, Advanced Drug Delivery Reviews, 47 (2001) 229-250.

[172] C.Himawan, V.M.Starov, and A.G.F.Stapley, Thermodynamic and kinetic aspects of fat crystallization, Advances in Colloid and Interface Science, 122 (2006) 3-33.

[173] R.H.Müller, R.D.Petersen, A.Hommoss, and J.Pardeike, Nanostructured lipid carriers (NLC) in cosmetic dermal products, Advanced Drug Delivery Reviews, 59 (2007) 522-530.

[174] E.B.Souto, S.A.Wissing, C.M.Barbosa, and R.H.Müller, Comparative study between the viscoelastic behaviors of different lipid nanoparticle formulations., Journal of Cosmetic Science, 55 (2004) 463-471.

[175] V.Jenning, M.Schäfer-Korting, and S.Gohla, Vitamin A-loaded solid lipid nanoparticles for topical use: drug release properties, Journal of Controlled Release, 66 (2000) 115-126.

[176] M.Uner, Preparation, characterization and physico-chemical properties of solid lipid nanoparticles (SLN) and nanostructured lipid carriers (NLC): their benefits as colloidal drug carrier systems., Pharmazie, 61 (2006) 375-386.

[177] M.Muchow, M.Phillipe, and R.H.Müller, Lipid Nanoparticles with a Solid Matrix (SLN®, NLC®, LDC®) for Oral Drug Delivery, Drug Development and Industrial Pharmacy, 34 (2008) 1394-1405.

[178] E.B.Souto and R.H.Müller, Lipid Nanoparticles (SLN and NLC) for drug delivery, in: A.J.Domb, M.N.V.Tabata, R.Kumar, and S.Farber (Eds.), American Scientific Publishers, 2007, pp. 103-122.

[179] A.C.Silva, E.González-Mira, M.L.García, M.A.Egea, J.Fonseca, R.Silva, D.Santos, E.B.Souto, and D.Ferreira, Preparation, characterization and biocompatibility studies on risperidone-loaded solid lipid nanoparticles (SLN): High pressure homogenization versus ultrasound, Colloids and Surfaces B: Biointerfaces, 86 (2011) 158-165.

[180] P.Prombutara, Y.Kulwatthanasal, N.Supaka, I.Sramala, and S.Chareonpornwattana, Production of nisin-loaded solid lipid nanoparticles for sustained antimicrobial activity, Food Control, 24 (2012) 184-190.

[181] S.Wang, T.Chen, R.Chen, Y.Hu, M.Chen, and Y.Wang, Emodin loaded solid lipid nanoparticles: Preparation, characterization and antitumor activity studies, International Journal of Pharmaceutics, 430 (2012) 238-246.

[182] R.Shegokar, K.K.Singh, and R.H.Müller, Production & stability of stavudine solid lipid nanoparticles–From lab to industrial scale, International Journal of Pharmaceutics, 416 (2011) 461-470.

[183] M.M.Mojahedian, S.Daneshamouz, S.M.Samani, and A.Zargaran, A novel method to produce solid lipid nanoparticles using n-butanol as an additional co-surfactant according to the o/w microemulsion quenching technique, Chemistry and Physics of Lipids, 174 (2013) 32-38.

[184] P.Fadda, M.Monduzzi, F.Caboi, S.Piras, and P.Lazzari, Solid lipid nanoparticle preparation by a warm microemulsion based process: Influence of microemulsion microstructure, International Journal of Pharmaceutics, 446 (2013) 166-175.

[185] M.Ghadiri, S.Fatemi, A.Vatanara, D.Doroud, A.R.Najafabadi, M.Darabi, and A.A.Rahimi, Loading hydrophilic drug in solid lipid media as nanoparticles: Statistical modeling of entrapment efficiency and particle size, International Journal of Pharmaceutics, 424 (2012) 128-137.

[186] S.Kumar and J.K.Randhawa, Preparation and characterization of Paliperidone loaded solid lipid nanoparticles, Colloids and Surfaces B: Biointerfaces, 102 (2013) 562-568.

[187] P.Severino, M.H.Santana, and E.B.Souto, Optimizing SLN and NLC by 22 full factorial design: Effect of homogenization technique, Materials Science and Engineering: C, 32 (2012) 1375-1379.

[188] J.Jaiswal, G.S.Kumar, and J.Kreuter, Preparation of biodegradable cyclosporine nanoparticles by high-pressure emulsification-solvent evaporation process, Journal of Controlled Release, 96 (2004) 169-178.

[189] D.Quintanar-Guerrero, D.Tamayo-Esquivel, A.Ganem-Quintanar, E.Allémann, and E.Doelker, Adaptation and optimization of the emulsification-diffusion technique to prepare lipidic nanospheres, European Journal of Pharmaceutical Sciences, 26 (2005) 211-218.

[190] F.Q.Hu, H.Yuan, H.H.Zhang, and M.Fang, Preparation of solid lipid nanoparticles with clobetasol propionate by a novel solvent diffusion method in aqueous system and physicochemical characterization, International Journal of Pharmaceutics, 239 (2002) 121-128.

[191] L.Montenegro, M.G.Sarpietro, S.Ottimo, G.Puglisi, and F.Castelli, Differential scanning calorimetry studies on sunscreen loaded solid lipid nanoparticles prepared by the phase inversion temperature method, International Journal of Pharmaceutics, 415 (2011) 301-306.

[192] L.Montenegro, C.Sinico, I.Castangia, C.Carbone, and G.Puglisi, Idebenone-loaded solid lipid nanoparticles for drug delivery to the skin: In vitro evaluation, International Journal of Pharmaceutics, 434 (2012) 169-174.

[193] M.Jumaa and B.W.Müller, The effect of oil components and homogenization conditions on the physicochemical properties and stability of parenteral fat emulsions, International Journal of Pharmaceutics, 163 (1998) 81-89.

[194] G.Tabanelli, P.Burns, F.Patrignani, F.Gardini, R.Lanciotti, J.Reinheimer, and G.Vinderola, Effect of a non-lethal High Pressure Homogenization treatment on the in-ávivo response of probiotic lactobacilli, Food Microbiology, 32 (2012) 302-307.

[195] R.H.Müller, W.Mehnert, J.S.Lucks, C.Schwarz, A.z.Mühlen, H.Weyhers, C.Freitas, and D.Rühl, Solid Lipid Nanoparticles (SLN) - An Alternative Colloidal Carrier System for Controlled Drug Delivery, European Journal of Pharmaceutics and Biopharmaceutics, 41 (1995) 62-69.

[196] C.M.Keck and R.H.Müller, Drug nanocrystals of poorly soluble drugs produced by high pressure homogenisation, European Journal of Pharmaceutics and Biopharmaceutics, 62 (2006) 3-16.

[197] F.Stern, Bernoulli Equation, Mechanics of Fluids and Transport Processes, 2008, pp. 1-24.

[198] A.Lippacher, R.H.Müller, and K.Mäder, Investigation on the viscoelastic properties of lipid based colloidal drug carriers, International Journal of Pharmaceutics, 196 (2000) 227-230.

[199] A.Lippacher, R.H.Müller, and K.Mäder, Semisolid SLN ™ dispersions for topical application: influence of formulation and production parameters on viscoelastic properties, European Journal of Pharmaceutics and Biopharmaceutics, 53 (2002) 155-160.

[200] A.Lippacher, R.H.Müller, and K.Mäder, Preparation of semisolid drug carriers for topical application based on solid lipid nanoparticles, International Journal of Pharmaceutics, 214 (2001) 9-12.

[201] A.Lippacher, R.H.Müller, and K.Mäder, Liquid and semisolid SLN dispersions for topical application: rheological characterization, European Journal of Pharmaceutics and Biopharmaceutics, 58 (2004) 561-567.

[202] B.Sjöström, A.Kaplun, Y.Talmon, and B.Cabane, Structures of nanoparticles prepared from oil-in-water emulsions., Pharmaceutical Research, 12 (2013) 39-48.

[203] L.Serpe, M.G.Catalano, R.Cavalli, E.Ugazio, O.Bosco, R.Canaparo, E.Muntoni, R.Frairia, M.R.Gasco, M.Eandi, and G.P.Zara, Cytotoxicity of anticancer drugs incorporated in solid lipid nanoparticles on HT-29 colorectal cancer cell line, European Journal of Pharmaceutics and Biopharmaceutics, 58 (2004) 673-680.

[204] C.Schwarz, W.Mehnert, J.S.Lucks, and R. H. R.H.Müller, Solid lipid nanoparticles (SLN) for controlled drug delivery. I. Production, characterization and sterilization, Journal of Controlled Release, 30 (1994) 83-96.

[205] S.Liedtke, S.Wissing, R.H.Müller, and K.Mäder, Influence of high pressure homogenisation equipment on nanodispersions characteristics, International Journal of Pharmaceutics, 196 (2000) 183-185.

[206] E.Marengo, R.Cavalli, O.Caputo, L.Rodriguez, and M.R.Gasco, Scale-up of the preparation process of solid lipid nanospheres. Part I, International Journal of Pharmaceutics, 205 (2000) 3-13.

[207] C.Schwarz and W.Mehnert, Freeze-drying of drug-free and drug-loaded solid lipid nanoparticles (SLN), International Journal of Pharmaceutics, 157 (1997) 171-179.

[208] E.Zimmermann, R.H.Müller, and K.Mäder, Influence of different parameters on reconstitution of lyophilized SLN, International Journal of Pharmaceutics, 196 (2000) 211-213.

[209] B.Heurtault, P.Saulnier, B.Pech, M.C.Venier-Julienne, J.E.Proust, R.Phan-Tan-Luu, and J.P.Benoît, The influence of lipid nanocapsule composition on their size distribution, European Journal of Pharmaceutical Sciences, 18 (2003) 55-61.

[210] B.Heurtault, P.Saulnier, B.Pech, J.E.Proust, and J.P.Benoit, Physico-chemical stability of colloidal lipid particles, Biomaterials, 24 (2003) 4283-4300.

[211] R.Cavalli, O.Caputo, M.E.Carlotti, M.Trotta, C.Scarnecchia, and M.R.Gasco, Sterilization and freeze-drying of drug-free and drug-loaded solid lipid nanoparticles, International Journal of Pharmaceutics, 148 (1997) 47-54.

[212] V.Jenning, A.F.Thünemann, and S.H.Gohla, Characterisation of a novel solid lipid nanoparticle carrier system based on binary mixtures of liquid and solid lipids, International Journal of Pharmaceutics, 199 (2000) 167-177.

[213] C.Freitas and R.H.Müller, Spray-drying of solid lipid nanoparticles (SLN^{TM}), European Journal of Pharmaceutics and Biopharmaceutics, 46 (1998) 145-151.

[214] E.Zimmermann and R.H.Müller, Electrolyte- and pH-stabilities of aqueous solid lipid nanoparticle (SLN ^{TM}) dispersions in artificial gastrointestinal media, European Journal of Pharmaceutics and Biopharmaceutics, 52 (2001) 203-210.

[215] H.Bunjes, K.Westesen, and M.H.J.Koch, Crystallization tendency and polymorphic transitions in triglyceride nanoparticles, International Journal of Pharmaceutics, 129 (1996) 159-173.

[216] V.B.Patravale and A.V.Ambarkhane, Study of solid lipid nanoparticles with respect to particle size distribution and drug loading., Pharmazie, 58 (2003) 392-395.

[217] P.Shahgaldian, J.Gualbert, K.Aîssa, and A.W.Coleman, A study of the freeze-drying conditions of calixarene based solid lipid nanoparticles, European Journal of Pharmaceutics and Biopharmaceutics, 55 (2003) 181-184.

[218] A.Radomska-Soukharev, Stability of lipid excipients in solid lipid nanoparticles, Advanced Drug Delivery Reviews, 59 (2007) 411-418.

[219] T.Echigo, D.M.Aruguete, M.Murayama, and Jr.Hochella, Influence of size, morphology, surface structure, and aggregation state on reductive dissolution of hematite nanoparticles with ascorbic acid, Geochimica et Cosmochimica Acta, 90 (2012) 149-162.

[220] A.Dubes, H.Parrot-Lopez, W.Abdelwahed, G.Degobert, H.Fessi, P.Shahgaldian, and A.W.Coleman, Scanning electron microscopy and atomic force microscopy imaging of solid lipid nanoparticles derived from amphiphilic cyclodextrins, European Journal of Pharmaceutics and Biopharmaceutics, 55 (2003) 279-282.

[221] S.J.Pennycook, A.R.Lupini, M.Varela, A.Y.Borisevich, Y.Peng, M.P.Oxley, K.van Benthem, and M.F.Chisholm. Scanning Transmission Electron Microscopy for Nanostructure Characterization. http://stem.ornl.gov/, 2012, Accessed 21/10/2012.

[222] D.Z.Hou, C.S.Xie, K.J.Huang, and C.H.Zhu, The production and characteristics of solid lipid nanoparticles (SLNs), Biomaterials, 24 (2003) 1781-1785.

[223] K.WaKasongo. An investigation into the feasability of incorporating didanosine into innovative solid lipid nanocarriers. Rhodes University, pp. 34-148, 2010.

[224] Y.C.Kuo and T.W.Lin, Electrophoretic Mobility, Zeta Potential, and Fixed Charge Density of Bovine Knee Chondrocytes, Methyl Methacrylate–Sulfopropyl Methacrylate, Polybutylcyanoacrylate, and Solid Lipid Nanoparticles, J. Phys. Chem. B, 110 (2006) 2202-2208.

[225] P.Leroy, C.Tournassat, and M.Bizi, Influence of surface conductivity on the apparent zeta potential of TiO2 nanoparticles, Journal of Colloid and Interface Science, 356 (2011) 442-453.

[226] C.Freitas and R.H.Müller, Effect of light and temperature on zeta potential and physical stability in solid lipid nanoparticle (SLN^{TM}) dispersions, International Journal of Pharmaceutics, 168 (1998) 221-229.

[227] K.Westesen, H.Bunjes, and M.H.J.Koch, Physicochemical characterization of lipid nanoparticles and evaluation of their drug loading capacity and sustained release potential, Journal of Controlled Release, 48 (1997) 223-236.

[228] K.Westesen and H.Bunjes, Do nanoparticles prepared from lipids solid at room temperature always possess a solid lipid matrix?, International Journal of Pharmaceutics, 115 (1995) 129-131.

[229] S.D.Clas, C.R.Dalton, and B.C.Hancock, Differential scanning calorimetry: applications in drug development, Pharmaceutical Science & Technology Today, 2 (1999) 311-320.

[230] M.H.Chiu and E.J.Prenner, Differential scanning calorimetry: An invaluable tool for a detailed thermodynamic characterization of macromolecules and their interactions, J Pharm Bioallied Sci, 3 (2011) 39-59.

[231] C.Freitas and R.H.Müller, Correlation between long-term stability of solid lipid nanoparticles (SLN^{TM}) and crystallinity of the lipid phase, European Journal of Pharmaceutics and Biopharmaceutics, 47 (1999) 125-132.

[232] V.Teeranachaideekul, E.B.Souto, V.B.Junyaprasert, and R.H.Müller, Cetyl palmitate-based NLC for topical delivery of Coenzyme Q_{10} − Development, physicochemical characterization and in vitro release studies, European Journal of Pharmaceutics and Biopharmaceutics, 67 (2007) 141-148.

[233] E.B.Souto, W.Mehnert, and R.H.Müller, Polymorphic behaviour of Compritol888 ATO as bulk lipid and as SLN and NLC., Journal of Microencapsulation, 23 (2006) 417-433.

[234] S.S.Bharate, S.B.Bharate, and A.N.Bajaj, Incompatibilities of Pharmaceutical Excipients with Active Pharmaceutical Ingredients: A Comprehensive Review, Journal of Excipients and Food Chemicals, 1 (2010) 3-26.

[235] J.You, F.Wan, F.de Cui, Y.Sun, Y.Z.Du, and F.Q.Hu, Preparation and characteristic of vinorelbine bitartrate-loaded solid lipid nanoparticles, International Journal of Pharmaceutics, 343 (2007) 270-276.

[236] D.Heng, D.J.Cutler, H.K.Chan, J.Yun, and J.A.Raper, What is a Suitable Dissolution Method for Drug Nanoparticles?, Pharm Res, 25 (2008) 1696-1701.

[237] S.A.Wissing and R.H.Müller, Solid lipid nanoparticles as carrier for sunscreens: in vitro release and in vivo skin penetration, Journal of Controlled Release, 81 (2002) 225-233.

[238] V.Venkateswarlu and K.Manjunath, Preparation, characterization and in vitro release kinetics of clozapine solid lipid nanoparticles, Journal of Controlled Release, 95 (2004) 627-638.

[239] Y.F.Luo, D.W.Chen, L.X.Ren, X.L.Zhao, and J.Qin, Solid lipid nanoparticles for enhancing vinpocetine's oral bioavailability, Journal of Controlled Release, 114 (2006) 53-59.

[240] L.D.Hu, X.Tang, and F.D.Cui, Solid lipid nanoparticles (SLNs) to improve oral bioavailability of poorly soluble drugs, Journal of Pharmacy and Pharmacology, 56 (2004) 1527-1535.

[241] H.Li, X.B.Zhao, Y.K.Ma, G.X.Zhai, L.B.Li, and H.X.Lou, Enhancement of gastrointestinal absorption of quercetin by solid lipid nanoparticles, Journal of Controlled Release, 133 (2009) 238-244.

[242] U.Bhardwaj and D.J.Burgess, A novel USP apparatus 4 based release testing method for dispersed systems, International Journal of Pharmaceutics, 388 (2010) 287-294.

[243] J.Liu, T.Gong, H.Fu, C.Wang, X.Wang, Q.Chen, Q.Zhang, Q.He, and Z.Zhang, Solid lipid nanoparticles for pulmonary delivery of insulin, International Journal of Pharmaceutics, 356 (2008) 333-344.

[244] M.Sznitowska, M.Gajewska, S.Janicki, A.Radwanska, and G.Lukowski, Bioavailability of diazepam from aqueous-organic solution, submicron emulsion and solid lipid nanoparticles after rectal administration in rabbits, European Journal of Pharmaceutics and Biopharmaceutics, 52 (2001) 159-163.

[245] R.Cavalli, M.R.Gasco, P.Chetoni, S.Burgalassi, and M.F.Saettone, Solid lipid nanoparticles (SLN) as ocular delivery system for tobramycin, International Journal of Pharmaceutics, 238 (2002) 241-245.

[246] P.Langmann, D.Schirmer, T.Vath, M.Zilly, and H.Klinker, High-performance liquid chromatographic method for the determination of HIV-1 non-nucleoside reverse transcriptase inhibitor efavirenz in plasma of patients during highly active antiretroviral therapy, Journal of Chromatography B: Biomedical Sciences and Applications, 755 (2001) 151-156.

[247] C.Z.Matthews, E.J.Woolf, R.S.Mazenko, H.Haddix-Wiener, C.M.Chavez-Eng, M.L.Constanzer, G.A.Doss, and B.K.Matuszewski, Determination of efavirenz, a selective non-nucleoside reverse transcriptase inhibitor, in human plasma using HPLC with post-column photochemical derivatization and fluorescence detection, Journal of Pharmaceutical and Biomedical Analysis, 28 (2002) 925-934.

[248] E.R.Montgomery, A.L.Edmanson, S.C.Cook, and P.K.Hovsepian, Development and validation of a reverse-phase HPLC method for analysis of efavirenz and its related substances in the drug substance and in a capsule formulation, Journal of Pharmaceutical and Biomedical Analysis, 25 (2001) 267-284.

[249] G.Ramachandran, A.K.H.Kumar, S.Swaminathan, P.Venkatesan, V.Kumaraswami, and D.J.Greenblatt, Simple and rapid liquid chromatography method for determination of efavirenz in plasma, Journal of Chromatography B, 835 (2006) 131-135.

[250] H.Rebiere, B.Mazel, C.Civade, and P.A.Bonnet, Determination of 19 antiretroviral agents in pharmaceuticals or suspected products with two methods using high-performance liquid chromatography, Journal of Chromatography B, 850 (2007) 376-383.

[251] M.Sarasa-Nacenta, Y.Lopez-Pua, L.F.Lopez-Cortes, J.Mallolas, J.M.Gatell, and X.Carne, Determination of efavirenz in human plasma by high-performance liquid chromatography with ultraviolet detection, Journal of Chromatography B: Biomedical Sciences and Applications, 763 (2001) 53-59.

[252] A.I.Veldkamp, R.P.G.Van Heeswijk, P.L.Meenhorst, J.W.Mulder, J.M.A.Lange, J.H.Beijnen, and R.M.W.Hoetelmans, Quantitative determination of efavirenz (DMP 266), a novel non-nucleoside reverse transcriptase inhibitor, in human plasma using isocratic reversed-phase high-performance liquid chromatography with ultraviolet detection, Journal of Chromatography B: Biomedical Sciences and Applications, 734 (1999) 55-61.

[253] A.Theron, D.Cromarty, M.Rheeders, and M.Viljoen, Determination of salivary efavirenz by liquid chromatography coupled with tandem mass spectrometry, Journal of Chromatography B, 878 (2010) 2886-2890.

[254] A.Rouzes, K.Berthoin, F.Xuereb, S.Djabarouti, I.Pellegrin, J.L.Pellegrin, A.C.Coupet, S.Augagneur, H.Budzinski, M.C.Saux, and D.Breilh, Simultaneous determination of the antiretroviral agents: amprenavir, lopinavir, ritonavir, saquinavir and efavirenz in human peripheral blood mononuclear cells by high-performance liquid chromatography-mass spectrometry, Journal of Chromatography B, 813 (2004) 209-216.

[255] P.Lemmer, S.Schneider, M.Schuman, C.Omes, V.Arendt, J.CTayari, L.Fundira, and R.Wennig, Determination of nevirapine and efavirenz in plasma using GC/MS in selected ion monitoring mode., Therapeutic Drug Monitoring, 4 (2012) 521-525.

[256] L.Jiaping, W.Jun, and C.Zongwei, Nucleoside reverse transcriptase inhibitors and their phosphorylated metabolites in human immunodeficiency virus-infected human matrices, Journal of Chromatography B, 868 (2008) 1-12.

[257] S.Notari, C.Mancone, T.Alonzi, M.Tripodi, P.Narciso, and P.Ascenzi, Determination of abacavir, amprenavir, didanosine, efavirenz, nevirapine, and stavudine concentration in human plasma by MALDI-TOF/TOF, Journal of Chromatography B, 863 (2008) 249-257.

[258] A.K.Manikanta, B.N.Sandhya, M.Nasare, V.V.L.N.Prasad, and P.V.Diwan, Development and validation of UV Spectrophotometric method for simultaneous estimation of Lamivudine and Efavirenz in the Pharmaceutical dosage form, Journal of Advanced Pharmacy Education & Research, 2 (2012) 210-214.

[259] D.G.Sankar, M.R.Kumar, and V.V.N.Reddy, UV spectrophotometric methods for the determination of saquinavir mesylate and efavirenz, Asian Journal of Chemistry, 15 (2003) 1856-1858.

[260] A.de Villiers, F.Leestremau, R.Szucs, S.Gélébart, F.David, and P.Sandra, Evaluation of ultra performance liquid chromatography: Part I. Possibilities and limitations, Journal of Chromatography A, 1127 (2006) 60-69.

[261] S.Lindsay, High Performance Liquid Chromatography, John Wiley and Sons,Inc, pp. 121-122 1992.

[262] F.A.Chaibva. Development And Assessment Of An Oxytocin Parenteral Dosage Form Prepared Using Pluronic® F127, Rhodes University, pp. 21-74, 2006.

[263] L.R.Snyder and J.J.Kirkland, Introduction to Modern Liquid Chromatography, John Wiley and Sons,Inc, pp. 552-555, 1979.

[264] C.F.Simpson, Practiacl High Performance Liquid Chromatography, Heyden and Son,Ltd, pp. 624-641, 1976.

[265] R.J.Hamilton and P.A.Sewell, Introduction To High Performance Liquid Chromatography, Chapman and Hall, pp. 127-140, 1977.

[266] R.R.Nageswara, S.Meena, and R.A.Raghuram, An overview of the recent developments in analytical methodologies for determination of COX-2 inhibitors in bulk drugs, pharmaceuticals and biological matrices, Journal of Pharmaceutical and Biomedical Analysis, 39 (2005) 349-363.

[267] R.A.Seburg, J.M.Ballard, T.L.Hwang, and C.M.Sullivan, Photosensitized degradation of losartan potassium in an extemporaneous suspension formulation, Journal of Pharmaceutical and Biomedical Analysis, 42 (2006) 411-422.

[268] B.J.Westenberger, C.D.Ellison, A.S.Fussner, S.Jenney, R.E.Kolinski, T.G.Lipe, R.C.Lyon, T.W.Moore, L.K.Revelle, A.P.Smith, J.A.Spencer, K.D.Story, D.Y.Toler, A.M.Wokovich, and L.F.Buhse, Quality assessment of internet pharmaceutical products using traditional and non-traditional analytical techniques, International Journal of Pharmaceutics, 306 (2005) 56-70.

[269] G.J.Threadgill, R.C.Conrad, L.M.Changchien, M.Cannon, and G.R.Craven, Application of high-performance liquid chromatography to the purification and characterization of ribosomal protein L3 from trichodermin-resistant yeast mutants., Biochemical Journal, 237 (1986) 421-426.

[270] G.J.Threadgill, R.C.Conrad, M.Cannon, and G.R.Craven, A rapid and preparative method for the separation of yeast ribosomal proteins by using high-performance liquid chromatography., Biochemical Journal, 244 (1987) 523-532.

[271] E.Gelpì, Biomedical and biochemical applications of liquid chromatography-mass spectrometry, Journal of Chromatography A, 703 (1995) 59-80.

[272] S.Passi, P.Fasella, M.Nazzaro-Porro, D.Whitehouse, and M.C.Rothschild-Boros, An application of high performance liquid chromatography to analysis of lipids in archaeological samples, Journal of Lipid Research, 22 (1981) 778-784.

[273] M.L.Chang and C.M.Chang, Simultaneous HPLC determination of hydrophilic whitening agents in cosmetic products, Journal of Pharmaceutical and Biomedical Analysis, 33 (2003) 617-626.

[274] Y.H.Lee, E.S.Jeong, H.E.Cho, and D.C.Moon, Separation and determination of polyethylene glycol fatty acid esters in cosmetics by a reversed-phase HPLC/ELSD, Talanta, 74 (2008) 1615-1620.

[275] A.M.Maia, A.R.Baby, W.J.Yasaka, E.Suenaga, T.M.Kaneko, and M.V.Velasco, Validation of HPLC stability-indicating method for Vitamin C in semisolid pharmaceutical/cosmetic preparations with glutathione and sodium metabisulfite, as antioxidants, Talanta, 71 (2007) 639-643.

[276] E.Sottofattori, M.Anzaldi, A.Balbi, and G.Tonello, Simultaneous HPLC determination of multiple components in a commercial cosmetic cream, Journal of Pharmaceutical and Biomedical Analysis, 18 (1998) 213-217.

[277] J.H.Lee and M.G.Choung, Determination of curcuminoid colouring principles in commercial foods by HPLC, Food Chemistry, 124 (2011) 1217-1222.

[278] M.J.Scotter, Synthesis and chemical characterisation of curcuminoid colouring principles for their potential use as HPLC standards for the determination of curcumin colour in foods, LWT - Food Science and Technology, 42 (2009) 1345-1351.

[279] Y.Tian, Y.Li, X.Xu, Z.Jin, A.Jiao, J.Wang, and B.Yu, A novel size-exclusion high performance liquid chromatography (SE-HPLC) method for measuring degree of amylose retrogradation in rice starch, Food Chemistry, 118 (2010) 445-448.

[280] J.P.Bergström and A.Helander, HPLC evaluation of clinical and pharmacological factors reported to cause false-positive carbohydrate-deficient transferrin (CDT) levels, Clinica Chimica Acta, 389 (2008) 164-166.

[281] M.Vogeser and C.Seger, A decade of HPLC–MS/MS in the routine clinical laboratory-Goals for further developments, Clinical Biochemistry, 41 (2008) 649-662.

[282] R.C.Williams, J.F.Edwards, A.S.Joshi, and A.F.Aubry, Chiral analysis of drug substance in clinical plasma extracts using achiral HPLC with circular dichroism detection, Journal of Pharmaceutical and Biomedical Analysis, 25 (2001) 501-509.

[283] D.Gunasekara, L.Byrnes, S.Brown, J.Beilby, and J.Kaye, Clinical implications of the early detection of urinary microalbumin in diabetic patients using a new high performance liquid chromatography (HPLC) method, Diabetes Research and Clinical Practice, 93 (2011) e61-e64.

[284] R.Raghavan and J.C.Joseph, Chromatographic methods of analysis- High performance liquid chromatography, Encyclopedia of Pharmaceutical Technology, 1 (2002) 414-425.

[285] D.E.Martire and R.E.Boehm, Unified theory of retention and selectivity in liquid chromatography. 2. Reversed-phase liquid chromatography with chemically bonded phases, J. Phys. Chem., 87 (1983) 1045-1062.

[286] R.J.M.Vervoort, A.J.J.Debets, H.A.Claessens, C.A.Cramers, and G.J.de Jong, Optimisation and characterisation of silica-based reversed-phase liquid chromatographic systems for the analysis of basic pharmaceuticals, Journal of Chromatography A, 897 (2000) 1-22.

[287] Y.V.Kazakevich, High-performance liquid chromatography retention mechanisms and their mathematical descriptions, Journal of Chromatography A, 1126 (2006) 232-243.

[288] C.Horváth, W.Melander, and I.Molnár, Solvophobic interactions in liquid chromatography with nonpolar stationary phases, Journal of Chromatography A, 125 (1976) 129-156.

[289] C.Horváth, W.Melander, I.Molnar, and P.Molnar, Enhancement of retention by ion-pair formation in liquid chromatography with nonpolar stationary phases, Anal. Chem., 49 (1977) 2295-2305.

[290] B.L.Karger, J.R.Gant, A.Martkopf, and P.H.Weiner, Hydrophobic effects in reversed-phase liquid chromatography, Journal of Chromatography A, 128 (1976) 65-78.

[291] P.E.Antle, A.P.Goldberg, and L.R.Snyder, Characterization of silica-based reversed-phase columns with respect to retention selectivity : Solvophobic effects, Journal of Chromatography A, 321 (1985) 1-32.

[292] K.A.Dill, The mechanism of solute retention in reversed-phase liquid chromatography, J. Phys. Chem., 91 (1987) 1980-1988.

[293] K.B.Sentell and J.G.Dorsey, Retention mechanisms in reversed-phase chromatography : Stationary phase bonding density and solute selectivity, Journal of Chromatography A, 461 (1989) 193-207.

[294] M.Jaroniec, Partition and displacement models in reversed-phase liquid chromatography with mixed eluents, Journal of Chromatography A, 656 (1993) 37-50.

[295] L.C.Tan and P.W.Carr, Study of retention in reversed-phase liquid chromatography using linear solvation energy relationships: II. The mobile phase, Journal of Chromatography A, 799 (1998) 1-19.

[296] F.Riedo and E.Kováts, Adsorption from liquid mixtures and liquid chromatography, Journal of Chromatography A, 239 (1982) 1-28.

[297] P.T.Ying, J.G.Dorsey, and K.A.Dill, Retention mechanisms of reversed-phase liquid chromatography: determination of solute-solvent interaction free energies, Anal. Chem., 61 (1989) 2540-2546.

[298] B.Buszewski and S.Noga, Hydrophilic interaction liquid chromatography (HILIC)—a powerful separation technique, Analytical and Bioanalytical Chemistry, 402 (2011) 231-247.

[299] J.H.Knox and A.Pryde, Performance and selected applications of a new range of chemically bonded packing materials in high-performance liquid chromatography, Journal of Chromatography A, 112 (1975) 171-188.

[300] F.Gritti and G.Guiochon, Critical contribution of nonlinear chromatography to the understanding of retention mechanism in reversed-phase liquid chromatography, Journal of Chromatography A, 1099 (2005) 1-42.

[301] D.V.McCalley, Effect of temperature and flow-rate on analysis of basic compounds in high-performance liquid chromatography using a reversed-phase column, Journal of Chromatography A, 902 (2000) 311-321.

[302] Y.C.Guillaume and E.Peyrin, Optimising mobile phase composition, its flow-rate and column temperature in HPLC using taboo search, Talanta, 51 (2000) 579-586.

[303] R.J.Flanagan and I.Jane, High-performance liquid chromatographic analysis of basic drugs on silica columns using non-aqueous ionic eluents : I. Factors influencing retention, peak shape and detector response, Journal of Chromatography A, 323 (1985) 173-189.

[304] J.K.Törnblom, T.F.W.Bureyko, and C.D.MacKinnon, Simulating phenol high-performance liquid chromatography retention times as the pH changes: Mobile phase pH versus buffer pH, Journal of Chromatography A, 1095 (2005) 68-73.

[305] M.Yang, S.Fazio, D.Munch, and P.Drumm, Impact of methanol and acetonitrile on separations based on pi-pi interactions with a reversed-phase phenyl column, Journal of Chromatography A, 1097 (2005) 124-129.

[306] J.W.Dolan, J.R.Gant, and L.R.Snyder, Gradient elution in high-performance liquid chromatography : II. Practical application to reversed-phase systems, Journal of Chromatography A, 165 (1979) 31-58.

[307] L.R.Snyder, J.W.Dolan, and J.R.Gant, Gradient elution in high-performance liquid chromatography : I. Theoretical basis for reversed-phase systems, Journal of Chromatography A, 165 (1979) 3-30.

[308] J.Lokajová, E.Tesarová, and D.W.Armstrong, Comparative study of three teicoplanin-based chiral stationary phases using the linear free energy relationship model, Journal of Chromatography A, 1088 (2005) 57-66.

[309] K.Valkó, M.Plass, C.Bevan, D.Reynolds, and M.H.Abraham, Relationships between the chromatographic hydrophobicity indices and solute descriptors obtained by using several reversed-phase, diol, nitrile, cyclodextrin and immobilised artificial membrane-bonded high-performance liquid chromatography columns, Journal of Chromatography A, 797 (1998) 41-55.

[310] A.Nasal, A.Buciñski, L.Bober, and R.Kaliszan, Prediction of pharmacological classification by means of chromatographic parameters processed by principal component analysis, International Journal of Pharmaceutics, 159 (1997) 43-55.

[311] R.Kaliszan, Quantitative structure-retention relationships applied to reversed-phase high-performance liquid chromatography, Journal of Chromatography A, 656 (1993) 417-435.

[312] R.Kaliszan, M.A.van Straten, M.Markuszewski, C.A.Cramers, and H.A.Claessens, Molecular mechanism of retention in reversed-phase high-performance liquid chromatography and classification of modern stationary phases by using quantitative structure–retention relationships, Journal of Chromatography A, 855 (1999) 455-486.

[313] L.Jedynak, M.Puchalska, M.Zezula, M.Laszcz, W.Luniewski, and J.Zagrodzka, Stability of sample solution as a crucial point during HPLC determination of chemical purity of temozolomide drug substance, Journal of Pharmaceutical and Biomedical Analysis, 83 (2013) 19-27.

[314] L.Dhooghe, K.Mesia, E.Kohtala, L.Tona, L.Pieters, A.J.Vlietinck, and S.Apers, Development and validation of an HPLC-method for the determination of alkaloids in the stem bark extract of Nauclea pobeguinii, Talanta, 76 (2008) 462-468.

[315] A.K.Dutta, B.A.Avery, and C.M.Wyandt, Development and validation of a stability-indicating reversed-phase high performance liquid chromatography method for NPC 1161C, a novel 8-aminoquinoline anti-malarial drug, Journal of Chromatography A, 1110 (2006) 35-45.

[316] L.R.Snyder, J.J.Kirkland, and J.L.Glajch, Practical HPLC method development, John Wiley and Sons, Inc, New York, pp. 657-662, 1997.

[317] Y.Xiong, K.P.Xiao, and A.M.Rustum, Development and validation of a stability-indicating RP-HPLC method to separate low levels of dexamethasone and other related compounds from betamethasone, Journal of Pharmaceutical and Biomedical Analysis, 49 (2009) 646-654.

[318] T.Radhakrishna, A.Narasaraju, M.Ramakrishna, and A.Satyanarayana, Simultaneous determination of montelukast and loratadine by HPLC and derivative spectrophotometric methods, Journal of Pharmaceutical and Biomedical Analysis, 31 (2003) 359-368.

[319] M.Murillo-Arbizu, E.González-Peñas, and S.Amézqueta, Comparison between capillary electrophoresis and high performance liquid chromatography for the study of the occurrence of patulin in apple juice intended for infants, Food and Chemical Toxicology, 48 (2010) 2429-2434.

[320] M.A.Korany, H.Mahgoub, O.T.Fahmy, and H.M.Maher, Application of artificial neural networks for response surface modelling in HPLC method development, Journal of Advanced Research, 3 (2012) 53-63.

[321] S.Agatonovic-Kustrin, M.Zecevic, L.Zivanovic, and I.G.Tucker, Application of artificial neural networks in HPLC method development, Journal of Pharmaceutical and Biomedical Analysis, 17 (1998) 69-76.

[322] D.Bas and H.Boyaci, Modeling and optimization I: Usability of response surface methodology, Journal of Food Engineering, 78 (2007) 836-845.

[323] S.M.Khamanga and R.B.Walker, The use of experimental design in the development of an HPLC–ECD method for the analysis of captopril, Talanta, 83 (2011) 1037-1049.

[324] I.Popovic, D.Ivanovic, M.Medenica, A.Malenovic, and B.Jancic-Stojanovic, LD Determination of Lercanidipine and its Impurities Using Drylab Software and Experimental Design Procedures, Chromatographia, 67 (2008) 449-454.

[325] R.M.Krisko, K.McLaughlin, M.J.Koenigbauer, and C.E.Lunte, Application of a column selection system and DryLab software for high-performance liquid chromatography method development, Journal of Chromatography A, 1122 (2006) 186-193.

[326] J.A.van Leeuwen, L.M.C.Buydens, B.G.M.Vandeginste, and G.Kateman, Expert systems in chemical analysis, Trends in analytical chemistry, 9 (1990) 50-54.

[327] J.A.van Leeuwen, B.G.M.Vandeginste, G.J.Postma, and G.Kateman, An evaluation of expert system tools on their use in high-performance liquid chromatography, Chemometrics and Intelligent Laboratory Systems, 6 (1989) 239-252.

[328] F.Maris and R.Hindriks, 5: Validation and Evaluation of Expert Systems for HPLC Method Development – Case Studies, in: M. C. B. Lutgarde (Ed.), Data Handling in Science and Technology Intelligent software for chemical analysis, Elsevier, (1993) 153-223.

[329] F.Erni, Use of high-performance liquid chromatography in the pharmaceutical industry, J Chromatogr A., 507 (1990) 141-149.

[330] I.K.Andre and S.Mukhopadhyay, Response surface methodology, WIREs Comp Stat, (2010) 128-149.

[331] M.A.Bezerra, R.E.Santelli, E.P.Oliveira, L.S.Villar, and L.A.Escaleira, Response surface methodology (RSM) as a tool for optimization in analytical chemistry, Talanta, 76 (2008) 965-977.

[332] S.L.C.Ferreira, R.E.Bruns, H.S.Ferreira, G.D.Matos, J.M.David, G.C.Brandão, E.G.P.da Silva, L.A.Portugal, P.S.dos Reis, A.S.Souza, and W.N.L.dos Santos, Box-Behnken design: An alternative for the optimization of analytical methods, Analytica Chimica Acta, 597 (2007) 179-186.

[333] N.Kettaneh-Wold, Use of experimental design in the pharmaceutical industry, Journal of Pharmaceutical and Biomedical Analysis, 9 (1991) 605-610.

[334] A.Müller, D.Flottmann, W.Schulz, W.Seitz, and W.H.Weber, Assessment of robustness for an LC–MS–MS multi-method by response-surface methodology, and its sensitivity, Anal Bioanal Chem, 390 (2008) 1317-1326.

[335] G.E.P.Box and D.W.Behnken, Some new three-level designs for the study of quantitative variables, Technometrics, 2 (1960) 455-475.

[336] L.Eriksson, Design of Experiments: Principles and Applications, Umetrics Academy, pp. 3-136, 2008.

[337] G.Srinubabu, K.Jaganbabu, B.Sudharani, K.Venugopal, G.Girizasankar, and J.V.L.N.S Rao, Development and validation of a LC method for the determination of pramipexole using an experimental design, Chromatographia, 64 (2006) 95-100.

[338] G.Srinubabu, C.Raju, N.Sarath, P.K.Kumar, and J.V.Rao, Development and validation of a HPLC method for the determination of voriconazole in pharmaceutical formulation using an experimental design, Talanta, 71 (2007) 1424-1429.

[339] T.A.Li, Y.Zhang, X.Feng, X.Xu, and D.H.Xu, Optimized preparation of naloxone microemulsion and its transdermal delivery effect, Chinese Pharmaceutical Journal, 44 (2009) 688-691.

[340] B.Chen, X.Shen, and J.Kong, Determining the purity of samples from natural products by coupling HPLC and CCD spectrometry, J Sep Sci., 28 (2005) 286-290.

[341] Agilent Technologies. Agilent Zorbax SB-CN. http://www.chem.agilent.com/Library/datasheets/Public/820644-005g.pdf . 8/6/2003. Accessed: 5/12/2013.

[342] Agilent Technologies. Agilent Zorbax SB-Phenyl. http://www.chem.agilent.com/Library/datasheets/Public/820644-012f.pdf . 8/11/2003. Accessed: 5/12/2013.

[343] P.D.Hamrapurka, P.S.Patil, M.D.Phale, N.Shah, and S.B.Pawar, Optimization and Validation of Rp-Hplc Stability-Indicating Method for Determination of Efavirenz and its Degradation Products, International Journal of Applied Science and Engineering, 8 (2010) 155-165.

[344] N.A.Raju and S.Begum, Simultaneous RP-HPLC Method for the Estimation of the Emtricitabine, Tenofovir Disoproxil Fumerate and Efavirenz in Tablet Dosage Forms, Research J. Pharm. and Tech, 1 (2009) 522-525.

[345] O.de Sá Viana, P.M.M.Flávia, G.Severino, A.M.Muniz, M.F.La Roca Sores, J.L.Sores-Sobrinho, L.D.S.Alves, L.A.Rolim, K.E.R.Silva, and P.J.Rolim-Neto, Development and validation of a HPLC analytical assay method for efavirenz tablets: a medicine for HIV infections, Brazilian Journal of Pharmaceutical Sciences, 47 (2011) 97-102.

[346] I.Madhusudhanareddy, R.M.Bhagavan, P.Y.Rajendra, R.K.Pavankumar, and C.R.Sarva, Simultaneous Quantification of Efavirenz and Lamivudine in Tablet Dosage Form by Liquid Chromatography, Indian Journal of Pharmaceutical Education and Research, 45 (2011).

[347] N.A.Raju, J.V.Rao, K.V.Prakash, K.Mukkanti, and K.Srinivasu, Simultaneous estimation of tenofovir disoproxil,emtricitabine and efavirenz in tablet dosage form by RP-HPLC, Oriental Journal of Chemistry, 24 (2008) 645-650.

[348] H.Pèlerin, S.Compain, X.Duval, F.Gimenez, H.Bénech, and A.Mabondzo, Development of an assay method for the detection and quantification of protease and non-nucleoside reverse transcriptase inhibitors in plasma and in peripherical blood mononuclear cells by liquid chromatography coupled with ultraviolet or tandem mass spectrometry detection, Journal of Chromatography B, 819 (2005) 47-57.

[349] S.Mogatle and I.Kanfer, Rapid method for the quantitative determination of efavirenz in human plasma, South African Medical Journal, 98 (2008) 945-949.

[350] G.Satyavathi, M.Sidhakar, V.Rajesh, K.Satyanarayana, D.R.Krishna, G.Prathap, J.Suvarchala, and R.Kuchi, Validation of an isocratic HPLC assay of efavirenz in pharmaceutical formulations of drug substance, Internation Journal of Research and Reviews in Pharmacy and Applied Sciences, 1 (2011) 20-26.

[351] D.Fox, R.O'Connor, P.Mallon, and G.McMahon, Simultaneous determination of efavirenz, rifampicin and its metabolite desacetyl rifampicin levels in human plasma, Journal of Pharmaceutical and Biomedical Analysis, 56 (2011) 785-791.

[352] J.J.Kirkland, F.A.Truszkowski, and R.D.Ricker, Atypical silica-based column packings for high-performance liquid chromatography, Journal of Chromatography A, 965 (2002) 25-34.

[353] J.J.Kirkland, M.A.van Straten, and H.A.Claessens, High pH mobile phase effects on silica-based reversed-phase high-performance liquid chromatographic columns, Journal of Chromatography A, 691 (1995) 3-19.

[354] J.J.Pesek and M.T.Matyska, Modified aluminas as chromatographic supports for high-performance liquid chromatography, Journal of Chromatography A, 952 (2002) 1-11.

[355] H.A.Claessens and M.A.van Straten, Review on the chemical and thermal stability of stationary phases for reversed-phase liquid chromatography, Journal of Chromatography A, 1060 (2004) 23-41.

[356] R.E.Majors. The Cleaning and Regeneration of Reversed-Phase HPLC Columns. http://www.chromatographyonline.com/ . 2003. Accessed: 5/20/2013.

[357] Agilent Technologies. Control pH During Method Development for Better Chromatography. www.agilent.com/chem . 2012. Accessed: 5/20/2013.

[358] A.S.Rathore, R.M.Kennedy, J.K.O'Donell, I.Bemberis, and O.Kaltenbrunner. Qualification of a Chromatographic Column. BioPharm International . 2003. Accessed: 5/21/2013.

[359] Center for Drug Evaluation and Research, U. S. Food and Drug Administration. Reviewer Guidance, Validation of Chromatographic Methods. http://www.fda.gov/downloads/Drugs/Guidances/UCM134409.pdf . 1994. Accessed: 5/22/2013.

[360] D.Song and J.Wang, Modified resolution factor for asymmetrical peaks in chromatographic separation, Journal of Pharmaceutical and Biomedical Analysis, 32 (2003) 1105-1112.

[361] World Heath Organisation. High-performance liquid chromatography. http://apps.who.int/phint/en/p/docf/ . 1997. Accessed: 5/24/2013.

[362] K.J.Bronsema, R.Bischoff, and N.C.Van de Merbel, Internal standards in the quantitative determination of protein biopharmaceuticals using liquid chromatography coupled to mass spectrometry, J Chromatogr B., 893-894 (2012) 1-14.

[363] F.Zhang and H.Li, Resolution of overlapping capillary electrophoresis peaks by using chemometric analysis: Improved quantification by using internal standard, Chemometrics and Intelligent Laboratory Systems, 82 (2006) 184-192.

[364] E.Dailly, F.Raffi, and P.Jolliet, Determination of atazanavir and other antiretroviral drugs (indinavir, amprenavir, nelfinavir and its active metabolite M8, saquinavir, ritonavir, lopinavir, nevirapine and efavirenz) plasma levels by high performance liquid chromatography with UV detection, J Chromatogr B., 813 (2004) 353-358.

[365] T.M.Vickrey, Liquid Chromatography Detectors, Marcel Dekker,Inc, pp. 23-165, 1983.

[366] R.P.W.Scott. Principles and Practice of Chromatography. http://www.chromatography-online.org/index.html . 2008. Accessed: 5/26/2013.

[367] C.Moreau and G.Douhéret, Thermodynamic and physical behaviour of water + acetonitrile mixtures. Dielectric properties, The Journal of Chemical Thermodynamics, 8 (1976) 403-410.

[368] G.E.P.Box and K.B.Wilson, On the Experimental Attainment of Optimum Conditions, Journal of the Royal Statistical Society. Series B (Methodological), 13 (1951) 1-45.

[369] V.S.Babu, S.S.Kumar, R.V.Murali, and M.M.Rao, Investigation and validation of optimal cutting parameters for least surface roughness in EN24 with response surface method, International Journal of Engineering, Science and Technology, 3 (2011) 146-160.

[370] M.U.Rahman, A.Gul, A.A.Odhano, I.Hafeez, R.B.Tareen, and M.M.Yasinzai, Optimization of Concentration of Medium Ingredients for Production of Citric Acid using Statistical Methods, Bangladesh J. Sci. Ind. Res, 46 (2011) 549-560.

[371] D.Ghodsiyeh, A.Golshan, N.Hosseininezhad, M.Hashemzadeh, and S.Ghodsiyeh, Optimizing Finishing process in WEDMing of Titanium Alloy (Ti6Al4V) by Zinc Coated Brass Wire based on Response Surface Methodology , Indian Journal of Science and Technology, 5 (2012) 3365-3377.

[372] NIST SEMATECH. Engineering Statistics Handbook. NIST/SEMATECH e-Handbook of Statistical Methods, http://www.itl.nist.gov/div898/handbook/, date . 4/1/2012. Accessed: 5/31/2013.

[373] A.F.B.Fauzee, S.M.Khamanga, and R.B.Walker, The impact of manufacturing variables on in vitro release of clobetasol 17-propionate from pilot scale cream formulations, Drug Development and Industrial Pharmacy, (2013) 1-10.

[374] U.S.Department of Health and Human Services, Food and Drug Administration, Center for Drug Evaluation and Research (CDER), and Center for Biologics Evaluation and Research (CBER). Guidance for Industry Q2B Validation of Analytical Procedures: Methodology. http://www.fda.gov/downloads/Regulator%20yInformation/Guidances/UCM128049.pdf . 1996. Accessed: 6/4/2013.

[375] Center for Drug Evaluation and Research (CDER). Validation of Chromatographic Methods:Reviewer Guidance. http://www.fda.gov/downloads/Drugs/Guidances/UCM134409.pdf , 1994. Accessed: 6/4/2013.

[376] European Medicines Agency. ICH Topic Q 2 (R1) Validation of Analytical Procedures: Text and Methodology. http://www.ema.europa.eu/docs/en_GB/document_library/Scientific_guideline/2009/09/WC500002662.pdf . 1995. Accessed: 6/4/2013.

[377] U.S.Department of Health and Human Services, Food and Drug Administration, Center for Drug Evaluation and Research (CDER), and Center for Biologics Evaluation and Research (CBER). Guidance for Industry Analytical Procedures and Methods Validation. http://www.fda.gov/ohrms/dockets/98fr/001424gl.pdf . 2000. Accessed: 6/4/2013.

[378] ICH Harmonised Tripartite Guideline. Validation of Analytical Procedures: Methodology, Q2 (R1). http://www.ich.org/fileadmin/Public_Web_Site/ICH_Products/Guidelines/Quality/Q2_R1/Step4/Q2_R1__Guideline.pdf . 1996. International Conference on Harmonisation of Technical Requirements for Registrations of Pharmaceuticals for Human Use(ICH),Geneva,Switzerland November, 2005. Accessed: 10/15/2012.

[379] Food and Drug Administration. Guidance for Industry: Bioanalytical Method Validation. http://www.fda.gov/downloads/Drugs/Guidances/ucm070107.pdf . 2011. Rockville, MD, US Department of Health and Human Services, FDA, Center for Drug Evaluation and Research, 2001. Accessed: 10/15/2012.

[380] M.Green, A Practical Guide to Analytical Method Validation, Anal. Chem., 68 (1996) 305A-309A.

[381] G.A.Shabir, Validation of high-performance liquid chromatography methods for pharmaceutical analysis.Understanding the differences and similarities between validation requirements of the US Food and Drug Administration, the US Pharmacopeia and the International Conference on Harmonization, J Chromatogr A., 987 (2003) 57-66.

[382] L.Huber. Validation of Analytical Methods and Procedures. Validation of Analytical Methods and Procedures . 3/29/2012. Accessed: 6/4/2013.

[383] A.G.Causey, H.M.Hill, and L.J.Phillips, Evaluation of criteria for the acceptance of bioanalytical data, Journal of Pharmaceutical & Biomedical Analysis, 8 (1990) 625-628.

[384] Biocides and Pesticides Unit. Guidlines for validation of analytical methods for non-agricultural pesticide active ingridients and products. http://www.hse.gov.uk/biocides/copr/pdfs/validation.pdf. 1995. Accessed: 6/4/2013.

[385] U.S.Food and Drug Administration. Guidelines for Submitting Samples and Analytical Data for Methods Validation. http://www.fda.gov/Drugs/GuidanceComplianceRegulatoryInformation/Guidances/ucm123124.htm . 4/27/2011. Accessed: 6/5/2013.

[386] O.von Richter, M.Eichelbaum, F.Schönberger, and U.Hofmann, Rapid and highly sensitive method for the determination of verapamil, [2H7]verapamil and metabolites in biological fluids by liquid chromatography–mass spectrometry, Journal of Chromatography B: Biomedical Sciences and Applications, 738 (2000) 137-147.

[387] A.Marin, E.Garcia, A.Garcia, and C.Barbas, Validation of a HPLC quantification of acetaminophen, phenylephrine and chlorpheniramine in pharmaceutical formulations: capsules and sachets, Journal of Pharmaceutical and Biomedical Analysis, 29 (2002) 701-714.

[388] J.W.Washington, J.J.Ellington, T.M.Jenkins, and J.J.Evans, Analysis of perfluorinated carboxylic acids in soils: Detection and quantitation issues at low concentrations, J Chromatogr A., 1154 (2007) 111-120.

[389] H.J.Kaiser and B.Ritts. Validation of Analytical Methods Used in Cleaning Validation. http://www.ivtnetwork.com/sites/default/files/Validation%20of%20Analytical%20Methods%20Used%20in%20Cleaning%20Validation.pdf . 8/1/2012. Accessed: 6/6/2013.

[390] J.Coleman, T.Wrzosek, R.Roman, J.Peterson, and P.McAllister, Setting system suitability criteria for detectability in high-performance liquid chromatography methods using signal-to-noise ratio statistical tolerance intervals, J Chromatogr A., 917 (2001) 23-27.

[391] S.De Baere, V.Eeckhaut, M.Steppe, C.De Maesschalck, P.De Backer, F.Van Immerseel, and S.Croubels, Development of a HPLC–UV method for the quantitative determination of four short-chain fatty acids and lactic acid produced by intestinal bacteria during in vitro fermentation, Journal of Pharmaceutical and Biomedical Analysis, 80 (2013) 107-115.

[392] N.A.Epshtein, Structure of chemical compounds,methods of analysis and process control, Pharmaceutical Chemistry Journal, 38 (2004) 40-56.

[393] T.C.Paino and A.D.Moore, Determination of LOD and LOQ of an HPLC Method Using Four Differnt techniques, Pharmaceutica Technology, 23 (1999) 86-92.

[394] International Conference on Harmonisation. Guidance for Industry Q1B Photostability Testing of New Drug Substances and Products. http://www.fda.gov/downloads/Drugs/GuidanceComplianceRegulatoryInformation/Guidances/ucm073373.pdf . 1996. Accessed: 6/11/2013.

[395] H.Rosing, W.Y.Man, E.Doyle, A.Bult, and J.H.Beijnen, Bioanalytical liquid chromatographic method validation . A review of current practices and procedures, Journal of Liquid Chromatography & Related Technologies, 23 (2000) 329-354.

[396] D.Dadgar and P.E.Burnett, Issues in evaluation of bioanalytical method selectivity and drug stability, Journal of Pharmaceutical & Biomedical Analysis, 14 (1995) 23-31.

[397] The United States Pharmacopeial Convention. USP Efavirenz Monograph. http://www.usp.org/sites/default/files/usp_pdf/EN/USPNF/pendingStandards/m3428.pdf . 2009. Accessed: 8/26/2012.

[398] B.Dogan-Topal, B.Uslu, and S.A.Ozkan, Voltammetric studies on the HIV-1 inhibitory drug Efavirenz: The interaction between dsDNA and drug using electrochemical DNA biosensor and adsorptive stripping voltammetric determination on disposable pencil graphite electrode, Biosensors and Bioelectronics, 24 (2009) 2358-2364.

[399] Y.Ni, L.Wang, and S.Kokot, Simultaneous determination of nitrobenzene and nitro-substituted phenols by differential pulse voltammetry and chemometrics, Analytica Chimica Acta, 431 (2000) 101-113.

[400] T.A.Ivandini, B.V.Sarada, C.Terashima, T.N.Rao, D.A.Tryk, H.Ishiguro, Y.Kubota, and A.Fujishima, Electrochemical detection of tricyclic antidepressant drugs by HPLC using highly boron-doped diamond electrodes, Journal of Electroanalytical Chemistry, 521 (2001) 117-126.

[401] Y.Yamauchi, M.Ido, M.Ohta, and H.Maeda, High performance liquid chromatography with an electrochemical detector in the cathodic mode as a tool for the determination of p-nitrophenol and assay of acid phosphatase in urine samples., Chem. Pharm. Bull., 52 (2004) 552-555.

[402] E.Kirchmann and L.E.Welch, High-performance liquid chromatographic separation and electrochemical detection of penicillins, J Chromatogr A., 633 (1992) 111-118.

[403] S.Altunata, R.L.Earley, D.M.Mossman, and L.E.Welch, Pulsed Electrochemical Detection Of Penicillins Using Three and Four Step Waveforms, Talanta, 42 (1994) 17-25.

[404] B.Paterson, C.E.Cowie, and P.E.Jackson, Determination of phenols in environmental waters using liquid chromatography with electrochemical detection, J Chromatogr A., 731 (1995) 95-102.

[405] R.B.Walker and I.Kanfer, Sensitive high-performance liquid chromatographic determination of cyclizine and its demethylated metabolite, norcyclizine, in biological fluids using coulometric

detection, Journal of Chromatography B: Biomedical Sciences and Applications, 672 (1995) 172-177.

[406] T.Grabowski, A.Świerczewska, B.Borucka, R.Sawicka, M.Sasinowska-Motyl, and S.W.Gumulka, Application of liquid chromatography method with electrochemical detection for bioequivalence study of trimetazidine in human plasma., Acta Poloniae Phamaceutica, 69 (2011) 1009-1016.

[407] B.Persson and S.Wendsjö, Oxygen effects in amperometric liquid chromatographic detection of omeprazole at a mercury electrode, J Chromatogr A., 321 (1984) 375-384.

[408] R.S.Martin, A.J.Gawron, S.M.Lunte, and C.S.Henry, Dual-Electrode Electrochemical Detection for Poly(dimethylsiloxane)-Fabricated Capillary Electrophoresis Microchips, Anal. Chem., 72 (2000) 3196-3202.

[409] J.Wang and L.D.Hutchins, Thin-layer electrochemical detector with a glassy carbon electrode coated with a base-hydrolyzed cellulosic film, Anal. Chem., 57 (1985) 1536-1541.

[410] T.N.Rao, B.V.Sarada, C.Terashima, and A.Fujishima, Electrochemical Detection of Carbamate Pesticides at Conductive Diamond Electrodes, Anal. Chem., 74 (2002) 1578-1583.

[411] S.Levin. Detection in HPLC. http://www.forumsci.co.il/HPLC/ .2013. Accessed: 5/26/2013.

[412] Thermo Scientific. How electrochemical detection for HPLC works. Thermo Scientific . 2013. Accessed: 5/26/2013.

[413] ESA.Inc. Hydrodynamic Voltammograms:Generation, Explanation, and Optimization of Applied Potentials. http://www.esainc.com/ . 2012. Accessed: 5/13/2013.

[414] N.Vanbeneden, F.Delvaux, and F.R.Delvaux, Determination of hydroxycinnamic acids and volatile phenols in wort and beer by isocratic high-performance liquid chromatography using electrochemical detection, J Chromatogr A., 1136 (2006) 237-242.

[415] I.N.Acworth and M.Bowers, Coulometric Electrode Array Detectors for Hplc, pp. 11-49, 1997.

[416] M.Joshi and V.Patravale, Formulation and Evaluation of Nanostructured Lipid Carrier (NLC)–based Gel of Valdecoxib, Drug Development & Industrial Pharmacy, 32 (2006) 911-918.

[417] R.H.Müller, S.A.Runge, V.Ravelli, A.F.Thünemann, W.Mehnert, and E.B.Souto, Cyclosporine-loaded solid lipid nanoparticles (SLN): Drug–lipid physicochemical interactions and characterization of drug incorporation, European Journal of Pharmaceutics and Biopharmaceutics, 68 (2008) 535-544.

[418] E.B.Souto, C.Anselmi, M.Centini, and R.H.Müller, Preparation and characterization of *n*-dodecyl-ferulate-loaded solid lipid nanoparticles (SLN), International Journal of Pharmaceutics, 295 (2005) 261-268.

[419] V.I.Mikla and V.V.Mikla, 1 - Advances in Imaging from the First X-Ray Images, in: V. I. Mikla and V. V. Mikla (Eds.), Medical Imaging Technology, Elsevier, Oxford, pp. 1-22, 2014.

[420] B.Li, G.Chen, H.Zhang, and C.Sheng, Development of non-isothermal TGA–DSC for kinetics analysis of low temperature coal oxidation prior to ignition, Fuel, 118 (2014) 385-391.

[421] D.Yu, M.Zhu, T.A.Utigard, and M.Barati, TGA kinetic study on the hydrogen reduction of an iron nickel oxide, Minerals Engineering, 54 (2013) 32-38.

[422] R.Chadha, P.Arora, A.Saini, and J.D.Singh, An insight into thermodynamic relationship between polymorphic forms of efavirenz, Journal of Pharmacy & Pharmaceutical Sciences, 15 (2012) 234-251.

[423] Gattefossé. Transcutol® HP. http://www.gattefosse.com/en/applications/ . 2013. Accessed: 12/8/2013.

[424] E.Zimmermann, E.B Souto, and R.H.Müller, Physicochemical investigations on the structure of drug-free and drug-loaded solid lipid nanoparticles (SLN ™) by means of DSC and ^{1}H-NMR, Die Pharmazie, 60 (2005) 508-513.

[425] L.Hernqvist, Crystal structures of fats and fatty acids, in : N.Garti, K.Sato (Editors), Crystallization and Polymorphism of Fats and Fatty Acids, Marcel Dekker Inc.,New York, Basel, 1998.

[426] J.Kreuter, Nanoparticulate systems for brain delivery of drugs, Advanced Drug Delivery Reviews, 47 (2011) 65-81.

[427] P.Blasi, S.Giovagnoli, A.Schoubben, M.Ricci, and C.Rossi. Solid lipid nanoparticles for targeted brain drug delivery. Lipid Nanoparticles: Recent Advances, 59 (2007) 454-477.

[428] N.A.Armstrong, Handbook of Pharmaceutical Excipients, The Pharmaceutical Press, London, pp. 290-292, 2009.

[429] European Communities-Commission. Reports for the Scientific Committee for Food. http://ec.europa.eu/food/fs/sc/scf/reports/scf_reports_16.pdf 15th[CD-NR-85-001-EN-C]. 1985. Luxembourg, Office of Official Publicationsof the European Communities. Accessed: 4/6/2012

[430] A.Rawat, E.Stippler, V.P.Shah, and D.J.Burgess, Validation of USP apparatus 4 method for microsphere *in vitro* release testing using Risperdal® Consta®, International Journal of Pharmaceutics, 420 (2011) 198-205.

[431] J.W.Moore and H.H.Flanner, Mathematical Comparison of curves with an emphasis on in vitro dissolution profiles, Pharm Tech, 20 (1996) 64-74.

[432] V.P.Shah, Y.Tsong, P.Sathe, and J.P.Liu, *In vitro* dissolution profile comparison–statistics and analysis of the similarity factor, f_2, Pharmaceutical Research, 15 (1998) 889-896.

[433] P. Costa and J. M. Sousa Lobo, Modeling and comparison of dissolution profiles, European Journal of Pharmaceutical Sciences, 13 (2001) 123-133.

[434] J. Siepmann and F. Siepmann, Mathematical modeling of drug delivery, International Journal of Pharmaceutics, 364 (2008) 328-343.

[435] J. Siepmann and F. Siepmann, Modeling of diffusion controlled drug delivery, Journal of Controlled Release, 161 (2012) 351-362.

[436] F.Lecomte, J.Siepmann, M.Walther, R.J.MacRae, and R.Bodmeier, Blends of enteric and GIT-insoluble polymers used for film coating: physicochemical characterization and drug release patterns, Journal of Controlled Release, 89 (2003) 457-471.

[437] S.R.Van Tomme, B.G.De Geest, K.Braeckmans, S.C.De Smedt, F.Siepmann, J.Siepmann, C.F.van Nostrum, and W.E.Hennink, Mobility of model proteins in hydrogels composed of oppositely charged dextran microspheres studied by protein release and fluorescence recovery after photobleaching, Journal of Controlled Release, 110 (2005) 67-78.

[438] F. Siepmann, K. Eckart, A. Maschke, K. Kolter, and J. Siepmann, Modeling drug release from PVAc/PVP matrix tablets, Journal of Controlled Release, 141 (2010) 216-222.

[439] M.Fathi, M.R.Mozafari, and M.Mohebbi, Nanoencapsulation of food ingredients using lipid based delivery systems, Trends in Food Science & Technology, 23 (2012) 13-27.

[440] N.V.Muyle and S.J.Turco, A simple model based on first order kinetics to explain release of highly water soluble drugs from porous dicalcium phosphate dihydrate matrices, Drug Development and Industrial Pharmacy, 21 (1995) 943-953.

[441] M.Ahuja, M.Yadav, and S.Kumar, Application of response surface methodology to formulation of ionotropically gelled gum cordia/gellan beads, Carbohydrate Polymers, 80 (2010) 161-167.

[442] A.R Madgulkar, M.R Bhalekar, V.J.Kolhe, and Y.D.Kenjale, Formulation and Optimization of Sustained Release Tablets of Venlafaxine Resinates Using Response Surface Methodology, Indian Journal of Pharmaceutical Sciences, 71 (2009) 387-394.

[443] I.A.W.Tan, A.L.Ahmad, and B.H.Hameed, Preparation of activated carbon from coconut husk: Optimization study on removal of 2,4,6-trichlorophenol using response surface methodology, Journal of Hazardous Materials, 153 (2007) 709-717.

[444] B. Singh, R. Kumar, and N. Ahuja, Optimizing drug delivery systems using systematic" design of experiments." Part I: fundamental aspects, Critical Reviews in Therapeutic Drug Carrier Systems, 22 (2005).

[445] J.Varshosaz, S.Ghaffari, M.R.Khoshayand, F.Atyabi, S.Azarmi, and F.Kobarfard, Development and optimization of solid lipid nanoparticles of amikacin by central composite design, Journal of Liposome Research, 20 (2010) 97-104.

[446] B.K.Körbahti and M.A.Rauf, Application of response surface analysis to the photolytic degradation of Basic Red 2 dye, Chemical Engineering Journal, 138 (2008) 166-171.

[447] C.Betianu, F.A.Caliman, M.Gavrilescu, I.Cretescu, C.Cojocaru, and I.Poulios, Response surface methodology applied for Orange II photocatalytic degradation in TiO2 aqueous suspensions, J. Chem. Technol. Biotechnol., 83 (2008) 1454-1465.

[448] F.Deyhimi, R.Salamat-Ahangari, M.Arabieh, and L.Parvin, Application of response surface methodology for modelling the enzymatic assay of hydrogen peroxide by Emerson–Trinder reaction using 4-iodophenol, International Journal of Environmental Analytical Chemistry, 86 (2006) 1151-1163.

[449] J. N. Sahu, B. C. Meikap, and A. V. Patwardhan, Optimization for the Production of Ammonia from Urea in a Semi-batch Reactor for Safe Feedstock in Power Plants: Experimental and Statistical Studies, CLEAN -Soil, Air, Water, 38 (2010) 533-542.

[450] R.Petkovska, C.Cornett, and A.Dimitrovska, Experimental design approach for the development and validation of an enantiospecific RP-HPLC method for simultaneous determination of clopidogrel and related compounds, Macedonian Journal of Chemistry and Chemical Engineering; 27 (2008) 53-64.

[451] A.A.Ahmad, B.H.Hameed, and A.L.Ahmad, Removal of disperse dye from aqueous solution using waste-derived activated carbon: Optimization study, Journal of Hazardous Materials, 170 (2009) 612-619.

[452] J.W.London, L.M.Shaw, L.Theodorsen, and J.H.Stromme, Application of response surface methodology to the assay of gamma-glutamyltransferase, Clinical Chemistry, 28 (1982) 1140-1143.

[453] Z.Rahman, A.S.Zidan, M.J.Habib, and M.A.Khan, Understanding the quality of protein loaded PLGA nanoparticles variability by Plackett–Burman design, International Journal of Pharmaceutics, 389 (2010) 186-194.

[454] Z.Rahman, A.S.Zidan, and M.A.Khan, Non-destructive methods of characterization of risperidone solid lipid nanoparticles, European Journal of Pharmaceutics and Biopharmaceutics, 76 (2010) 127-137.

[455] Y.Y.Yang, T.S.Chung, and N.N.Ping, Morphology, drug distribution, and in vitro release profiles of biodegradable polymeric microspheres containing protein fabricated by double-emulsion solvent extraction/evaporation method, Biomaterials, 22 (2001) 231-241.

[456] J. Weiss, E. A. Decker, D. J. McClements, K. Kristbergsson, T. Helgason, and T. Awad, Solid lipid nanoparticles as delivery systems for bioactive food components, Food Biophysics, 3 (2008) 146-154.

[457] F.Karacan, U.Ozden, and S.Karacan, Optimization of manufacturing conditions for activated carbon from Turkish lignite by chemical activation using response surface methodology, Applied Thermal Engineering, 27 (2007) 1212-1218.

[458] B.H.Hameed, L.F.Lai, and L.H.Chin, Production of biodiesel from palm oil (Elaeis guineensis) using heterogeneous catalyst: An optimized process, Fuel Processing Technology, 90 (2009) 606-610.

[459] A. Nath and P. K. Chattopadhyay, Optimization of oven toasting for improving crispness and other quality attributes of ready to eat potato-soy snack using response surface methodology, Journal of Food Engineering, 80 (2007) 1282-1292.

[460] N.K.Jain and A.Ram, Development and characterization of nanostructured lipid carriers of oral hypoglycemic agent:selection of surfactants, International Journal of Pharmaceutical Sciences Review and Research, 7 (2011) 125-130.

[461] J.Y.Fang, C.L.Fang, C.H.Liu, and Y.H.Su, Lipid nanoparticles as vehicles for topical psoralen delivery: Solid lipid nanoparticles (SLN) versus nanostructured lipid carriers (NLC), European Journal of Pharmaceutics and Biopharmaceutics, 70 (2008) 633-640.

[462] Y.C.Kuo and J.F.Chung, Physicochemical properties of nevirapine-loaded solid lipid nanoparticles and nanostructured lipid carriers, Colloids and Surfaces B: Biointerfaces, 83 (2011) 299-306.

[463] Y.C.Kuo and H.H.Chen, Entrapment and release of saquinavir using novel cationic solid lipid nanoparticles, International Journal of Pharmaceutics, 365 (2009) 206-213.

[464] P.Tangri and B.Bisht, Who Role And Guidelines in Stability Study of Pharmaceuticals: A Regulatory Perspective, International Journal of Research in Pharmaceutical and Biomedical Sciences, 3 (2012) 1379-1386.

[465] S.Bajaj, N.Singla, and N.Sakhuja, Stability Testing of Pharmaceutical Products, Journal of Applied Pharmaceutical Science, 2 (2012) 129-138.

[466] World Health Organization. WHO Expert Committee On Specifications For Pharmaceutical Preparations-Guidelines for registration of fixed-dose combination medicinal products. http://apps.who.int/prequal/info_general/documents/trs929/who_trs_929_annex5fdcs.pdf . 2005. Accessed: 12/9/2013.

[467] International Conference on Harmonization. Q1A(R2) Stability Testing of New Drug Substances and Products-International Conference on Harmonization (ICH) - Guidance for Industry: Q1A(R2) Stability Testing of New Drug Substances and Products. http://www.fda.gov/RegulatoryInformation/Guidances/ucm128179.htm. 2003. Accessed: 12/9/2013.

[468] Center for Drug Evaluation and Research, Food and Drug Administration Department of Health and Human Services. Guideline For Submitting Supporting Documentation In Drug Applications For The Manufacture Of Drug Substances. http://www.fda.gov/downloads/Drugs/GuidanceComplianceRegulatoryInformation/Guidances/ucm070632.pdf . 1987. Accessed: 12/9/2013.

[469] K.Vivek, H.Reddy, and R.Murthy.SR, Investigations of the effect of the lipid matrix on drug entrapment, in vitro release, and physical stability of olanzapine-loaded solid lipid nanoparticles, AAPS PharmSciTech, 8 (2007) 16-24.

[470] I. Zeta-Meter, Zeta-meter Manual, pp. 1-133, 1968.